23 February 2007 | S10

Science

AAAS

Volume 315, Issue 5815

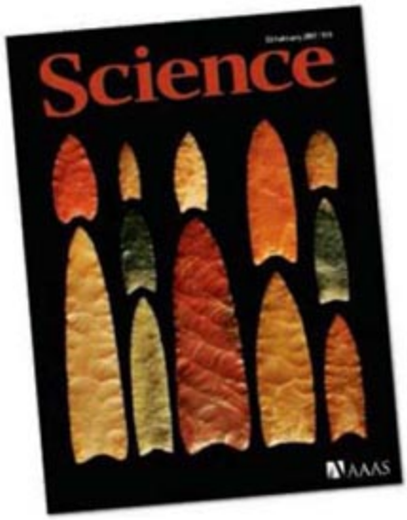

COVER

Projectile points of the prehistoric Clovis complex of North America are characterized by their lanceolate shape, concave base, distinctive basal flute, and basal edge grinding. The large point in the middle shows the distinctive outrepassé flaking pattern (broad flakes that extend across the width of the point) often found on Clovis points and other bifaces. See page 1122.

Photo of casts: Charlotte D. Pevny

DEPARTMENTS

EDITORIAL

NEWS OF THE WEEK

NEWS FOCUS

LETTERS

BOOKS *ET AL.*

EDUCATION FORUM

PERSPECTIVES

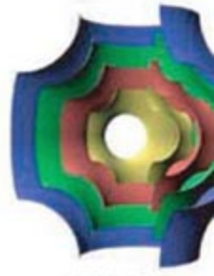

CONTENTS continued >>

Science

SCIENCE EXPRESS

www.sciencexpress.org

VIROLOGY

Suppression of MicroRNA-Silencing Pathway by HIV-1 During Virus Replication

R. Triboulet et al.

To protect itself from host defenses, the RNA virus HIV has evolved a way to dampen the host cell's RNA-silencing machinery.

10.1126/science.1136319

MOLECULAR BIOLOGY

A Slicer-Mediated Mechanism for Repeat-Associated siRNA 5′ End Formation in *Drosophila*

L. S. Gunawardane et al.

Tiny RNAs that silence potentially harmful transposons and repetitive sequences in germ cells are excised from larger RNAs by Argonaute proteins.

10.1126/science.1140494

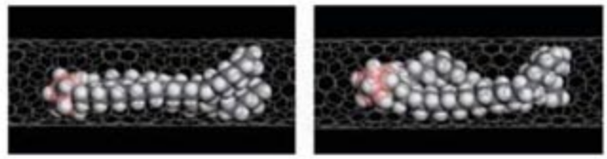

CHEMISTRY

BREVIA: Imaging of Single Organic Molecules in Motion

M. Koshino et al.

Sequential transmission electron microscopic images allow visualization of the motion of hydrocarbon chains confined within carbon nanotubes.

10.1126/science.1138690

MEDICINE

Disrupting the Pairing Between *let-7* and *Hmga2* Enhances Oncogenic Transformation

C. Mayr, M. T. Hemann, D. P. Bartel

Loss of miRNA binding sites in the mRNA for a chromatin-associated protein contributes to its overexpression and consequent cancer promoting ability.

10.1126/science.1137999

REVIEW

BREVIA

1086 & 1103

RESEARCH ARTICLE

REPORTS

CONTENTS continued >>

REPORTS *CONTINUED...*

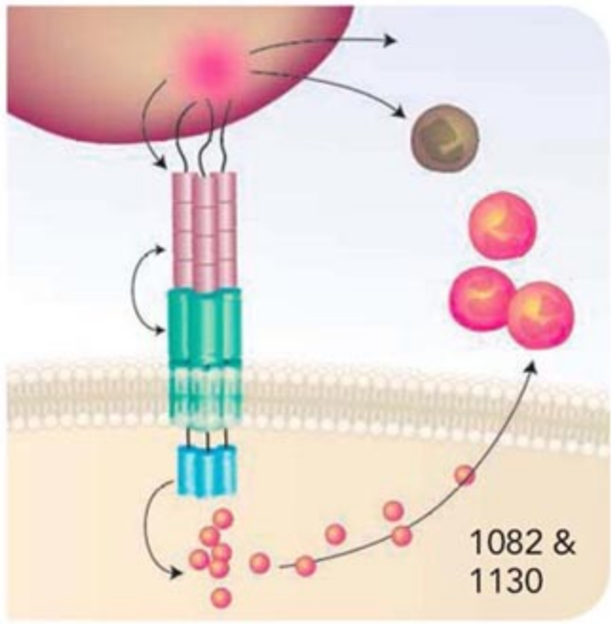

AAAS
ADVANCING SCIENCE, SERVING SOCIETY

SCIENCE (ISSN 0036-8075) is published weekly on Friday, except the last week in December, by the American Association for the Advancement of Science, 1200 New York Avenue, NW, Washington, DC 20005. Periodicals Mail postage (publication No. 484460) paid at Washington, DC, and additional mailing offices. Domestic individual membership and subscription (51 issues): $142 ($74 allocated to subscription). Domestic institutional subscription (51 issues): $710; Foreign postage extra: Mexico, Caribbean (surface mail) $55; other countries (air assist delivery) $85. First class, airmail, student, and emeritus rates on request. Canadian rates with GST available upon request, GST #1254 88122. Publications Mail Agreement Number 1069624. **Printed in the U.S.A.**

Change of address: Allow 4 weeks, giving old and new addresses and 8-digit account number. **Postmaster:** Send change of address to AAAS, P.O. Box 96178, Washington, DC 20090–6178. **Single-copy sales:** $10.00 current issue, $15.00 back issue prepaid includes surface postage; bulk rates on request. **Authorization to photocopy** material for internal or personal use under circumstances not falling within the fair use provisions of the Copyright Act is granted by AAAS to libraries and other users registered with the Copyright Clearance Center (CCC) Transactional Reporting Service, provided that $18.00 per article is paid directly to CCC, 222 Rosewood Drive, Danvers, MA 01923. The identification code for *Science* is 0036-8075. *Science* is indexed in the *Reader's Guide to Periodical Literature* and in several specialized indexes.

CONTENTS continued >>

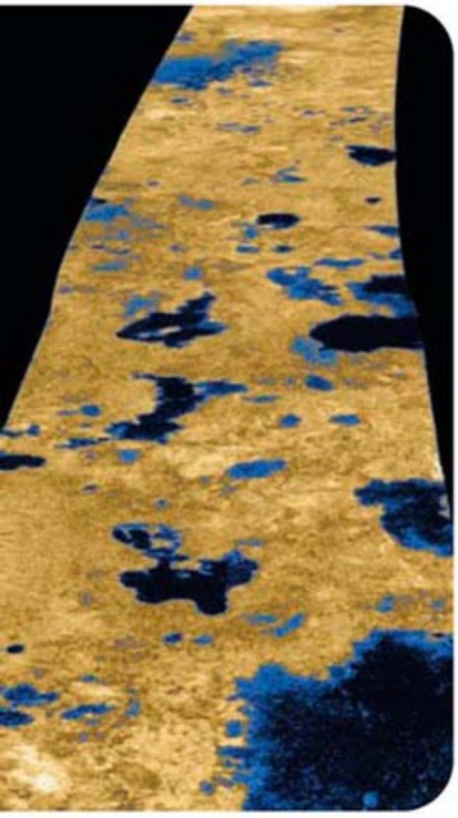

Clues to Earth's future on Titan?

SCIENCE**NOW**

www.sciencenow.org
DAILY NEWS COVERAGE

Titan's Dark Mirror
Saturn's giant moon is offering surprising clues about Earth's distant future.

Dirty Bombs Not Such a Blast
Radioactive dispersal devices may pose less threat to first responders than thought.

Lunar Observatories on a Budget
NASA scientists push small and cheap robotic craft to conduct astronomy from the moon.

HER2—now in the STKE Glossary.

SCIENCE'S **STKE**

www.stke.org
SIGNAL TRANSDUCTION KNOWLEDGE ENVIRONMENT

GLOSSARY
New additions include HER2 (a receptor), EPAC (an exchange factor), and GARP (a DNA binding domain).

ST NETWATCH: The Lipid Library
This site provides detailed information about lipid structure, biosynthesis, and biological functions; in Educator Sites.

ST NETWATCH: Yeast Resource Center
This site provides information to help researchers identify and characterize protein complexes in yeast; in Model Organisms.

Budget crunch at NASA.

SCIENCE **CAREERS**

www.sciencecareers.org CAREER RESOURCES FOR SCIENTISTS

US: Young Researchers Face NASA Budget Realities
A. Fazekas
NASA's tough funding climate is taking its toll on the next generation of space researchers.

EUROPE: FP7 Funding Opportunities at a Glance
E. Pain
Get the lowdown on funding for young scientists in the European Union's new Framework Programme.

MISCINET: Educated Woman, Postdoc Edition, Chapter 2—Palpable Neurosis
M. P. DeWhyse
Micella observes that people in her new place are even crazier than at her old place.

Separate individual or institutional subscriptions to these products may be required for full-text access.

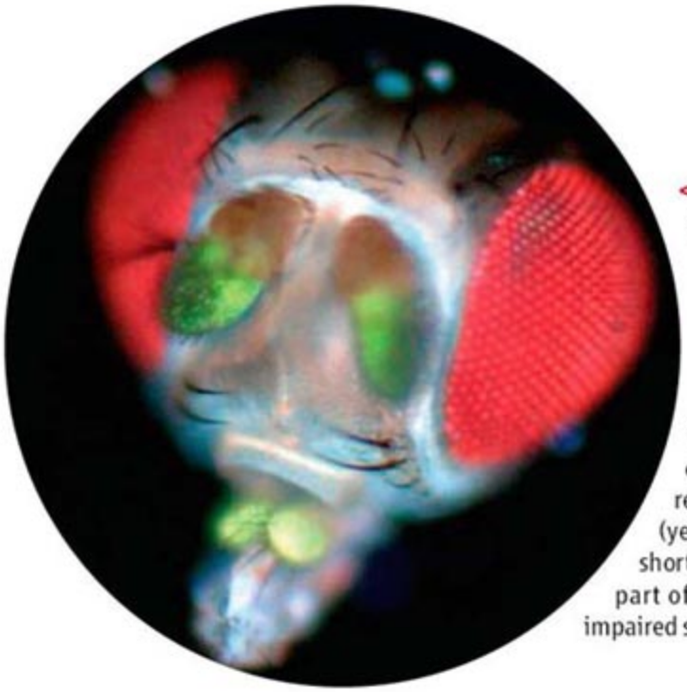

<< Smelling Their Way to an Early Grave

When animals are reared on a near-starvation diet, they live much longer than those that eat freely. Even the fruit fly *Drosophila* has this reaction to a low glucose diet, and lives considerably longer on a 5% than on a 15% sugar-yeast diet. This effect of dietary restriction is easily reversed when flies consume more food. **Libert *et al.*** (p. 1133, published online 1 February, see the 2 February news story by **Leslie**) report a less expected effect: Just the smell of the flies' food (yeast) can inhibit some of the effects of dietary restriction and shorten the flies' life span by 6 to 18%. Flies lacking an essential part of their odor receptors, which results in their having greatly impaired senses of smell, live longer than flies with intact odor sensation.

The Shape of Sheets to Come

When the sides of a flat piece of paper lying on a desk are slowly pushed together, the sheet will eventually buckle with a periodicity that depends on its thickness or stiffness. The same procedure applied to a piece of aluminum foil may also lead to buckling, but will also lead to crumpling or wrinkling on a local scale. If either material has been previously deformed, the change in shape and curvature will likely be affected by defect sites. **Klein *et al.*** (p. 1116) propose a general description for shrinking of thin sheets that depends only on the resting shape of the material and an accounting of the stresses placed on the material. Ideally, the thin sheet will deform in a competition between bending and stretching energies that maintains a shape near the resting shape. The authors demonstrate their concepts using a series of polymer films with nonlinear concentration gradients of monomers that swell to different extents across their surface. In a Perspective, **Kamien** shows how this approach can be applied to everyday objects, like potato chips, and how more complex shapes can be designed.

Outlook for Bright Neutron Source

X-ray and photon sources for spectroscopic and diffraction methods have increased in brightness by several orders of magnitude during the past 20 years, but the brightness of neutron sources for structural studies have increased by only an order of magnitude during the past 40 years. With conventional neutron source technologies (spallation and fission reactors) reaching a plateau in their output, **Taylor *et al.*** (p. 1092) propose that inertial fusion energy facilities and high-power lasers could run in tandem to provide neutron sources that would be three orders of magnitude brighter than those available at present.

Classical Quasicrystalline Tilings

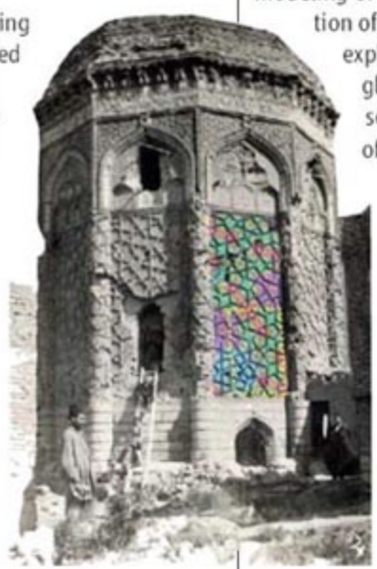

Islamic architecture beginning in the 10th century is marked by distinctive star and line patterns called girih. These figures were thought to be interwoven continuous lines, created by simple tools such as straightedge and compass. **Lu and Steinhardt** (p. 1106; see the news story by **Bohannon**) find that by the beginning of the 13th century, artisans began to create these patterns from tilings of decorated polygons. The tilings became increasingly complex, and by the 15th century the patterns had evolved into quasicrystalline designs, well before the mathematical description of these space-filling patterns that possess rotational symmetry yet lack translational symmetry.

Supernova Smoke Rings

Supernova 1987A, the first supernova that could be seen with the naked eye since Kepler's supernova in the 17th century, is of an unusual type, and its characteristics have suggested that its explosion resulted tens of thousands of years after the merger of two massive stars. However, a detailed model has eluded astronomers. **Morris and Podsiadlowski** (p. 1103; see the Perspective by **Soker**) have performed three-dimensional computer simulations of such a stellar merger that can explain many of these features. After the two stars merge, detailed modeling of the angular momentum and accretion of gas from the two stars predicts two explosions, one that causes an "hourglass" ejection of material and the second that produces a smaller puff of gas. Together, these events account for the three rings of gas around the remnant of the exploded stars—two from the projected hourglass explosion, and an inner one from the second explosion.

Empowering Powder

A central challenge in the structural elucidation of zeolites and related porous solids is the tendency of these materials to adopt highly polycrystalline morphologies that fail to yield clean x-ray diffraction data. The structures are nonetheless highly sought after in light of the catalytic significance of such materials. **Baerlocher *et al.*** (p. 1113; see the Perspective by **Gies**) present an algorithmic advance that facilitates combined analysis of powder diffrac-

Continued on page 1051

CREDITS (TOP TO BOTTOM): SERGIY LIBERT AND SCOTT PLETCHER/MCOA, BCM; LU AND STEINHARDT

Continued from page 1049

tion and electron microscopy data to solve particularly intractable zeolite structures. Using this method, they resolve the markedly complex 10-ring channel system forming the IM-5 zeolite, an active catalyst for hydrocarbon cracking and related reactions.

Beyond the Diffraction Limit

Most imaging techniques are diffraction limited, so that subwavelength information about an object is lost through the rapidly decaying evanescent waves. A number of techniques have been proposed, and some demonstrated, with the ability to form patterns beyond this diffraction limit, but these tend to operate in the near field. **Lerosey *et al.*** (p. 1120) use a time-reversal mirror—an antennae array that first detects the signal from a point source placed at the intended focus position, and then sends the signal back (time-reversal reflection)—to demonstrate the ability to focus microwaves on a receiver array to better than 1/30th of their wavelength. The technique was used to increase transmission rates for telecommunications by a factor of 3.

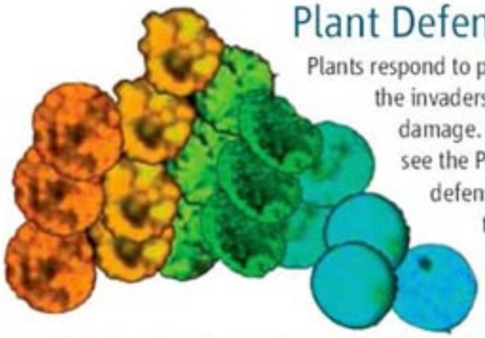

Plant Defense Coordination

Plants respond to pathogen attack by recognizing molecular signals from the invaders and instigating their own cellular responses to limit damage. **Shen *et al.*** (p. 1098, published online 21 December; see the Perspective by **Dangl**) now show that two of the plant's defense systems themselves interact at the level of gene transcription. Studying barley's mildew A proteins, part of one of the plant pathogen response pathways, the authors show how these proteins are localized to the nucleus, where they alter transcription of factors that regulate the other plant pathogen response pathway. The plant's response to pathogenic attack is thus coordinated and tuned to be appropriate to the challenge.

New Clovis Culture Dates

The first well-established culture in the New World has been long thought to be that of Clovis, characterized by a distinctive shape of their hunting points. **Waters and Stafford** (p. 1122; see the cover and the news story by **Mann**) present a series of new radiocarbon dates on several Clovis sites and reassess previous more scattered dates. Together, these imply that Clovis persisted for only a few hundred years and occurred somewhat later than was previously thought. The dates are similar to dates for other cultures such as Folsom and Goshen and may imply that the Clovis culture may have emerged in the New World after a previous colonization.

Customizing MicroRNAs

MicroRNAs (miRNAs) are ubiquitous small noncoding RNAs that regulate gene expression in eukaryotes. Because of the double-stranded nature of intermediates in their synthesis, miRNAs are potential targets for RNA editing. **Kawahara *et al.*** (p. 1137) now show that members of a mammalian miRNA cluster are edited in their seed regions, the region which determines their target specificity. This editing of adenosine bases to inosine, which is tissue specific, changes the potential target range of the miRNAs. The edited miRNA, but not the unedited version, acts to repress an enzyme involved in purine metabolism, and mice expressing this miRNA have elevated levels of uric acid in the cortex of the brain.

Reversal of Rett Syndrome in Mice

Rett syndrome is a rare genetic disease caused by a mutation in the X-linked gene *MECP2*, which causes mental retardation and autism-like symptoms in young girls. **Guy *et al.*** (p. 1143, published online 8 February; see the 9 February news story by **Miller**) engineered mice with an inserted sequence in the *MECP2* gene that blocks its expression and show that the mice exhibit many of the symptoms of Rett syndrome. Reactivation of *MECP2* in these mice before symptoms appear prevents disease. Reactivation in animals exhibiting Rett syndrome eliminated disease in both young adult males and mature females. Although such genetic manipulations are not possible in human patients, the apparent reversible nature of the disease suggests that therapy may be feasible.

CREDITS (TOP TO BOTTOM): IMAGE: QIAU-HUA SHEN, BASED ON DATA DESCRIBED IN Q.-H. SHEN *ET AL.*

Donald Kennedy is the Editor-in-Chief of *Science*.

Science, Information, and Power

NOW THAT THE 110TH UNITED STATES CONGRESS IS WELL SETTLED IN ITS SEATS, THINGS ARE heating up—and the decisive recent report from the United Nations Intergovernmental Panel on Climate Change will help. Some of the early action is on the legislative front: The well-publicized "First Hundred Hours" of the new House Democratic majority voted up some 40 hours' worth of the less controversial bills. The better news is that legislators made some serious-looking moves toward an emissions cap for greenhouse gases. That's a good start, but perhaps the most significant action has come from other sources.

One of these, improbably, is American industry. Quick digression: Earlier in this space, I noted a phenomenon arising when strong views in the polity bump up against administrative inertia in the federal government. For example, national polls show strong citizen preference for action to mitigate global warming and for revising the ban on federally supported embryonic stem cell research. Years of unresponsiveness from the Bush Administration have stimulated an unexpected downward jurisdictional migration, with some states floating bond financing for stem cell research and other states—even cities—adopting their own emissions targets. Now a new downstream locus for environmental activism has surfaced, and the White House might listen to this one.

Chief executive officers from 10 major U.S. companies have gathered to form a Climate Action Partnership. When General Electric, Alcoa, DuPont, and even Duke Energy are sufficiently convinced about global warming to recommend mandatory emissions reductions with targets, they are asking to be taken seriously. This corporate congregation was mobilized in part by the World Resources Institute and leading environmental organizations, whose collective clout once again demonstrates that enlightened leadership from civic society can sometimes reach useful ends more quickly than old-fashioned intercession in electoral politics.

Back in the political domain: The U.S. Congress does more than manufacture statutes. There's oversight of administrative agencies, and anyone who has been in charge of one knows how tough that process can be (even, as in my case, if the inquisitors are from your party). Now Henry Waxman, chair of the House Oversight Committee, is scheduling hearings—the first was on 30 January—about efforts by Administration officials to modify or rewrite the scientific findings of agency scientists. There promise to be more, and there should be. The Union of Concerned Scientists has just released a comprehensive report on such matters, and supplied witnesses to the Waxman hearing.

But there is a conveniently timed push-back from the White House. A new initiative announced late in January will affect the way in which executive agencies like the Environmental Protection Agency and the Occupational Safety and Health Administration generate guidelines and regulations. The plan places new responsibilities on a political appointee in each agency, claiming that it will smooth the process of rule-making and make it more consistent. Critics fear that its purpose is to enforce Administration control over the development of regulations affecting the environment and public health. Significantly, the announcement was published on the very day of the Waxman hearing.

Those who believe that convergences are often not mere coincidences will see these events as a typical, garden-variety struggle between a Democratic Congress and the White House over the use of science in informing policy. But this confrontation is about more than whether politics can trump science. At its core, it is a struggle for authority between a presidency wanting control over information so that the public will accept its version of reality, and a Congress insistent on its responsibility to find facts needed to shape national policy.

This contest over the power of the presidency could not be more fundamental to the democratic values of American society. Presidential claims to exclusive power over knowledge may sometimes be justifiable in our national interest, but we should not be misled. We are not an empire—and our president is neither an emperor nor, as author and historian Garry Wills reminds us, the commander-in-chief of anyone who doesn't happen to be in the army or the navy.

– Donald Kennedy

10.1126/science.1140872

EDITED BY GILBERT CHIN AND JAKE YESTON

APPLIED PHYSICS

Squeeze Play

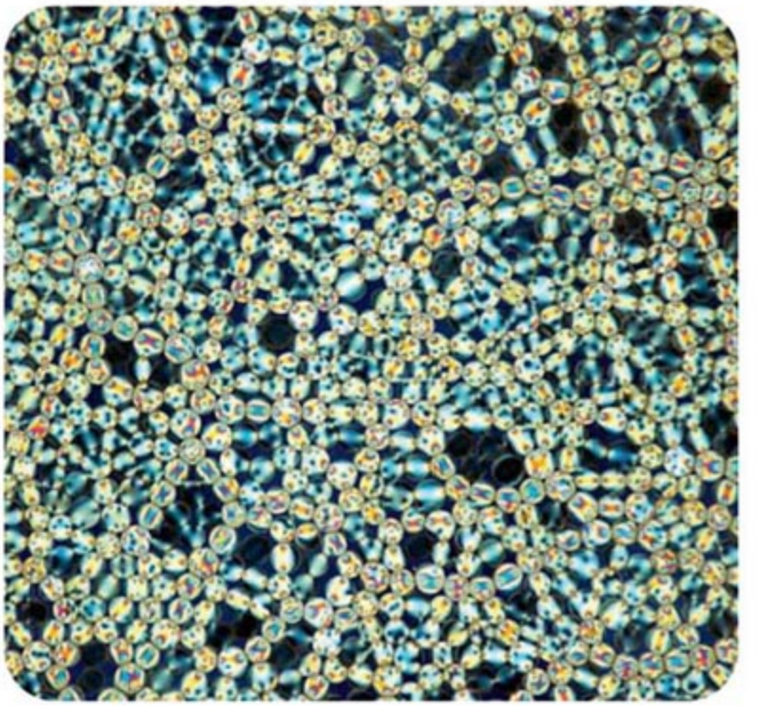

Cereals in grain silos, coal in freight cars, and powders in processing vats are all examples of granular materials that show similar flow properties despite the differences in size and shape of the particles. During flow, loosely packed granular materials are similar to fluids in that the particles are not closely connected but nonetheless interact with each other through periodic collisions. Above a critical packing fraction, the number of contacts between neighboring particles increases and creates mechanical stability leading to a jamming transition. In a set of elegant experiments, Majmudar *et al.* have tracked the jamming transition in two dimensions for a bidisperse mixture of disk-shaped particles (shown at right), with a size ratio and composition designed to guarantee a disordered system. The particles were made from a birefringent polymer so that contacts between particles and their stress fields could be measured with polarized light, while a second image taken without polarizers tracked the particle centers. The authors observed critical values at the jamming transition consistent with recent simulations, although the sharpness of the transition was diminished because of residual stress effects from the walls of the container. — MSL

Phys. Rev. Lett. **98**, 058001 (2007).

NEUROSCIENCE

Supplying a Start-Up

After an injury to its axon, a neuron must reorganize rapidly in order to establish a new growth cone at the tip of the transected segment. The growth cone can then search for and reestablish synaptic contacts, but the axon must supply the requisite materials to promote regrowth.

By imaging cultured *Aplysia* neurons after axotomy, Erez *et al.* have followed the events by which axons establish new growth cones. Soon after an axon has been cut, the end of the portion still attached to the cell body partitions into two compartments. In the proximal region, vesicles can be observed en route to the plasma membrane from the Golgi complex; if the production of Golgi-derived vesicles is blocked, a new growth cone cannot be established. In the distal region, vesicles also accumulate, but these arise via the retrieval of membrane from the cell surface. What drives this traffic are the microtubules, which form the structural scaffold of the axon and rearrange to establish a region that segregates the two classes of vesicles. This process, which involves the reorientation of polarized microtubules, collects and concentrates the components needed to regenerate a motile growth cone. — SMH

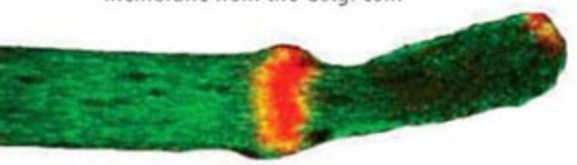

Vesicles (red) are delivered by microtubules (green) to the site of the new growth cone.

J. Cell Biol. **176**, 497 (2007).

MATERIALS SCIENCE

Freezing in the Glow

Polymer light-emitting electrochemical cells (PLECs) have mobile ions within the polymer layer, a feature that fosters low turn-on voltages and skirts the need for low-work-function cathodes or interfacial layers between the cathodes and polymer. However, in comparison with light-emitting diodes, PLECs tend to have slow response times and short operating lifetimes. Ion mobility limits the device speed, and performance can degrade as phase separation occurs between the emitting polymer and the second polymer used to store the mobile ions.

Shao *et al.* have fabricated PLECs with a simple sandwich structure, in which an organic ionic liquid, methyltrioctylammonium trifluoromethanesulfonate (MATS), acts as the reservoir for the mobile ions. Because MATS has a melting temperature of 56°C, the authors could freeze p-type–intrinsic–n-type (p-i-n) junctions into the devices at room temperature through heating/cooling cycles under an applied voltage bias. The consequent improved contact between the mobile ions and the luminescent polymer led to fast response times. Moreover, the compatibility of MATS with the luminescent polymer—in this case a substituted poly(*para*-phenylene vinylene) compound—precluded phase separation. The devices functioned with stable high brightness over days of continuous operation. — MSL

Adv. Mater. **19**, 365 (2007).

APPLIED PHYSICS

Reflecting X-rays into Focus

Coherent x-rays produced by synchrotrons have provided an invaluable tool for studying the static and dynamical structural properties of matter on the macroscopic scale. There is now a desire, in both biological and condensed-matter systems, to shift toward the probing of microscopic samples on the nanoscale. Although hard (short-wavelength) x-rays can be focused to approximately 100-nm spot sizes using reflection, refraction, or diffraction techniques, it is reflection from a high-quality surface that is expected to hone the focus down to the 20-nm level and thereby provide the capability of a true nanometer-scale structural probe. Using a combination of surface machining and surface interferometry, Mimura *et al.* have designed a platinum-coated, silicon-based elliptical mirror with a surface roughness better than 2 nm from peak to valley. After fabricating the mirror to match the optical requirements of their 1-km-long beamline, they demonstrate focusing of 15-keV hard x-rays to a beam

CREDITS (TOP TO BOTTOM): MAJMUDAR *ET AL.*, *PHYS. REV. LETT.* **98**, 058001 (2007); EREZ *ET AL.*, *J. CELL BIOL.* **176**, 497 (2007)

width of ~25 nm. By combining two such mirrors in orthogonal planes, they expect the x-rays to be focused to a spot size of ~30 nm. — ISO

Appl. Phys. Lett. **90**, 051903 (2007).

CHEMISTRY

Metal-Free Ringing

Chiral Brønsted acids have recently proven effective alternatives to metallic Lewis acids in a range of enantioselective catalysis applications. Rueping *et al.* extend this approach to electrocyclic ring closures. Specifically, they explored the capacity of binaphthyl phosphate derivatives to catalyze the Nazarov cyclization, a reaction in which two alkenyl groups flanking a carbonyl moiety connect at the β carbons to form a cyclopentenone ring. The resulting product bears two new chiral centers, which the optimized catalyst (at 2 mol % loading) produced with enantiomeric excesses up to 93% for the major diastereomer. The cis diastereomer was generally favored (with selectivities ranging from 1.5 to 9.3), though the products could be epimerized selectively at the α carbon to the corresponding trans isomers by treatment with basic alumina. The selectivity is sensitive to solvent, because it relies on the nature of the ion pair formed after proton transfer from the chiral anion to the substrate, and was found to be highest in chloroform. — JSY

Angew. Chem. Int. Ed. **46**, 10.1002/anie.200604809 (2007).

MICROBIOLOGY

Stepwise Sabotage of Susceptibility

Streptomycin was the first antibiotic found to target the ribosome; specifically, it works by promoting the misreading of the genetic code during translation. Although resistance to high levels of streptomycin has been assigned to mutations in *rrs*, the gene encoding 16*S* ribosomal RNA (rRNA), this mechanism does not account for the observed high prevalence of resistance to low levels of the drug.

Okamoto *et al.* have found that spontaneous mutations occur rapidly within the bacterially conserved gene *gidB*, which encodes a 7-methylguanosine methyltransferase specific for 16*S* rRNA. As a consequence of these mutations, there is a failure to methylate the invariant nucleotide G527, and hence low-level streptomycin resistance is conferred. Even though resistance to most drugs that interact with the ribosome occurs via changes in rRNA sequence, this finding suggests that this mechanism of resistance could be more frequent among bacteria than previously expected. Moreover, it is worrisome that these mutations do not appear to exact any fitness cost and seem to constitute a first step toward the evolution of high-level resistance. — CA

Mol. Microbiol. **63**, 1096 (2007).

Science STKE AAAS

www.stke.org

<< An Unkind Cut Can Lead to a Broken Heart

Postpartum (or peripartum) cardiomyopathy (PPCM), which occurs up to a few months after delivery (or late in pregnancy), is associated with an acute onset of heart failure in women with no history of heart disease. Hilfiker-Kleiner *et al.* have linked cardiomyocyte STAT3 (signal transducer and activator of transcription 3) to PPCM. Normally, pregnancy is associated with cardiac hypertrophy and increased capillary density—physiological changes that also were found to occur in mice lacking cardiac STAT3. However, postpartum mice lacking cardiac STAT3 lost the increased capillary density. These mice suffered an attenuated increase in cardiac manganese superoxide dismutase, which led to excessive levels of reactive oxygen species, which led, in turn, to an increased abundance of the proteolytic enzyme cathepsin D. Furthermore, the STAT3-deficient mice exhibited enhanced cleavage of full-length prolactin, which is a cathepsin D substrate, into a shorter, antiangiogenic form. Increasing the amount of circulating prolactin stimulated cardiac damage in mice that overexpressed cardiac cathepsin D. In contrast, pharmacological inhibition of prolactin secretion prevented PPCM. A preliminary study suggested that inhibiting prolactin release by administering bromocriptine was protective of cardiac function in women at high risk of PPCM. Thus, the authors suggest that cardiac STAT3 is critical to postpartum cardiac function and propose that inhibiting prolactin release may be a viable approach to PPCM treatment. — EMA

Cell **128**, 589 (2007).

CREDIT: HILFIKER-KLEINER *ET AL.*, *CELL* **128**, 589 (2007)

www.sciencemag.org

Science

1200 New York Avenue, NW
Washington, DC 20005
Editorial: 202-326-6550, FAX 202-289-7562
News: 202-326-6500, FAX 202-371-9227

Bateman House, 82-88 Hills Road
Cambridge, UK CB2 1LQ
+44 (0) 1223 326500, FAX +44 (0) 1223 326501

Subscription Services For change of address, missing issues, new orders and renewals, and payment questions: 866-434-AAAS (2227) or 202-326-6417, FAX 202-842-1065. Mailing addresses: AAAS, P.O. Box 96178, Washington, DC 20090-6178 or AAAS Member Services, 1200 New York Avenue, NW, Washington, DC 20005

Institutional Site Licenses please call 202-326-6755 for any questions or information

Reprints: Author Inquiries 800-635-7181
Commercial Inquiries 803-359-4578
Corrections 202-326-6501

Permissions 202-326-7074, FAX 202-682-0816

Member Benefits Bookstore: AAAS/BarnesandNoble.com bookstore www.aaas.org/bn; Car purchase discount: Subaru VIP Program 202-326-6417; Credit Card: MBNA 800-847-7378; Car Rentals: Hertz 800-654-2200 CDP#343457, Dollar 800-800-4000 #AA1115; AAAS Travels: Betchart Expeditions 800-252-4910; Life Insurance: Seabury & Smith 800-424-9883; Other Benefits: AAAS Member Services 202-326-6417 or www.aaasmember.org.

science_editors@aaas.org (for general editorial queries)
science_letters@aaas.org (for queries about letters)
science_reviews@aaas.org (for returning manuscript reviews)
science_bookrevs@aaas.org (for book review queries)

Published by the American Association for the Advancement of Science (AAAS), *Science* serves its readers as a forum for the presentation and discussion of important issues related to the advancement of science, including the presentation of minority or conflicting points of view, rather than by publishing only material on which a consensus has been reached. Accordingly, all articles published in *Science*—including editorials, news and comment, and book reviews—are signed and reflect the individual views of the authors and not official points of view adopted by the AAAS or the institutions with which the authors are affiliated.

AAAS was founded in 1848 and incorporated in 1874. Its mission is to advance science and innovation throughout the world for the benefit of all people. The goals of the association are to: foster communication among scientists, engineers and the public; enhance international cooperation in science and its applications; promote the responsible conduct and use of science and technology; foster education in science and technology for everyone; enhance the science and technology workforce and infrastructure; increase public understanding and appreciation of science and technology; and strengthen support for the science and technology enterprise.

Information for Authors

See pages 120 and 121 of the 5 January 2007 issue or access www.sciencemag.org/feature/contribinfo/home.shtml

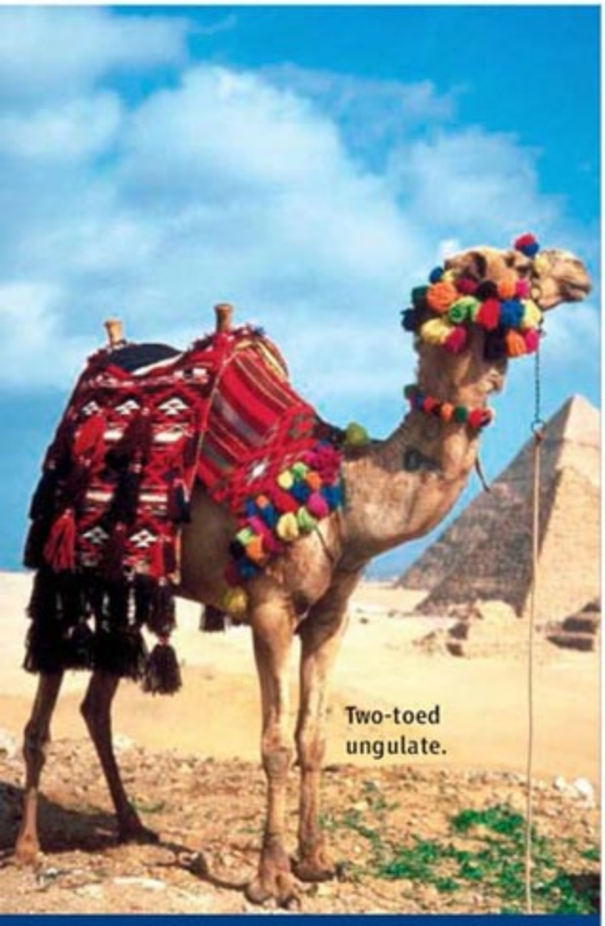
Two-toed ungulate.

ON THE HOOF

NET WATCH

What does a dromedary camel loping across a sand dune have in common with a Lippizaner stallion high-stepping around a ring and a rhinoceros luxuriating in a mud puddle? They are all ungulates, mammals that typically sport the overgrown toenails known as hooves. To learn more about the group or individual species, drop by the Ultimate Ungulate page from Brent Huffman, a keeper at the Toronto Zoo in Canada.

Introductory pages summarize some of the surprises from recent molecular studies on mammalian evolution, which distanced the ungulates from elephants and aardvarks, long thought to be their next of kin. Hoofed animals are actually more closely related to bats. Species accounts cover most of the more than 250 ungulates, offering details on the animals' diet, habitat, behavior, and range. >>
www.ultimateungulate.com

CREDITS (TOP TO BOTTOM): PHOTOS.COM; ALEX BORISENKO 2006, ROYAL ONTARIO MUSEUM

Birds, Bats, and Bar Codes

Fifteen bird species have been newly discovered by a DNA identification technique called bar coding, researchers reported online 19 February in *Molecular Ecology Notes*. They've also uncovered six new bat species in bat-rich Guyana.

The Barcode of Life project seeks to determine the DNA sequence of the same mitochondrial gene in millions of Earth's fauna. The variations in the sequence provide a unique, easy-to-read species identifier, scientists say.

Until now, bar coding hadn't been tested in either mammals or widespread bird populations. For the bird probe, evolutionary biologist Paul Hebert of the University of Guelph in Canada and colleagues cataloged DNA from 2500 specimens supplied by museums and bird banders in the United States and Canada. The samples represent 643 of the 690 known North America–based species. Bar codes supplied some surprises, revealing 15 "cryptic" species: birds so similar to other birds that they had not been seen as distinct. What's more, eight supposed gull species turned out to be just one, and birds from 14 other supposed species were virtually identical to at least one other species.

In the mammalian end of the project, Hebert's team turned to Guyana, taking tissue samples from 840 bat specimens in the Royal Ontario Museum. There was concern that the species would be too closely related to reveal genetic differences. Yet the researchers easily distinguished the 80 or so species in the collection and discerned several new ones, Hebert says.


A different bat.

Such studies have the potential to "break bar coding" by proving to skeptics that species can't always be distinguished on the basis of just one gene, says project member Mark Stoeckle of Rockefeller University in New York City. "But it's worked everywhere it's been applied."

Diabetes Genes Go Public

As genomic information piles up at an exponential rate, sorting through it all has become overwhelming. In the hopes that with enough eyes, breakthroughs will materialize, the Swiss drug company Novartis has helped create a free and open database on the genetics of type 2 diabetes.

Posted at www.broad.mit.edu/diabetes, the Diabetes Genetics Initiative is a collaboration between Novartis, the Broad Institute of the Massachusetts Institute of Technology and Harvard University, and Lund University in Sweden. Launched in 2004 and completed last week, it contains information on the genomes of 1500 people with diabetes and 1500 without in Sweden and Finland.

Alan Shuldiner, an endocrinologist and geneticist at the University of Maryland School of Medicine in Baltimore, suspects that the Novartis collaboration is "proactively providing their data in anticipation that others will do the same." A dozen teams are working along the same lines with different populations, from the Pima Indians in Arizona to Massachusetts residents in the Framingham Heart Study.

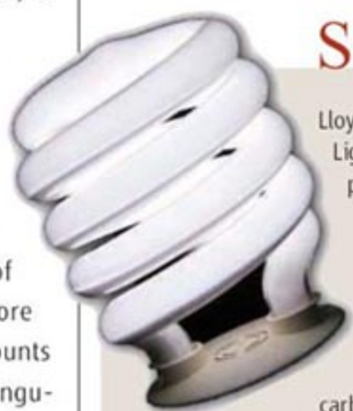

Seeing the Light

Lloyd Levine doesn't intend the "How Many Legislators Does It Take to Change a Light Bulb Act" of 2007 as a joke. The California assemblyman, a Democrat, is preparing a bill that would effectively ban the sale of household incandescent bulbs in the state by 2012. Compact fluorescents, called twisties by some, are cheaper and more energy-efficient, he says.

The Levine ban "is probably the most aggressive proposal we've heard to date," says R. Neal Elliot of the nonprofit American Council for an Energy-Efficient Economy. Elliot says compact fluorescents are a green "no-brainer" because they use less electricity—and thus reduce carbon emissions—and with life spans of up to 8 years, they last more than long enough to recoup their high initial cost. John Geesman of the California Energy Commission says he thinks the proposal might fly if it exempts certain fixtures, such as the lights inside microwave ovens, for which there aren't effective substitutes.

Q: Where's the only place you can buy AAAS/*Science* merchandise?

A: Exclusively from the new AAAS Online Store!

AAAS members get your 10% discount

Visit www.apisource.com/aaas

If you're proud to be an AAAS member, here you can find carefully selected quality items that will let you wear your membership with pride. And, as another great benefit of AAAS membership, all members receive a discount of 10% or more on every item! To receive your discount, enter code SBN5 at the checkout.

As with all AAAS programs, a portion of each sale goes toward our vital educational outreach programs.

Don't wait—visit www.apisource.com/aaas and enter SBN5 for your discount.

Science
AAAS

EDITED BY YUDHIJIT BHATTACHARJEE

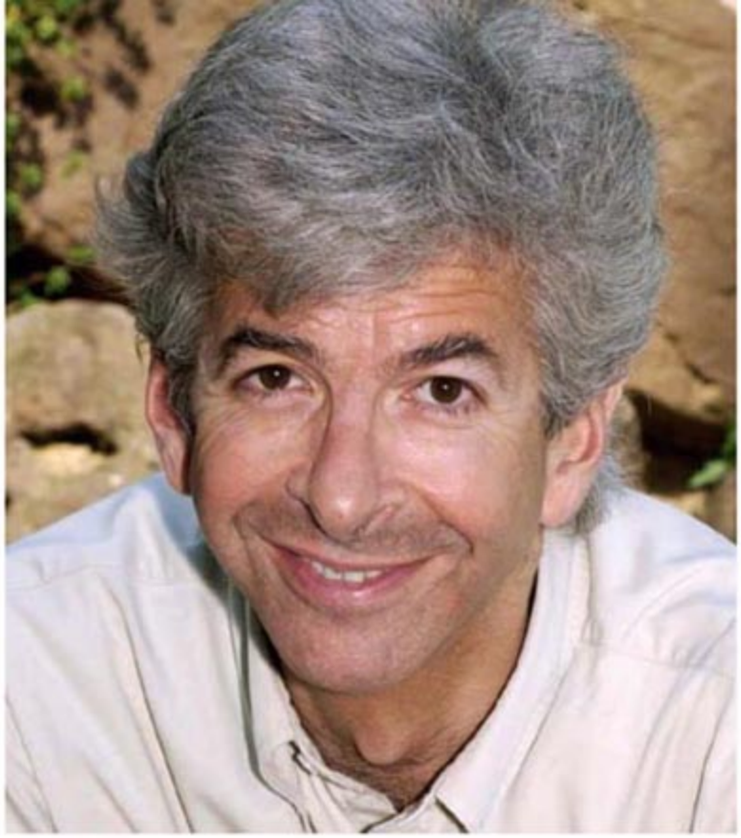

Politics

INSIDE KNOWLEDGE. For more than a decade, Dutch molecular biologist Ronald Plasterk has told others how to run science policy. Now, he'll be in the driver's seat himself. Plasterk, who heads the Hubrecht Laboratory in Utrecht and moonlights as a sharp-tongued newspaper and TV columnist (*Science*, 5 September 2003, p. 1311), is the minister of science, education, and culture in the new Dutch government. "I'm sad. He's a great scientist," says Stanford University researcher and Nobelist Andrew Fire. "But it's wonderful for Holland."

Plasterk helped pen the Labor Party's election platform last fall, and longtime colleague Piet Borst of the Netherlands Cancer Institute expects him to make some "radical changes." One likely move is to boost merit-based project funding through the Netherlands Organization for Scientific Research.

Borst says Plasterk's presence in the new Cabinet, which includes two Christian parties, is also "a huge relief for atheist intellectuals." Two years ago, Plasterk blasted his Christian-Democratic predecessor, Maria van der Hoeven, for supporting intelligent design.

MOVERS

BACK IN THE FOLD. After a period of self-imposed exile, Carlo Rubbia, one of Italy's best-known scientists, has made peace with the Italian government and is returning home to a new role as a special counselor to the environment ministry. "Above all, as an Italian living abroad, I do care about the future of my country," he says.

A former director of the CERN particle physics lab near Geneva, Switzerland, and joint winner of the 1984 physics Nobel, Rubbia has focused on energy research in recent years. He was made president of ENEA, Italy's energy research agency, in 1999, but in 2005, after beginning work in Sicily on a solar thermal energy project called Archimedes, funding for the project was suddenly axed by Silvio Berlusconi's conservative government. Rubbia openly criticized energy policies in the Rome daily *La Repubblica* and was removed from his ENEA post (*Science*, 22 July 2005, p. 542). Undaunted, Rubbia moved to Spain and continued work on Archimedes in Andalucia.

On 11 February, however, during an Italian TV debate about climate change and energy, Alfonso Pecoraro Scanio, Italy's environment minister in the new center-left government, asked Rubbia to accept Italy's apologies and join a government energy policy committee. On accepting his new appointment, Rubbia said: "The sun is one of Italy's great resources, and it's something we must learn to use."

IN BRIEF

ANTI-GM. Uprooting a field trial of transgenic corn in 2004 may land French presidential candidate José Bové in prison. On 7 February, an appeals court upheld a 4-month sentence issued in November. (Another judge may yet commute the penalty to home imprisonment.) A farmer and "alter globalist" who previously served time for ransacking a McDonald's, Bové launched his bid for the April elections on 8 February, billing himself as "the first political prisoner who's also running for president."

NAE. The National Academy of Engineering has elected 64 new members and 9 foreign associates. The list is at www.nae.edu.

Three Q's >>

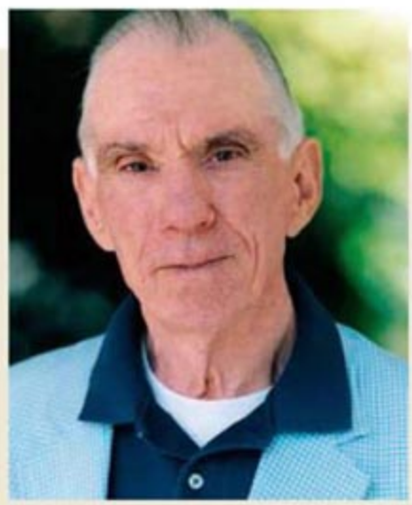

The Princeton Engineering Anomalies Research laboratory is closing down at the end of this month. Since 1979, the lab, headed by aerospace scientist **Robert Jahn**, 76, has stirred controversy with claims that human thought and emotion can influence physical reality.

Q: Has it been a worthwhile effort?
I think so. We certainly have learned a lot ourselves. We certainly understand much more about the nature of the phenomena than we did going in, and I think we have been faithful in sharing our insights with others.

Q: Do you think these phenomena will ever be proved in a way that will satisfy the skeptics?
That raises the whole question of where the skepticism stems from. I have to tell you that I was not totally prepared for the intensity of recalcitrance we have encountered. … For skepticism to be useful, it has to be informed. It doesn't help if the people haven't read your papers or visited your laboratory or talked with you personally.

Q: What's the worst snub you ever received from a scientist?
[One wrote that] "It's not worth my time to inform myself [about your research] because it is so obviously impossible." This is not a scientific attitude.

CREDITS (BOTTOM TWO IMAGES/LEFT TO RIGHT): AP PHOTO; ANDREA KANE PHOTOGRAPHY/PEAR LABORATORY

Got a tip for this page? E-mail people@aaas.org

Polygon pattern puzzle
1066

Getting to the point
1067

U.S. 2007 BUDGET

NSF Enjoys a Heartfelt Ending To a Difficult Budget Year

On Valentine's Day, the U.S. Congress sent the National Science Foundation (NSF) a long-delayed token of its warm feelings for the $6 billion basic science agency. It came at the end of a marathon budgetmaking process that stretched 4½ months past its intended deadline. The card was signed by the new House Speaker, Representative Nancy Pelosi (D–CA).

The valentine was a $334 million increase in NSF's $4.4 billion research budget that matches its 2007 request. It was tucked into a $463 billion, yearlong spending plan that displays little budgetary love for most of the other civilian agencies in the package. The National Institutes of Health (NIH) and the Department of Energy's (DOE's) science programs were also modest winners, picking up $620 million and $200 million, respectively, while NASA's space science programs continue to be squeezed by plans to explore the moon and Mars. Most agencies get no increase over 2006 in the bill, which covers the rest of the 2007 fiscal year that began 1 October.

For many scientists, the year began on a high note some 54 weeks ago, when President George W. Bush proposed major increases for the physical sciences as part of his American Competitiveness Initiative (*Science*, 10 February 2006, p. 762). The increases, part of a proposed 10-year doubling for NSF, DOE science, and the core labs at the National Institute of Standards and Technology (NIST), were embraced last summer by House and Senate spending panels. But those efforts went by the boards after the outgoing Republican-led Congress failed to pass a spending bill and the new Democratic majority announced that it planned to hold 2007 spending to 2006 levels (*Science*, 5 January, p. 24).

Any boost for research in the so-called joint funding resolution is a tribute to the bipartisan support for science within Congress, say lobbyists. In particular, the bill tracks with an innovation agenda released by congressional Democrats, led by Pelosi, nearly 1 year before they were voted into power. And although science advocates pushed hard for increases that would match the president's levels, they were not optimistic about the outcome of negotiations that took place behind closed doors from mid-December to late January. So the result, which was approved without amendments by the House on 31 January (*Science*NOW, sciencenow.sciencemag.org/cgi/content/full/2007/130/1) and by the Senate 2 weeks later, was a pleasant surprise. NSF's research account received its full 2007 request, DOE's $3.6 billion Office of Science received 40% of its $506 million request, and NIST's core labs gained half of a proposed $104 million boost.

Be mine. Lobbyists credit House Speaker Nancy Pelosi (D–CA) for research gains.

"There are two words why any research money was added to the House bill: Nancy Pelosi," says John Palafoutas, chief lobbyist for AeA (formerly the American Electronics Association). "The [congressional] staff was telling us not to get our hopes up and that research would be flat-lined along with everything else." Despite strong letters from high-tech CEOs and university and scientific society presidents urging support for basic research, he said, all indications were that adding money "was too big a lift."

An appropriations staffer who requested anonymity describes a free-for-all in which members' priorities were matched up with the money on the table. "We all submitted our lists [of exceptions to the 2006 spending levels], and some of them included offsets," says the aide. "And I have to tell you, I was stunned by the NSF level."

The 2007 spending bill contains a special valentine for agencies whose budgets are riddled with congressional earmarks, projects inserted by individual legislators that were not requested by the agency. The Democrats' decision to erase all 2006 earmarks allows agencies to spend the "extra" money as they see fit, subject to the approval of their operating plan by appropriators. There was $128 million in such earmarks in DOE's 2006 science budget, for example, and $137 million in NIST's budget.

Even so, some legislators are keeping close tabs on their favorite projects. For example, this year was to see the second of five $15 million awards, funneled through the Department of Veterans Affairs (VA), to the University of Texas Southwestern Medical Center in Dallas for research on a controversial theory linking neurotoxins to the mysterious symptoms that plagued veterans after the first Gulf War. Marc Short, a spokesperson for porkbarreling Senator Kay Bailey Hutchison (R–TX), says that the VA "signed a contract with UT Southwestern, … [and] we certainly would expect the VA to honor that commitment."

The biggest wrinkle yet to be ironed out of the bill is whether agencies can use their money to start projects and programs. The previous spending measure that governed the first 4½ months of the 2007 fiscal year said no, but the final bill contains no such restrictions.

NSF Director Arden Bement hopes to begin construction on three major research facilities in his 2007 budget: the Ocean Observatories Initiative, the Arctic Research Vessel, and the National Ecological Observatory Network, although each one is being "rescoped" to reconcile their scientific objectives with rising costs. But DOE appears to be taking a ▶

CREDIT: JIM YOUNG/REUTERS

Restoring a rainforest
1070

Birdbrain? Why, thank you
1074

different tack, according to lab officials. Brookhaven National Laboratory in Upton, New York, foresees a 20-week run of its Relativistic Heavy Ion Collider—which last year relied on a $13 million private donation—but no new design work for the proposed $775 million National Synchrotron Light Source II. A delay also seems likely for a suite of instruments known as SING-II at the Spallation Neutron Source at Oak Ridge National Laboratory in Tennessee, and a neutrino experiment called NOvA at Fermi National Accelerator Laboratory in Batavia, Illinois. At the same time, the Thomas Jefferson National Accelerator Facility in Newport News, Virginia, hopes to press ahead with an upgrade of its CEBAF particle accelerator even if it means running fewer experiments this year.

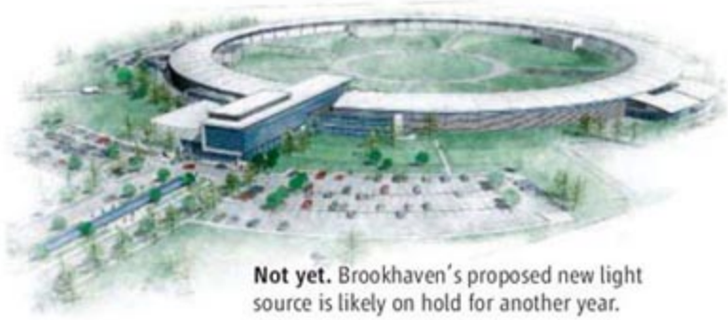

Not yet. Brookhaven's proposed new light source is likely on hold for another year.

NIH hopes to make an additional 500 research grants, including $91 million for a new investigator fund, $40 million for short-term, high-risk "junior pioneer" awards, and $69 million for the National Children's Study (*Science*, 9 February, p. 751). The 2% overall boost may look small for a $28.3 billion agency, but it is a "tremendous victory," says Jon Retzlaff, legislative director of the Federation of American Societies for Experimental Biology, compared to flat funding in the president's 2007 request and some 450 programs that have been cut from 2006 levels.

NASA is among that group, and the chair of the agency's spending panel, Senator Barbara Mikulski (D–MD), apologized for not doing better during the negotiations. "This joint funding resolution is not what anyone wanted," she declared immediately after the vote. The only silver lining Mikulski could find in a $16.2 billion budget that falls $400 million below 2006 levels is that science accounts were not raided to provide some $460 million designated for new exploration vehicles.

Despite the expectation that 2008 will be another tough budget year, Pelosi's spokesman, Drew Hammill, says that the 2007 budget "is the first step of good things to come for science funding." Lobbyists sure hope he's right. "Science continues to win bipartisan support," says Joel Widder of Lewis-Burke Associates in Washington, D.C. "But the arithmetic still stinks." **–JEFFREY MERVIS**

With reporting by Adrian Cho, Jennifer Couzin, and Eliot Marshall.

PRIMATE BEHAVIOR

Spear-Wielding Chimps Seen Hunting Bush Babies

The right to bear arms has long been considered a distinctly human privilege. But apparently the Second Amendment to the U.S. Constitution applies to chimpanzees too, at least while they're out hunting small game.

Researchers in Senegal recently spotted wild chimpanzees biting the tips of sticks, which they then used like spears to jab small primates called bush babies. Anthropologist Jill Pruetz of Iowa State University in Ames was astonished when her project manager saw a chimp thrust a sharpened stick into a hole in a tree and pull out a limp bush baby to eat, according to a report in the 6 March issue of *Current Biology*.

Bush baby, beware. Senegal chimps like this one attacked bush babies with sharpened sticks (*inset*).

"This is stunning," says primatologist Craig Stanford of the University of Southern California in Los Angeles. It's the first time a nonhuman primate has been known to make a lethal weapon for hunting other animals, he says. "This is no anecdote, as they have 22 cases," adds primatologist William McGrew of Cambridge University in the U.K. "Once again, chimpanzees exceed our imaginations."

Anthropologists have known for some time that chimpanzees are adept at making and using stick and stone tools, for example to probe termite mounds or crack nuts. And researchers have seen gangs of male chimps kill monkeys by beating and biting. But they thought only humans used tools to hunt.

Pruetz's team, working at the Fongoli research site in the wooded savanna of Senegal, observed chimps breaking off green branches and in four cases using their incisors to sharpen the points. The chimps, which typically weigh 26 to 60 kilograms, were hunting nocturnal bush babies, 100- to 300-gram primates that hide by day in holes in trees. In all, Pruetz and Paco Bertolani, a graduate student at Cambridge University, documented 10 different chimps thrusting the tools into holes in 22 instances. "This is habitual," says Pruetz, whose team logged 2500 hours of observations.

Other researchers were impressed by the observations, although some noted that the researchers saw only one bush baby actually killed. "Could they have been rooting around for something else?" asks primate behavior ecologist John Mitani of the University of Michigan, Ann Arbor.

Pruetz says the chimps' intent was clear: They jabbed the sticks in the holes with enough force to injure prey and far more vigorously than when probing for termites. And bush baby remains were common in chimp feces, indicating they were regular fare.

In another surprising twist, most hunters were females. "It's a double whammy," says Pruetz. "It doesn't fit the old paradigm of Man the Hunter." Make that Chimp the Hunter.

–ANN GIBBONS

CREDIT (TOP TO BOTTOM): BROOKHAVEN NATIONAL LABORATORY; P. BERTOLANI/CAMBRIDGE (PHOTO AND INSET)

SCIENTIFIC PUBLISHING

European Union Steps Back From Open-Access Leap

BRUSSELS—Europe took center stage last week in the growing battle for free access to the results of publicly funded research. An online petition, signed by almost 14,000 researchers and 500 research organizations in the European Union (E.U.) and presented here at the start of a 2-day meeting, asked the European Commission to take bold action on so-called open access. Traditional scientific publishers launched a counteroffensive, arguing that the future of scientific communication—as well as their €3 billion European industry—is at stake.

For the moment, the publishers' argument has carried the day: In a policy brief, the commission failed to enact a mandatory open-access policy for E.U.–funded scientists, to the disappointment of ardent supporters of the petition. "This doesn't reflect the spirit of what's happening in Europe," says cognitive scientist Stevan Harnad of the University of Southampton in the United Kingdom.

Open-access proponents argue that scientific papers should be available to everyone for free, instead of only from publishers at a cost. One way to achieve this goal is to ask researchers to make a copy of each paper freely available online, perhaps on their institute's Web site—a step called "self-archiving." The U.S. National Institutes of Health asks researchers to do this on a voluntary basis; legislation to make it compulsory for most taxpayer-funded researchers has stalled in the U.S. Congress.

Meanwhile, five research councils in the United Kingdom have made self-archiving within 6 months of publication mandatory, as have other research funding agencies. If the E.U. required the same from the scientists it funds through its €50 billion Seventh Framework Programme, many individual countries—within and outside the E.U.—might follow suit, contends Harnad. "It would be terrific if this big domino fell," he says. Indeed, a commission-sponsored study of the publishing industry by Belgian and French academics recommended mandatory self-archiving in January 2006, as did a December report by the commission's European Research Advisory Board. The brand-new E.U.–funded European Research Council also supports the idea.

But mandatory self-archiving has met stiff resistance from most scientific publishers. Making papers freely available after just 6 months may lead librarians to cancel subscriptions, threatening the entire publication system, they said at the 2-day, commission-sponsored meeting here. Publishers also questioned the economics of new-style online journals—such as the *Public Library of Science* (*PLoS*)—in which authors pay to publish and access is free. Such a business model is too young to know if it can work, they said.

Putting on the pressure. Sijbolt Noorda (*right*), who chairs a European University Association working group on open access, presented the petition to Research Commissioner Janez Potočnik last week.

CREDIT: LESLIE CHAN

The commission agrees, for now. In a 14 February policy statement, it acknowledged that data from publicly funded research "should in principle be accessible to all" and offered steps to move in that direction, such as a promise to reimburse scientists publishing in journals such as *PLoS*. But it didn't endorse a mandate to self-archive, asking for more studies and debate instead.

Robert Campbell, president of Blackwell Publishing, calls it a "sensible and encouraging" position. But Harnad says the commission's steps are "wishy-washy." It appears to be protecting publishers' interests without realizing that open access would have much greater economic benefits overall, he says. Other supporters of open access take a more optimistic view. The commission is still new to the debate and may come around, notes Sijbolt Noorda, chair of the Association of Universities in the Netherlands. "Rome wasn't built in one day."

–MARTIN ENSERINK

"Hobbit" Finders to Return

The team that discovered the remains of tiny humans in Indonesia's Liang Bua Cave plans to restart excavations in May. After controversy arose over whether the tiny bones were a new species or pathological *Homo sapiens*, Indonesian authorities closed the cave to anthropological digs. Now they are again allowing excavation, says team co-director Mike Morwood of the University of Wollongong in Australia.

Two digs are planned: Last August, a paleoenvironmental team led by Michael Gagan of Australian National University in Canberra uncovered a chamber below Liang Bua that contains bone material. Indonesian and Australian researchers plan to return to that chamber in June, says Gagan. Morwood says he hopes they find "fresh" remains that could yield DNA. **–ELIZABETH CULOTTA**

A Wave of Approval

The world's three large gravitational wave detectors will work together to measure the minuscule stretching of space. The Virgo detector near Pisa, Italy, will share data with the Laser Interferometer Gravitational-Wave Observatory (LIGO), which has detectors in Livingston, Louisiana, and Hanford, Washington. Scientists proposed joining forces months ago (*Science*, 6 October 2006, p. 33), and funding agencies in the United States, Italy, and France sealed the deal last week. LIGO already collaborates with GEO600, a detector near Hannover, Germany. Any one detector could sense the waves, says Jay Marx, executive director for LIGO at the California Institute of Technology in Pasadena, but together, the three should be able to better pinpoint the sources. **–ADRIAN CHO**

Indonesia, WHO Patch Up

Indonesia and the World Health Organization (WHO) appear to have resolved an impasse on the sharing of avian influenza samples after two of the agency's flu experts met with Indonesian health minister Siti Fadillah Supari in Jakarta last week.

Indonesia had announced it would stop sharing H5N1 strains with WHO's four collaborating centers without an agreement to limit commercial use of the virus. The country did so after discovering that an Australian company had developed a vaccine based on an Indonesian H5N1 strain. A 16 February joint declaration said that Indonesia would resume sharing strains while WHO would help the country and its neighbors find ways to ensure access to vaccines at an affordable cost. **–MARTIN ENSERINK**

MATHEMATICS

Quasi-Crystal Conundrum Opens a Tiling Can of Worms

The mosques and palaces of the medieval Islamic world are wonders of design. Because tradition forbids any pictorial decorations, they are covered with complex and intricate mosaics. These geometric patterns, called *girih* in Arabic, may be even more sophisticated than has been appreciated.

On page 1106, physicists Peter Lu of Harvard University and Paul Steinhardt of Princeton University propose that architects made a conceptual breakthrough sometime between the 13th and 15th centuries. By first visualizing a surface as a tiling of polygons, these unknown scholars created *girih* patterns that conform almost exactly to a pattern called a quasi-crystal. If Lu and Steinhardt are right, then the Islamic world discovered a piece of mathematics 500 years before it was formally described in the West. But the paper has also sparked a rancorous dispute over who first made this insight, and whether it is true at all.

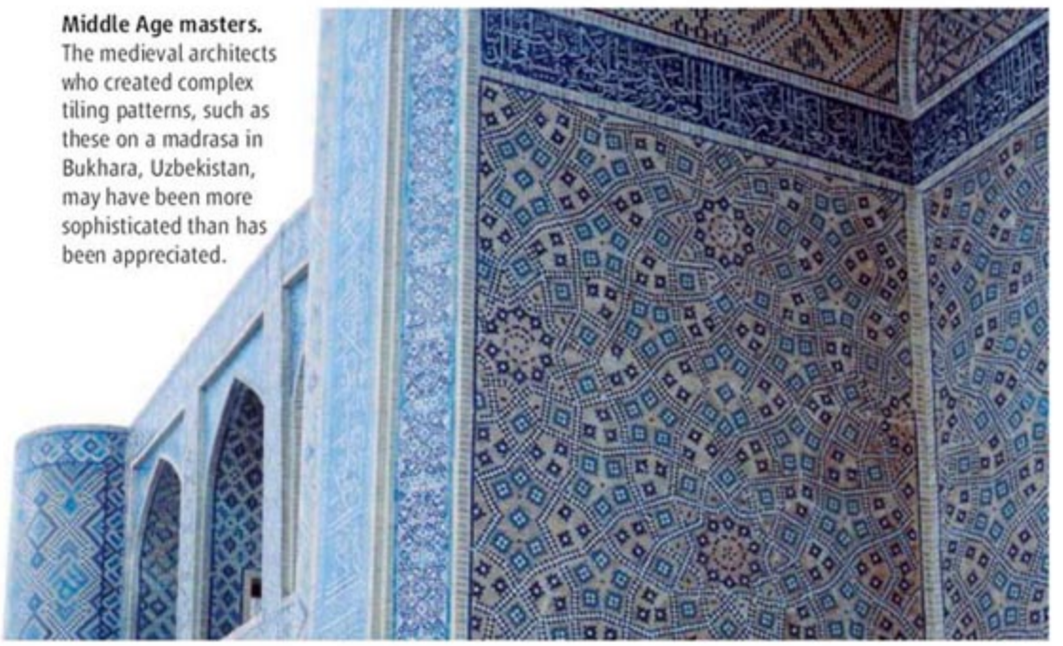

Middle Age masters. The medieval architects who created complex tiling patterns, such as these on a madrasa in Bukhara, Uzbekistan, may have been more sophisticated than has been appreciated.

Starting in the 1960s, mathematicians studying the geometry of tiling came up with the concept of the quasi-crystal. Tiling is crystalline if it is made up of an infinitely repeating pattern of some finite set of units. Quasi-crystals are also made up of a finite set of interlocking units, but their pattern never repeats even if tiled infinitely in all directions. Researchers also found that although pentagons and decagons don't fit easily into normal tiling, in a quasi-crystal such fivefold and 10-fold rotational symmetries are integral. The most famous quasi-crystal pattern is "Penrose tiling," named after Oxford University mathematician and cosmologist Roger Penrose.

In 2005, Lu, a doctoral student at Harvard, noticed a geometric pattern on the wall of an Islamic school in Uzbekistan with surprisingly complex decagonally symmetric motifs. "It got me thinking that maybe quasi-crystals had been discovered by Islamic architects long ago," he says. Islamic architects began to explore motifs with fivefold and 10-fold rotational symmetry during a flourishing of geometric artistry between the 11th and 16th centuries.

Back at Harvard, Lu began to study architectural scrolls from that period. On many scrolls, faintly sketched beneath the intricate lines of the *girih* design, was a polygonal tiling pattern. "I found the outlines of the same tile shapes appearing over and over," he says. Lu realized that Islamic architects could have used a pattern of polygonal shapes—which he calls *girih* tiles—as the starting point for their designs, creating a wonderfully complex *girih* pattern by tracing lines from tile to tile following local rules. And if the right shape of *girih* tiles were laid together just so, the resulting pattern could be extended forever without repeating—a quasi-crystal.

Lu examined "a few thousand" photos of real mosques and found that although decagonal *girih* patterns became increasingly common from 1200, nearly all are periodic and so are not quasi-crystals. But then he found a photo of the Darb-i Imam shrine in Isfahan, Iran, built in 1453. Its decagonally symmetric motifs on two different length scales are a telltale sign of a quasi-crystal. Working with Steinhardt, his former undergraduate adviser and a quasi-crystal expert, Lu found that the Darb-i Imam *girih* pattern can map onto a Penrose tiling. There were a few defects, but these are superficial, says Lu, and were likely introduced by workers during construction or repair. "We realized that by the 15th century, these architects had the makings of quasi-crystals," says Lu.

The paper has had a mixed reception. Crystal expert Emil Makovicky of the University of Copenhagen, Denmark, studied *girih* patterns for 2 decades. His analysis of the patterns on a tomb in Maragha, Iran, built in 1197, concluded that they map onto Penrose tiles and was published in a 1992 book about fivefold symmetry. Lu and Steinhardt cite his work, he says, but "without proper quoting and … in a way that [the ideas] look like their own."

Physicist Dov Levine of the Israel Institute of Technology in Haifa agrees that Makovicky deserves more credit than he is given in the paper. "His analysis of [the Maragha tomb] patterns anticipates some of the ideas in the Lu and Steinhardt paper," he says. Joshua Socolar, a physicist at Duke University in Durham, North Carolina, agrees that Makovicky deserves credit for discovering "an interesting relation between the Maragha pattern and a Penrose tiling with a few defects." Both Levine and Socolar doubt that the architects truly understood quasi-crystals but say Lu and Steinhardt have generated interesting and testable hypotheses.

Lu and Steinhardt say they were aware of Makovicky's published work on the subject, but "we have found serious problems with both his technical reconstruction and general conclusions." They say that they decided to limit their references to Makovicky "to avoid having to address the serious technical problems with his work." Makovicky disagrees that his work is flawed.

Beyond the question of credit, just how mathematically sophisticated these medieval architects really were remains open. "We haven't done an exhaustive search of Islamic architecture by any means," says Lu. "There could be a perfect quasi-crystal pattern waiting to be found."

–JOHN BOHANNON

CREDIT: P. LU/HARVARD UNIVERSITY

ARCHAEOLOGY

Clovis Technology Flowered Briefly And Late, Dates Suggest

For almost 80 years, one of the most enduring puzzles in the archaeology of the Americas has been the "Clovis culture," known for its elegant, distinctively shaped projectile points. Was Clovis the progenitor of all later Native American societies, as many researchers have long maintained, and, if so, how and when did it arrive in the Americas?

On page 1122 of this week's issue, Michael R. Waters of Texas A&M University in College Station and Thomas W. Stafford Jr., proprietor of a private-sector laboratory in Lafayette, Colorado, use new radiocarbon data to argue that Clovis was a kind of brilliant flash in the pan—a movement that may have flourished across North America for as little as 2 centuries around 13,000 years ago. The new dates also put Clovis a bit later than thought, making it harder to accept that it was the first in the Americas.

"What this paper does is reinforce how unusual was the phenomenon we call Clovis," says Michael R. Bever of the University of Texas, Austin. "To have it rise and fall [throughout North America] in as little as 2 centuries" is a phenomenon with few equivalents in the archaeological record.

Waters says that he and Stafford, an expert in the complex art of radiocarbon dating, set out "to nail down the most basic question: When was Clovis?" The heyday of the technology has typically been set between 11,500 and 10,900 radiocarbon years B.P. (The radiocarbon calibration is disputed for this period, but the widely used IntCal04 calibration puts the dates at 13,300 to 12,800 calendar years B.P.). In a controversial move, Waters and Stafford argue that no fewer than 11 of the 22 Clovis sites with radiocarbon dates are "problematic" and should be disregarded—including the type site in Clovis, New Mexico. They argue that the datable samples could have been contaminated by earlier material.

Of the remaining 11 sites, Waters and Stafford found that five had been recently dated by higher-precision techniques. The pair decided to redate the others, succeeding in all but one case. The results, Waters says, "were a real surprise." All of the new dates—as well as all of the previous acceptable dates—occurred within, at most, a 450-year band. Indeed, they say, Clovis probably existed for as little as 200 years, between 11,050 and 10,800 radiocarbon years B.P.—a cultural flowering both somewhat later and considerably shorter than thought.

The later, more precise dates support the emerging view that Clovis was not the progenitor culture, because it overlaps or occurred after other cultures, including one in Monte Verde, Chile, dated to 1000 years before Clovis.

The real surprise of the paper, according to David Meltzer of Southern Methodist University in Dallas, Texas, "is the compressed time frame for Clovis writ large." So fast was its apparent spread that Stafford suggests that Clovis may have been a set of technologies that were picked up by a mosaic of different cultures across North America rather than a single, fast-moving society. "These tight dates, if they hold up, may help us resolve that long-standing debate," says Meltzer, who questions the decision to discard the 11 sites.

Meltzer stresses that the dates used are from a minority of North American sites, most in the west, whereas most Clovis points have been found in the east. Until more data are compiled, he says, researchers "can't know whether this is a real effect or simply a consequence of sampling." In a sense, Stafford agrees. "We need to get more people out in the field," he says. "We hope these dates motivate that."

–CHARLES C. MANN

CREDITS: M. WATERS/TEXAS A&M UNIVERSITY

Clovis up close. Researchers say more dates are needed at sites such as this one in Gault, Texas.

Stem Cell Grants Awarded

The California Institute for Regenerative Medicine (CIRM), which is funding human embryonic stem (ES) cell research in that state, last week announced its first $45 million in research grants to 20 California institutions. The top recipient is Stanford University, with 12 awards totaling $7.6 million over 2 years. Faculty with the University of California, San Francisco, came in second with 11 grants.

Among the awards are some novel attempts at reprogramming differentiated cells to a pluripotent—or ES cell–like—state. And the Burnham Institute for Medical Research in San Diego is getting $638,000 to generate a library of ES cell lines that model a number of human genetic diseases. A second, $80 million round of grants is slated to be announced this spring. CIRM is moving ahead with the aid of private donations and a $150 million state loan, pending resolution of lawsuits that have delayed bond sales.

CIRM is also hunting for a president to succeed Zach Hall, who plans to retire in June. National Institutes of Health stem cell chief James Battey is rumored to be a top contender for the job.

–CONSTANCE HOLDEN

Kaiser to Set Up Gene Bank

The health care provider Kaiser Permanente hopes that 500,000 of its 2 million adult members in northern California will participate in a massive genetics research program containing DNA samples with health information to find links between genes, environment, and disease. Kaiser has started asking members about their family history, lifestyle, and other matters and plans to collect saliva or blood samples from willing participants in the next few years. The venture "is contingent on our acquiring additional funding," says Catherine Schaefer, director of the program, which has raised $7 million of the tens of millions of dollars needed. It will safeguard the confidentiality of participants, and Kaiser will make data available on a case-by-case basis to outside scientists, she says.

Kaiser "is in a strong position," but its plan won't include a geographically diverse cohort nor the uninsured, notes Francis Collins, director of the National Human Genome Research Institute in Bethesda, Maryland. Collins would like to start a broader study from scratch, which he admits would cost hundreds of millions of dollars a year.

–JENNIFER COUZIN

AAAS ANNUAL MEETING

Wedging Sustainability Into Public Consciousness

SAN FRANCISCO, CALIFORNIA—In a darkened ballroom in the Hilton San Francisco, 413 people tap numbers onto slate-gray keypads, each the size of a thick paperback book. Around them, almost 600 others watch as two screens at the front of the room reveal the results of their manipulations: a selection of strategies for taking wedge-shaped bites out of a graph of projected levels of atmospheric carbon over the next 50 years. Their mission: to whittle future CO_2 levels down to a plateau in time to avert intolerable greenhouse warming.

The "Wedge Game," based on "stabilization wedges"—a concept developed by Robert Socolow and Stephen Pacala of Princeton University (*Science*, 13 August 2004, p. 968)—was part of a town hall–like session for teachers and students at the AAAS Annual Meeting, held here from 15 to 19 February. The game, designed to convey the scale of the effort needed to stabilize carbon emissions and the pros and cons of possible options, was just one of some 200 sessions, ranging from "Addiction and the Brain" to "Education, Learning, and Public Diplomacy in Virtual Worlds." (For coverage of selected sessions, visit www.sciencenow.org.) But one theme dominated the meeting: "Science and Technology for Sustainable Well-Being."

AAAS President John Holdren of Harvard University and the Woods Hole Research Center in Massachusetts set the stage with an opening address in which he warned of the dangers of complacently expecting technological fixes such as nuclear fusion to solve our problems. "I'm a great believer in science and technology, but the notion that science and technology will ride to the rescue is a pernicious one," Holdren told reporters at a morning briefing before the talk. "Believing in technological miracles is usually a mistake." Instead, he said, a huge effort on many fronts will be needed. Holdren urged scientists to "tithe" 10% of their time to working on four key challenges: global poverty, the competition for resources, the "energy-economy-environment dilemma," and the threat from nuclear weapons.

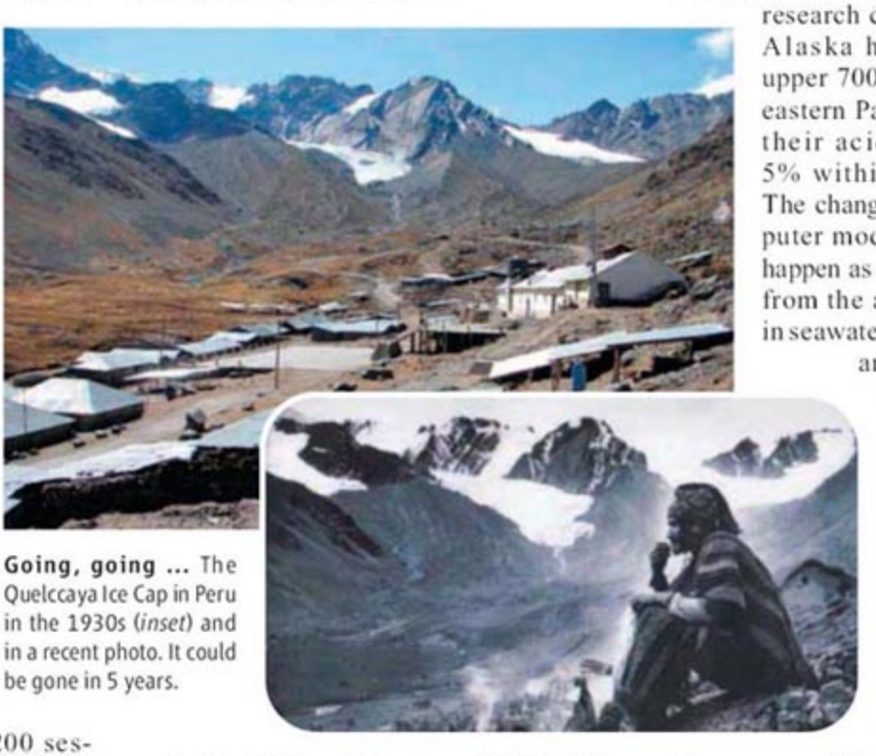

Going, going ... The Quelccaya Ice Cap in Peru in the 1930s (*inset*) and in a recent photo. It could be gone in 5 years.

For its 4000 participants and 3000 visitors, including some 1000 reporters, the meeting offered a crash course in those challenges and how scientists are tackling them, from "big picture" strategies to technical nuts and bolts.

Researchers monitoring the state of the planet reported warning signs from several quarters. Glaciologist Lonnie Thompson of Ohio State University in Columbus said ice cores from the Quelccaya Ice Cap in Peru—the largest body of ice in the world's tropics, 5670 meters above sea level—show that the ice is now melting faster than precipitation can replenish it. "All things being equal, those glaciers should be growing," he said. Thompson, who has been studying such glaciers for decades, estimates that the 5000-year-old glacier could be gone within 5 years. Because temperatures at high altitudes are more stable than those below, he says, melting tropical mountain glaciers could be a "canary in the coal mine" for global climate change. Their loss could devastate the millions of people who depend on them for water.

> "I'm a great believer in science and technology, but **the notion that science and technology will ride to the rescue is a pernicious one.**" —John Holdren, AAAS

Meanwhile, in the Pacific Ocean, a research cruise from Tahiti to Alaska has shown that the upper 700 meters of the northeastern Pacific have increased their acid content by about 5% within the past 15 years. The change matches what computer models predicted would happen as more carbon dioxide from the atmosphere dissolves in seawater, said Richard Feely, an oceanographer with the U.S. National Oceanic and Atmospheric Administration in Seattle, Washington. Largely as a result, Feely calculates that the zone within which marine creatures can grow calcium carbonate shells is growing shallower by 1 to 5 meters per year.

Even some of the supposed good news about climate change is looking less rosy. "You tell farmers in high latitudes they're going to get warming temperatures and longer growing seasons—end of story, they're happy," plant ecologist David Wolfe of Cornell University said at one session. But recent outdoor field studies with carbon dioxide suggest that "yield benefits are about half what we thought they were," he said. Also, hotter weather could damage milk production and crop yields. New work suggests that high levels of atmospheric CO_2 emboldens weeds more than crops and could require farmers to double the amount of herbicide they use.

Problems dominated news reports from the meeting, but more than three times as many sessions focused on the quest for solutions: economically competitive biofuels, better-managed water resources, and more efficient fish farms, fisheries, and ▶

CREDIT: L. THOMPSON/OHIO STATE UNIVERSITY

livestock grazing. The tone ranged from matter-of-fact to unabashedly techno-optimistic. In a fast-paced pep talk in the run-up to the Wedge Game, for example, long-time alternative-energy advocate Amory Lovins of the Rocky Mountain Institute in Snowmass, Colorado, hymned the virtues of greener living through engineering. Ultralight low-drag cars, better-insulated houses, and decentralized low-carbon "micropower" energy sources, he predicted, would stabilize Earth's climate while reaping huge profits for businesses that seize the opportunities they present. "The low-hanging fruit is mushing up around our ankles," Lovins said.

Perhaps influenced by Lovins, the Wedge Gamers voted for a deep-green mix of two parts increased efficiency and one part each solar electricity, wind power, driving less, switching from petroleum to natural gas, and "biostorage" (planting forests to absorb CO_2). It's far from current U.S. energy policy, but it reflects much of the thinking on display at many other sessions at this meeting. **–ROBERT COONTZ**

With reporting by David Grimm, Eli Kintisch, Greg Miller, and Erik Stokstad.

ENVIRONMENTAL REGULATION

U.S. Courts Say Transgenic Crops Need Tighter Scrutiny

Citing a broad range of risks, U.S. federal judges in three separate cases have asked the U.S. Department of Agriculture (USDA) to examine genetically engineered crops more closely. The courts said the department had violated the National Environmental Protection Act (NEPA) in approving commercial sales of transgenic alfalfa and field trials of turf grass and plants engineered to produce pharmaceuticals.

Critics of genetically engineered crops say the decisions, two issued this month and one last August, will compel tighter regulation of transgenic crops. Will Rostov, an attorney for the Center for Food Safety in Washington, D.C., which filed all three lawsuits, called the alfalfa decision, rendered 12 February by U.S. District Judge Charles Breyer in San Francisco, California, "another nail in the coffin for USDA's hands-off approach to regulation." But Stanley Abramson, a lawyer who represents several biotech companies, pointed out that the courts raised questions about USDA's procedures, not its substantive decisions. He predicted that USDA's final judgments would hold up in court.

The alfalfa verdict could have the most significant impact. In 2005, USDA approved the sale of Roundup Ready alfalfa, jointly developed by Monsanto and Forage Genetics International, which can withstand the popular herbicide glyphosate. But last week, Breyer said that the department should have first prepared an environmental impact statement (EIS) as required under NEPA.

Joseph Mendelson of the Center for Food Safety said that his group may demand an end to sales of genetically engineered alfalfa or even a ban on planting transgenic seed already in farmers' hands. USDA officials declined to discuss the government's position or whether it plans to appeal. A spokesperson for Monsanto, which sells genetically engineered alfalfa but was not a party to the lawsuit, said he did not expect sales to be halted. Breyer gave both sides until next week to propose regulatory fixes.

On the farm. Alfalfa is the third most valuable crop grown in the United States.

CREDIT: DOUG WILSON/USDA

The second verdict, handed down 5 February by a Washington, D.C., district judge, found that USDA should have carried out an EIS or a more modest environmental assessment before it allowed a 162-hectare field trial of transgenic turf grass near Madras, Oregon, in 2003. And last August, a federal court in Hawaii faulted USDA for approving field trials in Hawaii of corn and sugar cane engineered to produce experimental pharmaceuticals without considering the state's numerous endangered species.

In two of the cases, the judges expressed concerns about potential risks that USDA has dismissed as insignificant or outside its mandate. Breyer, for instance, complained that USDA ignored the cumulative impact of glyphosate-tolerant alfalfa, corn, and soybeans. Greater use of glyphosate increases the odds that weeds will develop resistance to it.

Breyer also said USDA erred when it dismissed as not "significant" the concerns of organic farmers who don't want Roundup Ready pollen or seeds spreading to their alfalfa fields. The possible replacement of traditional varieties is itself significant, he noted. "An action which eliminates or … greatly reduces the availability of a particular plant—here, nonengineered alfalfa—has a significant effect on the human environment," he wrote.

USDA argued that cross-pollination wasn't a serious problem in alfalfa, because farmers typically harvest their fields before the plants have a chance to flower, much less produce seeds. Producers of commercial alfalfa seed, however, would have to make sure their conventional and transgenic fields were widely separated. Alfalfa is pollinated by bees, which can carry pollen at least 3 kilometers.

In the turf grass case, Judge Henry Kennedy found that transgenic bentgrass from a large field trial in Oregon threatened a nearby area's "aesthetic and recreational" value. Pollen from the bentgrass spread up to 20 kilometers into the nearby Crooked River National Grassland.

Many scientists, including some critics of genetically engineered crops, say the bentgrass poses no real ecological threat in that area because it isn't well adapted to the region's arid climate. But the spread of this "confined" field trial proved embarrassing to the Scotts Co., which hopes eventually to sell bentgrass seed to golf courses.

–DAN CHARLES

Dan Charles is a Washington, D.C.–based science writer.

Some reforestation projects result in little more than tree plantations. An ambitious project in Brazil's São Paulo state is trying to go further and create a real working ecosystem

Reconstructing Brazil's Atlantic Rainforest

CUNHA, BRAZIL—Benedito de Carvalho Filho strides across his yard, through an empty cow pen and uphill. He clambers over rocks and searches, pushing aside shreds of barbed wire and vegetation, as his 12-year-old son shadows him. Finally, the farmer stops and points to the eye of a spring that barely percolates up from the earth. His water—or what's left of it.

Throughout this pastoral region that was once the heart of Brazil's Atlantic rainforest, extensive deforestation has not only changed land cover, it has also altered the hydrologic cycle. The forest once stretched over 1 million square kilometers along Brazil's coastal region with extensions inland. Today, only 7% of that original extent persists. And now, de Carvalho and other farmers are grappling with a growing realization: The fresh and abundant ground water they have relied on for decades is disappearing. For his family and his crops to have water, de Carvalho needs the rainforest back. He may be in luck.

With little fanfare, this past December, biologists and farmers planted the first seedlings of an ambitious project that ultimately aims to reforest 1 million hectares (2.47 million acres) of riparian rainforest across São Paulo, Brazil's most populous state. The goal is not just to recreate this globally unique ecosystem but also to reclaim the so-called services the rainforest once provided, from the maintenance of natural springs and soil fertility to the sequestration of carbon.

It's a tall order. Funded with seed money from the state and the Global Environment Facility (GEF), the Riparian Forest Restoration Project (RRP) will require an estimated 2 billion seedlings of hundreds of species of trees and take decades to complete. The total bill could top $2 billion—about $2000 per hectare—just a fraction of which has been raised.

"It is hard to think of a reforestation project undertaken anywhere that is quite this ambitious," says Thomas Lovejoy, formerly the World Bank's chief biodiversity advisor. Even if the RRP achieves only some of its ambitious goals, say conservation scientists, it appears set to test the limits of nature's resilience, the science of ecological restoration, and societal commitment.

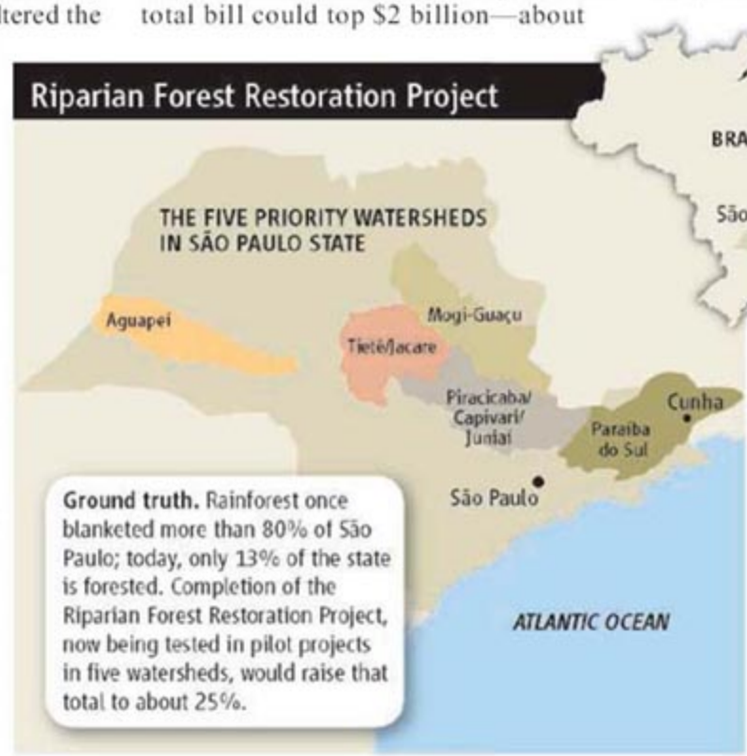

CREDIT: BERNICE WUETHRICH

Dimensions of diversity

The RRP will focus on restoring forest along the denuded margins of rivers and streams that establish migratory corridors for animals and plants and protect the ecological health of waterways. The eventual goal is to recover a significant portion of the staggering diversity of the rainforest's flora and fauna—its bromeliads, lianas, shrubs, grasses, birds, bats, butterflies, insects, microbes, mammals, and amphibians.

How exactly to do that is being tested in pilot projects in five watersheds across São Paulo state, with $19 million in start-up funds provided primarily by the state, GEF, and the World Bank. Each of the

Mother lode. Rainforest preserved in the Serra do Mar State Park is a source of trees and seeds needed to reforest riverbanks and streams. Benedito de Carvalho Filho (*above*), a farmer in Cunha, Brazil, points to his diminished natural springs on a deforested hillside overtaken by ferns.

CREDIT: BERNICE WUETHRICH

five watersheds is in turn divided into three "microwatersheds" that represent a range of ecological as well as social challenges. In Cunha, for instance, located within the larger Paraíba do Sul watershed, subsistence farmers work within a mosaic of forest fragments. It is a sharp contrast to the large northwest watershed, Aguapeí, where sugar cane is king and any remnant forest is hard to find.

In these pilot projects, the state Department of the Environment and its partners are experimenting with a variety of restoration methods. Some emphasize replanting trees alone; others aim to return a variety of plants and animals simultaneously. "We want to see how the forest can best develop on its own after a starting push," says project director Helena Carrascosa von Glehn.

At each site, the selection of trees and methods will depend on local conditions and the specific goals for the area, whether that be soil stabilization, water maintenance, or production of fruit and nuts from rainforest trees. "Our emphasis is on bringing people to this for 20 to 30 years and involving them in restoration," Carrascosa says.

Search for Mother Trees

At the heart of the effort is the Mother Tree project: a detailed plan for identifying the starting stock for the forest's regeneration. Conceived by Ricardo Rodrigues at the Laboratorio de Ecologia e Restauração Florestal in Piracicaba, Brazil, the Mother Tree project aims to find and mark the location of 15,000 trees of 800 different species to support seed collection programs and ensure adequate genetic diversity in the replanted forests. There is now a master list of 780 species appropriate for reforestation in designated watersheds.

To find the seeds, biologists are scouring remnants of the Atlantic forest across the state. So far, says Rodrigues, 20 biologists have recorded 10,200 mother trees.

One of those biologists is forest engineer Renato Lorza, who conducts his search for mother trees in the mountainous terrain of Cunha on foot, aided by a long-handled scissor. On a morning last December, a fine mist laces the air as he scoops up a handful of gleaming seeds from the forest floor. Most plentiful are the soft, marble-sized seeds of the Jussara palm (*Euterpe edulis*). Severely overharvested to extract heart of palm, the tree grows up to 25 meters to reach the light through the forest's dense canopy. The palm is but one of some 1300 tree species in the Serra do Mar State Park in Cunha that Lorza has come to know well during 2 years of collecting.

University researchers analyze and sometimes genetically sequence the material he collects. After the species is definitively identified, Lorza returns to nail a small metal label into the trunk of each mother tree. He has tagged 750 individual trees, representing 250 species in this remnant forest. Each one must be in a reproductive stage of life, but some species flower only every 20 years.

One giant, Number 2496, is *Sapium glandulatum*, a bird-dispersed pioneer tree. Number 2497 is a climax species, *Aspidosperma parvifolium*. Slow growing, the tree is a rare find, as it has been overharvested for use in construction. Both pioneer and climax species are essential to the reforestation effort. Fast-growing pioneer species are the first to establish in gaps that form when trees fall in the forest. They germinate and grow in light. The secondary species that follow germinate in light but grow in shadow; slow-growing and long-lived climax species germinate, establish, and grow in the shadows.

A state law—the most far-reaching of its kind in Brazil—mandates that each reforested hectare include a minimum of 80 tree species, with each represented by at least 12 mother trees from distinct populations to ensure good genetic variability. The law also mandates that the 80 trees reflect the different successional stages of the forest, which means a mix of both pioneer and nonpioneer species, in a ratio that is close to 1:1.

This basic approach grows out of the work of Paulo Kageyama, director of biodiversity conservation at the Brazilian Ministry of the Environment, who spent decades planting experimental forests for the hydroelectric industry to restore biodiversity around dams. Beginning in 1988, he began growing diverse plantations that included species representative of each major successional stage.

One such plantation, the state's Paraibuna forest, has stood as an emblem of success. Its 100 different tree species have thrived, and now that "other kinds of plants are arriving by wind or birds, the biodiversity is increasing," Kageyama says.

It took well over a decade, however, for the Paraibuna forest to cross that threshold and begin recruiting the other species needed to recycle nutrients, disperse seeds, and pollinate plants. It is now a functioning forest rather than a plantation that must be maintained, says Kageyama.

But many other reforested areas in Brazil have failed to make that transition. Of some 98 publicly funded reforested areas evaluated in 2000, only two did well, according to Luiz Mauro Barbosa, director of the São Paulo Botanical Institute and a co-director of the RRP. In most areas, after initially flourishing, the trees died, and weeds took over.

Barbosa says that diversity is a key ingredient of success: Forests with 30 tree species generally did better than those with only three or four. The premise is that if a sufficient and balanced diversity of trees is planted with species appropriate to the local conditions, the flourishing forest will recruit the other flora and fauna—essentially, build it and they will come.

Trees in context

Yet species diversity in and of itself has not always been sufficient. For instance, one reforestation effort in western São Paulo state began with 42 tree species, but after 10 years, just four pioneer species dominated the upper canopy, says Daniel Piotto, a forest engineer who has worked on industry-financed reforestation projects in São Paulo and is now a Ph.D. candidate at Yale University. Piotto thinks that the difficulty may lie in the limited availability of factors such as water, mineral nutrients, and suitable microclimate that put slow-growing climax species at a competitive disadvantage relative to faster growing pioneer tree species and grasses.

In addition, some biologists believe that the rainforest restoration will require more than a narrow focus on trees. Ademir Reis, now at the University of Santa Catarina, and Fernando Bechara, now at the Casa da Floresta Assessoria Ambiental in Piracicaba, have developed an experimental technique known as "nucleation."

It aims to jump-start the establishment of ecological relationships essential to plant and animal life through creating a wide variety of niches. In test plots, the biologists have combined a number of techniques: They erected perches to attract birds and bats, built shelters for small mammals, and planted herbs and shrubs (shunned as competitors to trees in traditional reforestation) to attract butterflies. They also transposed squares of topsoil from intact forest, delivering soil microbes, earthworms, and fungi. After just 1 year, Bechara has noted the return of 35 species of birds to one experimental area.

"Forest restoration is extremely expensive and labor-intensive. Anything that can mimic natural succession in depleted areas is worthwhile," says Gustavo Fonseca, chief conservation and science officer with Conservation International.

Building support

Equally important to testing restoration methods is ensuring the support of the local community: "We can do nothing without the involvement and support of the people," Lorza says. The RRP aims to build this support by convincing people that devoting some portion of their land to rainforest restoration would benefit them in the long run, even if it means giving up some hectares used for farming or pasture.

In Cunha, that means educating the community about the role of the rainforest in maintaining their natural springs, which have slowly disappeared over the past 40 years. Honario Eliane, a farmer who has lived in Cunha all of his 71 years, is convinced. "About two-thirds of the natural springs that once irrigated my land are gone. The river I used to swim in when I was a kid now barely covers my feet. We need this," he says. Honario's daughter is one of 19 teenage "environmental monitors" who work with a local nonprofit group known as Living in the Atlantic Forest, one of many partners in the state's reforestation effort.

Today, after some initial opposition, about 60 farmers in Cunha want to reforest some of their land, says Leila Pires, who directs the RRP in Cunha. Due to limited resources, reforestation has begun on just six farms.

To speed the project along and ensure its financial sustainability, São Paulo state is exploring the establishment of a fund for ecosystem services, says Carrascosa. The state has already implemented new environmental legislation in two watersheds, charging industry, large-scale farmers, and the government for water use. Other possibilities include GEF payment for carbon sequestration achieved through reforestation and the establishment of a private market for rainforest seedlings, Carrascosa says. She suggests that the RRP could prove to be a model for both the Amazon and the nation.

–BERNICE WUETHRICH

Bernice Wuethrich usually writes from Maryland. Marcelo Rideg provided translations in São Paulo.

CREDIT: BERNICE WUETHRICH

House calls. Forest engineer Renato Lorza (*left*) and Ednei Marques of the nonprofit Living in the Atlantic Forest visit farmers in Cunha to enlist their support in the restoration project.

U.S. DEPARTMENT OF AGRICULTURE

Farm Bill May Contain Seeds For More Robust Research

The Bush Administration wants to trim farm subsidies, restructure USDA, and do more research on biofuels, fruits, and vegetables

CREDIT: JACK DYKINGA

For the past decade, advocates for U.S. agricultural research have watched with envy as the federal government has pumped money into other disciplines, notably medical research. Despite daunting environmental problems and growing international competition for producing cheap food, the research budget of the U.S. Department of Agriculture (USDA) has been stuck at roughly $2 billion. But advocates say that a new proposal by the Bush Administration to revamp agricultural subsidies provides an ideal cue for pitching research to a Democratic-controlled Congress that intends to pass some sort of legislation this year.

Congress periodically adjusts the nation's agricultural policies in a massive farm bill, and the Administration's latest proposal, submitted 31 January, does more than tinker: It would cut $10 billion over 10 years from subsidies paid to farmers. The president's plan also proposes a restructuring of USDA by merging two research agencies and creating an Office of Science. And it would add $100 million for research on specialty crops—fruits, vegetables, tree nuts, and nursery plants, for example—and $50 million for biofuels.

Ag lobbyists say the move is a good start, although it falls short of the doubling of basic research that a major panel recommended several years ago. "USDA should be in a much stronger leadership role" if the bill is approved, says Jeffrey Armstrong, dean of the College of Agriculture and Natural Resources at Michigan State University in East Lansing. "To integrate and create an Office of Science—it's huge." And although the science reorganization is relatively uncontroversial, the bid for additional spending could run afoul of a push by growers to protect their subsidies as appropriators try to tighten belts.

USDA's research is divided into three main parts: the $1.3 billion intramural Agricultural Research Service (ARS); the Cooperative State Research, Education, and Extension Service (CSREES), which gives out $180 million in competitive grants through the National Research Initiative and $180 million in so-called formula research grants to agricultural universities; and the $340 million research effort at the U.S. Forest Service. Each program has its own staff, and there's considerable duplication in areas such as plant genetics, soil science, and air quality. "An integrated approach would be more effective," says Fred Cholick of Kansas State University in Manhattan.

Change has been in the air for several years. In 2004, a blue-ribbon panel called for an independent research agency (*Science*, 10 December 2004, p. 1879). But USDA disliked the idea, and a bill to implement the findings died. Last year, the National Association of State Universities and Land-Grant Colleges (NASULGC) proposed a suite of reforms, called CREATE-21, that included unifying USDA research efforts.

The Administration's bill, expected out in the next few weeks, would merge ARS and CSREES and give a chief scientist control over both intramural and extramural programs. "We'll be better able to plan and coordinate comprehensive programs like food safety," says Lowell Randel of USDA's research policy shop, as well as pursue pressing topics such as obesity. Forest Service research would remain separate, Randel says, because it focuses on forest issues. (It's also overseen by a different congressional committee, he notes.)

The farm bill would nearly double research on specialty crops and biofuels. USDA spent $44 million on biofuels research in fiscal year 2006 and somewhere between $120 million and $150 million on specialty crops. The new initiatives, totaling $150 million a year for 10 years, would be financed by the government's Commodity Credit Corporation, which places them outside the annual appropriations cycle.

Even so, appropriators could divert some of the money, as they did repeatedly with the $200 million Initiative for Future Agriculture and Food Systems (IFAFS), a competitive grants program set up in 1998 (*Science*, 21 January 2000, p. 402). IFAFS also garnered little support outside the academic community, as growers which didn't see its value for specific crops or agricultural problems. Randel says that focusing on specialty crops and biofuels is a better way to "show that our science is world class and [that it is] solving problems that matter to all Americans."

Research advocates hope Randel is right. But they would like the bill to go further. "I don't have any quarrel with the targeted areas, but there are other areas that are equally critical," says Ian Maw, vice president for food, agriculture, and natural resources at NASULGC, which is asking for the USDA research budget to double over 7 years. The group also wants competitive funding, now 10% of the department's total research budget, to grow to 58%.

Research advocates admit that farmers' cries for maintaining subsidies could drown out their call for a bigger research pot. But they argue that international pressure to eliminate farm subsidies may work in their favor. In 2005, the World Trade Organization (WTO) ruled that USDA cotton subsidies were illegal because they undermined fair trade. But getting Congress to listen is another matter. The chairs of the two committees that will write the bill have said that they don't feel bound by WTO rules. Their goal is to complete work on it by September.

–ERIK STOKSTAD

Bird watcher. Clayton with her rooks.

PROFILE: NICOLA CLAYTON

Nicky and the Jays

Experimental psychologist Nicola Clayton and her colleagues are proving that birds are more intelligent than most of us give them credit for

"I'm very birdlike, don't you think?" chirps Nicola Clayton. In fact, the petite Clayton *does* indeed remind one of a bird: She stands just 1.62 meters tall even in her stilettos and has a slightly beaked nose, a plume of blond hair, flashy clothes, and a hummingbird's quick, darting moves. So apparent is the similarity that her students at the University of Cambridge, U.K., have dubbed this 44-year-old experimental psychologist a new bird species, *Claytonia professorii*.

But Clayton's "birdiness" is not just a matter of style. She's a keen student of bird behavior, drawing on natural history to investigate experimentally a trait that most scientists did not believe existed in birds: cognition. Over the past 9 years, she and her colleagues have pumped out 75 papers on the surprisingly humanlike mental skills of food-storing birds, particularly the western scrub jay (*Aphelocoma coerulescens*). In this week's issue of *Nature*, Clayton's lab chips away at another "human-only" cognitive ability by showing that scrub jays can plan for the future.

"They've devised a clever experiment for these jays which does fulfill the [psychological] criteria for future planning—which makes this a first," says Sara Shettleworth, a comparative psychologist at the University of Toronto in Canada. Other papers have argued that monkeys, bonobos, and orangutans plan ahead (*Science*, 19 May 2006, pp. 1006, 1038), but because the animals were given numerous trials, they might have been "trained" to act as though they foresaw the future, Shettleworth points out.

Although it might seem that some animals prepare for the future, for instance by moving to a cave for hibernating, researchers consider these behaviors to be merely mechanistic responses to a seasonal cue. In contrast, Clayton's graduate students Caroline Raby and Dean Alexis placed the scrub jays in a novel situation. The birds first spent the night in a suite with two adjoining rooms. In the morning, the researchers moved the jays to one of the end rooms. One end room was like a bed and breakfast, and the jays received breakfast pine nuts; the other room was more like a cheap motel, and the jays went hungry.

After a few days, the jays were allowed access to either end room and provided with pine nuts in the main compartment. Spontaneously, the jays stashed the nuts in the breakfastless room, hiding them in a sand-filled ice cube tray (the jay's equivalent of a refrigerator). They seemed to recall going hungry during their past stay in the motel room and, based on that experience, saved the nuts for a future breakfastless morning.

"Who would have thought you could ask a bird what it understands about the future?" asks Joan Silk, a primatologist at the University of California (UC), Los Angeles. "It's incredibly difficult to design an experiment that would demonstrate this. But they have. It adds to a growing body of work that shows that jays, crows, and rooks can do anything primates can do, especially things that we once thought were important links to understanding the emergence of cognition in humans."

For the birds

Clayton's talent for designing such ingenious experiments comes, she says, from understanding what scrub jays do in the wild. During the early 1990s, in John Krebs's University of Oxford lab, Clayton worked on memory development in food-caching Eurasian jays and tits, species known to have excellent memories. Her work there showed that the hippocampus region of these birds' brains responded like a muscle to their food-hiding

CREDIT: PHILIP MYNOTT/UNIVERSITY OF CAMBRIDGE

behaviors, growing markedly in size as they stored seeds in numerous locations.

When she moved to UC Davis in 1995, she found that the western scrub jays—gray-and-blue birds with a raucous squawk—were common, making it easy for her to observe them in their natural setting. "One thing I noticed almost immediately was that the scrub jays would steal bits and pieces from people's lunches and hide these," she says. "Later on, they'd return to these caches and move them. But why?"

She decided to use this food-stashing behavior as a starting point for her experiments, using what she knew about the jays' wild activities to reveal their psychology. For these tests, Clayton provides them with sand-filled ice-cube trays. Previous studies have shown that in the wild, food-stashing birds use nearby landmarks to remember their stashes. To give the lab jays similar cues, Clayton attaches a colorful stack of Lego pieces to each cube of the tray. She offers the birds nuts and fresh wax worms and films the birds' behaviors.

She had observed that wild scrub jays stole one another's caches, if they could, and also stored worms and bugs, which decay relatively quickly, as well as longer-lasting seeds and nuts. "They not only had to remember where they buried things but *when* they did," she points out. That observation led to a controversial *Nature* paper in 1998.

With her co-author, University of Cambridge comparative psychologist Anthony Dickinson, she asserted that scrub jays have "episodic-like memory," the ability to remember specific things they did in the past, a skill akin to what humans do. "People seemed to think that if a monkey had done it, that would be one thing," Clayton says, "but a *bird*?"

Dickinson says he would never have considered making such a claim prior to meeting Clayton. Indeed, Dickinson, a learning theorist, confesses that when they met at a 1996 conference, he was initially dismissive of Clayton's research, saying there was absolutely no reason an animal needed to have personal, episodic memories. "It was an outrageous statement," recalls Clayton, who countered that the birds had to remember when they buried something, particularly fresh food, otherwise they'd be wasting time and energy flying back and forth constantly to make sure the food was still edible. "That wouldn't be at all adaptive," says Clayton. Intrigued, Dickinson soon found himself collaborating with Clayton on experiments designed to investigate whether the birds were making cognitive decisions or behaving mechanistically.

"I wouldn't have thought of using a natural behavior—such as the food-caching—to ask a psychological question, prior to meeting Nicky," says Dickinson. "But that's her strength: She's a biologist who's capable of thinking about psychological processes."

Clayton met her other main collaborator (and husband), Nathan Emery, at about the same time. He was then studying primates at UC Davis and delighted in boasting to Clayton about his monkeys' many talents. "He made so many 'ape-ist' remarks, about how they could do things that no other animal could do, and I'd say, 'But that's not true!' and tell him all about my jays," Clayton recalls. To his credit, she adds, Emery immediately grew interested in the jays, and soon he and Clayton were also collaborating on papers, adding his primatologist's credentials to their claims that jays and their relatives are as smart as apes. They moved to England in 2000, bringing the jays with them.

Pilferers and physicists

In her lab at Cambridge, Clayton leads the way into a room with large wire enclosures lining the walls. Inside, the scrub jays squawk and leap from the sides of the cages to their perches and back, watching her every move. "I find it so curious, the way they look you right in the eye," says Clayton, who hand-raised most of her charges. "I think it's because they recognize individuals—that's not a scientific finding, just a gut feel. But I think it's another factor in their pilfering; they know each other as individuals."

She, Emery, and postdoc Joanna Dally have shown that the jays are well aware of each other's thieving natures and, once they themselves have stolen the cache of a fellow jay, learn to watch out for thieves. "They might know something about what the other bird is thinking; they seem to take his point of view," says Clayton. "They keep track of who was watching when" (*Science*, 16 June 2006, p. 1662).

Many researchers think that such an ability, called "theory of mind," is something that requires language and therefore can only be done by humans. But Clayton disagrees. "I think [thievery] is one reason they've become so cognitive: When they stash their nuts, they have a lot to worry about—they have to think about it from their own perspective, as well as the thief's."

Other comparative psychologists are not persuaded, however. "It's a giant controversy," says Shettleworth, explaining that a jay stashing a nut may simply be mentally recording the presence of another bird near its cache; the jay returns to hide its food elsewhere when the other bird is gone. "The hoarder doesn't need to know what the other guy is thinking to act this way."

If jays are thieves, then it seems that rooks (*Corvus frugilegus*)—raven-sized birds with dark plumage—are physicists. Or, at the very least, the birds' ability to manipulate things suggests they have some basic understanding of the properties of objects and gravity, even though rooks don't use tools—and therefore don't need this knowledge—in the wild.

Clayton, Emery, and graduate student Amanda Seed reported in the April 2006 issue of *Current Biology* that rooks easily mastered the simple physics required to retrieve a piece of meat from inside a tube, using a twig to push or pull as necessary until the food fell to the ground. "You can see them assessing the tube and the stick and the bit of food" to arrive at a solution, says Clayton. This behavior again suggests that these birds are quite cognitive creatures.

Clayton, Emery, and University of Cambridge postdoc Lucie Salwiczek plan to expand their lab's investigation of bird intelligence this year by testing young jays newly arrived from California for their understanding of object permanence: that is, their ability to know that something is still there even if they can't see it. The adult birds must have this ability, because after burying a nut, they return to retrieve it. But Clayton and her colleagues want to know at what age they develop this sense.

Despite her intense curiosity about these birds' brains, Clayton says she will stay away from neuroanatomical studies, as she is loath to sacrifice any jays. "I'm too attached," she says. That may limit her progress, as that's the logical next step, says neurobiologist Erich Jarvis of Duke University in Durham, North Carolina, who compares bird and mammalian brains. Yet even without taking this step, Clayton is changing the way neurobiologists think, he notes. "There's a general belief that the further away a group is from humans, the less intelligent it will be. So people are surprised—even scientists are surprised—that some birds can do many of these things." For *Claytonia professorii*, that's something to crow about.

–VIRGINIA MORELL

Virginia Morell is a writer in Ashland, Oregon.

CREDIT: GEORGE D. LEPP/CORBIS

LETTERS

edited by Etta Kavanagh

Developing Drugs for Tuberculosis

IN THEIR POLICY FORUM "A PORTFOLIO MODEL OF DRUG DEVELOPMENT FOR TUBERCULOSIS" (3 Mar. 2006, p. 1246), S. W. Glickman *et al.* conclude that achieving 95% confidence of at least one new tuberculosis (TB) drug takes 12 years and up to $400 million, and that there is a less than 5% chance of a new TB drug by 2010.

Their first Monte Carlo simulation is based on only 11 of the 27 compounds in the global portfolio (confusingly, still labeled the "global TB drug portfolio" in the first diagram). The policy relevance of such subportfolio simulation is unclear.

The finding of a less than 5% chance may be a bit on the low side, too. Gatifloxacin and moxifloxacin—the two drugs listed as Phase II/III in Glickman *et al.*'s reference (*8*)—are previously licensed anti-infectives for other purposes, now being re-indicated for anti-TB activity. Gatifloxacin is already in Phase III and moxifloxacin is about to enter Phase III with the TB Alliance, U.S. Centers for Disease Control, and Bayer. Both come from the same subclass of fluoroquinolones, and evidence suggests that their anti-TB efficacy is likely to be similar. Given extensive prior clinical experience and proven safety records, the likelihood of success of these two compounds is better and more predictable, and development time and costs lower, than for any of the other compounds should any of them reach Phase III.

The second simulation, still generating a less than 5% chance, "doubled the number of phase I and II compounds in the [first] portfolio." Yet diagram 2 and the background paper refer to "double the number of compounds in preclinical and clinical tests." Which of these did the authors do? What is the policy relevance? Building up to "optimal" portfolio size inevitably creates a cost bulge with little immediate outcome.

The third simulation, and the $400 million figure, is based on 30 phase I compounds only. How this relates to the current 27-compound global portfolio is not fully explained, although any funding shortfall depends on it.

And is the 11% per year cost of capital nominal or real (i.e., adjusting for inflation)? It seems to be treated as nominal, although the figure it is derived from (*1*) is real.

The point is to build a portfolio that will generate a rolling supply of new TB drugs and not only the chance of the first one. According to the transition probabilities used by Glickman *et al.*, the 30-compound portfolio generates on average 2.925 drugs. If the $400 million is right, this means $136.75 million each, which compares favorably with current funding into TB drug development. Policy-makers, and funders, need to hold their nerve (*2*).

ANDREW FARLOW

Saïd Business School, University of Oxford, Park End Street, Oxford, OX1 1HP, U.K.

References

1. J. A. DiMasi, R. W. Hansen, H. G. Grabowski, *J. Health Econ.* **22**, 151 (2003).
2. See www.economics.ox.ac.uk/members/andrew.farlow/FarlowTBPortfolio.pdf for more details on these issues.

Response

WE APPRECIATE THE LETTER BY FARLOW ON OUR Policy Forum, and we reiterate that the TB Alliance's support and facilitation are immeasurable contributions toward the success of bringing new antituberculosis drugs to market. One goal of our analysis was to focus attention on the critical need for new antituberculosis drugs in the developing world by quantifying the gap between what is being spent and what needs to be spent to bring new drugs to market. Whether it will take 10 years or 20 years to develop the next effective antituberculosis drug is not certain. What is certain is that the need for such drugs is growing, and greater resources would help to shorten the development time. Since our Policy Forum was published, an outbreak of extensively drug-resistant tuberculosis has been reported (*1*), further highlighting the urgency of the problem. Therefore, we join in calls for increased support of antituberculosis drug development.

The first simulation model described in our Policy Forum is based on all 11 compounds in the global antituberculosis drug portfolio that were in preclinical or clinical testing at the time of our analysis. We derived this information from a report by the Stop TB Partnership (*2*). The remaining 16 compounds in the global portfolio were in discovery phase. The time required to bring any of these 16 compounds to market was well beyond the timeline of our analysis (through 2019), and their inclusion in the portfolio model would have simply inflated development costs without providing precise estimates around the eventual timing or likelihood of their development. Our model did include gatifloxacin and moxifloxacin, compounds that were in phase II testing for use in antituberculosis regimens at the time of our analysis. Phase III testing of gatifloxacin was in planning stages (*3*). To our knowledge, there was no publicly available information about phase III testing of moxifloxacin at that time. We are pleased to learn that the drug may soon enter phase III clinical trials.

We conducted two additional exercises to illustrate the magnitude of the challenges that policy-makers face in antituberculosis drug development efforts. In one exercise, we repeated the first simulation but doubled the number of compounds in preclinical and clini-

CREDIT: PETER HOEY

Supernova birthday 1086

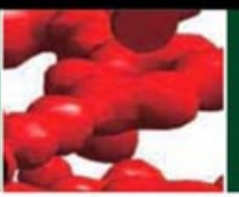

Solving crystal structures 1087

cal testing. In another exercise, we examined how increasing the number of phase I compounds affects drug development timeline and costs. Despite large increases in the number of compounds in these hypothetical portfolios, our findings indicate that substantial challenges remain in bringing new antituberculosis drugs to market in a manner that is timely and not cost-prohibitive. Resources would ideally be directed toward compounds in late stages of development. However, given the limited number of such compounds in the current portfolio, resources should be devoted to increasing the number of compounds in early clinical testing.

As described in our Supporting Online Material, we used a 4% annual cost of capital, not 11%. Our choice of 4% reflects our belief that this is an appropriate (risk-free) discount rate for projects that are intended to generate social benefits, rather than the higher discount rate typically assumed by the pharmaceutical industry for profit-maximizing purposes.

We believe that the model accurately reflects the drug development process from the perspective of a public-private partnership, but could be improved with more reliable and timely input. We would welcome an opportunity to contribute to dialogue and planning for antituberculosis drug development by expanding the model to include all public and nonpublic information about potential therapies for tuberculosis. Such a model would allow the TB Alliance and the funding community to better understand the status of public-private partnerships in antituberculosis efforts and to assess the full range of unmet needs.

SETH W. GLICKMAN,[1,2] EMMA B. RASIEL,[3] CAROL DUKES HAMILTON,[1] KEVIN A. SCHULMAN[1,2]*

[1]Duke University School of Medicine, Durham, NC 27710, USA. [2]Health Sector Management Program, The Fuqua School of Business, Duke University, Durham, NC 27708, USA. [3]Department of Economics, Duke University, Durham, NC 27708, USA.

*Address for correspondence: Center for Clinical and Genetic Economics, Duke Clinical Research Institute, PO Box 17969, Durham, NC 27715, USA. E-mail: kevin.schulman@duke.edu

References

1. N. R. Gandhi *et al.*, *Lancets* **368**, 1575 (2006).
2. Working Group on New TB Drugs, Stop TB Partnership, *Strategic Plan: Prepared for the Global Plan to Stop TB: 2006-2015* (www.stoptb.org/wg/new_drugs/documents.asp).
3. World Health Organization, New tuberculosis therapy offers potential shorter treatment (press release) (www.who.int/mediacentre/news/releases/2005/pr71/en/index.html).

Letters to the Editor

Letters (~300 words) discuss material published in *Science* in the previous 3 months or issues of general interest. They can be submitted through the Web (www.submit2science.org) or by regular mail (1200 New York Ave., NW, Washington, DC 20005, USA). Letters are not acknowledged upon receipt, nor are authors generally consulted before publication. Whether published in full or in part, letters are subject to editing for clarity and space.

A Way to Deal with Image Enhancement

THE PROBLEMS RAISED IN THE NEWS FOCUS article "Don't pretty up that picture just yet" (J. Couzin, 22 Dec. 2006, p. 1866) on image editing in scientific publications can be ameliorated in the near term. For every published image, authors should be required to add the original, unaltered image to their supporting online data. First, this will allow the authors to gussy up their images for clarity and emphasis of specific points without being disingenuous. If they wish, aficionados in the field and other interested readers will be able to view the "raw data" and judge scientific validity. Second, by imposing the requirement for all images, regardless of the amount or type of editing, ambiguity as regards "literary license" is removed. Duplicity is not addressed, but unintentional missteps would be minimized.

LAWRENCE BODENSTEIN

Columbia University, New York, NY 10032, USA. E-mail: lb2126@columbia.edu

Recognizing William Bateson's Contributions

IN THEIR REPORT "A COMPLEX OSCILLATING network of signaling genes underlies the mouse segmentation clock" (8 Dec. 2006, p. 1595), M.-L. Dequéant *et al.* expand on Pourquié's (*1*) work demonstrating that the precursors of vertebrae (somites) are rhythmically produced from the presomitic mesoderm (PSM), specifically, how "during the formation of each somite [the gene coding for the transcription factor], *Lfng* is expressed in the PSM as a wave that sweeps across the tissue in a posterior-to-anterior direction" (p. 1595).

Historically, however, the idea of a rhythmical element in the development of repeated or meristic parts, such as somites and vertebrae, belongs to William Bateson. By 1888, Bateson had become consumed by studying variation in plants and animals as differences of expression of repeated parts. In September 1891, Bateson wrote to his sister that his "vibratory theory of repetition of parts" (also called the "Undulatory Hypothesis") explained "all the *patterns* and *recurrence* of patterns in animals and plants" In *Materials*, Bateson suggested that as waves of differing intensities create different numbers and spacings of sandy furrows, so, too, will developmental waves of differing intensities determine the expression and number of elements in series of repeated structures (*2*).

Although scientists usually concentrate on recent literature, the work of past scholars may still sometimes enlighten. In addition to translating into English Mendel's sole article and expanding Mendelism to include animals, Bateson struggled with issues such as the origin of species and of the features that distinguish them. His thoughts on alterations of development as the basis of evolutionary or specific novelty may have its roots in Victorian saltationism, but his appreciation of the achievement of difference through alteration of the developmental mechanisms underlying repeated parts foreshadowed by almost a century the current incarnation of developmental biology and the theoretical field of "evo-devo" (*3*).

JEFFREY H. SCHWARTZ

Departments of Anthropology and History and Philosophy of Science, University of Pittsburgh, Pittsburgh, PA 15260, USA.

References

1. O. Pourquié, *Science* **301**, 328 (2003).
2. W. Bateson, *Materials for the Study of Variation, Treated with Especial Regard to Discontinuity in the Origin of Species* (Macmillan, New York, 1894).
3. J. H. Schwartz, *Sudden Origins: Fossils, Genes, and the Emergence of Species* (Wiley, New York, 1999).

CORRECTIONS AND CLARIFICATIONS

Reports: "Electric field–induced modification of magnetism in thin-film ferromagnets" by M. Weisheit *et al.* (19 Jan., p. 349). The first affiliation was incorrect. It should be [1]Institut Néel, CNRS/Université Joseph-Fourier, 25 Avenue des Martyrs, Boite Postale 166, F-38042 Grenoble Cedex 9, France.

Perspectives: "Negative refractive index at optical wavelengths" by C. M. Soukoulis *et al.* (5 Jan., p. 47). In the figure, the scale for the green panel should have been 200 nm, and the scale for the blue panel should have been 500 nm.

NEUROSCIENCE

Dangers of Brain-o-vision

Daniel M. Wegner

Imagine a gadget, call it "brain-o-vision," for brain scanning that doesn't create pictures of brains at all. That's right, no orbs spattered with colorful "activations" that need to be interpreted by neuroanatomists. Instead, with brain-o-vision, what a brain sees is what you get—an image of what that brain is experiencing. If the person who owns the brain is envisioning lunch, up pops a cheeseburger on the screen. If the person is reading a book, the screen shows the words. For that matter, if the brain owner is feeling pain, perhaps brain-o-vision could reach out and swat the viewer with a rolled-up newspaper. Brain-o-vision could give us access to another person's consciousness (*1*).

Technologies for brain-o-vision are beginning to seem possible. We are learning how brain activations map onto emotions, memories, and mental processes, and it won't be long before we might translate activations into Google searches for images of what the brain is thinking. There is a specific brain area linked with face perception (*2*), for instance, and even a neuron that fires when it sees Jennifer Aniston (*3*). So why, in principle, shouldn't we be able to scan a brain and discover when it is looking at her—and eventually even learn what she's wearing? Of course, it may be many years to the beta version. But imagine that everything works out and brain-o-vision goes on sale at Wal-Mart. Could the device solve the problem of whether consciousness causes behavior?

With direct evidence of a person's consciousness, we could do science on the question. We could observe regularities in the relation between consciousness (say, a thought of sipping coffee) and behavior (the actual drink). If the consciousness always preceded the behavior (and never occurred without being followed by the behavior), we could arrive at the inductive inference of causation and, as scientists, be quite happy that we had established a causal connection.

The reviewer is at the Department of Psychology, Harvard University, 33 Kirkland Street, Cambridge, MA 02138, USA. E-mail: wegner@wjh.harvard.edu

In fact, this is the project about which several of the contributors to *Does Consciousness Cause Behavior?* (Marc Jeannerod, Richard Passingham and Hakwan Lau, Suparna Choudhury and Sarah-Jayne Blakemore) give masterful reports (using measures of consciousness other than brain-o-vision). So what's the problem? Why is the issue so vexing that this book and many others have taken up the question? Certainly, one snag is that we don't yet have brain-o-vision. But that's not the full story. There is a key sidetrack on the way to establishing this causal inference that has left philosophers and scientists in a muddle for years.

Does Consciousness Cause Behavior?

Susan Pockett, William P. Banks, and Shaun Gallagher, Eds.

MIT Press, Cambridge, MA, 2006. 372 pp. $50, £32.95. ISBN 9780262162371.

The problem is that we each have our own personal brain-o-vision shimmering and blaring in our heads all day long. We have our own consciousness, and we find its images mesmerizing. The picture that our minds produce shows what looks exactly like a causal relationship: I thought of drinking the coffee and then I did it. This apparent relationship anchors our intuition about the conscious causation of behavior so deeply that it is difficult to understand that this causal inference is something that ought to be a scientific matter, not an intuitive one. We can't turn off the inner television and try to figure out what really happened. Each of the volume's contributors struggles to find some rapprochement between the personal experience of conscious causation and the possibility that consciousness might not cause behavior—leaving the experience an illusion.

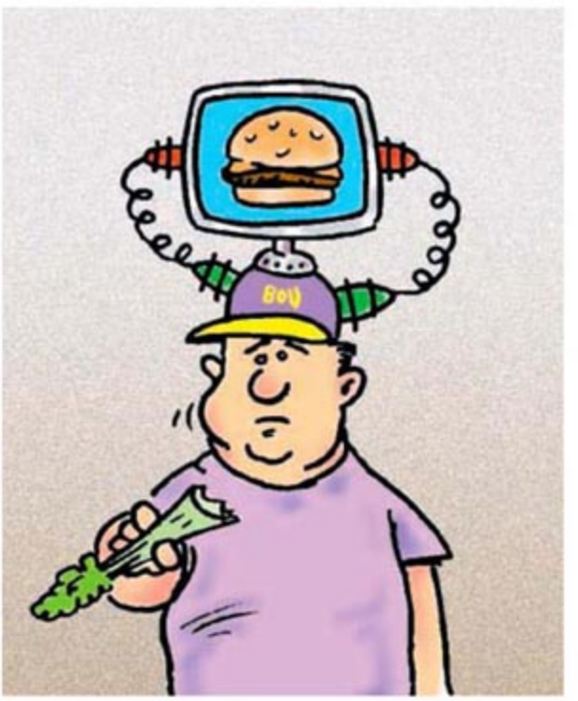

CREDIT: JOE SUTLIFF

An occasional undercurrent in the volume is the idea that exceptions to the standard inner experience of conscious causation should be discarded as uninformative. For example, Libet's classic finding (*4*) that brain activation precedes the reported conscious experience of willing action is often cited as evidence that consciousness is not the initial cause of behavior, and that it instead occurs in a chain of events initiated by brain events. Several contributors examine this finding in creative ways—but, curiously, others belittle the finding as a laboratory-bound oddity. The dismissal of exceptional cases extends to some chapters that question the value of examining any unusual lapses of conscious causation—such as those in hypnosis, facilitated communication, schizophrenia, or psychogenic movement disorders or in automatisms such as dowsing and table-turning. These anomalous cases sometimes reveal that the experience of conscious causation can diverge from the actual causal circumstances surrounding behavior. We need to understand such cases to establish when it is that consciousness thinks it is causing behavior. Exploring a phenomenon by studying its boundaries is a standard operating procedure of science, and it is curious that some students of mind would wish such informative exceptions swept under the rug.

Research into conscious causation is complicated by the fact that the scientists and philosophers studying the problem are people. Our own personal brain-o-vision leads us to idealize apparent conscious causation and disparage exceptions. We may not be able to turn off our own consciousness and consider the question dispassionately, but it probably would help.

References and Notes

1. Thanks to D. Dennett for this idea.
2. N. Kanwisher, J. McDermott, M. M. Chun, *J. Neurosci.* **17**, 4302 (1997).
3. R. Q. Quiroga, L. Reddy, G. Kreiman, C. Koch, I. Fried, *Nature* **435**, 1102 (2005).
4. B. Libet, *Behav. Brain Sci.* **8**, 529 (1985).

10.1126/science.1138463

NEUROSCIENCE

Perceptions of a Receptor

David Colquhoun

I like history. Nothing gives one a better feel for a subject than knowing how it developed. *Nicotinic Acetylcholine Receptors* concentrates on the French contribution to knowledge about these neurotransmitter receptors, and it's a good (if, at times, idiosyncratic) read.

The nicotinic acetylcholine receptors are often referred to as the most investigated and best understood type of ligand-gated ion channel. That is probably true of the type that occurs in electric eels and rays, and the very similar receptor that mediates neuromuscular transmission in vertebrates, but the sorts of nicotinic receptor that occur in the central nervous system are much less well understood.

I can remember well the April 1972 meeting at which, with a flourish, Jean-Pierre Changeux produced from his pocket a tube with a thin blue band and proclaimed, "We have the receptor." Beginning in the early 20th century, most people had supposed that a receptor must be something like an enzyme, and here at last was the proof. After that, progress was fast. Soon cloning (largely in Japan) determined the primary sequence of the receptor subunits, and the invention of the patch clamp method led to much better functional studies of the receptor. Collaborative work (at first, largely between German and Japanese researchers) revealed the nature of the adult and embryonic forms of the receptor and the location of the ion channel within it.

This book covers everything about the nicotinic receptors from purification, function, and structure through to speculations about the role of the neuronal type of nicotinic receptors that are found in the brain. Many parts are good, but Changeux (Institut Pasteur) and Stuart Edelstein (University of Geneva), like all of us, are perhaps victims of their own backgrounds. They deal much more authoritatively with the biochemical and structural aspects of the receptors than the functional aspects.

Nicotinic Acetylcholine Receptors
From Molecular Biology to Cognition

by Jean-Pierre Changeux and Stuart J. Edelstein

Odile Jacob, New York. 296 pp. $99. ISBN 9780976890805.

Throughout the book, the authors contrast two types of models for receptor activation by agonists: allosteric models ("good") and sequential models (as used by electrophysiologists, "bad"). In my view, this distinction is totally spurious. The authors never really define "sequential," but usually it seems to mean that the unliganded open state is omitted from a postulated mechanism. When that is done, it is done for practical reasons. The authors are speaking theoretically, but when working with experimental results, one can't fit parameters about which the data contain no information. It is obvious that unliganded open channels must exist: in principle, from Boltzmann's law; in practice, from mutant receptors that open in the absence of agonist at a rate fast enough to measure. Any apparent difference in approach is a difference between those who have data and those who haven't.

Such misapprehensions give rise to some surprising assertions. For example, "these [single channel] studies do not give the exact relationship between binding events and channel opening events. The [Monod-Wyman-Changeux] formalism, on the other hand, makes specific experimental predictions for these relationships." In fact, all postulated mechanisms make such predictions.

Or, "In conclusion, experimental data—particularly the data concerning pleiotropic pathological mutations in the nicotinic receptor …—that are readily accounted for by the allosteric schema cannot be satisfactorily represented by the sequential schema." (Here, "pleiotropic" means that when you mess with the structure of a protein it can have complicated and unpredictable effects.) This is simply untrue. The authors present two pages devoted to simulations (based on numbers from the literature) that purport to show that the effect of a mutation is mediated by changing the equilibrium constant L_0 for the conformation change (shut to open) of the unliganded receptor. The simulations bear a qualitative resemblance to observations made by Ohno *et al.* (*1*), but they do not fit them. Nevertheless, the authors conclude that their postulated mechanism is correct. Although, the idea that mutations change L_0 is attractive, the evidence is not strong. Perhaps the best evidence comes from some very thorough work by Auerbach's lab (*2*), but that work is not cited. Even more surprising, in discussing transduction of the signal from the binding site to the channel gate, the authors ignore the whole body of work by Auerbach and Grosman (*3*) on phi-analysis as well as related work on the flip mechanism (*4*).

A lack of precision also appears in the discussion of "allosteric diseases." Since around 1980, it has been appreciated that the physiological event triggered by the agonist is a short burst of channel openings, the duration of which controls the decay rate of the synaptic current. Mutations can slow this decay either by making the individual openings longer or by producing more (re-)openings without changing the length of each. The latter occurs when the mutation slows the dissociation of agonist. Several mutations of this sort have been described, the classical one being αG153S. Sine *et al.* noted that "its prolonged activation episodes arise primarily from a decreased rate of dissociation of [acetylcholine], allowing repetitive opening during [acetylcholine] occupancy" (*5*). Yet the book incorrectly states that the effect is to produce "longer openings," thus ignoring the last 25 years of developments in the understanding of synaptic currents.

The word allosteric seems to appear on almost every page, although in most cases it could be omitted without changing the meaning. I have never found the word very useful, if only because it is used in so many different senses (*6*). To the list we can now add "allosteric diseases."

The authors give an informative account of their behavioral studies with knockout mice, but, for me, it is rather spoiled by a hyperbolic style: "In conclusion, from the cognitive perspective, these findings clearly illustrate the involvement of nicotinic receptors in regulating the transition between states of consciousness." And if you don't quite follow that, you are referred to a network diagram that strikes me as little more than fantasy. The fact is that cholinesterase inhibitors do little or no good for Alzheimer's disease (*7*), never mind regulating consciousness.

The account Changeux and Edelstein provide in *Nicotinic Acetylcholine Receptors* is very good in parts. Nonetheless, as an overall view of the current state of our understanding, it is not only incomplete but sometimes positively misleading.

The reviewer is at the Department of Pharmacology, University College London, Gower Street, London WC1E 6BT, UK. E-mail: d.colquhoun@ucl.ac.uk

References

1. K. Ohno *et al.*, *Proc. Natl. Acad. Sci. U.S.A.* **92**, 758 (1995).
2. S. Chakrapani, T. D. Bailey, A. Auerbach, *J. Gen. Physiol.* **122**, 521 (2003).
3. C. Grosman, M. Zhou, A. Auerbach, *Nature* **403**, 773 (2000).
4. V. Burzomato, M. Beato, P. J. Groot-Kormelink, D. Colquhoun, L. G. Sivilotti, *J. Neurosci.* **24**, 10924 (2004).
5. S. M. Sine *et al.*, *Neuron* **15**, 229 (1995).
6. D. Colquhoun, *Br. J. Pharmacol.* **125**, 923 (1998).
7. M. Maggini, N. Vanacore, R. Raschetti, *PLoS Med.* **3**, 456 (2006).

10.1126/science.1132059

ASSESSMENT

Standardized Tests Predict Graduate Students' Success

Standardized admissions tests are valid predictors of many aspects of student success across academic and applied fields.

Nathan R. Kuncel[1] and Sarah A. Hezlett[2]

Accurately predicting which students are best suited for postbaccalaureate graduate school programs benefits the programs, the students, and society at large, because it allows education to be concentrated on those most likely to profit. Standardized tests are used to forecast which students will be the most successful and obtain the greatest benefit from graduate education in disciplines ranging from medicine to the humanities and from physics to law. However, controversy remains about whether such tests effectively predict performance in graduate school. Studies of standardized test scores and subsequent success in graduate school over the past 80 years have often suffered from limited sample size and present mixed conclusions of variable reliability.

Several meta-analyses have been conducted to extract more reliable conclusions about standardized tests from a variety of disciplines. To date, these review studies have been conducted on several tests commonly used in the United States: the Graduate Record Examination (GRE-T) (*1*), Graduate Record Examination Subject tests (GRE-S) (*1*), the Law School Admissions Test (LSAT) (*2–4*), the Pharmacy College Admissions Test (PCAT) (*5*), the Miller Analogies Test (MAT) (*6*), the Graduate Management Admissions Test (GMAT) (*7*), and the Medical College Admissions Test (MCAT) (*8*, *9*).

We collected and synthesized these studies. Four consistent findings emerged: (i) Standardized tests are effective predictors of performance in graduate school. (ii) Both tests and undergraduate grades predict important academic outcomes beyond grades earned in graduate school. (iii) Standardized admissions tests predict most measures of student success better than prior college academic records do (*1–5*, *7*, *8*). (iv) The combination of tests and grades yields the most accurate predictions of success (*1–4*, *7*, *8*).

Structure of Admissions Tests

Most standardized tests assess some combination of verbal, quantitative, writing, and analytical reasoning skills or discipline-specific knowledge. This is no accident, as work in all fields requires some combination of the above. The tests aim to measure the most relevant skills and knowledge for mastering a particular discipline. Although the general verbal and quantitative scales are effective predictors of student success, the strongest predictors are tests with content specifically linked to the discipline (*1*, *5*).

Estimating Predictive Validity

The predictive validity of tests is typically evaluated with statistics that estimate the linear relationship between predictors and a measure of academic performance. Meta-analyses synthesizing primary studies of test validity aggregate Pearson correlations. In many primary studies, the correlations are weakened by statistical artifacts, thus contributing to misinterpretation of conclusions. The first attenuating factor is the restriction of range that occurs when a sample is selected on the basis of a predictor variable that has a nonzero correlation with an outcome measure (*10*). The second attenuating factor is unreliability in the success measure resulting from inconsistency in human judgment (*11*). Where possible, recognized corrections were used (*12*) to account for these artifacts.

Research has been conducted on the correlation between test scores and various measures of student success: first-year grade point average (GPA), graduate GPA, degree attainment, qualifying or comprehensive examination scores, research productivity, research citation counts, licensing examination performance, and faculty evaluations of students. These results are based on analyses of 3 to 1231 studies across 244 to 259,640 students. The programs represented include humanities, social sciences, biological sciences, physical sciences, mathematics, and professional graduate programs in management, law, pharmacy, and medicine. For all tests across all relevant success measures, standardized test scores are positively related to subsequent meas-

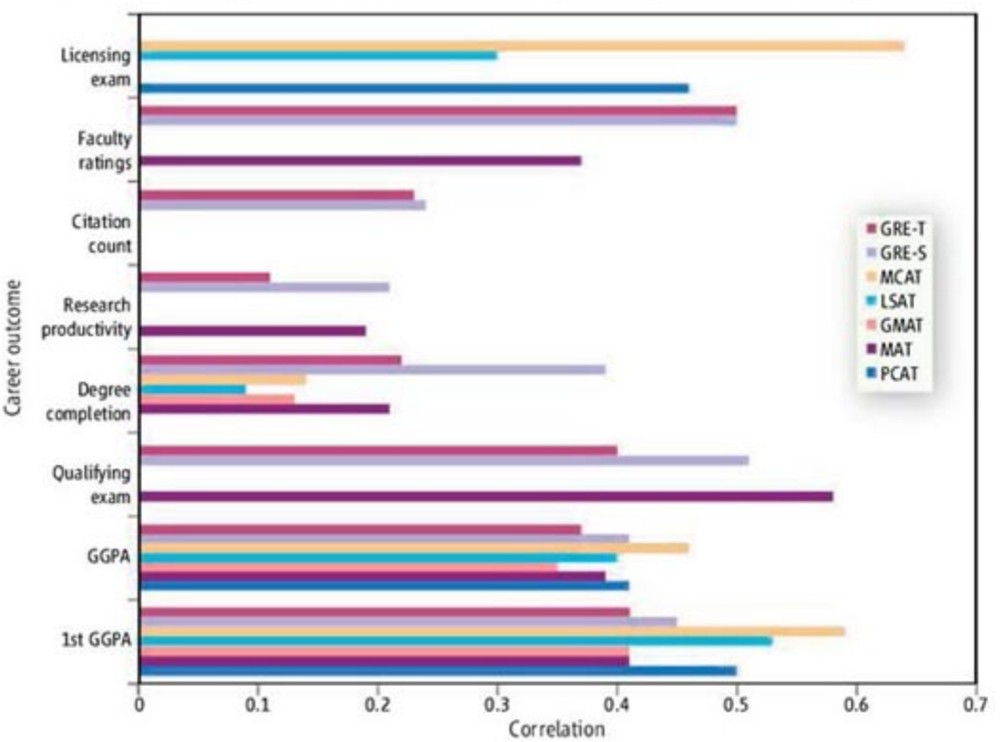

Tests as predictors. Standardized test scores correlate with student success in graduate school. See table S1 for detailed data.

[1]Department of Psychology, University of Minnesota, 75 East River Road, Minneapolis, MN 55455, USA. [2]Personnel Decisions Research Institutes, 650 Third Avenue South, Suite 1350, Minneapolis, MN 55402, USA.

*Author for correspondence. E-mail: kunce001@umn.edu

ures of student success [see chart, table S1, and supporting online material (SOM) text].

Utility of Standardized Tests

The actual applied utility of predictors is not easily inferred from the correlations shown in the chart. The number of correct and incorrect admissions decisions for a specific situation can be estimated from the correlation (*13*) (SOM text). In many cases, frequency of correct decisions can be increased from 5% to more than 30% (SOM text). In addition, correlations were converted into odds ratios using standard formulae (*14*) to facilitate interpretation (table S1).When an institution can be particular about whom it admits, even modest correlations can yield meaningful improvements in the performance of admitted students.

The worry that students' scores might contaminate future evaluations that, in turn, influence outcomes appears to be unfounded. The predictive validity of tests when evaluators do or do not know the individual's score is unaffected (*15*, *16*) and, some outcomes, such as publication record, are not directly influenced by test scores.

Bias in Testing

One concern is that admissions tests might be biased against certain groups, including racial, ethnic, and gender groups. To test for bias, regression analyses of an outcome measure are compared for different groups (*12*, *17*). If regression lines do not differ, then there is evidence that any given score on the test is associated with the same level of performance in school regardless of group membership. Overall and across tests, research has found that regression lines frequently do not differ by race or ethnic group. When they do, tests systematically favor minority groups (*18*–*23*). Tests do tend to underpredict the performance of women in college settings (*24*–*26*) (SOM text) but not in graduate school (*18*–*20*, *23*).

Items from most professionally developed tests were screened for content bias and for differential item functioning (DIF). DIF examines whether performance on an item differs across racial or gender groups when overall ability is controlled. Most items do not display DIF but some content patterns have emerged over time (see SOM text). To avoid negative effects, DIF items can be rewritten, eliminated before finalizing the test, or left unscored. Research has found that the DIF effects remaining in tests have effectively zero impact on decision-making (*27*).

Coaching Effects in Testing

If test preparation yields large gains, then concerns about the gain's effects on differential access to higher education and the predictive validity of tests are understandable. Scores on any test can be increased to some degree because standardized tests are, like all ability tests, assessments of developed skills and knowledge. The major concern is that coaching may produce gains that are unrelated to actual skill development.

In controlled studies, gains on standardized tests used for college or graduate admissions are consistently modest. The typical magnitude for coached preparation is about 25% of one standard deviation (*28*–*33*). Longer and longer periods of study and practice are needed to attain further equal increments of improvement. Those item types that have been demonstrated to be most susceptible to coaching have been eliminated from tests (*34*). Test preparation or retaking does not appear to adversely affect the predictive validity of standardized tests (*35*–*37*).

Future Directions

Standardized admission tests provide useful information for predicting subsequent student performance across many disciplines. However, student motivation and interest, which are critical for sustained effort though graduate education, must be inferred from various unstandardized measures including letters of recommendation, personal statements, and interviews. Additional research is needed to develop measures that provide more reliable information about these key characteristics.

These efforts will be facilitated with more information about the actual nature of student performance. Researchers have examined a number of important outcomes but have not captured other aspects of student performance including networking, professionalism, leadership, and administrative performance. A fully specified taxonomy of student performance dimensions would be invaluable for developing and testing additional predictors of student performance.

Results from a large body of literature indicate that standardized tests are useful predictors of subsequent performance in graduate school, predict more accurately than college GPA, do not demonstrate bias, and are not damaged by test coaching. Despite differences across disciplines in grading standards, content, and pedagogy, standardized admissions tests have positive and useful relationships with subsequent student accomplishments.

References and Notes

1. N. R. Kuncel, S. A. Hezlett, D. S. Ones, *Psychol. Bull.* **127**, 162 (2001).
2. R. L. Linn, C. N. Hastings, *J. Educ. Meas.* **21**, 245 (1984).
3. L. F. Wrightman, "Beyond FYA: Analysis of the utility of LSAT scores and UGPA for predicting academic success in law school" (RR 99-05, Law School Admission Council, Newton, PA, 2000).
4. L. F. Wrightman, "LSAC national longitudinal bar passage study" (Law School Admission Council, Newton, PA, 1998).
5. N. R. Kuncel *et al.*, *Am. J. Pharm. Educ.* **69**, 339 (2005).
6. N. R. Kuncel, S. A. Hezlett, D. S. Ones, *J. Pers. Soc. Psychol.* **86**, 148 (2004).
7. N. R. Kuncel, M. Crede, L. L. Thomas, *Acad. Manage. Learn. Educ.*, in press.
8. E. R. Julian, *Acad. Med.* **80**, 910 (2005).
9. R. F. Jones, S. Vanyur, *J. Med. Educ.* **59**, 527 (1984).
10. R. L. Thorndike, *Personnel Selection: Test and Measurement Techniques* (Wiley, New York, 1949).
11. J. E. Hunter, F. L. Schmidt, *Methods of Meta-Analysis: Correcting Error and Bias in Research Findings* (Sage, Newbury Park, CA, 1990).
12. American Educational Research Association (AERA), *Standards for Educational and Psychological Testing* (AERA, Washington, DC, 1999).
13. H. C. Taylor, J. T. Russell, *J. Appl. Psych.* **23**, 565 (1939).
14. J. P. T. Higgins, S. Green, Eds., *Cochrane Handbook for Systematic Review of Interventions 4.2.5* (The Cochrane Collaboration, Oxford, UK, 2005).
15. B. B. Gaugler, D. B. Rosenthal, G. C. Thornton, C. Bentson, *J. Appl. Psych.* **72**, 493 (1987).
16. N. Schmitt, R. Z. Gooding, R. A. Noe, M. Kirsch, *Pers. Psych.* **37**, 407 (1984).
17. T. A. Cleary, *J. Educ. Meas.* **5**, 115 (1968).
18. J. A. Koenig, S. G. Sireci, A. Wiley, *Acad. Med.* **73**, 1095 (1998).
19. R. L. Linn, *J. Legal Educ.* **27**, 293 (1975).
20. S. G. Sireci, E. Talento-Miller, *Educ. Psych. Meas.* **66**, 305 (2006).
21. J. B. Vancouver, *Acad. Med.* **65**, 694 (1990).
22. L. F. Wrightman, D. G. Muller, "An analysis of differential validity and differential prediction for black, Mexican American, Hispanic, and white law school students" (RR 90-03, Law School Admission Council, Newton, PA, 1990).
23. H. I. Braun, D. H. Jones, "Use of empirical Bayes method in the study of the validity of academic predictors of graduate school performance" (GRE Board Professional Report 79-13P, Educational Testing Service, Princeton, NJ, 1985).
24. R. Zwick, *Fair Game?* (RoutledgeFalmer, New York, 2002).
25. L. J. Stricker, D. A. Rock, N. W. Burton, *J. Educ. Psych.* **85**, 710 (1993).
26. J. W. Young, *J. Educ. Meas.* **28**, 37 (1991).
27. S. Stark *et al.*, *J. Appl. Psych.* **89**, 497 (2004).
28. B. J. Becker, *Rev. Educ. Res.* **60**, 373 (1990).
29. L. F. Leary, L. E. Wrightman, "Estimating the relationship between use of test-preparation methods and scores on the Graduate Management Admission Test" (GMAC RR 83-1, Princeton, NJ, 1983).
30. D. E. Powers, *J. Educ. Meas.* **22**, 121 (1985).
31. S. Messick, A. Jungeblut, *Psychol. Bull.* **89**, 191 (1981).
32. D. E. Powers, D. A Rock, *J. Educ. Meas.* **36**, 93 (1999).
33. J. A. Kulik *et al.*, *Psychol. Bull.* **95**, 179 (1984).
34. D. E. Powers, S. S. Swinton, *J. Educ. Psych.* **76**, 266 (1984).
35. M. Hojat, *J. Med. Educ.* **60**, 911 (1985).
36. L. F. Wightman, "The validity of Law School Admission Test scores for repeaters: A replication" (LSAC RR 90-02, Law School Admission Council, Newton, PA, 1990).
37. A. Allalouf, G. Ben-Shakhar, *J. Educ. Meas.* **35**, 31 (1998).

Supporting Online Material

www.sciencemag.org/cgi/content/full/315/5815/1080/DC1

10.1126/science.1136618

MICROBIOLOGY

Mayhem in the Lung

Insights on how a lethal strain of bacteria causes necrotic pneumonia may guide development of drugs and vaccines that combat dangerous respiratory pathogens.

Barbara C. Kahl, Georg Peters

Infection by the pathogenic bacterium *Staphylococcus aureus* can cause a wide range of conditions, from mild skin infections to life-threatening endocarditis, pneumonia, and sepsis (*1*). Until recently, severe infections caused by strains that are resistant to multiple drugs including β-lactam antibiotics (penicillin and cephalosporin)—the so-called methicillin-resistant *S. aureus* (MRSA) strains—were found exclusively in health-care institutions and hospitals, and strong hygiene procedures were used to prevent transmission and destroy the bacteria. But in 1999, fatal infections caused by MRSA were unexpectedly reported in the community (*2*). Since then, the spread of community-acquired MRSA to healthy individuals has been worldwide (*3*–*5*), resulting in severe fatal infections including fasciitis necroticans ("flesh-eating bacteria") (*6*), Waterhouse-Friedrichsen syndrome (*7*), and highly lethal necrotizing pneumonia (*8*). On page 1130 of this issue, Labandeira-Rey *et al*. (*9*) report that MRSA strains that cause necrotizing pneumonia rely on the dual action of a single bacterial toxin that results in the destruction of respiratory tissue and bacteria-engulfing immune cells and exacerbated inflammation. This new understanding may help guide the design of effective therapeutic regimens for *S. aureus* infections and other infectious respiratory illnesses.

Both community-acquired MRSA and methicillin-susceptible strains can secrete Panton-Valentine leukocidin (PVL), a protein whose active form creates a pore in the cell membrane of leukocytes such as neutrophils. Most patients dying from necrotizing pneumonia have low numbers of leukocytes in their bloodstream, supporting leukotoxicity by PVL in vivo (*8*). It seems that the combined presence of the PVL-encoding gene and *mecA*, the gene that encodes resistance to methicillin, has created superadapted MRSA strains that are spreading in the community (*10*). Yet the precise role of PVL during pathogenesis has been an open question, as mouse models of *S. aureus* infections (sepsis and abscess development) do not implicate the protein as a major virulence factor (*11*).

To investigate the function of PVL in the pathogenesis of necrotizing pneumonia, Labandeira-Rey *et al*. established a new mouse model of acute pneumonia. The authors used clinical PVL-positive *S. aureus* strains as well as strains that were engineered to express PVL or not. The gene encoding PVL can be transmitted among bacteria by a virus (phage). The authors generated isogenic strains of *S. aureus* harboring either PVL-carrying phage or phage lacking the PVL locus, and PVL-negative bacteria carrying extrachromosomal DNA (plasmid) with the PVL gene. After 2 days, mice infected with PVL-positive bacteria showed changes in lung tissue comparable to those observed in human necrotizing pneumonia—an abundance of infiltrating neutrophils, inflammation of the lung parenchyma, tissue necrosis, and hemorrhage. In contrast, the lungs of mice infected with PVL-negative strains were mostly normal. Presence of the toxin in the lungs of animals infected with PVL-positive strains was also detected with PVL-specific antibodies. Furthermore, administration of the toxin resulted in dose-dependent tissue damage. In other words, the toxin alone was enough to destroy lungs.

Increased binding of clinical PVL-positive strains to injured human airway epithelium in vitro has been described previously (*12*). Bacteria bind to epithelial cells and extracellular matrix proteins through proteins that are covalently anchored to the cell wall and act as adhesins. In *S. aureus*, the expression of adhesins and secreted proteins (such as toxins) is tightly regulated during the bacterial growth phase. Adhesin expression is activated during the early log phase, whereas toxin expression is activated during late log phase, when the expression of adhesins is suppressed. This differential expression of virulence factors depends on environmental signals and is thought to achieve optimal spatial and temporal adaptation of the pathogen.

One of the most important adhesins of *S. aureus* is staphylococcal protein A (or SpA), which has long been known to block the engulfing action of phagocytic immune cells. Labandeira-Rey *et al*. demonstrate that PVL causes changes in gene expression that may affect strain virulence. The authors found that in a PVL-positive strain, adhesins such as protein A are highly expressed in all growth phases, and not inhibited as might be expected in late log and stationary phases. In contrast, secreted proteins such as proteases are not expressed. Therefore, PVL seems to act at the transition from logarithmic to stationary growth phases by an as yet unidentified mechanism. Such negative regulation of bacterial toxin expression has been shown to occur in *S. aureus* strains harboring the gene for toxic shock syndrome toxin (*13*). The surprising new finding is that PVL also acts as a positive regulator of adhesion expression.

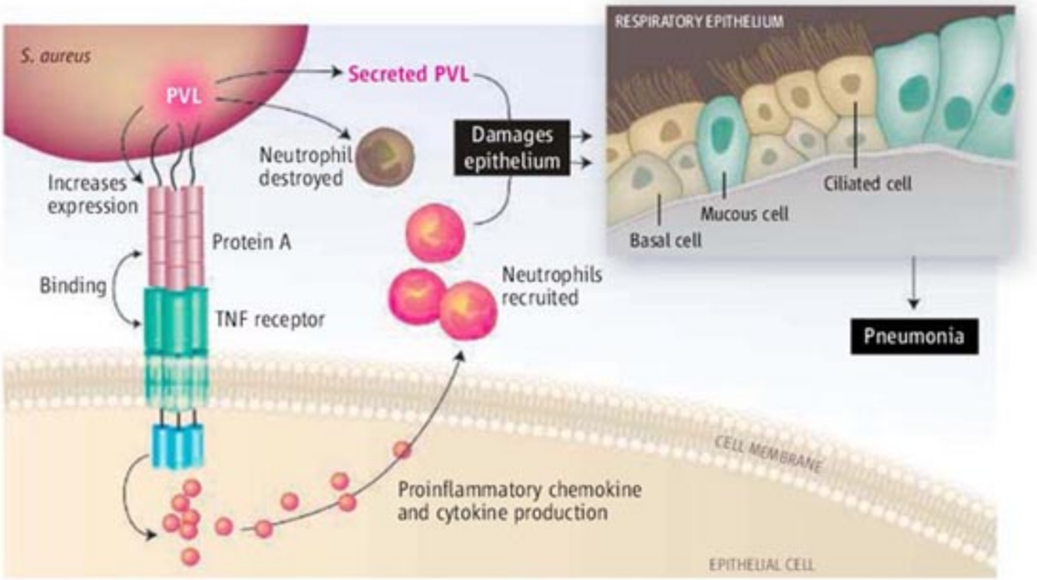

Busy toxin. The *S. aureus* protein PVL triggers a combination of events in an infected lung including the destruction of respiratory tissue and host defense cells (neutrophils) and increased inflammation. This ultimately leads to fatal necrotic pneumonia.

The authors are in the Institute of Medical Microbiology, University of Münster, Domagkstrasse 10, D-49149 Münster, Germany. E-mail: georg.peters@uni-muenster.de

The Labandeira-Rey *et al.* finding is especially important in light of the new proinflammatory role recently defined for protein A in pneumonia (see the figure). Protein A activates a receptor on the surface of respiratory epithelial cells that normally binds to the proinflammatory cytokine tumor necrosis factor–α. This triggers the recruitment of neutrophils to the lung, thus mimicking the effect of the cytokine (*14*). Using PVL-positive strains that cannot express protein A, Labandeira-Rey *et al.* show decreased severe infections in mice, and no animal deaths.

A clearer picture thus emerges of the lethal events that lead to hemorrhagic, necrotizing pneumonia. Concerted action of the bacterial adhesin protein A as well as the dual actions of PVL to boost protein A expression and lyse host cells reveal a new type of synergism among pathogenic factors. This is good reason to seek new diagnostics and therapeutics to fight the havoc that *S. aureus* can wreak.

References

1. F. D. Lowy, *N. Engl. J. Med.* **339**, 520 (1998).
2. *JAMA* **282**, 1123 (1999).
3. B. A. Diep *et al.*, *Lancet* **367**, 731 (2006).
4. S. K. Fridkin *et al.*, *N. Engl. J. Med.* **352**, 1436 (2005).
5. F. Vandenesch *et al.*, *Emerg. Infect. Dis.* **9**, 978 (2003).
6. L. G. Miller *et al.*, *N. Engl. J. Med.* **352**, 1445 (2005).
7. P. V. Adem *et al.*, *N. Engl. J. Med.* **353**, 1245 (2005).
8. Y. Gillet *et al.*, *Lancet* **359**, 753 (2002).
9. M. Labandeira-Rey *et al.*, *Science* **315**, 1130 (2007); published online 18 January 2007 (10.1126/science.1137165).
10. P. Dufour *et al.*, *Clin. Infect. Dis.* **35**, 819 (2002).
11. J. M. Voyich *et al.*, *J. Infect. Dis.* **194**, 1761 (2006).
12. S. deBentzmann *et al.*, *J. Infect. Dis.* **190**, 1506 (2004).
13. N. Vojtov, H. F. Ross, R. P. Novick, *Proc. Natl. Acad. Sci. U.S.A.* **99**, 10102 (2002).
14. M. I. Gomez *et al.*, *Nat. Med.* **10**, 842 (2004).

10.1126/science.1139628

MATERIALS SCIENCE

Better Geometry Through Chemistry

Chemically patterned flat surfaces can be made to crumple and fold in a controlled way.

Randall D. Kamien

In his lectures on physics, Feynman explained the properties of surfaces from the point of view of bugs living on them (*1*). Consider a bug that lives on a surface having a temperature that changes from place to place. Assume also that the bug and any ruler it uses to measure distance are made of the same material and expand and contract together as the temperature varies. The spatially varying temperature thus becomes a spatially varying distance scale. Feynman then shows how, by appropriately varying the temperature, we can convince the bug that it lives on a sphere, or a piece of a saddle, and so forth. In a similar vein, we can deduce that the world is round by measurements on the surface and do not need to view it from outer space.

This abstraction in which local measurements tell us about the global geometric properties of an object is known as intrinsic or Riemannian geometry (*2*). Although it forms the basis for Einstein's theory of general relativity, in which curved space-time causes gravitational attraction, Riemannian geometry is not only unnecessary but also incomplete when it comes to physical, two-dimensional surfaces in three dimensions. As reported on page 1116 of this issue, Klein *et al.* (*3*) have made clever use of the connection between the intrinsic geometry of a surface and how it sits in space. Instead of a temperature that changes from place to place on a sheet, they have locally altered the chemistry to make it locally expand and contract, changing the bug's ruler at each point. In so doing, they are able to force the sheets to twist, bend, and distort controllably and reversibly. Instead of molding materials into complex three-dimensional surfaces, Klein *et al.* have created self-folding materials through a beautiful connection between two- and three-dimensional geometry.

Why do potato chips curve into three-dimensional shapes, as shown in the top panel of the figure? Imagine drawing on the uncooked chip a regular grid that can be used to measure distances—the so-called "flat metric." As the slice is fried, different regions shrink by different amounts, warping the original grid. If we now try to draw a new regularly spaced grid on the deformed surface there will be, in general, no registry with the original grid. This is familiar: The lines of latitude and longitude on Earth cannot be laid onto a square grid without stretching the northernmost and southernmost land masses. Indeed, the whole point of Feynman's parable of the bugs is that merely by measuring distances on the surface of Earth, we can deduce its shape.

Can this shrinkage be controlled to fold a flat disc into a sphere or an even more complex object? Klein *et al.* have done just that. By changing the spatial concentration of *N*-isopropylacrylamide, a molecule that undergoes a dramatic, reversible reduction in volume at 33°C, they have programmed the final metric of the surface. Above the transition temperature, the flat gel discs fold into controllable three-dimensional shapes.

How does this happen? To accommodate the change in the grid, the thin sheet can either stretch or bend. Because thin sheets bend more easily than they stretch, they can more easily crumple into the third dimension than stretch (*4*), and the stresses are relieved through buckling. For instance, as shown in the middle panel of the figure, consider a disc with a wedge cut out of it. We can connect the two dashed lines to form a contiguous surface by stretching the disc until they meet. Alternatively, we can make a cone without stretching the original surface if we allow the

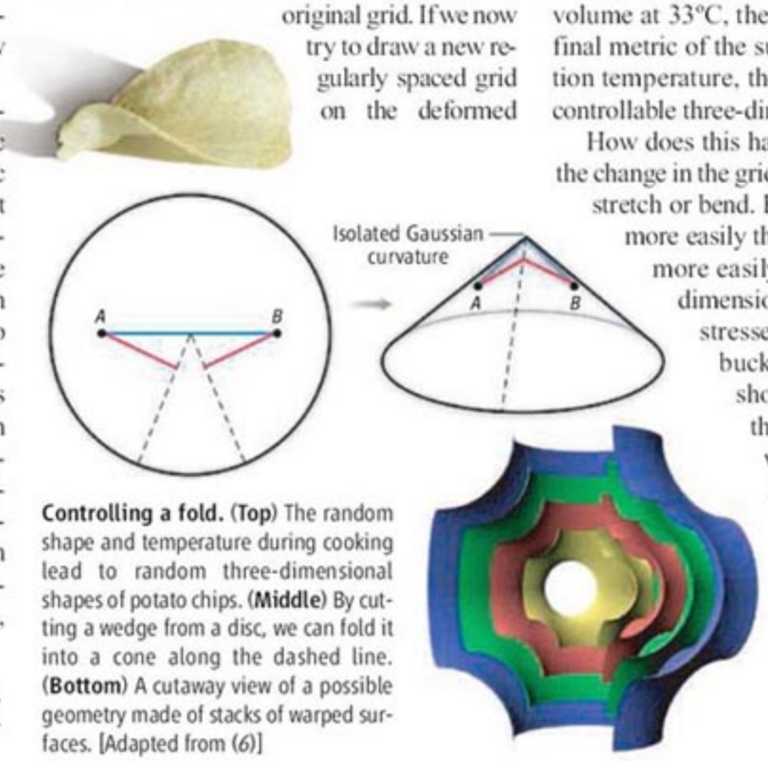

Controlling a fold. (**Top**) The random shape and temperature during cooking lead to random three-dimensional shapes of potato chips. (**Middle**) By cutting a wedge from a disc, we can fold it into a cone along the dashed line. (**Bottom**) A cutaway view of a possible geometry made of stacks of warped surfaces. [Adapted from (*6*)]

The author is in the Department of Physics and Astronomy, University of Pennsylvania, Philadelphia, PA 19104–6396, USA. E-mail: kamien@physics.upenn.edu

surface to buckle out into the third dimension. On the unstretched disc, the shortest distance between A and B is a straight line, the blue path. On the cone, however, the red path is connected and shorter than the blue path. The cone is flat except at the vertex, where there is intrinsic, or Gaussian, curvature. That is precisely what happens in these gel discs. Although a bug on the stretched surface and on the cone will observe the same two-dimensional, intrinsic geometry, our extrinsic view from outside the surface will be different.

In general relativity, there is no need for our four-dimensional, curved space-time to be embedded in a higher-dimensional space, but when it comes to materials, we see that this buckling into more dimensions enables Klein *et al.* to create, control, and manipulate surfaces, containers, and actuators. Moreover, controlling the geometry of sheets should make it possible for layered systems to self-assemble with intrinsic curvature, as shown in the bottom panel of the figure. These base units would come together to form triply periodic structures and, if mixed and matched properly with diblock copolymer architectures, can stabilize new and yet unseen morphologies. It may even be possible to assemble structures that are known for their useful photonic properties (*5*). This beautiful control of geometry only scratches the surface of how to create complex topologies and structures.

References

1. R. P. Feynman, R. B. Leighton, M. Sands, *The Feynman Lectures in Physics* (Addison Wesley, Reading, 1963), vol. 2, chap. 42.
2. M. Berger, *A Panoramic View of Riemannian Geometry* (Springer-Verlag, Berlin, 2003).
3. Y. Klein, E. Efrati, E. Sharon, *Science* **315**, 1116 (2007).
4. A. E. Lobkovsky, T. A. Witten, *Phys. Rev. E* **55**, 1577 (1997).
5. M. Maldovan *et al.*, *Phys. Rev. B* **65**, 165123 (2002).
6. B. A. DiDonna, R. D. Kamien, *Phys. Rev. Lett.* **89**, 215504 (2002).

10.1126/science.1138506

OCEANS

Climate Drives Sea Change

Changes in Arctic climate have contributed to shifts in abundances and seasonal cycles of a variety of species in the northwest Atlantic.

Charles H. Greene and Andrew J. Pershing

Ecosystems can shift rapidly from one state to another as a result of natural environmental variability, human activities (such as overfishing or human-induced climate change), or both. Recently, Frank *et al.* reported such an ecosystem regime shift in the northwest Atlantic during the early 1990s (*1*). To understand the likely causes for this shift, we here consider changes in the climate system that occurred at the same time.

Changes in climate beginning in the late 1980s resulted in an enhanced outflow of low-salinity waters from the Arctic (*2*) and a general freshening of shelf waters from the Labrador Sea to the Mid-Atlantic Bight (*3*–*5*). This freshening altered circulation and stratification patterns on the shelf and has been linked to changes in the abundances and seasonal cycles of phytoplankton, zooplankton, and fish populations (*6*, *7*).

In recent decades, the Arctic has experienced a period of historically unprecedented changes (*2*, *8*). In 1987, atmospheric pressure at the sea surface began to decline in the central Arctic. Two years later, this sea level pressure dropped precipitously, and a strongly cyclonic atmospheric regime emerged. This cyclonic regime increases the delivery of warmer, higher-salinity Atlantic water into the Arctic Ocean, mainly via the Barents Sea (see the first figure).

The ocean responds. Between the late 1980s and early 1990s, upper-ocean circulation in the Arctic Ocean changed substantially after an atmospheric regime shift. These changes included an increased inflow of relatively warm high-salinity Atlantic water into the Arctic Ocean through the Barents Sea and Fram Strait, a shift of the front separating Atlantic and Pacific water masses, a weakening and deflection of the Transpolar Drift, a reduction in size and intensity of the Beaufort Gyre, a thickening and intensification of the Arctic Ocean Boundary Current, and an increased discharge of relatively low-salinity water into the North Atlantic through both the Canadian Archipelago and Fram Strait.

C. H. Greene is in the Department of Earth and Atmospheric Sciences, Cornell University, Ithaca, NY 14853, USA. E-mail: chg2@cornell.edu A. J. Pershing is at the University of Maine and the Gulf of Maine Research Institute, 350 Commercial Street, Portland, ME 04101, USA.

Associated with these changes in the atmosphere and Atlantic water inflow, circulation in the upper layers of the Arctic Ocean changed substantially between the late 1980s and early 1990s (see the first figure). From an Atlantic perspective, the most important consequence of these changes was a redirection of the shallow outflow from the Arctic Ocean. Instead of entering the North Atlantic mainly via Fram Strait as before, much of this low-salinity outflow began to exit the Canadian Basin and enter the Labrador Sea via the Canadian Archipelago.

The cryosphere has also responded to changes in climate. During the past three decades, continental melting of permafrost, snow, and ice has increased substantially, which, combined with increased precipitation, has led to greater river discharge into the Arctic Ocean (*8*). Arctic sea ice has declined in both extent and thickness, with extensive summertime ice-free conditions observed to the north of Canada and Russia since 1978. Lindsay and Zhang (*9*) recently hypothesized that the atmospheric regime shift in 1989 and its effects on Arctic Ocean circulation patterns pushed the cryosphere into a new, internally perpetuating state of accelerated sea ice melting. An ice-albedo feedback mechanism may have maintained this accelerated melting even after the atmosphere shifted out of its strongly cyclonic mode during the mid-1990s (*10*).

Although anthropogenic climate forcing is considered to be responsible for the accelerated ice melting, the relative importance of human-induced versus natural climate forcing in driving the observed changes in atmospheric and oceanic circulation has not been fully resolved (*8*). Whether forced by human-induced climate change, natural climate variability, or some combination of the two, relatively low-salinity waters began to emerge from the Canadian Archipelago during 1989 and started to affect shelf ecosystems downstream from the Labrador Sea to the Mid-Atlantic Bight.

The first pulse of low-salinity water passed Georges Bank and reached the Mid-Atlantic Bight by 1991. Several years later, a second pulse advected even lower salinity waters downstream. This second pulse, although moving downstream from the Labrador Sea as well, probably originated from Fram Strait rather than the Canadian Archipelago (*2, 11*).

Northwest Atlantic shelf ecosystems shifted rapidly as they became notably fresher during the 1990s relative to the 1980s (see the second figure, top). This freshening enhanced stratification, resulting in greater phytoplankton production and abundance during the autumn (second figure, middle), a period when primary production would otherwise be expected to decline as thermal stratification breaks down and algae are mixed deeper in the water column and become increasingly light-limited (*6*). The increase in phytoplankton abundance coincided with a reorganization of the zooplankton assemblage: The abundance of smaller, shelf-associated copepods increased markedly (second figure, bottom) (*1, 7*). The largest of these increases occurred in late autumn/early winter, a change associated with the enhanced autumn phytoplankton abundance.

Early juvenile stages of the larger copepod species *Calanus finmarchicus* also increased in abundance with these smaller species; however, older stages became less abundant (*1, 7*). Increased size-selective predation by herring populations, which became much more abundant in the 1990s, may explain these observations.

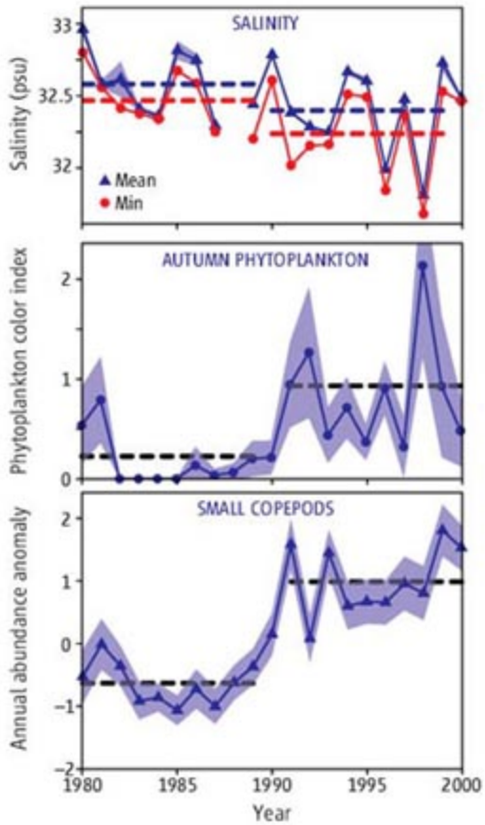

The ecosystem responds. Salinity, phytoplankton, and zooplankton data from the Gulf of Maine and Georges Bank illustrate ecosystem changes associated with regime shift. Dashed lines: mean values during 1980 to 1989 and 1990 to 1999; shaded areas: 95% confidence intervals. (**Top**) Decadal mean salinities, based on annual mean (blue) and annual minimum (red) salinities reported in (*5*), decrease after the regime shift. (**Middle**) Decadal mean autumn phytoplankton abundances, based on annual mean phytoplankton color index values reported in (*12*), increase after the regime shift. (**Bottom**) Decadal mean copepod abundances, based on annual mean small copepod abundance anomaly values reported in (*7*), increase after the regime shift.

Commercially harvested fish and crustacean populations have also undergone large changes in the northwest Atlantic since 1990 (*1, 7, 12–14*). Of particular importance is the collapse of cod stocks in the early 1990s. Overfishing is considered the main cause of this collapse, but the cold, Arctic-derived waters in the northern part of their range have probably hampered their recovery despite a decade-long fishing moratorium in the Canadian Maritime Provinces (*13*). Other fish and crustaceans have become more abundant during this period (*1, 7, 13*); for certain species, such as snow crab and shrimp, a release from cod predation appears to be the most likely explanation (*1, 14*).

In their original paper on this ecosystem regime shift, Frank *et al.* reported alternating changes in groundfish, benthic crustacean, zooplankton, and phytoplankton abundances (*1*). They attributed these observations to a "trophic cascade" initiated by the overfishing of cod. Certain prey species have indeed increased in abundance with a release from top-down control by cod, but it remains open to what extent the trophic cascade proposed by Frank *et al.* affects lower links in the food chain, especially phytoplankton and zooplankton. We suggest that, with or without the collapse of cod, a bottom-up, climate-driven regime shift would have taken place in the northwest Atlantic during the 1990s.

The resilience of northwest Atlantic shelf ecosystems is being tested by climate forcing from the bottom up and predator overexploitation from the top down. Predicting the fate of these ecosystems will be one of oceanography's grand challenges for the 21st century.

References and Notes

1. K. T. Frank *et al.*, *Science* **308**, 1621 (2005).
2. M. Steele *et al.*, *J. Geophys. Res.* **109**, 10.1029/2003JC002009 (2004).
3. S. Häkkinen, *Geophys. Res. Lett.* **29**, 10.1029/2002GL015243 (2002).
4. P. C. Smith *et al.*, *Deep-Sea Res., Part II* **48**, 37 (2001).
5. D. G. Mountain, *J. Geophys. Res.* **108**, 10.1029/2001JC001044 (2003).
6. E. G. Durbin *et al.*, *Mar. Ecol. Prog. Ser.* **254**, 81 (2003).
7. A. J. Pershing *et al.*, *ICES J. Mar. Sci.* **62**, 1511 (2005).
8. ACIA, *Arctic Climate Impact Assessment* (Cambridge Univ. Press, Cambridge, UK, 2005).
9. R. W. Lindsay, J. Zhang, *J. Clim.* **18**, 4879 (2005).
10. J. Morison *et al.*, *Geophys. Res. Lett.* **33**, 10.1029/2006GL026826 (2006).
11. I. M. Belkin. *Geophys. Res. Lett.* **31**, 10.1029/2003GL019334 (2004).
12. K. T. Frank *et al.*, *Ecol. Lett.* **9**, 1096 (2006).
13. H. Vilhjálmsson *et al.*, in *Arctic Climate Impact Assessment*, ACIA (Cambridge Univ. Press, Cambridge, UK, 2005), pp. 691–780.
14. B. Worm, R. A. Myers, *Ecology* **84**, 162 (2003).
15. This Perspective was developed during the synthesis phase of the U.S. GLOBEC Northwest Atlantic/Georges Bank Program.

10.1126/science.1136495

ASTRONOMY

Nebulae Around Evolved Stars

Noam Soker

How intricate nebula structures form has been a mystery, but a model based on a 20-year-old supernova explosion now suggests answers.

Despite many observations of impressive nebular structures around evolved stars, there is no acceptable theory that explains their formation. Such structures include multiple-ring systems, hourglass-shaped nebulae, and butterfly-type morphologies, and they are found around quietly dying Sun-like stars as well as around massive stars that explode as supernovae (see the figure). The formation mechanism of these structures is connected to the most puzzling questions regarding stellar evolution: What is the role of rotation as matter collapses to form a star, and how does stellar rotation evolve from the birth to the death of stars?

As reported on page 1103 of this issue, Morris and Podsiadlowski (*1*) propose a model for the formation of the triple-ring system of supernova (SN) 1987A, a supernova whose explosion was detected 20 years ago. The model is based on fast rotation of the progenitor star, and the authors nicely pinpoint the crucial role of stellar rotation. In particular, they attribute the fast rotation of the progenitor of SN 1987A to a stellar companion that was swallowed by the progenitor about 20,000 years before the explosion.

Knowledge of stellar processes does not come easily. For about a hundred years, from the middle of the 19th century to the middle of the 20th century, the major question in the field of stellar structure and evolution was the energy source of stars. Fierce arguments raged between scientists who thought that gravitational energy powered the stars and those who thought another process was at work. At the beginning of the 20th century it became clear that nuclear reactions are the source of energy in the Sun and other stars. It took another 50 years and the efforts of great scientists such as Arthur Eddington and Hans Bethe to identify the major nuclear reactions in stars.

In the past 40 years, the major open questions in the field of stellar evolution have been related to the role and evolution of rotation (or angular momentum) in stars and in gaseous disks around stars. Are magnetic fields required to transport angular momentum in gaseous disks around stars? How can two oppositely directed and well-collimated jets be emitted by such disks? How are jets responsible for the gamma-ray burst phenomena formed from collapsing rotating massive stars? What is the mechanism that shapes gaseous nebulae around evolved stars?

Morris and Podsiadlowski address this last question. The gaseous nebulae around evolved stars are made of gas that once was part of the envelope of the central star. This gas was expelled via a strong wind from the stellar surface when the star was a red giant star close to the end of its nuclear activity. At this stage, the star was several hundred times the present size of the Sun and its surface temperature was a few thousand kelvin. With a huge luminosity and low surface gravity, these stars eject mass at a very high rate.

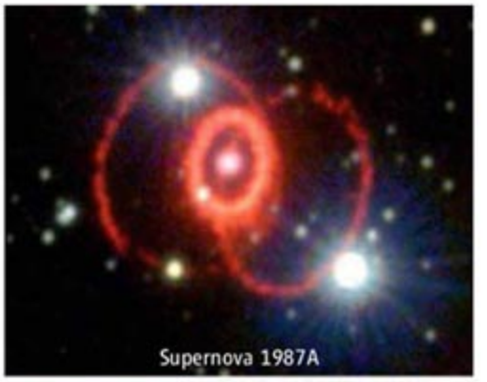

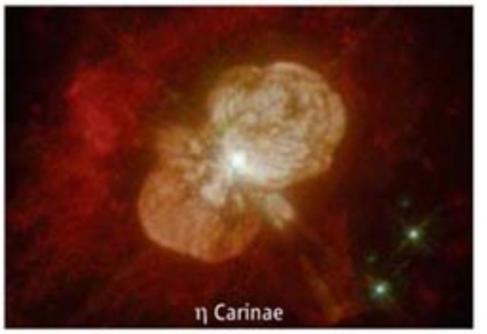

Sun-like stars completely deplete their envelopes because of this wind, leaving behind the compact core, which evolves to become a compact hot star termed a white dwarf. The core then ionizes and heats the nebula to 10,000 K, allowing the nebula to glow and form a planetary nebula. Stars more massive than about 10 times the mass of the Sun explode as supernovae and light up the surrounding nebula with a bright flash of light. SN 1987A was a star about 20 times as massive as the Sun; on 23 February 1987 it was observed to explode and light up its surrounding triple-ring system.

For about 40 years, researchers have debated whether single stars can form such nonspherical structures (as seen in the figure) or whether a binary companion is required for this nonspherical mass loss geometry from evolved stars. This debate intensified about 15 years ago with the analysis of highly detailed images from the Hubble Space Telescope and several other large telescopes, as well as data from the triple-ring system observed around SN 1987A (*2*). It is now becoming clear that a single evolved star cannot rotate fast enough to form nonspherical nebulae, and a binary companion is required. In some cases, even a massive planet is sufficient to lead to a nonspherical wind.

There are several processes by which a companion can lead to the different structures

A gallery of nebulae. (**Top**) Supernova 1987A with its triple-ring system was first observed on 23 February 1987. The rings were formed thousands of years before the explosion. One large ring is in front of the star and the other one is behind the star; a small ring is located around the star. All the rings are circular but appear elliptical because of the angle of observation. (**Upper middle**) The massive binary star η Carinae has a bipolar nebula called Homunculus. The star is 120 times as massive as the Sun and is expected to become a supernova in the relatively near future. (**Lower middle**) The Red Rectangle is a star evolving to become a planetary nebula and has a stellar companion. (**Bottom**) The Hourglass planetary nebula (MyCn 18) was ejected by the central star, now a dying Sun-like star seen as a white dot in the center.

CREDITS: (TOP TO BOTTOM) C. BURROWS/ESA/STSCI AND NASA; J. HESTER/ARIZONA STATE UNIVERSITY/NASA; H. VAN WINCKEL/CATHOLIC UNIVERSITY OF LEUVEN, BELGIUM AND M. COHEN/UNIVERSITY OF CALIFORNIA, BERKELEY/NASA/ESA; R. SAHAI AND J. TRAUGER/JPL/WFPC2 SCIENCE TEAM/NASA

The author is in the Department of Physics, Technion, Haifa 32000, Israel. E-mail: soker@physics.technion.ac.il

observed. They can be classified into two groups. In one, the companion is swallowed by the primary star, and it spirals inward inside the primary envelope toward the primary core. In some cases the companion survives; in other cases it is destroyed in the envelope. In the second type of process, the companion stays outside the envelope and influences the primary stellar wind from outside. Morris and Podsiadlowski consider the first scenario and build a model where the progenitor of SN 1987A swallowed a companion about 20,000 years before the explosion. The companion caused the progenitor's envelope to spin at such a high speed that the envelope became extremely flat, resulting in a wind geometry that led to the formation of the two large outer rings (upper panel in the figure).

Although their model has several advantages, such as providing a good explanation for the required amount of rotation (angular momentum), and it sheds some light on the formation of the outer rings of SN 1987A, it cannot be considered as a general model for other similar objects, and it is not the last word on the formation of the rings of SN 1987A. The reason is that in some other systems we see similar nebulae, but the companion is outside the primary envelope and has not been swallowed by it. Examples are η Carinae and the Red Rectangle (see the figure).

Astrophysicists must continue their quest for the different mechanisms that shape nebulae formed by evolved stars. Projecting from the hundred years that were required to understand the production of energy in stars, we may expect that this research will take tens of years more before we fully understand how nebulae form around dying stars.

References

1. T. Morris, P. Podsiadlowski, *Science* **315**, 1103 (2007).
2. B. Balick, A. Frank, *Annu. Rev. Astron. Astrophys.* **40**, 439 (2002).

10.1126/science.1139937

CHEMISTRY

Charge Flipping and Beyond

By combining different kinds of structural data and an innovative analysis method, crystal structures of materials previously thought too complex or disordered can now be solved.

Hermann Gies

In recent decades, solving crystal structures has become routine for crystals of moderate complexity (with several hundred atoms in the unit cell). Automated procedures now exist for the entire structure-solving process. But challenges remain, both in extending computational methods to macromolecules (*1*, *2*) and solving crystal structures from powder diffraction data of limited resolution (*3*). Powder diffraction is used for crystal structure determination in cases where sufficiently large crystals cannot be obtained. For example, zeolite catalysts are often synthesized as microcrystalline powders, precluding single-crystal techniques for structural elucidation. However, powder diffraction data suffer from severe signal overlap, making interpretation difficult.

On page 1113 of this issue, Baerlocher *et al.* (*4*) present a new and possibly revolutionary approach to solving crystal structures. Their approach is based on the "charge flipping" method, which uses information both in reciprocal space (the diffraction data) and in physical space (the crystal structure) in a recursive manner to determine the unknown crystal structure. By combining this method with results from electron microscopy, the authors can solve complex structures from powder diffraction data.

The idea of charge flipping was first introduced by Oszlányi and Sütő (*5*, *6*). For this extremely simple structure solution method, no information on the crystal's chemical composition or its symmetry is required. All one needs is a crystal of sufficient quality for diffraction experiments.

Information about the composition and spatial arrangement of atoms in the unit cell of the crystal can be derived from experimentally measured diffraction intensities. In charge flipping, these structure factors are combined with a random set of phases. From this information in reciprocal space, an electron density grid is calculated in physical space. Next, the calculated electron density grid is analyzed and the sign for all values below a chosen threshold value is changed (flipped). From this modified electron density grid, new structure factors are calculated. The iteration cycle is completed by calculating the electron density again.

Once the investigator has picked the threshold values, the subsequent iteration

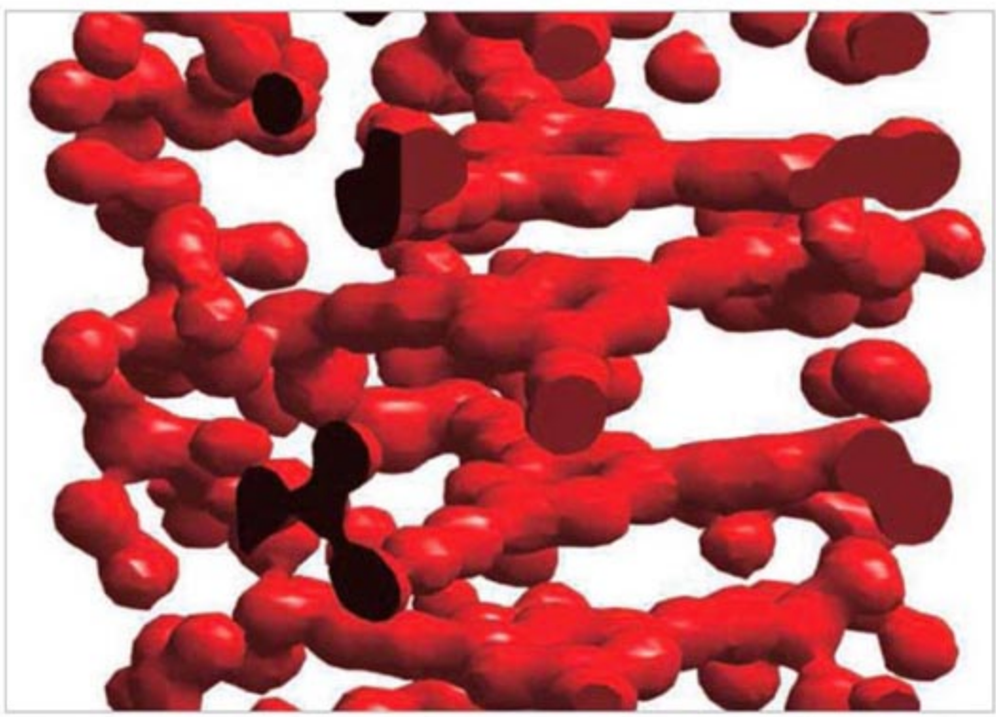

Structures from charge flipping. This isosurface plot shows the electron density distribution of a molecular crystal, as revealed from the charge-flipping process. The density maxima represent atomic positions. [Reproduced with permission from (*8*)]

The author is in the Department of Geology, Mineralogy, and Geophysics, Ruhr-Universität Bochum, 44801 Bochum, Germany. E-mail: hermann.gies@ruhr-uni-bochum.de

process proceeds without human interference until convergence. Depending on the starting set of random phases, the whole process might take several thousand iterations. For the examples studied so far, convergence was reached after a minute or so. The result is the true electron density map of the unknown crystal structure.

Baerlocher *et al.* previously applied charge flipping to powder diffraction data of moderate complexity (*7*). They now combine this approach with information from high-resolution electron microscopy. Phases can be determined from the electron microscope images and can be used to guide the otherwise random charge-flipping process.

To test the new approach, the authors use the most complicated known zeolite material, IM-5, whose crystal structure has resisted determination for almost 10 years (*4*). IM-5 has a large unit cell of 864 atoms and is pseudosymmetric (that is, parts of the crystal structure are similar but not the same), making it extremely challenging to solve its structure. The success in solving this crystal structure proves the power of the combined approach.

Structure solution by charge flipping does not yield a set of spatial coordinates for the atomic positions of the constituents, but rather the electron density distribution in physical space (see the figure). Where high-resolution diffraction data are available, interpretation of the data is straightforward. The electron density data easily provide atomic positions as electron density maxima. Interpretation is less straightforward for materials with restricted crystallinity, such as disordered materials. Here, broadened diffraction peaks lead to low-intensity maxima and peak overlap for reflections at high diffraction angles. The resulting lower-resolution data would only yield electron densities from structure fragments. However, chemists should easily be able to identify these fragments based on complementary information.

The inventors of the charge-flipping technique cautiously proposed that the technique might succeed where other methods fail. Baerlocher *et al.*'s visionary work goes well beyond these original expectations. By solving a highly complicated crystal structure, the authors demonstrate the power of the technique and show how complementary information can assist the structure-solving process. They open up new horizons for solving crystal structures of any complexity and size, of any type of material—be it inorganic, organic, or biological.

References

1. T. R. Schneider, G. M. Sheldrick, *Acta Crystallogr. D* **58**, 1772 (2002).
2. G. M. Sheldrick, *Z. Kristallogr.* **217**, 644 (2002).
3. J. Rius, *Z. Kristallogr.* **219**, 826 (2004).
4. C. Baerlocher *et al.*, *Science* **315**, 1113 (2007).
5. G. Oszlányi, A Sütő, *Acta Crystallogr. A* **60**, 134 (2004).
6. G. Oszlányi, A Sütő, *Acta Crystallogr. A* **61**, 147 (2005).
7. C. Baerlocher, L. B. McCusker, L. Palatinus, *Z. Kristallogr.* **222**, 47 (2007).
8. G. Oszlányi, A. Sütő, M. Czugler, L. Parkanyi, *J. Am. Chem. Soc.* **128**, 8392 (2006).

10.1126/science.1140022

PLANT SCIENCE

Nibbling at the Plant Cell Nucleus

When plants recognize certain pathogens, an activated immune receptor moves to the nucleus where it affects transcription to initiate a successful response.

Jeffery L. Dangl

Plants deploy an innate immune system that recognizes and responds to different sorts of molecules produced by microbes (*1*). At a quick glance, the system seems segregated into two distinct branches, each using different "molecular antennae," or protein receptors, to sense microbes. But activation of receptors in either branch triggers a largely overlapping set of plant cellular responses, including a major reprogramming of gene expression that can halt microbial growth. On page 1098 of this issue, Shen *et al.* (*2*) show that specific recognition of a fungal pathogen requires the function of the relevant receptor, surprisingly, in the plant cell nucleus. A similar publication in *PLoS Biology* from Burch-Smith *et al.* suggests the same (*3*). Together, the studies reveal a means by which the plant innate immune system can balance the requirement for a swift and effective defense response with the possible dangers of autoimmunity. These results, if generalized to the function of other plant immune receptors, could point to a basic operating mechanism for the pathogen-specific branch of the plant immune system.

Immune receptors at the cell surface recognize common microbial-associated molecular patterns (MAMPs) (*4*), such as bits of bacterial flagellin or cell wall. These receptors are akin to the well-studied Toll-like receptors of animal innate immune systems. The output from this extracellular branch of the immune system is a defense response sufficient to stop growth of nonpathogenic microbes. Yet pathogens can, by definition, overcome this defense by secreting effector molecules, which act as virulence factors to dampen or inhibit it.

The second branch of the plant immune system, composed of intracellular receptors, responds to these virulence factors. The intracellular receptors are characterized by nucleotide-binding and leucine-rich repeat domains [so-called NB-LRR ("Nibbler") proteins]. NB-LRR proteins are structurally analogous to the animal NOD/NLR/CATERPILLAR superfamily of intracellular proteins. They also act as microbial sensors, some of which play critical roles in human diseases such as Crohn's disease and cold-induced autoinflammatory syndrome (*5*). Plant NB-LRR proteins are activated upon delivery of a virulence factor into the cell's interior by viral, bacterial, fungal, oomycete, or insect pathogens (*1*). Receptor activation involves intramolecular rearrangements that are likely to "open" the NB domain, allowing cleavage and cycling of its bound nucleotide. This presumably allows the amino-terminal domain of the receptor to interact with downstream signaling molecules that trigger the defense response (*6*).

Although defense responses from the two immune system branches are qualitatively similar, activation of NB-LRRs leads to a faster and stronger response that can include rapid cell death at and surrounding the infection site. Chronic or auto-activation of this output response is dangerous—cell death, stunting of plant growth, and loss of seed yield can result (*7*, *8*). Hence, the plant immune system must discern the difference between a harmless or helpful microbe and a pathogenic one, and translate that recognition into an appropriately graded output, which can include host cell death. The output is controlled in the nucleus by plant-specific transcriptional regulators, many of which are members of the WRKY family (*9*).

NB-LRR proteins inhabit a variety of subcellular locations, from the inner face of the cell membrane to the cytosol (*1*). Biochemical fractionation of barley NB-LRR proteins (MLA proteins) indicates localization to solu-

The author is in the Department of Biology, the Curriculum in Genetics, and the Carolina Center for Genome Sciences, University of North Carolina, Chapel Hill, NC 27599, USA. E-mail: dangl@email.unc.edu

ble and intracellular membrane fractions. These experiments used transgenic barley plants expressing native levels of MLA (*10*). However, transient overexpression of a functional fusion protein consisting of MLA and a fluorescent protein (MLA-YFP) revealed cytoplasmic and nuclear localization in barley cells (*2*). Shen *et al.* demonstrate that if MLA-YFP is fused to an amino acid sequence that excludes MLA-YFP from the nucleus, then function is lost. Moreover, the authors show that a very small fraction of native MLA is constitutively present in the nucleus. Hence, MLA proteins function in the nucleus despite their lack of a discernible nuclear localization signal. This result should serve as a caution to all biologists that the location of a functional protein may not be its site of action.

Shen *et al.* further demonstrate that the amino terminus of MLA interacts with two closely related WRKY transcriptional regulators. These WRKY proteins belong to a small clade within this large protein family in both barley and the model plant *Arabidopsis thaliana*. Members of this clade are negative regulators of defense gene transcription, shutting down the expression of genes normally triggered by MAMPs and the extracellular branch of the plant innate immune system. Shen *et al.* demonstrate that this is true for both barley and *Arabidopsis* defense responses against otherwise virulent pathogens. The ability of these particular WRKY proteins to repress plant defense extends to blocking MLA-dependent disease resistance as well, indicating that the defense response is generic and that NB-LRR proteins somehow hyperactivate it.

The two WRKY proteins in question are constitutively located in the nucleus. When transiently overexpressed as fluorescent fusion proteins, WRKY and MLA proteins interact with each other in the nucleus, but only when a functional fungal effector protein is also present in the plant cell. Recall that these specific effectors are likely to be pathogen virulence factors whose activity inside the plant cell is sensed by specific NB-LRR proteins, in this case MLA. Shen *et al.* demonstrate that only the expression of specific alleles of a MLA gene and pathogen effector gene will lead to interaction of MLA and WRKY in the nucleus. It is not yet known whether the pathogen effector protein interacts with cytosolic or nuclear MLA. However, Burch-Smith *et al.* (*3*) demonstrate that another NB-LRR protein also acts in the nucleus, and that effector molecule recognition clearly occurs in the cytoplasm. Hence, either the activation of these NB-LRR receptors drives relocalization of a subfraction into the nucleus, or an activation signal is transduced into the nucleus where it acts on the receptor pool already present there.

Shen *et al.* conclude that the WRKY proteins of this small clade repress defense responses, and that activation of MLA proteins by pathogens blocks this repressor activity, allowing for rapid and efficient disease resistance responses (see the figure). The switch from repression to activation of the defense response may be simple in that both WRKY proteins—bound to target defense genes but also in contact with activated MLA—might become transcriptional activators. Alternatively, the WRKY-MLA interaction might preclude repressor function, allowing for assembly of transcriptional activators to kick-start the transcriptional reprogramming required for a successful defense response.

There is precedence for the former model from studies of the mammalian CIITA protein, the original member of the NOD/NLR/CATERPILLAR superfamily (*5*). Expression of defense genes (in this case, of the major histocompatibility complex) requires binding of activated CIITA to a complex of transcription factors (called the enhanceosome). Recall that a minute fraction of MLA is present in uninfected plant cell nuclei. It will be important to define chromatin-bound versus unbound MLA levels, and to understand whether MLA is constantly cycling into and out of the nucleus, waiting to be activated.

Other tantalizing results suggest that NB-LRR association with transcriptional regulators may be a common mechanism to activate the plant immune system. The plasma membrane–localized NB-LRR protein RPM1 interacts with a transcriptional regulator (polymerase II accessory protein) that also acts as a repressor of the plant defense response (*11*). There is also an intriguing "Rosetta Stone" fusion of an NB-LRR and a WRKY called RRS1 (*12*). This type of fusion unites proteins, or protein domains that are typically encoded by separate genes but that function together, in much the way that MLA and WRKY come together in the nucleus, following activation. It may be the case that the expansion of plant-specific transcriptional regulator gene families is evolutionarily driven, at least in part, by the need for their continued functional coupling to NB-LRR proteins, whose evolution is, in turn, pathogen-driven.

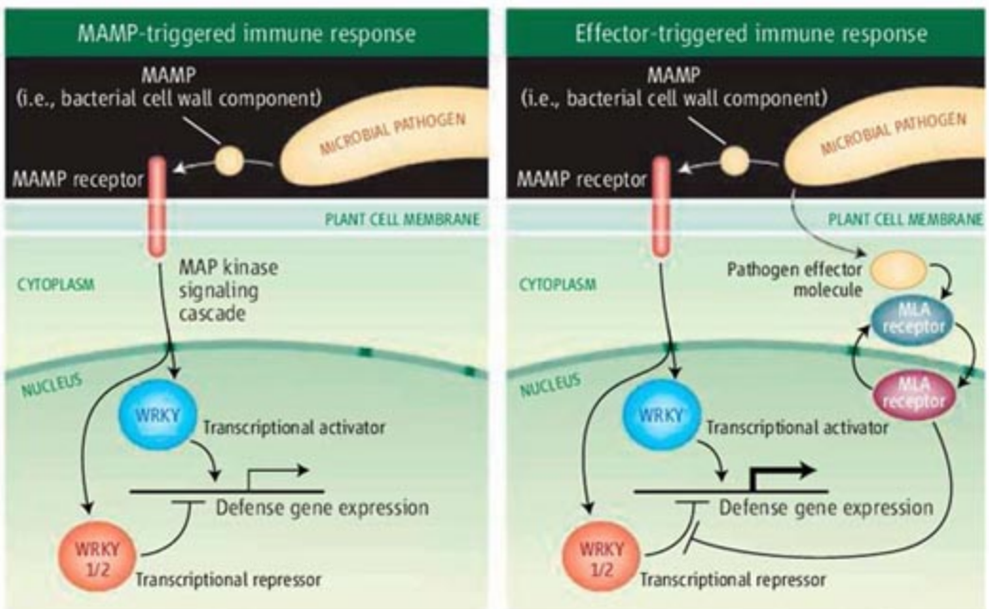

A balanced defense. Plant immnue system receptors are poised both at the cell surface and within the cell to sense microbial molecules. A weak, basal response to a pathogen (**left**) does not harm the plant itself. A stronger and more rapid response (**right**) may drive the attacked host cells to their death. The latter response requires one receptor pathway to interact with, and modulate, the other, as shown, to potentiate expression of defense genes.

References

1. J. D. G. Jones, J. L. Dangl, *Nature* **444**, 323 (2006).
2. Q.-H. Shen *et al.*, *Science* **315**, 1098 (2007); published online 21 December 2006 (10.1126/science.1136372).
3. T. M. Burch-Smith, *PLoS Biol.* **5**, e68 (2007).
4. F. M. Ausubel, *Nat. Immunol.* **6**, 973 (2005).
5. J. P. Ting, D. L. Kastner, H. M. Hoffman, *Nat. Rev. Immunol.* **6**, 183 (2006).
6. F. L. Takken, M. Albrecht, W. I. Tameling, *Curr. Opin. Plant Biol.* **9**, 383 (2006).
7. Y. Zhang, S. Goritschnig, X. Dong, X. Li, *Plant Cell* **15**, 2636 (2003).
8. A. J. Heidel, J. D. Clarke, J. Antonovics, X. Dong, *Genetics* **168**, 2197 (2004).
9. T. Eulgem, *Trends Plant Sci.* **10**, 71 (2005).
10. S. Bieri *et al.*, *Plant Cell* **16**, 3480 (2004).
11. B. F. Holt III *et al.*, *Dev. Cell* **2**, 807 (2002).
12. L. Deslandes *et al.*, *Proc. Natl. Acad. Sci. U.S.A.* **100**, 8024 (2003).

10.1126/science.1138991

SCIENCE DIPLOMACY

Arab, U.S. Women Scientists Build Network at Landmark Kuwait Forum

KUWAIT CITY—It was, in some respects, a typical science conference, with panels on career development, workshops on publishing and grant-writing, and a busy schedule of social events each night. But this one was different: It brought scientists and engineers from throughout the Middle East, Northern Africa, and the United States to an Arab capital for talks that stressed partnerships and cooperation—and virtually all of the participants were women.

Samira Islam, head of the Drug Monitoring Unit at King Fahd Medical Research Center in Jeddah, Saudi Arabia

At the opening of the International Conference on Women Leaders in Science, Technology, and Engineering, co-sponsored by AAAS, many of them said they'd never attended anything like it. Accomplished Arab women often "are not only unseen, but are hidden from each other," said Ikhlas Abdalla, an expert in human resources development for the Arab Fund for Economic and Social Development.

While it explored challenges still confronting women scientists and engineers in the Arab world—and in many other parts of the world—the conference also revealed diversity and progress not often conveyed in Western news reports from the region. And in a time of rising mistrust and conflict, the conference showed a way toward constructive engagement of nations and cultures based on science and technology.

"In addition to just meeting people and learning about the diversity in the region, there was a hopefulness that filled the room," Shirley Malcom, head of Education and Human Resources at AAAS, said afterward. "You had a sense that many of the women came out of this conference with a new realization of some possibilities for the future, and they were going to go home and apply that in their work. And you could say the same for many people in the U.S. group, too."

Held 8–10 January at the elegant Arab Organizations Headquarters Building, the conference drew more than 200 scientists and engineers from 18 nations in the Middle East and Northern Africa and a delegation of about 20 from the United States. It was held under the patronage of Kuwaiti Prime Minister Sheikh Nasser Al Mohammed Al Ahmed Al Sabah. It was organized by the Kuwait Institute for Scientific Research; the Kuwait Foundation for the Advancement of Science; the Arab Fund for Economic and Social Development; the U.S. State Department; and AAAS.

AAAS's delegation was led by Chief Executive Officer Alan I. Leshner, who also serves as executive publisher of *Science*, and also included Malcom; *Science* Executive Editor Monica Bradford; and Chief International Officer Vaughan Turekian, who played a central role in organizing the event.

AAAS in recent years has been building its engagement with the Middle East and Northern Africa. Officials have written and held conferences on the state of science in Iraq. AAAS Science & Technology Policy Fellows have organized the creation of the Iraq Virtual Science Library and a conference in Jordan on the uses of geographic information systems to foster sustainable urban development. This month, on 19 February, a half-day symposium on the role of women and innovation in the Arab world was held at the AAAS Annual Meeting in San Francisco.

On the morning that the Kuwait conference opened, the *Kuwait Times* published a commentary co-authored by Leshner and Farkhonda Hassan, a professor of geology at the American University in Cairo, a member of the Egyptian Parliament, and secretary-general for the National Council for Women in Egypt.

"In a world growing ever-smaller, no single nation, no region or culture, owns science," they wrote. "While researchers may speak many languages, they share a common dedication to science as a rational process of problem-solving that holds enormous promise for the well-being and advancement of all humanity."

In the opening address delivered on behalf of the Kuwaiti prime minister, Deputy Prime Minister Mohammad Sabah Al-Salem Al-Sabah said young women "are becoming an important asset" to the nation's advancement. "We want more women to take part in the developmental process of the nation through their contributions to the society on firmly rational grounds," said Al-Sabah, who also serves as foreign minister.

Paula Dobriansky, the U.S. undersecretary of state for democracy and global affairs and a leader in developing the idea for the event, expanded on that sentiment in a later address. "International science cooperation is at its best when it provides opportunities for women, and draws on their resources and strengths, thus greatly expanding our capacity for achievement," she said. "Science and technology empower individuals, and empowerment gives hope—which is the antithesis of many of the problems that fuel the world's current conflicts."

Leshner, in one of the opening talks of the forum, emphasized the theme of global S&T collaboration in the post-9/11 world. His talk elicited a poignant exchange with epidemiological psychiatrist Rafia Ghubash, president of both Arabian Gulf University in Bahrain and the Arab Network of Women in Science and Technology. She expressed regret for the attacks of 9/11 and acknowledged that in the current climate it will take time to repair relations between Arabs and Americans.

"I would like, at this conference, to talk seriously that we would like to work with the American people—but outside the political agenda," Ghubash said.

Leshner immediately agreed. "We believe science is the apolitical, or nonpolitical, vehicle, and should be used for far greater communication generally around the world," he said. "[It] can be a very important vehicle for peace."

SCIENCE POLICY

New Site Tracks S&T Legislation

With climate change, national security, innovation, and other science- and technology-related issues prominent on the U.S. national agenda, AAAS has launched a new site that will track S&T legislation as it moves through Congress.

You can find the list at www.aaas.org/spp/legtracker.

The site details the names, sponsors, and status of bills pending in the U.S. Senate and House of Representatives and includes links to other useful resources. It will be managed and updated regularly by the AAAS Center for Science, Technology, and Congress.

Paula Dobriansky (center), U.S. undersecretary of state for democracy and global affairs

The progress made by Arab women—and the challenges still confronting them—were captured in a presentation by Samira Islam, a pioneering Saudi Arabian pharmacologist and scholar who serves as head of the Drug Monitoring Unit at King Fahd Medical Research Center in Jeddah. In earlier writings, she noted that the tenets of Islamic belief stress gender equality and that the teachings of the Prophet Muhammad require every Muslim to seek knowledge.

But, she said at the conference, the West often sees the Arab world—and Arab women—simplistically. With 321 million people in 22 countries, the region "cannot be viewed as a single monolithic community in term of endowment or human development," she said.

Citing 2005 statistics reported by UNESCO, Islam reported that women comprised 74% of science graduates in Bahrain, 71% in Qatar, and 47% in Lebanon; in the U.S., 43% of science graduates were women, and in Japan, 25%. In Saudi Arabia, among six major universities that admit women, nearly 45% of science graduates in 2004-05—nearly 8700 in all—were women.

Once out of school, however, the opportunities available to Arab women are diminished, Islam found. In Saudi Arabia and other countries, jobs in S&T education and research go disproportionately to men, as do government grants for research. "The glass ceiling is still existing for women in the Arab region and around the world," she said.

In presentations and informal discussions, the Arab women detailed the cultural practices that create obstacles: family values that often are biased toward the success of male children; expectations that women are responsible for cooking and child-rearing; social restrictions on interacting with men, which makes networking difficult; and limited options for mentoring.

"The problem is not the number of women attending schools, or high schools or universities—the problem is what are they doing afterwards," said microbiologist Maysa Azzeh, a Palestinian and assistant professor in the Department of Immunology and Microbiology at al-Quds University in Jerusalem. "Most of them and their parents are actually more worried about are they going to get married and have kids or not. And this is not only an Arabic problem—it is an international problem. But it is more focused and clear in our society."

By the meeting's end, participants had identified strategies for further progress: mentoring; local and international networking; establishing local science centers for students; giving boys and girls the same opportunities.

And whether from the Middle East, Northern Africa or the United States, they expressed hope that the Kuwait conference would be followed by sustained action—exchanges, research collaborations, workshops, and conferences—that would contribute to a cross-cultural engagement of women, and men, in S&T.

In the closing minutes of the forum, Fatima Ahmed Alhadi, an assistant professor of plant physiology at the University of Sanaá in Yemen, asked for the microphone. She was dressed conservatively—a black robe, her hair covered in a black scarf, her face hidden behind a black veil, except for her eyes.

Fatima Ahmed Alhadi, assistant professor of plant physiology at the University of Sanaá in Yemen

"Women scientists in Yemen are very much underestimated," she said confidently in English, "maybe because we come from a country that really doesn't believe in woman as a woman in any field, especially in science. We have very distinguished scientists and very active girls who would like to be distinguished in science, but they don't have that chance, or they don't get that chance.... We would like, after we come home, to be more distinguished in our country and be more active and achieve all our expectations in the field of science."

EDUCATION

Project 2061 Offers Climate Change Teaching Guide

Project 2061, AAAS's influential science literacy initiative, has released a new guide that will help prepare educators to teach today's students about the science and societal implications of changes in the global climate that are already shaping the future.

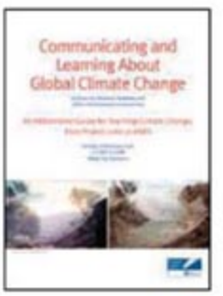

The teaching guide, *Communicating and Learning About Global Climate Change*, is based on *Science for All Americans* and the *Atlas of Science Literacy*, two seminal science education documents published by Project 2061. Using these two resources, the guide describes what adults should know about climate change and then shows how students work toward that knowledge as they move from kindergarten through high school. The guide was included in a special teachers' kit distributed during a town hall event on climate change held this month at the AAAS Annual Meeting in San Francisco.

"This guide brings together several different strands—from the water cycle and the atmosphere and the dynamic nature of ecosystems to evaluating scientific evidence, using energy resources, and making decisions about technology—that are essential to understanding the science of climate change and its implications," said Jo Ellen Roseman, director of Project 2061. "By laying out the basic science concepts that are important for understanding climate change and showing how they relate to one another, teachers can gain a good picture of what a science-literate person should know and be able to do as a concerned and well-informed citizen."

For instance, the guide shows how lessons on the Earth's resources can wend their way from a first-grader's discovery of the kinds of fuel used to heat homes around the world, to a fifth-grader's understanding of pollution and a high school student's grasp of the economic and social tradeoffs in using different fuel resources.

Project 2061, a long-term project of AAAS to boost American understanding of science and mathematics, produced a similar teachers' guide on evolution for the 2006 Annual Meeting in St. Louis, which "was very popular," according to Mary Koppal, Project 2061 communications director.

The teachers' kit also included a classroom version of the game "Stabilization Wedges," developed by Princeton University's Carbon Mitigation Initiative (CMI). Teams play the game by choosing a variety of strategies—from more fuel-efficient cars to nuclear power—to keep world carbon emissions from doubling over the next 50 years. The game has its roots in a 2004 *Science* article by Princeton researchers Robert Socolow and Stephen Pacala. There are no right or wrong answers in the game, but judges pick a winner based on how well they defend the merits of their particular mix of strategies.

"It's always worked well in the environments we've played with, researchers and industry folk, but we thought if we put it in the hands of 500 teachers, they would probably come up with all kinds of fantastic ideas," said Roberta Hotinski, a science communicator at CMI who helped develop the game.

Along with the guide and game, teachers at the town hall received a copy of AAAS's new video on climate change, which focuses in part on the Alaskan village of Shishmaref, and a letter of participation reflecting three hours' worth of professional development. To receive a copy of the Project 2061 teaching guide, contact Mary Koppal at (202) 326-6643 or mkoppal@aaas.org.

—*Becky Ham*

A Route to the Brightest Possible Neutron Source?

Andrew Taylor,[1*] Mike Dunne,[1] Steve Bennington,[1] Stuart Ansell,[1] Ian Gardner,[1] Peter Norreys,[1] Tim Broome,[1] David Findlay,[1] Richard Nelmes[2]

We review the potential to develop sources for neutron scattering science and propose that a merger with the rapidly developing field of inertial fusion energy could provide a major step-change in performance. In stark contrast to developments in synchrotron and laser science, the past 40 years have seen only a factor of 10 increase in neutron source brightness. With the advent of thermonuclear ignition in the laboratory, coupled to innovative approaches in how this may be achieved, we calculate that a neutron source three orders of magnitude more powerful than any existing facility can be envisaged on a 20- to 30-year time scale. Such a leap in source power would transform neutron scattering science.

Neutron scattering provides a powerful probe of the structure and dynamics of condensed matter, complementary to x-ray and other techniques, across a wide range of science from solid state physics to biology (*1*, *2*). Although there have been remarkable advances in the sensitivity and scope of neutron scattering experiments, there has not been the transformation that can come from the multiple orders of magnitude increase in source power seen in x-ray synchrotron facilities. The 20 years from 1980 to 2000 brought an increase in flux of 10^6 in going from the second-generation synchrotron sources to the third-generation machines, and there is every prospect of a further 10 orders of magnitude increase with the construction of x-ray free-electron lasers (*3*, *4*). In contrast, the source power of neutron scattering facilities has only enjoyed gains of only about one order of magnitude over the past 40 years, with at most another factor of 10 or so currently in prospect.

Neutron scattering can be used to study the structure and dynamics of almost any solid or liquid, and as such it spans the whole range of condensed matter research from electron correlations in quantum critical systems to the hydration of biopolymers in solution. Neutron techniques are intrinsically more effective than x-rays in locating hydrogen atoms in structures, in resolving detail of atomic thermal motion and structural disorder, in studying collective excitations like phonons, and in determining magnetic structures. The most powerful source for which a design study has been funded is the 5-MW European Spallation Source (ESS), which would provide flux 10 to 20 times as high as the ISIS facility in the United Kingdom (*5*) (for many years the world's most powerful spallation neutron source). This full order-of-magnitude increase in neutron flux would allow experiments to be performed with far greater spatial or temporal resolution (or momentum and energy resolution in conjugate space) and provide access to measurements that have so far been impossible because the samples are too small or exist for too short a time. For example, it would make it possible to study enzyme action in much greater detail; or to study materials at more extreme pressures and temperatures, under conditions similar to those found deep inside Earth; or to study more complex materials—the kinds of materials that we use in the real world rather than the idealized samples that we study in the laboratory; or to study smaller microstructures or the action of faster catalysts.

The prospect of these advances is exciting, but they are essentially incremental. Here, we describe a way in which it might be possible to create a neutron source three or more orders of magnitude brighter by using foreseeable developments in inertial fusion energy (IFE) technologies to take neutron scattering into completely new areas. These could include problems like the dynamics of molecular motors, protein folding, diffusion through membranes, and proton transfer mechanisms; and, given that even at these fluxes there is no measurable beam heating, much of this biochemical work could be done in vivo. As well, such a large gain in source power would completely transform neutron scattering studies of materials, condensed matter physics, chemical reactions, engineering, and geoplanetary science.

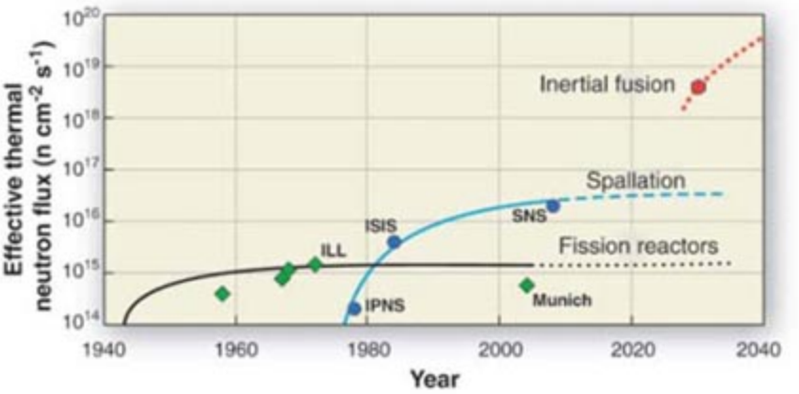

Fig. 1. Neutron source flux versus year. A comparison between reactors, spallation sources, and the proposed inertial fusion source. "Effective flux" values are notional equivalent reactor core fluxes that provide an accepted approximate comparison between the different types of sources for many classes of experiments [adapted from (*14*)]. The figure includes the Intense Pulsed Neutron Source (IPNS) at Argonne and the new high-flux reactor FRM-II in Munich. The other named sources are identified in the text.

Present Limits

Figure 1 illustrates how currently available neutron sources are reaching the limits of existing technologies. There are two distinct approaches: pulsed spallation sources, in which accelerated protons smash or "spall" neutrons out of a heavy-metal target, and nuclear fission reactors.

A reactor designed to provide beams for scattering experiments has to have a compact high-flux core to maximize thermal source brightness (see Fig. 2). The limiting factor is the degree to which a large amount of heat can be extracted from a small and highly confined volume. Reactor-based facilities already began to approach their maximum power in the 1970s with the 58-MW Institut Laue-Langevin (ILL) in France (*6*), and the (unfunded) Advanced Neutron Source's ~330-MW reactor (*7*) would have reached the water-cooling limit for a compact reactor core.

Spallation sources also have to use compact target assemblies to provide high-flux beams for experiments, but the crucial factors are the density of power deposition and radiation damage rather than total power. The effect of depositing the power in a short pulse (on the order of a μs) is to induce stress in the target material for a solid target or in the container for

[1]Council for the Central Laboratory of the Research Councils, Rutherford Appleton Laboratory, Chilton, Didcot, Oxon OX11 0QX, UK. [2]Scottish Universities Physics Alliance, School of Physics and Centre for Science at Extreme Conditions, The University of Edinburgh, Mayfield Road, Edinburgh EH9 3JZ, UK.

*To whom correspondence should be addressed. E-mail: andrew.taylor@rl.ac.uk

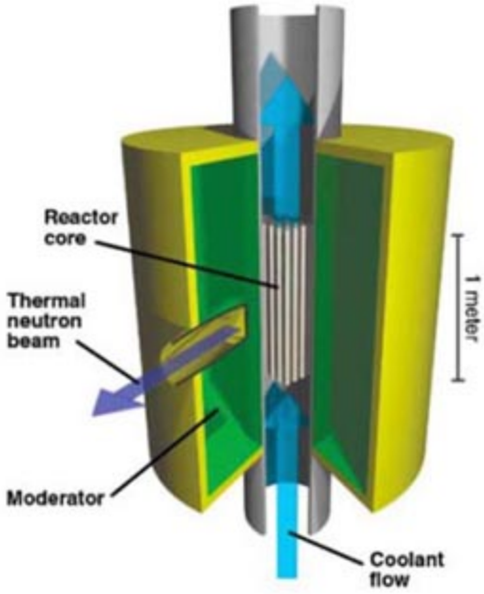

Fig. 2. Schematic of a high-flux reactor core. To maximize the flux brightness of the thermal neutron beams, it is necessary to make the core as small as possible, typically less than 1 m^3. The limiting factor then becomes the maximum achievable rate of cooling. Current high-flux reactors like the ILL produce 58 MW of power, which is cooled by fast-flowing D_2O. The design of the (unfunded) 330-MW Advanced Neutron Source in the United States took reactor sources close to their practical limit.

a liquid metal target (see Fig. 3). The 1-MW Spallation Neutron Source (SNS), which is currently in its commissioning phase (*8*), uses a liquid mercury target to remove the heat deposited by the proton beam and cope with the pulsed power and radiation damage. The ESS design (*2*) is close to the acceptable limit for these effects.

In assessing the prospects for future neutron scattering science, we turn to another field of research that could be adapted to the benefit of the neutron community. As shown, the conventional approaches are reaching the limits of the survivability of their core or target. In the field of IFE, this issue is neatly sidestepped by allowing the target to be destroyed and then replacing it, several times a second. This field is likely to mature over the coming decade, such that it is now timely to consider how it might affect neutron scattering science.

Inertial Fusion

In IFE research, lasers are used to compress a very small mass of deuterium (^2H) and tritium (^3H) to sufficiently high densities and temperatures to initiate a propagating thermonuclear reaction in which these nuclei combine to form an energetic alpha particle (3.5 MeV) and a high-energy neutron (14 MeV). The achievable neutron yield is considerably higher than can be envisaged from any reactor- or accelerator-based approach, and there are no limitations imposed by target survivability. The means by which this high-energy neutron source could be adapted to provide low-energy neutron beamlines for scattering applications is explored in the next section.

The history of IFE is long, with many problems having being encountered along the way. The initial concept, suggested in the 1960s and developed through the 1970s (*9*), calculated that a laser with energy on the order of 1 kJ would be sufficient to implode a fuel pellet to the degree required for fusion to self-initiate (a threshold known as "ignition"). It is now believed that this estimate was wrong by three orders of magnitude because of an incomplete treatment of hydrodynamic and plasma instabilities. Conclusive demonstration experiments were performed in a classified program by the United States in the 1980s, which defined the energy required to drive a small capsule to ignition. What now remains is to demonstrate this process with a laboratory driver and to develop the technology associated with a fusion energy power plant. The next major milestone along this path is almost upon us, with a new generation of lasers with energy ~2 MJ being constructed in the United States and France to finally realize the goal of ignition (*10*), with every anticipation of success in the period 2010 to 2015.

As a result of this upcoming demonstration of ignition, there has been much research into the techniques by which IFE can be developed into a viable high-repetition source for a future power plant. The current generation of fusion lasers has a woefully low repetition rate, with the time between shots measured in hours. The rate required for a viable power plant is on the order of 5 Hz. The capital investment and technological hurdles associated with a high-repetition-rate laser capable of delivering energy in the multi-MJ regime has been a principal concern of the fusion community for many years. To address this issue, an innovative approach to IFE—"fast ignition"—has been suggested (*11*, *12*). This approach has the potential to reduce the laser energy requirements by an order of magnitude, thus lowering the facility costs and easing the route to high repetition rates.

In fast ignition, a capsule is first compressed to moderately high density at low temperature, creating an isochoric (uniform density) rather than isobaric (uniform pressure) fuel assembly. Ten nanoseconds later, at the point of maximum compression, a second high-intensity short-pulse beam is used to ignite this compressed core (Fig. 4), resulting in an intense, isotropic burst of 14 MeV neutrons. For this to be effective, it may be necessary to insert a metallic cone (typically gold) in the pellet to allow the ignition pulse access to the center of the compressed plasma. With this method, the gain is limited only by the size of plasma that can be assembled. Experiments to verify the physics underlying fast ignition are well under way with very encouraging results (*11*), such that it is now reasonable to explore the likely applications of this scheme. If successful, ~300 kJ of laser energy is calculated to produce some 30 MJ of total fusion energy, of which 22 MJ is in high-energy neutrons (*13*). This would open up the potential for adaptation of fast-ignition fusion to alternative science applications.

The potential for application to neutron sources arises because a 22-MJ yield translates into a remarkable 10^{19} neutrons per pulse, and the replacement of the source for each shot means that there is no longer any source-conserving limit. That is, the principal limitation of the

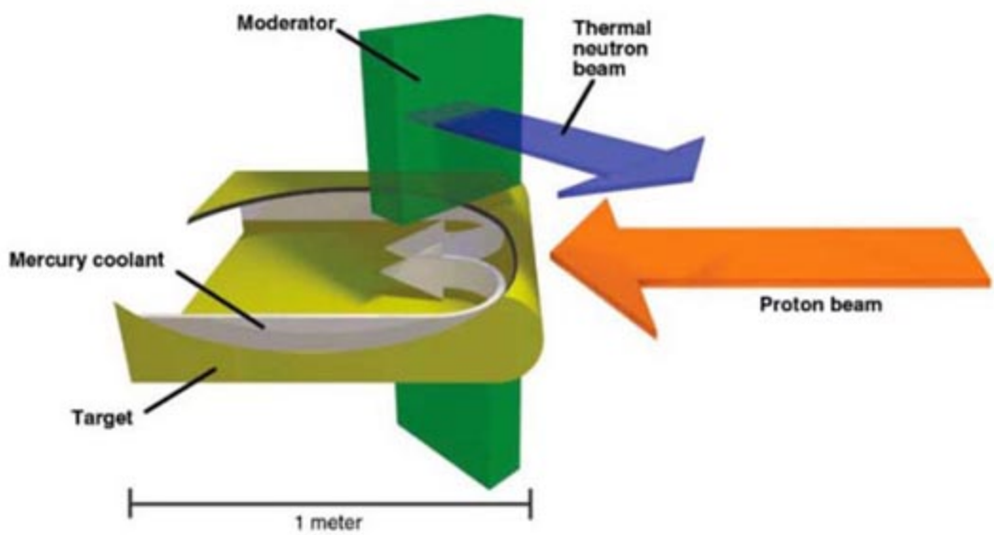

Fig. 3. Schematic of a high-power spallation neutron source. The latest designs of spallation neutron source, such as the SNS at Oak Ridge in the United States or the as-yet-unfunded ESS, are designed to run at powers in the 1- to 5-MW range. The thermal shock is too great for a solid target; liquid mercury is used instead and flows at high speed to remove the deposited heat. The limiting factor for the target design is the material erosion caused by the shock wave when the proton beam hits the target and its container. This liquid mercury design is close to the practical limit on power.

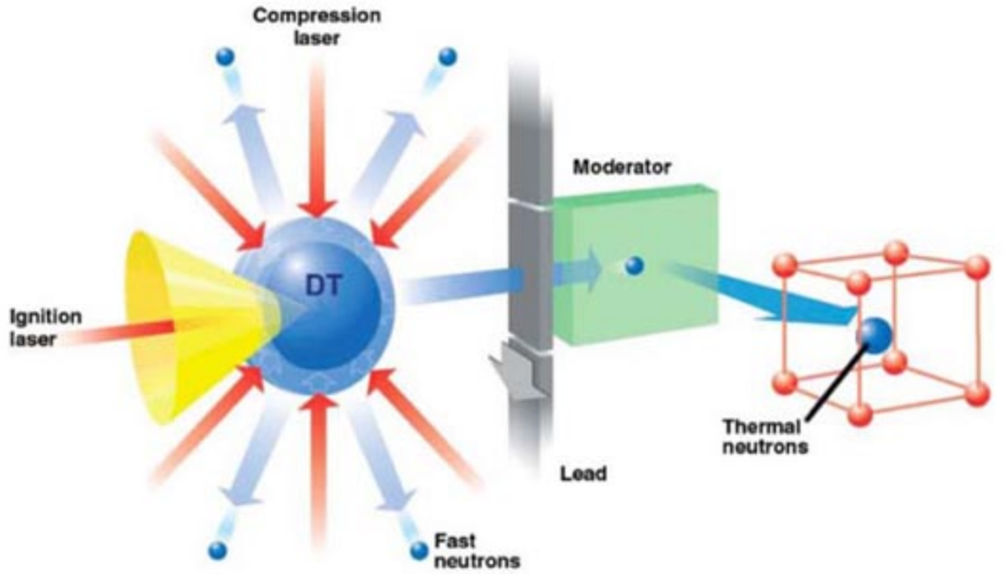

Fig. 4. Schematic of a conceptual design for an inertial fusion neutron source. Compression laser beams are focused on the millimeter-diameter Deuterium-Tritium capsule. The ignition short-pulse beam enters ~10 ns later via a gold cone through the compressed plasma. Some of the 14-MeV "fast" neutrons that are produced enter a moderator through a moving, sacrificial Pb converter. A flowing water moderator ~15 cm long, ~15 cm high, and ~5 cm wide provides sufficient moderator efficiency and a pulse width suitable for neutron scattering experiments. Several such moderators are placed in the equatorial plane, 1 m from the target. Moderated "thermal" neutrons are emitted from each 15-cm-by-15-cm face to provide beams that interact with experimental samples, as shown. Several neutron-beam instruments can view each moderator. The moderator assemblies occupy only ~±2° about the equatorial place, easily clear of the incident laser beams, which can be removed from a region up to ±30° about the equator and still retain adequate symmetry to drive the implosion in this fast ignition geometry.

reactor and spallation approaches would be completely removed.

Several more years of research are needed before there can be confidence that fast ignition represents a viable route for energy production or for alternative applications such as those proposed here. However, IFE research in this area is proceeding at a very fast pace, both on driver technology development and in the construction of a number of new facilities to test the physics underpinning the basic target design for fast ignition. These facilities (in Japan and the United States) will demonstrate in the next 5 years whether it is possible to heat highly compressed matter to the temperature required for hot spark formation. If this is proven, then the construction of lasers designed to provide high repetition rate and high-energy gain through thermonuclear burn propagation should begin, along with accelerated development of the engineering solutions required for a practical high-throughput facility. One might expect experimental programs studying the physics of high-gain fusion to start in the middle of the next decade.

A Conceptual Design

To be useful for scattering studies of structures and excitations in condensed matter, the initial 14-MeV neutrons need to be slowed to energies of less then 1 eV (*14*, *15*). This can be achieved by allowing the neutrons to reach thermal equilibrium with a cool (300 K) bath of material in a process known as moderation (Fig. 4). In a collision with a proton, a neutron will on average lose half its energy, so the most effective moderator materials are those with the highest density of hydrogen atoms. Water is particularly effective, not only because of its hydrogen content but also because its liquid nature allows heat to be removed quickly through mass transport. A pulse of neutrons from the target quickly moderates in the water, and the slowed neutrons then diffuse out over a period of time (typically a few tens of microseconds). The time constant of the process is determined by the size of the moderator and the diffusion constant of the neutrons within the material. Therefore, it is possible to control the time width of the thermal neutron pulse by changing the dimension of the moderator along the direction of the emitted neutron beam.

Water moderation is inefficient at 14 MeV because the bath is semitransparent to such high-energy neutrons, but the moderation efficiency can be considerably enhanced by placing a layer of lead (~30 mm thick) on the leading surface of the water container to first convert the 14-MeV neutrons to lower energies, around 2 MeV, through inelastic reactions in which each incident neutron gives rise to two or more emitted neutrons. Moving from 14 MeV to 2 MeV, the scattering efficiency (cross section) of water more than doubles; for our 15-cm-long moderator, more than 20% of 14-MeV neutrons will pass through without interacting, whereas at 2 MeV, this drops to 2 to 3%.

This lead layer on the leading surface of the moderator containment also serves to protect the moderator assembly. A conveyor system that moves the sacrificial lead layer past the front wall of each moderator will be needed so that a cool and unablated surface is presented for each pulse. This will reduce heating of the moderator, counter the problem of shockwaves in the water that is otherwise likely to be caused by the fast neutron and gamma flux, and protect the moderator assembly from ablation by high-energy x-rays and charged ions.

In practice, there are likely to be several moderators, each viewed by a number of experimental beamlines. To achieve the highest neutron brightness, these moderators need to be as close to the fusion source as possible. However, this has to be balanced with their ability to survive the hostile irradiation environment and allow access for the lasers.

To explore the feasibility of the scheme, we have designed a notional target and moderator assembly using a Monte Carlo neutron transport code (*16*). This models the moderation process to provide values to within 5 to 10% for the neutron flux, radiation damage, and heat deposition. In our conceptual design (Fig. 4), we placed four moderators 1 m from the fusion target, with a width of water (5 cm) chosen to produce short pulses of neutrons similar to those found in existing spallation sources. By using these Monte Carlo calculations, it is also possible to show that the heat deposition will be comfortably within the cooling limit of fast-flowing water. The overall moderating process is a factor of 20 less efficient than it is in optimized spallation designs, but despite this, the useful flux per pulse will still be more than 1000 times as high as that from an ISIS water moderator (*17*), primarily because the initial neuron yield is so high.

At most neutron sources, the flux of low-energy neutrons is enhanced by the use of cold moderators; a moderator at 20 K can provide gains in excess of a factor of 50 below 1 meV, compared to one at room temperature. The current state-of-the-art design on a pulsed source is to surround the hydrogen with a water premoderator to boost efficiency (*18*) and protect the hydrogen from excessive heat deposition. The heating will still set limits, but we estimate that by running a water-protected cold moderator at its cooling limit, it will be possible to achieve a cold neutron flux at least 100 times that from a comparable ISIS moderator. However, the cooling limit is mostly governed by the mass transport achievable with current circulator technology and, because this has never been a limiting factor before, very little effort has been invested in obtaining higher performance. There is plenty of room for improvement over the coming decades to match the 1000-fold gain estimated for water moderators.

We envisage the source running at a repetition rate of 10 Hz, which is ideal for neutron scattering experiments and only a factor of two greater than the 5 Hz typically planned for IFE power plant designs (*19*). Progress is such that operation at 10 Hz is likely to be achieved within the 20- to 30-year time frame, with the limiting factor being the reactor chamber dynamics (e.g., cooling) rather than provision of the laser source. On a longer time scale, it also appears probable that a further factor-10 increase in neutron flux could be envisaged by making use of baseline (500 MJ) IFE reactor designs and/or more closely coupled moderators. This would mainly require detailed design of the vacuum system and an efficient cooling and remote replacement capability for the converter/moderator assembly.

Design and Operation Issues

There are, of course, many difficult challenges to confront, but these are principally ones that already need to be overcome for IFE power plant designs.

As well as the deposited heat, the moderator assemblies have to cope with the materials damage caused by the neutron, fast ion, and thermal x-ray flux from the fusion reaction. The capsule implosion releases an energy equivalent to 7 kg of high explosive, but instead of producing a shock wave, this energy mostly goes into producing neutrons with relatively low momentum. However, the reactions produce a large number of x-rays and high-energy charged ions that, if they were allowed to hit the moderator assembly, would cause substantial radiation damage and would rapidly ablate away surfaces. Experience shows that this begins to occur if the flux exceeds 1 to 5 J/cm^2, and, because the current IFE power plant designs typically predict 5 to 20 J/cm^2 in fast ions and 0.5 to 1.5 J/cm^2 in x-rays at the chamber wall, sophisticated flux mitigation techniques will need to be developed by the fusion community (*20*). The estimated fluence on our Pb neutron converter is ~50 J/cm^2 in fast ions and ~3 J/cm^2 in x-rays, or within a factor of 2 to 3 of the problems already faced by the IFE community, so that we can reasonably expect to adopt similar mitigating procedures.

To cope with this highly hostile environment, we propose to use the lead layer as a sacrificial shield as well as an energy converter. We estimate it will be ablated at about 100 mm/hour, so it will need to be a moving strip as shown in Fig. 4. In practice, we would envisage a thin plastic layer on the front of the lead, because replacing as much as possible of the ablated lead with ablated plastic is preferable with respect to waste management. The level of ablation from the converter equates to ~10^{21} atoms per pulse, which is comparable to the debris associated with IFE target designs, so we can adopt similar vacuum and waste-collection technology.

As well as ablation, the radiation will weaken materials through radiation damage. The neutron fluence at the front face of the moderator assembly (~1 m from the fusion target) is ~ 8×10^{13} n/cm^2 per shot. Over a lifetime of 1 month, the moderator has therefore to withstand irradiation by ~10^{21} n/cm^2. This is sufficient to induce on the order of 100 displacements per atom, which is beyond the limit of structural survivability for the assembly. Put another way, this means that each atom is displaced on average once every 7 hours. We estimate that the effects of radiation damage will require a design in which the whole moderator assembly can be routinely replaced each month—an operationally acceptable frequency.

The facility would likely consume >10 kg a year of tritium, which is equivalent to 50% of the world's current inventory. However, techniques are being developed in the fusion program that will make it possible to "breed" all the tritium required by reacting neutrons with a layer of lithium and lead built into the walls of the outer containment vessel. This will capture 14-MeV neutrons and generate the tritium required for subsequent fuel pellets through the reaction $^6\mathrm{Li} + \mathrm{n} \rightarrow {}^4\mathrm{He} + {}^3\mathrm{T}$. Because the neutron capture efficiency is only ~80%, there is a need to compensate through neutron multiplication in this blanket. This is achieved by inelastic reactions in the lead atoms (*21*). For our purposes, the neutron scattering infrastructure results in only a small additional reduction in the total neutron population (~1-2%), such that it is reasonable to assume the tritium breeding scheme can absorb this perturbation. Interestingly, the fast ignition scheme adopted here may even permit the use of designs in which only trace amounts of tritium are required within the capsule, so the complexity of external breeding can be avoided or minimized (*22*).

The tritium requirements and the materials survival are all difficult issues, but they are already being addressed very actively by the fusion energy community. Considerable progress in this field is expected in the next decade as a result of the decision to proceed with the ITER fusion project (*23*–*25*).

Concluding Remarks

The merging of neutron scattering science with IFE research offers the potential for a revolutionary increase in neutron-source brightness. Although a source of this kind poses considerable challenges, we have not discovered any barrier, technical or physical, that would make it obviously unfeasible. The great challenges are balanced by the huge gains that such a source would offer. This suggestion anticipates the demonstration of thermonuclear ignition within the next few years and builds on innovative work from the fusion community into how such a demonstration could be developed into a viable high-repetition source. The IFE community has a long history of tying a broad range of scientific applications into its long-term goal of energy production, and the advent of ignition now opens up these tantalizing prospects for neutron scattering science.

We believe it is timely for the neutron scattering community to pay close attention to developments in IFE and to imagine the rich possibilities presented by such an increase in source power.

References and Notes

1. Opinion, *Nature* **417**, 883 (2002).
2. ESS Science Case, http://neutron.neutron-eu.net/n_ess.
3. European X-ray Free-Electron Laser, www.xfel.net/XFELpresse/en/index.html.
4. Linac Coherent Light Source, www-ssrl.slac.stanford.edu/lcls/index.html.
5. ISIS Spallation Neutron Source, www.isis.rl.ac.uk.
6. Institut Laue-Langevin, www.ill.fr.
7. Advanced Neutron Source (eventually not constructed), www.ornl.gov/info/ornlreview/rev27-12/text/xcontents.html.
8. Spallation Neutron Source, www.sns.gov.
9. J. Nuckolls, L. Wood, L. Thiessen, G. Zimmerman, *Nature* **239**, 139 (1972).
10. J. Lindl, *Phys. Plasmas* **2**, 3933 (1995).
11. R. Kodama *et al.*, *Nature* **418**, 933 (2002).
12. M. Tabak *et al.*, *Phys. Plasmas* **1**, 1626 (1994).
13. S. Atzeni, M. Tabak, *Plasma Phys. Contr. Fusion* **47**, B769 (2005).
14. K. Sköld, D. L. Price, Eds., *Neutron Scattering: Methods of Experimental Physics, Part C* (Academic Press, London, 1987).
15. Neutrons produced in a fission or fusion process are in thermal equilibrium with the nucleus and have energies in the megaelectron volt range and wavelengths that are commensurate with the size of the nucleus, ~10^{-15} m. These neutrons are of little or no use for studies of condensed matter, where the energy scales are millielectron volts and the wavelengths needed are on the order of angstroms (~10^{-10} m).
16. *The MCNPX Version 2.5.0 User's Manual* (LA-CP-05-0359, Los Alamos National Laboratory, NM, April 2005).
17. Monte Carlo neutron transport code simulations (*16*) of the conceptual design show that it will be possible to moderate the 14-MeV neutrons to 1 eV, by using water, with an efficiency of ~10^{-7} n eV^{-1} Sr^{-1} cm^{-2} per fast neutron (the probability of a source neutron being thermalized and leaving one of the moderator faces). This is less by a factor of about 20 than current optimized spallation source designs, which typically have efficiencies of ~2×10^{-6} n eV^{-1} Sr^{-1} cm^{-2} per fast neutron, as is the case for the ISIS target station. ISIS produces ~5×10^{14} fast neutrons per pulse and hence delivers ~10^9 n eV^{-1} Sr^{-1} cm^{-2} per pulse (at 1 eV) from each of the moderator faces. The fusion target will produce in excess of 10^{19} neutrons per pulse and thus around 10^{12} n eV^{-1} Sr^{-1} cm^{-2} per pulse, or some 1000 times as much as the flux per pulse from an equivalent ISIS moderator.
18. D. J. Picton, S. M. Bennington, T. A. Broome, T. D. Beynon, *Nucl. Instr. Meth. Phys. Res. A* **545**, 363 (2005).
19. J. Sethian *et al.*, *Nucl. Fusion* **43**, 1693 (2003).
20. S. Nakai, K. Mima, *Rep. Prog. Phys.* **67**, 321 (2004).
21. J. Coen, *Nucl. Mater.* **133-134**, 46 (1985).
22. S. Atzeni, M. L. Ciampi, *Nucl. Fusion* **37**, 1665 (1997).
23. ITER project, www.iter.org.
24. *Fusion Eng. Design* **55** (2-3) (2001).
25. Although magnetically confined fusion reactors such as ITER have integrated neutron fluences comparable to the laser-driven reactor of ~5×10^{14} n cm^{-2} s^{-1}, because ITER is steady-state, it would offer no advantage over current sources of neutrons.

26. We thank M. Simon from ISIS for helpful discussions about cooling limits in cryogenic moderators, and two anonymous reviewers for perceptive and constructive comments on the manuscript.

10.1126/science.1127185

Electrical Activity During the 2006 Mount St. Augustine Volcanic Eruptions

R. J. Thomas,[1*] P. R. Krehbiel,[1] W. Rison,[1] H. E. Edens,[1] G. D. Aulich,[1] W. P. Winn,[1] S. R. McNutt,[2] G. Tytgat,[2] E. Clark[2]

It has long been known that volcanic eruptions can produce vigorous lightning. Early investigations of volcanic lightning were made during the Surtsey and Heimay eruptions in Iceland in 1963 and 1973 (*1*, *2*). Despite increasing interest (*3*–*5*), volcanic lightning continues to be poorly understood, because there are few direct scientific observations of the phenomena. We report observations of lightning during the recent eruptions of Mt. Augustine in Alaska that provide a more detailed picture of volcanic lightning than heretofore available.

After the initial eruptions of Mount St. Augustine on 11 and 13 January 2006, two of which produced lightning, we deployed two time-of-arrival mapping stations on the east coast of Cook Inlet 100 km east of Augustine (fig. S1). The stations constituted a minimal network capable of determining the azimuthal direction of impulsive radio emissions from electrical discharges (*6*).

Within 2 days of the stations being set up Augustine erupted again, producing four explosive eruptions during the night of 27 to 28 January 2006 (*7*). Although not observed visually because of stormy weather, the data showed that the first and largest of the eruptions produced a spectacular lightning sequence (Fig. 1). Seismic data indicate that the eruption lasted about 11 min, from 05:24 to 05:35 UTC, with a particularly energetic explosion occurring between 05:31 and 05:33.

The main explosion, and a smaller explosion ~3 min earlier, were accompanied by continuous backgrounds of strong, impulsive radiation and by several embedded lightning-like bursts (Fig. 1A). The bursts were detected by both measurement stations and originated from the direction of Augustine's summit (Fig. 1B). The background radiation, although strong, was not detected at the northern station and is believed to have originated at low altitude immediately above or within Augustine's vent. Its presence is indicative of a myriad of small discharges within the superheated ejecta as it exited the volcano.

The main explosion was followed after a delay of ~3 min by a sequence of about 300 well-defined lightning discharges between 05:34:11 and 05:45:31 UTC. The discharges drifted southward from Augustine's summit (Fig. 1B), in the same direction as the Nexrad-detected radar plume. One of the final discharges lasted 650 ms and had a transverse extent of 15 km, extending to 22 km away from the volcano (Fig. 1C). The discharges undoubtedly occurred within the volcano's plume, which developed up to 8 to 10 km in altitude.

Although not planned, the southern station fortuitously functioned as a sea-surface interferometer, in which direct and water-reflected signals interfered constructively or destructively at the receiving antenna depending on the height of the radiation source above the volcano. The interference effects were clear for a radiation burst at 05:32:14 during the main explosion (fig. S3). Together with the azimuthal data, the results show that the burst was produced by an upward-initiated, ~4-km-long discharge from Augustine's summit that developed horizontally into the downwind plume (Fig. 1D). The radiation was characteristic of negative-polarity breakdown into net positive charge in the plume (*8*) [Supporting Online Material (SOM) text]. Some discharges of the delayed lightning sequence may have been initiated upward from the summit, but most were undoubtedly intracloud discharges.

Overall, the observations of the 27–28 January eruptions indicate that Augustine's electrical activity had two modes or phases: first, a newly identified explosive phase in which the ejecta from the explosion appeared to be highly charged upon exiting the volcano, resulting in numerous apparently disorganized discharges and some simple lightning (Fig. 1D). The net charge exiting the volcano appears to have been positive, the same polarity observed for the Icelandic volcanoes involving direct contact with sea water (*1*, *2*). In the second phase, conventional lightning discharges occurred within the plume cloud produced by the explosion. Although the plume was undoubtedly charged as a result of the explosion, the fact that the plume lightning was delayed and continued after and well downwind of the eruption indicates that in situ charging also occurred within the plume, for example as a result of particle interactions involving tephra, ash, and ice hydrometeors. Volcanoes are known to release copious amounts of water and may behave as "dirty" thunderstorms (*9*).

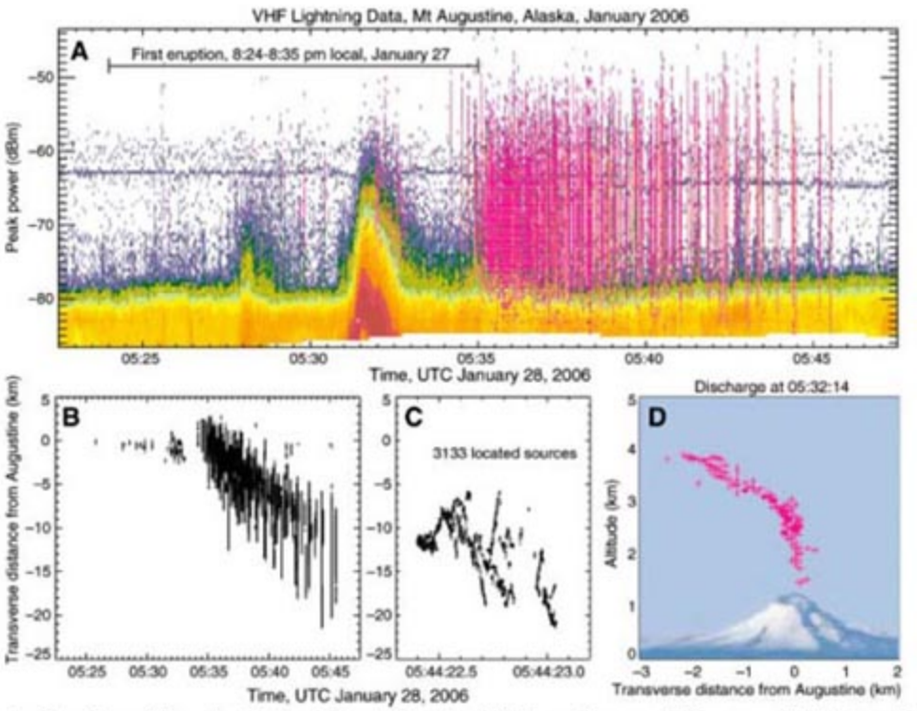

Fig. 1. Overview of the electrical activity during the initial eruption on 27 January. (**A**) Peak radiated power values at the southern station, with azimuthally located events shown in magenta. VHF, very high frequency. (**B**) Transverse distance of the located discharges relative to Augustine. (**C**) Temporal development of a final lightning discharge near the end of the activity. (**D**) Vertical projection of an upward discharge during the main explosion.

References

1. R. Anderson *et al.*, *Science* **148**, 1179 (1965).
2. M. Brook, C. B. Moore, T. Sigurgeirsson, *J. Geophys. Res.* **79**, 472 (1974).
3. R. P. Hoblitt, *J. Volcanol. Geotherm. Res.* **62**, 499 (1994).
4. S. R. McNutt, C. M. Davis, *J. Volcanol. Geotherm. Res.* **102**, 45 (2000).
5. K. S. Vogfjörd *et al.*, *Eos* **86**, 245 (2005).
6. R. J. Thomas *et al.*, *J. Geophys. Res.* **109**, D14207 (2004).
7. J. A. Power *et al.*, *Eos* **87**, 373 (2006).
8. S. A. Behnke, R. J. Thomas, P. R. Krehbiel, W. Rison, *J. Geophys. Res.* **110**, D10207 (2005).
9. E. R. Williams, S. R. McNutt, *Eos* **85** (suppl.), abstr. AE23A-0842 (2004).

Supporting Online Material

www.sciencemag.org/cgi/content/full/315/5815/1097/DC1
Materials and Methods
SOM Text
Figs. S1 to S4
References and Notes

10 October 2006; accepted 19 December 2006
10.1126/science.1136091

[1]Langmuir Laboratory, New Mexico Tech, Socorro, NM 87801, USA. [2]Alaska Volcano Observatory, University of Alaska, Fairbanks, AK 99775, USA.

*To whom correspondence should be addressed. E-mail: thomas@nmt.edu

Nuclear Activity of MLA Immune Receptors Links Isolate-Specific and Basal Disease-Resistance Responses

Qian-Hua Shen,[1] Yusuke Saijo,[1] Stefan Mauch,[1] Christoph Biskup,[2] Stéphane Bieri,[3] Beat Keller,[3] Hikaru Seki,[1]* Bekir Ülker,[1]† Imre E. Somssich,[1] Paul Schulze-Lefert[1]‡

Plant immune responses are triggered by pattern recognition receptors that detect conserved pathogen-associated molecular patterns (PAMPs) or by resistance (R) proteins recognizing isolate-specific pathogen effectors. We show that in barley, intracellular mildew A (MLA) R proteins function in the nucleus to confer resistance against the powdery mildew fungus. Recognition of the fungal avirulence A10 effector by MLA10 induces nuclear associations between receptor and WRKY transcription factors. The identified WRKY proteins act as repressors of PAMP-triggered basal defense. MLA appears to interfere with the WRKY repressor function, thereby de-repressing PAMP-triggered basal defense. Our findings reveal a mechanism by which these polymorphic immune receptors integrate distinct pathogen signals.

Plants have evolved two classes of immune receptors, each of which recognizes non-self molecular structures. One class involves membrane-resident pattern recognition receptors (PRRs) that detect pathogen-associated molecular patterns (PAMPs) such as bacterial flagellin or chitin, a component of fungal cell walls (*1*). During interactions with virulent parasites, PRRs confer weak immune responses that attenuate pathogen growth and contribute to basal defense (*1*). Reduced PAMP-mediated defense probably results from successful host defense suppression by pathogen effectors (*1*). Resistance (R) proteins represent a second, mainly intracellular, immune receptor class having the capacity to directly or indirectly detect isolate-specific pathogen effectors, encoded by avirulence (*AVR*) genes (*1*). PRR-triggered immune responses are tightly linked to mitogen-activated protein kinase signaling, the accumulation of reactive oxygen species (ROS), and the activation of defense-related genes involving WRKY transcription factors (TFs) (*2*). Immediate signaling components of effector-activated R proteins are unknown. However, R protein–triggered immune responses are also linked to ROS accumulation and defense-gene activation but differ quantitatively and kinetically from basal defense, often leading to host cell suicide at invasion sites (*3*). This points to a convergence of PRR- and R protein–triggered signaling, but the nodes and mechanisms enabling plants to integrate signals from these two receptor classes remain elusive.

The polymorphic barley *mildew A* (*MLA*) *R* locus encodes allelic receptors containing an N-terminal coiled-coil (CC) structure, a central nucleotide-binding (NB) site, and a leucine-rich repeat (LRR) region. MLA receptors share >90% sequence identity but recognize isolate-specific *Blumeria graminis* f sp. *hordei* effectors (*4*–*7*). *MLA1*/*MLA6* hybrid analyses revealed that recognition specificity is determined by different but overlapping LRRs and a C-terminal non-LRR region (CT) (*6*). MLA steady-state levels are critical for effective resistance and are subject to control by cytosolic heat-shock protein 90 (Hsp90) and the co-chaperone–like proteins RAR1 and SGT1 (*8*, *9*). Recently, the *B. graminis* effector AVR_{A10}, which is recognized by MLA10, was isolated and shown to belong to a diversified gene family comprising more than 30 paralogs (*5*, *10*). The availability of the cognate *MLA10* and AVR_{A10} gene pair, as well as the cell-autonomous nature of MLA resistance to *B. graminis* upon transient gene expression in single epidermal cells, enabled us to elucidate effector-dependent receptor functions (*5*, *7*, *10*).

Nuclear activity of MLA receptors. Biochemical fractionation of leaf protein extracts from transgenic barley lines expressing epitope-tagged *MLA1* or *MLA6* detected the majority of the receptor in the soluble fraction (*8*). To examine the subcellular distribution of MLA, we biolistically delivered a DNA plasmid encoding MLA10 tagged with yellow fluorescent protein (YFP) into leaf epidermal cells and recorded YFP fluorescence by confocal imaging (Fig. 1A, upper panel). MLA10-YFP localized to the cytoplasm and the nucleus. Biolistic delivery of wild-type *MLA10* or *MLA10-YFP* constructs into single epidermal cells comparably restricted *B. graminis* growth in an AVR_{A10}-dependent manner (Fig. 1B), demonstrating activity of the MLA10-YFP fusion protein. To determine the functional role of the nuclear MLA10 pool, we fused a nuclear export signal (NES) to the C terminus of MLA10-YFP (*11*). Expression of the MLA10-YFP-NES construct revealed undetectable nuclear fluorescence signals in the majority (>80%) of epidermal cells despite clearly visible cytoplasmic YFP fluorescence. In the remaining cells, nuclei were indirectly marked by a YFP halo (Fig. 1A, middle panel). If this difference in the subcellular distribution between MLA10-YFP-NES– and MLA10-YFP–expressing cells were due to a functional NES, then amino acid substitutions predicted to render the NES nonfunctional (nes) (*11*) should restore nuclear accumulation of a corresponding MLA10-YFP-nes fusion protein. Indeed, the subcellular YFP fluorescence distribution patterns of cells expressing MLA10-YFP-nes or MLA10-YFP were indistinguishable (Fig. 1A, bottom panel). Inoculation with *B. graminis* expressing AVR_{A10} showed that the MLA10-YFP-NES receptor variant was inactive, whereas MLA10-YFP-nes restored activity to MLA10 wild-type–like levels (Fig. 1B). Together these data strongly imply that the nuclear pool of MLA10 is essential for its disease-resistance function. This is unexpected because MLA lacks known nuclear localization signals.

We next analyzed stable transgenic barley lines containing a single copy of functional epitope-tagged *MLA1* driven by native 5′ regulatory sequences (*8*). We purified nuclei from leaves of 7-day-old seedlings before and after inoculation with *B. graminis* isolates expressing or lacking the cognate AVR_{A1} effector. Immunoblot analyses detected MLA1-HA in both nuclear extracts and nuclei-depleted soluble fractions (Fig. 1C). A time-course experiment revealed an apparent increase of the nuclear MLA1-HA pool in the incompatible interaction (12, 18, and 24 hours after spore inoculation) as compared to the compatible interaction (Fig. 1C; similar results were obtained with protein extracts from leaf epidermal tissue). This demonstrates the existence of a nuclear pool for a second MLA receptor, is indicative of dynamic changes of the nuclear pool during the immune response, and suggests that the intracellular distribution of MLA10-YFP observed in the single-cell system probably reflects its physiological locations.

***Hv*WRKY1/2 TFs interact with the MLA CC domain.** We constructed yeast two-hybrid baits encoding single or multiple domains of MLA1 or MLA6 CC-NB-LRR-CT receptors and screened a barley prey cDNA library derived from healthy and *B. graminis*–challenged leaf epidermal tissue (Fig. 2A) (*8*, *12*). The bait MLA

[1]Department of Plant Microbe Interactions, Max-Planck-Institut für Züchtungsforschung, Carl-von-Linné-Weg 10, D-50829 Köln, Germany. [2]Institute of Physiology II, Friedrich-Schiller-University of Jena, Teichgraben 8, D-07740 Jena, Germany. [3]Institute of Plant Biology, University of Zürich, Zollikerstrasse 107, 8008 Zürich, Switzerland.

*Present address: RIKEN Plant Science Center, 1-7-22 Suehirocho, Tsurumi-ku, Yokohama, Kanagawa, 230-0045, Japan.

†Present address: School of Biological and Biomedical Sciences, Durham University, Science Site, South Road, Durham DH1 3LE, UK.

‡To whom correspondence should be addressed. E-mail: schlef@mpiz-koeln.mpg.de

CC_{1-46} (an invariant sequence in all known MLA receptors) identified four interactors. Two were dismissed because of their predicted localization in chloroplasts and mitochondria. One identified prey cDNA encoded an N-terminally truncated version of a WRKY domain–containing TF, designated *Hv*WRKY2 (*Hv*, *Hordeum vulgare*) (Fig. 2A; GenBank accession number AJ853838). A highly sequence-related homolog, designated *Hv*WRKY1 (GenBank accession number AJ536667), sharing 72% sequence similarity and identical domains and motifs (fig. S2), was subsequently isolated and also found to interact with the MLA CC_{1-46} bait by targeted yeast two-hybrid experiments. To characterize MLA and *Hv*WRKY1/2 TFs interactions, we performed directed yeast two-hybrid assays using truncated and full-length receptor and TF variants. Although interactions were found with truncated forms of the receptor and the TFs (Fig. 2A), the full-length MLA6 bait failed to interact with all tested *Hv*WRKY1 or *Hv*WRKY2 prey variants despite the presence of comparable amounts of the LexA-MLA fusion proteins (fig. S1). This might indicate requirements for intra- and intermolecular interactions in vivo.

To examine whether MLA directly interacts with *Hv*WRKY1/2, we performed in vitro pull-down assays. A hemagglutinin (HA) epitope–tagged MLA1 CC_{1-166} fragment was expressed in a wheat germ in vitro translation system and subsequently incubated with glutathione *S*-transferase (GST)–*Hv*$WRKY2_{107-319}$ or GST alone purified from *Escherichia coli* lysates. Immunoblot analysis of GST pull-down precipitates with HA antibodies revealed the presence of MLA1 CC_{1-166} in GST-*Hv*$WRKY2_{107-319}$ but not GST precipitates (Fig. 2B). This is consistent with a physical interaction between the MLA1 CC and the *Hv*WRKY2 TF.

***HvWRKY1/2* repressor functions.** To elucidate the functional role of *HvWRKY1* and *HvWRKY2* in immune responses to *B. graminis*, we first examined their contribution to basal defense mechanisms by virus-induced gene silencing (VIGS) during a compatible interaction. Barley seedlings were inoculated with a barley stripe mosaic virus (BSMV) vector harboring antisense fragments of *HvWRKY1* (BSMV-WRKY1as) or *HvWRKY2* (BSMV-WRKY2as) or control vectors (Fig. 3A) (*13*). Two weeks after BSMV infection, leaves were inoculated with a virulent *B. graminis* isolate, and the frequency of fungal microcolonies on the leaf surface was microscopically scored 48 hours later. Whereas leaves inoculated with the control vectors supported a frequency of 15 ± 2% and 19 ± 2% microcolonies, respectively, significantly reduced levels were found with BSMV-WRKY1as and BSMV-WRKY2as [7 ± 2% and 9 ± 3% (Fig. 3A); the fourth leaf was used for VIGS experiments that show a higher level of basal defense than did the first true leaf used for single-cell gene expression studies]. This is consistent with and extends previous data showing heightened resistance to a different virulent *B. graminis* iso-

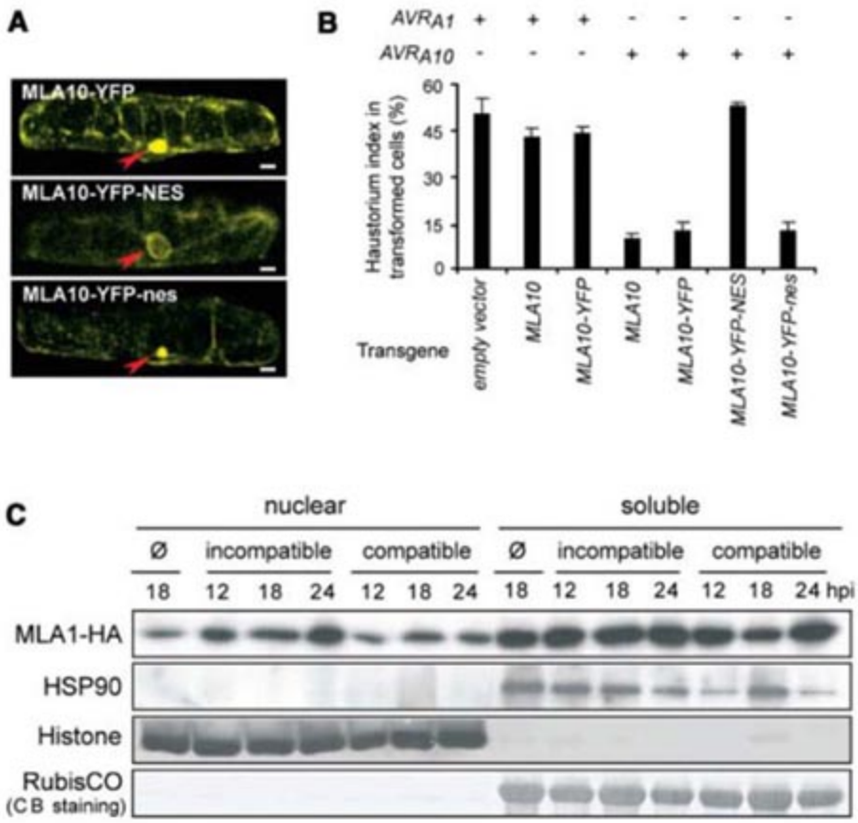

Fig. 1. The nuclear MLA10 fraction mediates race-specific resistance. (**A**) Confocal image of a barley leaf epidermal cell expressing MLA10-YFP [upper panel, three-dimensional (3D) reconstruction], MLA10-YFP-NES (middle, 2D *z* plane), and MLA10-YFP-nes (lower panel, 2D *z* plane). Cytoplasmic strands traversing the vacuole are also visible. Arrowheads mark the nuclei, Scale bar, 10 μm. (**B**) Haustorium index in leaf epidermal cells upon biolistic codelivery of the indicated plasmid vectors and *GUS* reporter. Bombarded leaves were inoculated with *B. graminis* isolates expressing AVR_{A1} or AVR_{A10}. Fungal haustoria were microscopically scored 48 hours after inoculation. Data were obtained from three independent experiments. (**C**) Western blot of MLA1-HA in nuclear and soluble fractions of healthy or *B. graminis*–challenged leaves. Purified nuclear and nuclei-depleted soluble fractions were prepared from leaves of a transgenic line expressing MLA1-HA (*8*) at the indicated time points [hours post inoculation (hpi)] after inoculation with *B. graminis* isolates expressing or lacking AVR_{A1} (incompatible or compatible). All fractions were subjected to immunoblot analyses. This loading represents an approximately 16-fold overrepresentation of nuclear proteins on a per-tissue amount basis. Ø, non-inoculated controls. Histone H3, cytosolic Hsp90, and Coomassie blue (CB) staining of ribulose-1,5-bisphosphate carboxylase-oxygenase (RubisCO) were used as fraction markers.

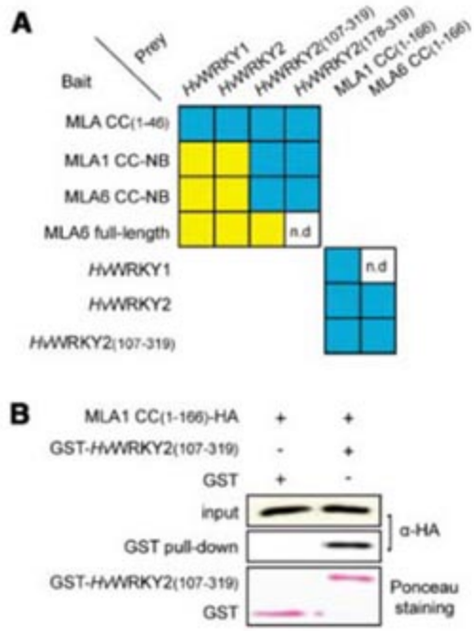

Fig. 2. *Hv*WRKY1/2 TFs interact with the MLA CC domain. (**A**) Results of yeast two-hybrid assays between bait fusions of the LexA DNA binding domain and prey fusions of the B42 activation domain containing either MLA1/6 or *Hv*WRKY1/2 sequences as indicated. Blue, detected interactions; yellow, undetectable interactions; n.d., not determined. (**B**) Immunoblot analysis of GST and GST-*Hv*$WRKY2_{107-319}$ pull-down precipitates. GST or GST-*Hv*$WRKY2_{107-319}$ were incubated with HA epitope–tagged MLA1 CC_{1-166} before GST pull-downs. Ten μl of the mixtures was subjected to immunoblot analysis with antiserum to HA as an input control. MLA1 CC_{1-166} was detected by antiserum to HA, GST-$WRKY2_{107-319}$, and GST by Ponceau staining.

late upon *HvWRKY1* single-cell silencing in the leaf epidermis (*14*), suggesting that *Hv*WRKY1 and *Hv*WRKY2 act as repressors of basal defense to virulent *B. graminis*.

We tested this hypothesis through *HvWRKY2* overexpression experiments during compatible interactions. Biolistic delivery of a *HvWRKY2* construct, driven by the strong ubiquitin promoter, into single leaf epidermal cells resulted in supersusceptibility in different genetic backgrounds harboring *MLA1-HA*, *MLA6-HA*, or wild-type *MLA10* (Fig. 3B; similar results were obtained with *HvWRKY1*). Overexpression of *SUSIBA2*, a barley WRKY TF functioning in sugar signaling (*15*), did not alter the *B. graminis* infection type (Fig. 3B), indicating that sequence motifs other than the shared WRKY DNA binding domain (*16*) contribute to the *HvWRKY1/2*-dependent supersusceptible phenotype. The contrasting infection phenotypes observed upon overexpression or gene silencing of *HvWRKY1/2* are consistent with their presumed roles as repressors of basal defense. *HvWRKY1* and *HvWRKY2* expression was strongly (≥20 fold), rapidly (within 3 hours), and transiently activated upon *B. graminis* challenge in both compatible and *MLA*-specified incompatible interactions (fig. S3A) approximately 10 hours before differential infection phenotypes became microscopically visible. This, and the observation that a similarly strong and even faster *HvWRKY1* and *HvWRKY2* activation occurred upon treatment of leaves with the bacterial flg22 PAMP (fig. S3B), support our hypothesis that both genes are components of PAMP-triggered basal defense.

Next we investigated the importance of the physical association between the invariant MLA CC domain and *Hv*WRKY1/2 during incompatible interactions. We reasoned that if MLA receptors function through interference with *Hv*WRKY1/2 repressor activity in basal defense, then single-cell overexpression of *HvWRKY1/2* might block MLA function because of inappropriate timing and/or TF levels. Indeed, single-cell *HvWRKY2* overexpression fully compromised tested *MLA1-HA*–, *MLA10*-, and *MLA12*-specified immune responses to *B. graminis* isolates expressing cognate Avr_A effectors (Fig. 3C; similar results were obtained with *HvWRKY1*). We previously showed that *MLA12* single-cell overexpression alters the resistance kinetics, but not specificity, so that the growth of a larger proportion of fungal germlings is terminated earlier in comparison to *MLA12* wild-type plants (*6*). To test whether overexpression of the receptor can negate the effect of overexpressed *HvWRKY2*, we co-delivered *HvWRKY2* with *MLA10* or *MLA12*. This still compromised both MLA-specified immune responses (Fig. 3C), indicating that in wild-type plants *HvWRKY2* expression must be tightly controlled to ensure proper MLA function. *SUSIBA2* WRKY overexpression did not interfere with tested *MLA1-HA*–triggered immunity, again illustrating that only particular WRKY TFs can interfere with immune responses to *B. graminis* (Fig. 3C). *HvWRKY2* overexpression also failed to compromise *MLG*-triggered race-specific as well as *mlo*-mediated race-nonspecific resistance to *B. graminis* (Fig. 3C) (*17*, *18*). This is consistent with previous results demonstrating separate genetic pathways for race-specific and *mlo*-mediated resistance (*19*) and revealing the existence of at least one *HvWRKY2* independent *R* gene–triggered immune response to *B. graminis*.

Effector-dependent association between MLA and *Hv*WRKY2. To directly test associations between the MLA receptor and *Hv*WRKY2 in plants, we labeled the proteins with the yellow (YFP)– or blue [cyan fluorescent protein (CFP)]–shifted variants of the green fluorescent protein (GFP), respectively. Upon biolistic delivery of the corresponding DNA plasmids into epidermal cells, functional MLA10-YFP and functional CFP-*Hv*WRKY2 fusion proteins colocalized in epidermal nuclei (fig. S4, A and B; CFP-*Hv*WRKY2 exclusively localizes to the nucleus in all experiments described below). To test protein associations in the presence or absence of the cognate AVR_{A10} pathogen effector (*10*), we monitored for Förster resonance energy transfer (FRET) between the fluorescence tags of MLA10-YFP and CFP-*Hv*WRKY2. In this study, we adopted a quantitative non-invasive fluorescence lifetime imaging (FLIM) approach to detect FRET (fig. S5). To calculate FRET efficiency (E) the lifetime of the donor in the presence of the acceptor (τ_{DA}) only needs to be compared with its lifetime in the absence of the acceptor (τ_D): $E = 1 - \tau_{DA}/\tau_D$. This approach has the advantage that FRET and control measurements can be performed in different cells because fluorescence lifetimes are independent of the actual fluorophore concentration.

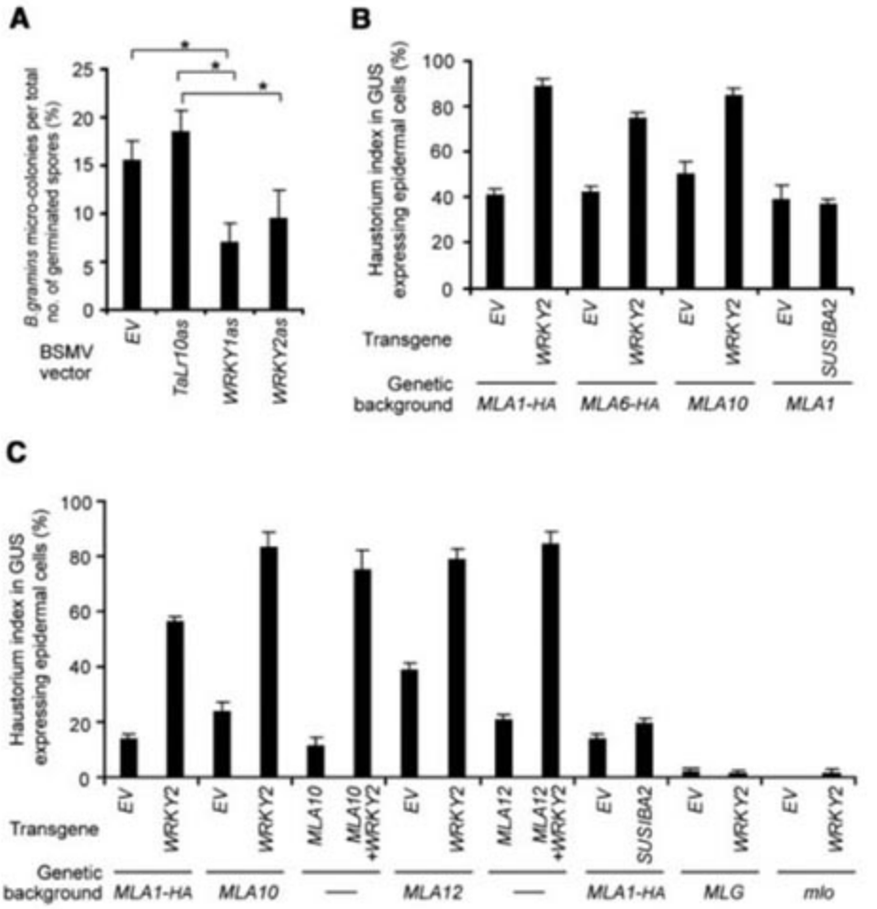

Fig. 3. *Hv*WRKY1/2 TFs repress basal and interfere with *MLA*-triggered immune responses. (**A**) *B. graminis* microcolony formation on barley leaves after BSMV-mediated *HvWRKY1* or *HvWRKY2* silencing. BSMV empty vector (BSMV-EV) and BSMV-TaLr10as were used as controls. BSMV-TaLr10as harbors an antisense fragment of the 3′ untranslated region of wheat *TaLr10* that is of similar length to BSMV-WRKY1as or BSMV-WRKY2as. Mean values of microcolony formation are based on the microscopic analysis of at least 600 interaction sites at 48 hours after inoculation with *B. graminis* conidiospores of virulent isolate A6. Asterisk indicates significant difference at $P < 0.05$. (**B**) Haustorium index in leaf epidermal cells after inoculation with *B. graminis* conidiospores of virulent isolates A6 or K1. Empty DNA vectors (EV) or plasmids expressing *HvWRKY2* or *HvSUSIBA2* were biolistically codelivered with the *GUS* reporter into epidermal cells of the indicated genetic backgrounds. (**C**) Haustorium index in leaf epidermal cells after inoculation with *B. graminis* conidiospores of avirulent isolates A6 or K1. EVs or plasmids expressing the indicated transgenes were biolistically codelivered with the *GUS* reporter into epidermal cells of the indicated genetic backgrounds.

We measured the lifetimes of free CFP and CFP fusion proteins as a control. The average lifetime of free CFP was 2.53 ± 0.02 ns (mean ± SEM, n = 8 nuclei) (fig. S6F). Unexpectedly, the average CFP lifetime in nuclei expressing the CFP-*Hv*WRKY2 fusion was reduced to 2.12 ± 0.02 ns (n = 24; Fig. 4A and fig. S6F), indicating possible homo-FRET between the CFP tags of associated CFP-*Hv*WRKY2 fusion proteins (*20*). In contrast, the average CFP lifetime of CFP-SUSIBA2 (2.47 ± 0.01 ns, n = 5; fig. S6, C and F) was close to that of unfused CFP (2.53 ± 0.02). To directly test for *Hv*WRKY2 dimerization, we generated a YFP-*Hv*WRKY2 construct and co-delivered it with CFP-*Hv*WRKY2 into epidermal cells. A dramatic reduction of the average CFP lifetime to 1.29 ± 0.04 ns (n = 7) was recorded in nuclei coexpressing the fusion proteins (fig. S6, A and F). To rule out the possibility that CFP lifetime reduction was due to unspecific associations between the fluorescent tags, we coexpressed as a control CFP-*Hv*WRKY2 and unfused YFP. Nuclei coexpressing these two proteins showed an average CFP lifetime of 2.03 ± 0.01 ns (n = 12; fig. S6, B and F), which is close to the average CFP lifetime of CFP-WRKY2 alone (2.12 ± 0.02 ns). Collectively, this provides strong in vivo evidence for homomeric *Hv*WRKY2 associations.

In the coexpression experiments, a measured lifetime was considered to be significantly (P < 0.003) shorter when it was more than 3 SD lower than the respective control values. For CFP-WRKY2, the threshold was calculated to be 1.92 ns. Thus, upon coexpression with potential interactors, lifetimes <1.92 ns can be attributed to FRET. For CFP-SUSIBA2, the calculated threshold was 2.39 ns. We measured the CFP lifetime upon coexpression of functional CFP-*Hv*WRKY2 and MLA10-YFP (2.00 ± 0.03 ns, n = 12; Fig. 4B and fig. S6F) and found that it did not differ significantly (P < 0.01) from the average CFP lifetime of nuclei coexpressing CFP-*Hv*WRKY2 and free YFP (2.03 ± 0.01 ns). Thus, there is no evidence for constitutive associations between the immune receptor and the TF, which is consistent with undetectable interactions between full-length MLA and *Hv*WRKY1/2 in the yeast two-hybrid experiments (Fig. 2). However, cells subjected to cotransformation of CFP-*Hv*WRKY2, MLA10-YFP, and the *B. graminis* AVR_{A10} effector, which is recognized by MLA10, produced a broad CFP lifetime distribution not seen in any other tested combinations, ranging from 1.32 to 2.17 ns (Fig. 4C and fig. S6F). Ten out of 27 (37%) CFP lifetime measurements yielded lifetimes that were significantly shorter than that of the CFP-*Hv*WRKY2 control (Fig. 4A), indicating AVR_{A10}-stimulated associations between MLA10 and *Hv*WRKY2. That a portion of the measured CFP lifetimes does not differ from the control measurements could indicate that the stoichiometry between the three proteins and putative auxiliary factors is critical and/or that the association between receptor and WRKY TF is only transient by nature.

When we coexpressed CFP-*Hv*WRKY2, MLA10-YFP, and the *B. graminis* effector AVR_{K1} [an AVR_{A10} homolog recognized by the MLK R protein (*10*)], the average CFP lifetime (2.06 ± 0.03 ns, n = 14) did not differ significantly from the lifetime found in nuclei coexpressing CFP-*Hv*WRKY2 and MLA10-YFP (Fig. 4D and fig. S6F). Furthermore, replacement of CFP-*Hv*WRKY2 by CFP-SUSIBA2 in combinations with MLA10-YFP and AVR_{A10} or AVR_{K1} failed to generate a pronounced broadening of the CFP lifetime distribution [lifetimes were 2.42 ± 0.03 ns (n = 11) and 2.43 ± 0.02 ns (n = 11), respectively; fig. S6, D to F]. Together, this corroborates the ability of MLA immune receptors to interact with particular WRKY family members in the nucleus and supports the notion of an AVR_{A10}-dependent physical association between MLA10 and *Hv*WRKY2.

The FLIM-FRET data were substantiated by using the conventional acceptor photobleaching method (APB-FRET). To estimate the extent of FRET, the donor fluorescence intensity is measured before and after the acceptor chromophore is bleached. Donor fluorescence intensity increases in those cases where FRET has occurred before bleaching. Such an increase in CFP intensity was observed only in nuclei coexpressing CFP-*Hv*WRKY2, MLA10-YFP, and AVR_{A10} (fig. S7) but not in nuclei coexpressing CFP-*Hv*WRKY2 and YFP, or CFP-*Hv*WRKY2, MLA10-YFP, and AVR_{K1} (fig. S7). This independently confirms the AVR_{A10}-dependent physical association between MLA10 and *Hv*WRKY2 in nuclei.

***AtWRKY18/40* repressor functions.** WRKY TFs belong to large gene families in *Arabidopsis* and in rice (*21*, *22*). *Arabidopsis AtWRKY18*, *AtWRKY40*, and *AtWRKY60* (*At*, *Arabidopsis thaliana*) and rice *OsWRKY28* and *OsWRKY71* (*Os*, *Oryza sativa*) show the highest sequence relatedness to *HvWRKY1* and *HvWRKY2* (fig. S2). The deduced proteins form a distinct subgroup of group II WRKYs containing a leucine zipper (LZ) domain thought to be involved in homo- and/or heterocomplex formation (*23*, *24*). *AtWRKY18*, *AtWRKY40*, and *AtWRKY60* have been recently implicated in repressing basal defense to virulent hemibiotrophic *Pseudomonas syringae* (*24*). We tested mutant lines of these *Arabidopsis WRKY* family members by inoculation with the virulent powdery mildew

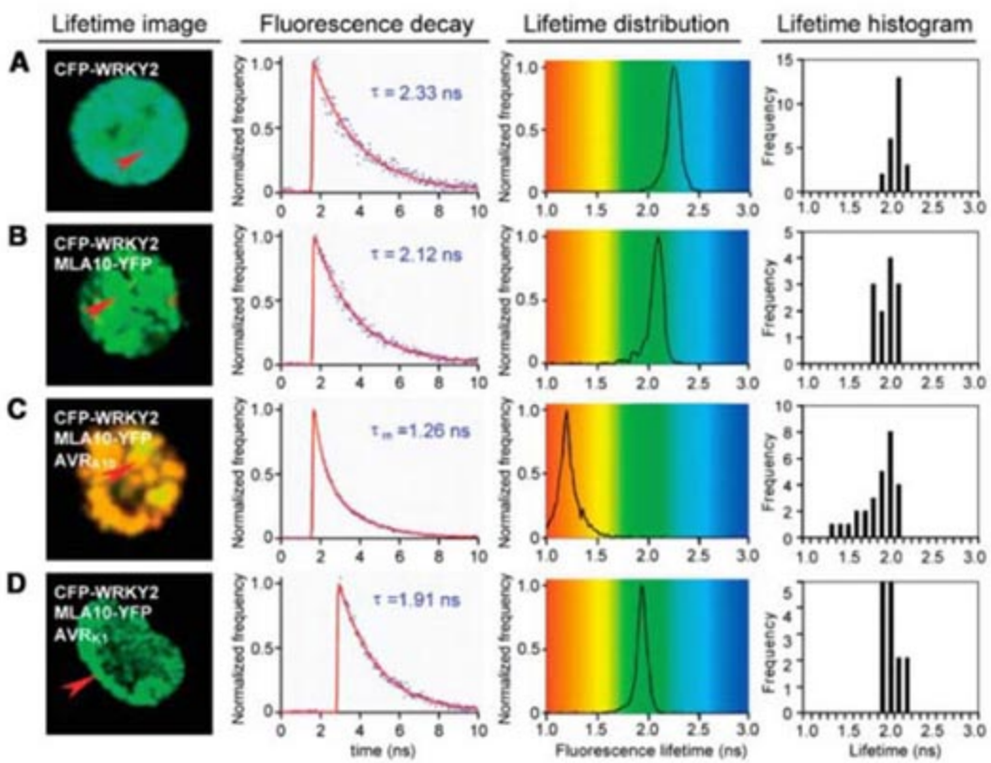

Fig. 4. (**A** to **D**) *Hv*WRKY2 and MLA10 association is AVR_{A10}-dependent. FLIM measurements in barley epidermal nuclei expressing the indicated protein(s) are shown. (Left column) CFP fluorescence lifetime image of the nucleus of a representative cell expressing the indicated protein(s). The average fluorescence lifetime obtained for each pixel is encoded by color as indicated by the scale in the middle right column. (Middle left column) CFP fluorescence decay curve measured for the pixel marked by the red arrowhead in the left column. The decay curve was approximated by a mono- or biexponential function as described in the supporting online material. (Middle right column) CFP fluorescence lifetime distribution throughout the nucleus shown in the lifetime image. (Right column) Histogram of mean CFP fluorescence lifetimes obtained for all measured nuclei expressing the indicated protein(s). Bar heights represent the number of nuclei whose mean lifetime falls within the indicated 0.1-ns range.

Golovinomyces orontii (*24*) (and our collections). Although single *Atwrky18*, *Atwrky40*, or *Atwrky60* mutant plants and *Atwrky18/60* or *Atwrky40/60* double mutants retained Col-0 wild-type–like susceptibility, the *Atwrky18/40* and *Atwrky18/40/60* triple mutant lines were almost fully resistant (Fig. 5, A and B). This reveals redundant *At*WRKY18 and *At*WRKY40 activities and points to a conserved repressor function of the dicot and monocot homologs in basal defense.

Although *Atwrky18/40* double mutants do not constitutively express defense-associated genes (*24*), genome-wide gene expression profiling experiments upon inoculation with virulent *P. syringae* DC3000 revealed that a subset of 23 genes accumulates earlier and is 3.5-fold or more up-regulated in the *Atwrky18/40* double mutant but not in *Atwrky18* or *Atwrky40* single mutants (table S1). This subset contains 21 PAMP-responsive genes, including the 6-fold up-regulated *SID2*, which encodes isochorismate synthase 1, required for salicylic acid biosynthesis, and is a major contributor to basal defense against *G. orontii* (*25*, *26*). Thus, mutants lacking the *At*WRKY18/40 repressors retain the ability to execute stimulus-dependent defense-gene expression and the response appears to be exaggerated. These findings imply the existence of an *At*WRKY18/40-dependent feedback repression system as an intrinsic control feature of basal defense.

Conclusions. Few host factors have been identified that directly interact with intracellular NB-LRR proteins and participate in receptor function. A subset of these, including cytosolic Hsp90, determines R protein steady-state levels, possibly by regulated folding of monomeric R proteins and/or preactivated R protein–containing complexes (*27*). *Arabidopsis* RIN4 interacts with the NB-LRR type R proteins RPM1 and RPS2, forming a preactivation receptor complex at the plasma membrane that permits indirect recognition of the cognate *P. syringae* effectors AvrRpm1 and AvrRpt2, respectively (*28*, *29*). Whether AVR_{A10} is directly or indirectly recognized by the cytoplasmic and/or nuclear MLA10 pool remains unknown. However, unrestricted growth of AVR_{A10}-expressing *B. graminis* after coexpression of *MLA10* and *HvWRKY2* (Fig. 3C) is difficult to reconcile with a scenario in which the TF serves as the effector target that indirectly activates the receptor. We could not detect association of the functional, fluorochrome-tagged MLA10 and *Hv*WRKY2 by FRET-FLIM in the absence of AVR_{A10}. This suggests that the specific, AVR_{A10}-stimulated nuclear association between receptor and TF is a postrecognition event involving activated MLA. Altered intramolecular interactions in the NB-LRR R proteins Rx and Bs2 probably accompany their effector-dependent activation (*30*, *31*). Because MLA recognition specificity is determined by the sequence-divergent LRR-CT region (*6*), direct or indirect effector-induced modulations of the MLA LRR-CT may similarly lead to intramolecular interaction changes, in turn permitting an association of the invariant CC domain with *Hv*WRKY1/2.

Our data suggest that the transcriptional machinery of PAMP-triggered basal defense is a direct target of MLA, thereby providing a link between PRR- and R protein–triggered immunity. Although transcriptional reprogramming of the host during incompatible versus compatible interactions differs only quantitatively and kinetically (*3*), it is difficult to determine whether the typically weaker and/or less sustained defense-related gene expression during compatible interactions is the consequence of effector-mediated defense suppression or is an intrinsic feature of PAMP-triggered basal defense. The retained pathogen-dependent but exaggerated activation of a subset of defense-related genes in *Arabidopsis Atwrky18 wrky40* double mutants is consistent with the existence of at least one negative feedback system operating in PAMP-mediated basal defense. Because enhanced defense against virulent *G. orontii* in *Atwrky18/40* plants was accompanied by extensive leaf cell death (Fig. 5), *At*WRKY18/40-dependent repression might restrict the output of PAMP-triggered basal defense below a detrimental threshold and, at the same time, function as a hair trigger of the primed immune system for R protein–dependent defense potentiation driving host cells into suicide. Given that *AtWRKY18/40* are functionally homologous to *HvWRKY1/2*, it is reasonable to hypothesize that the observed genetic interference (Fig. 3C) and physical association (Figs. 2 and 4) between MLA and *Hv*WRKY1/2 during incompatible interactions with *B. graminis* result in derepression of PAMP-triggered basal defense (fig. S8). This regulatory logic of MLA function could explain why, after biolistic delivery of AVR_{A10} into host epidermal cells of *MLA10* genotypes (that is, in the absence of PAMPs), most cells remain alive (*10*). Direct targeting of PAMP-activated *Hv*WRKY1/2 repressors by MLA receptors also implies a short signaling pathway that may not require genuine *R* gene–specific signaling components.

Plant and animal innate immune systems are thought to have evolved independently from each other (*32*). Accordingly, biochemical constraints might have contributed to the engagement of structurally related components for immune functions in both phyla, including the CATERPILLER superfamily, which encompasses plant NB-LRR R and mammalian NOD proteins (*33*, *34*). CATERPILLER proteins have either demonstrated or anticipated roles as microbial component sensors to control immune and inflammatory responses. In this context, direct targeting of *Hv*WRKY1/2 repressors by MLA R proteins in the nucleus is reminiscent of the nuclear CATERPILLER CIITA function, which acts through direct association with DNA binding proteins to regulate the expression of all major histocompatibility complex class II and other genes important in antigen presentation (*34*). Domain fusion events between a WRKY and NB-LRR domain in two *Arabidopsis* proteins, including the RRS1-R R protein–to–*Ralstonia solanacearum* infection (*35*), suggest similar transcription machinery–associated functions of plant immune receptors.

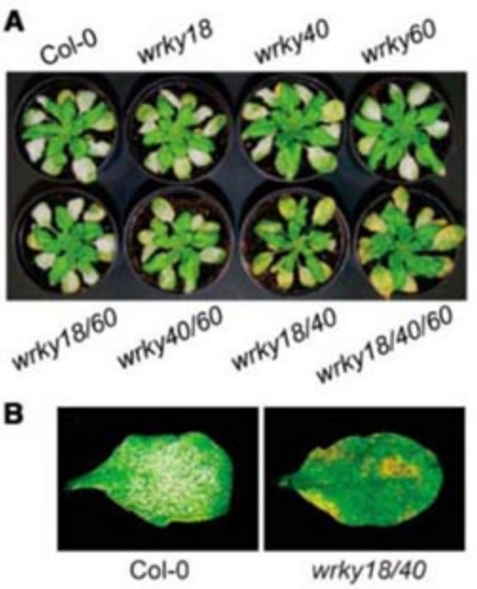

Fig. 5. *Atwrky18/40* double mutant plants are resistant to *G. orontii*. (**A**) Infection phenotypes of *Arabidopsis* plants 10 days after inoculation with virulent *G. orontii*. Plant genotypes are indicated. (**B**) Macroscopic leaf infection phenotype of a representative Col-0 and *Atwrky18/40* plant shown in (A).

References and Notes

1. J. D. G. Jones, J. L. Dangl, *Nature* **444**, 323 (2006).
2. T. Asai *et al.*, *Nature* **415**, 977 (2002).
3. Y. Tao *et al.*, *Plant Cell* **15**, 317 (2003).
4. D. Halterman, F. Zhou, F. Wei, R. P. Wise, P. Schulze-Lefert, *Plant J.* **25**, 335 (2001).
5. D. A. Halterman, R. P. Wise, *Plant J.* **38**, 215 (2004).
6. Q. H. Shen *et al.*, *Plant Cell* **15**, 732 (2003).
7. F. Zhou *et al.*, *Plant Cell* **13**, 337 (2001).
8. S. Bieri *et al.*, *Plant Cell* **16**, 3480 (2004).
9. I. Hein *et al.*, *Plant Physiol.* **138**, 2155 (2005).
10. C. J. Ridout *et al.*, *Plant Cell* **18**, 2402 (2006).
11. W. Wen, J. L. Meinkoth, R. Y. Tsien, S. S. Taylor, *Cell* **82**, 463 (1995).
12. Materials and methods are available as supporting material on *Science* Online.
13. S. Holzberg, P. Brosio, C. Gross, G. P. Pogue, *Plant J.* **30**, 315 (2002).
14. C. Eckey *et al.*, *Plant Mol. Biol.* **55**, 1 (2004).
15. C. X. Sun *et al.*, *Plant Cell* **15**, 2076 (2003).
16. K. Yamasaki *et al.*, *Plant Cell* **17**, 944 (2005).
17. R. Büschges *et al.*, *Cell* **88**, 695 (1997).
18. R. Görg, K. Hollricher, P. Schulze-Lefert, *Plant J.* **3**, 857 (1993).
19. C. Peterhänsel, A. Freialdenhoven, J. Kurth, R. Kolsch, P. Schulze-Lefert, *Plant Cell* **9**, 1397 (1997).
20. I. Gautier *et al.*, *Biophys. J.* **80**, 3000 (2001).
21. B. Ulker, I. E. Somssich, *Curr. Opin. Plant Biol.* **7**, 491 (2004).
22. Z. Xie *et al.*, *Plant Physiol.* **137**, 176 (2005).
23. R. S. Cormack *et al.*, *Biochim. Biophys. Acta Gene Struct. Express.* **1576**, 92 (2002).
24. X. P. Xu, C. H. Chen, B. F. Fan, Z. X. Chen, *Plant Cell* **18**, 1310 (2006).

25. J. Dewdney *et al.*, *Plant J.* **24**, 205 (2000).
26. M. C. Wildermuth, J. Dewdney, G. Wu, F. M. Ausubel, *Nature* **414**, 562 (2001).
27. P. Schulze-Lefert, *Curr. Biol.* **14**, R22 (2004).
28. M. J. Axtell, B. Staskawicz, *Cell* **112**, 369 (2003).
29. D. Mackey, B. F. Holt III, A. Wiig, J. L. Dangl, *Cell* **108**, 743 (2002).
30. R. T. Leister *et al.*, *Plant Cell* **17**, 1268 (2005).
31. G. J. Rairdan, P. Moffett, *Plant Cell* **18**, 2082 (2006).
32. F. M. Ausubel, *Nat. Immunol.* **6**, 973 (2005).
33. W. Strober, P. J. Murray, A. Kitani, T. Watanabe, *Nat. Rev. Immunol.* **6**, 9 (2006).
34. J. P. Y. Ting, D. L. Kastner, H. M. Hoffman, *Nat. Rev. Immunol.* **6**, 183 (2006).
35. L. Deslandes *et al.*, *Proc. Natl. Acad. Sci. U.S.A.* **100**, 8024 (2003).
36. We thank C. Ridout and C. Jansson for providing various plasmids; Z. Chen (Purdue University) for providing *Arabidopsis wrky* single and triple mutants; and E. Schmelzer, E. Logemann, A. Reinstaedler, M. Hallstein, and H. Häweker for technical support. This work was supported by funds from the Max Planck Society, a Deutsche Forschungsgemeinschaft grant (SFB670) to Q.-H. S., and a European Union–BIOEXPLOIT grant to Y.S.

Supporting Online Material
www.sciencemag.org/cgi/content/full/1136372/DC1
Materials and Methods
Figs. S1 to S8
Table S1
References

16 October 2006; accepted 14 December 2006
Published online 21 December 2006;
10.1126/science.1136372
Include this information when citing this paper.

The Triple-Ring Nebula Around SN 1987A: Fingerprint of a Binary Merger

Thomas Morris[1,2] and Philipp Podsiadlowski[1]*

Supernova 1987A, the first naked-eye supernova observed since Kepler's supernova in 1604, defies a number of theoretical expectations. Its anomalies have long been attributed to a merger between two massive stars that occurred some 20,000 years before the explosion, but so far there has been no conclusive proof that this merger took place. Here, we present three-dimensional hydrodynamical simulations of the mass ejection associated with such a merger and the subsequent evolution of the ejecta, and we show that this accurately reproduces the properties of the triple-ring nebula surrounding the supernova.

Supernova 1987A in the Large Magellanic Cloud was one of the major astronomical events of the 1980s, but it was highly unusual. The progenitor star, Sk −69°202, was one of the surprises. Massive stars similar to the progenitor of SN 1987A are expected to end their evolution as red supergiants, but Sk −69°202 was a blue supergiant. Moreover, the outer layers of the star were highly enriched in helium (*1*), suggesting that some nuclear processed material from the core had been mixed into the envelope by a nonstandard mixing process (*2*). Most notably, the supernova was surrounded by a complex triple-ring nebula (*3*, *4*) consisting of material that was ejected from the progenitor some 20,000 years before the explosion in an almost axi-symmetric but very nonspherical manner. Together, this evidence indicates that a dramatic event affected the progenitor some 20,000 years before the explosion, most likely the merger of two massive stars (*5*).

A merger was first suggested to explain some of the asymmetries of the supernova ejecta (*6*). Later it was realized that a binary merger would also explain the blue progenitor and its main chemical anomalies (*7*–*9*). This hypothesis has since been confirmed by detailed stellar, hydrodynamical simulations of the slow merger of two massive stars (*10*). However, the origin of the triple-ring nebula has so far not found a satisfactory explanation.

The triple-ring nebula consists of three overlapping rings in projection. The supernova occurred at the center of the inner ring, and the outer rings are in planes almost parallel to the central ring plane but displaced by 0.4 pc above and below the central ring plane. Notably, these outer rings do not form the limb-brightened projection of an hourglass nebula, as in some of the early models for the nebula (*11*–*13*), but form instead dense, ringlike density enhancements (*4*). Previous attempts to model the nebula have involved interacting winds in a binary (*14*, *15*), a photoionization-driven instability (*16*), mass ejection during a binary merger (*17*), or magnetically controlled ejection (*18*), but none of these has been able to fully explain both the detailed geometry and the kinematical properties of the nebula.

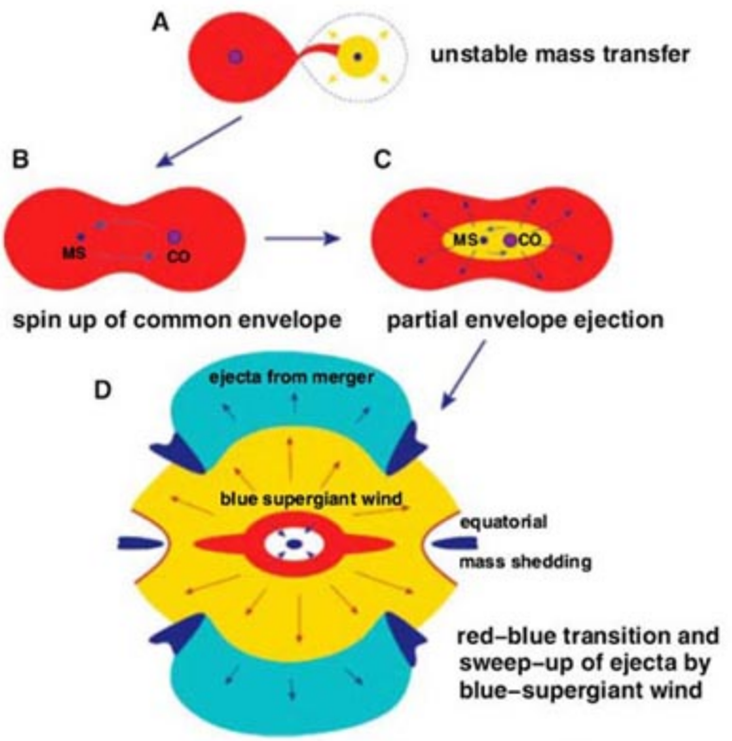

Fig. 1. Schematic diagram showing the formation of the triple-ring nebula. The system initially consisted of a binary with two stars of ~15 and ~5 $M_{\odot}$ with an orbital period longer than ~10 years. Mass transfer is dynamically unstable, leading to the merger of the two components in (**A**) a common envelope and (**B**) the spin-up of the envelope. MS, main-sequence companion; CO, carbon-oxygen core. (**C**) The release of orbital energy due to the spiral in of the companion leads to the partial ejection of the envelope. (**D**) After the merging has been completed, the merged object evolves to become a blue supergiant, shedding its excess angular momentum in an equatorial outflow. In the final blue-supergiant phase, the energetic wind from the blue supergiant sweeps up all of the previous structures, producing the triple-ring nebula.

[1]Department of Astrophysics, University of Oxford, Oxford OX1 3RH, UK. [2]Max-Planck Institut für Astrophysik, Garching 85741, Germany.

*To whom correspondence should be addressed. E-mail: podsi@astro.ox.ac.uk

The axi-symmetric but very nonspherical structure immediately suggests that rotation may have played a role in the formation. However, simple angular-momentum conservation arguments show that any single star that is rotating rapidly in its early evolution could rotate slowly only after it has expanded by a factor of ~100 to red-supergiant dimensions. On the other hand, a binary merger provides a simple and effective means of converting orbital angular momentum into spin angular momentum and of producing a single, rapidly rotating supergiant.

A typical binary merger model for SN 1987A (*9*) assumes that the system initially consisted of two massive stars with masses of ~15 and ~5 solar masses ($M_\odot$) in a fairly wide orbit with an orbital period longer than ~10 years. Given these parameters, the more massive component started to transfer mass to its companion only after it had completed helium burning in the core. Because of the large mass ratio, mass transfer was unstable, leading to a common envelope phase during which the secondary star was engulfed within the primary star's envelope (Fig. 1). In this phase, most of the orbital angular momentum of the binary was deposited in the common envelope, spinning the envelope up in the process. The friction with the envelope caused the secondary star's orbit to decay (i.e., to spiral in) inside the common envelope. Because the density increased inward, the spiral-in process accelerated until enough orbital energy had been released and deposited in the envelope to affect the envelope dynamically. The time scale of this energy ejection is comparable to the dynamical time scale of the envelope, meaning that the energy injection into the envelope was essentially impulsive; this led to a dynamical expansion of the envelope and substantial mass ejection. After the envelope expanded, the spiral in of the secondary star slowed down and occurred in a self-regulated manner, in which

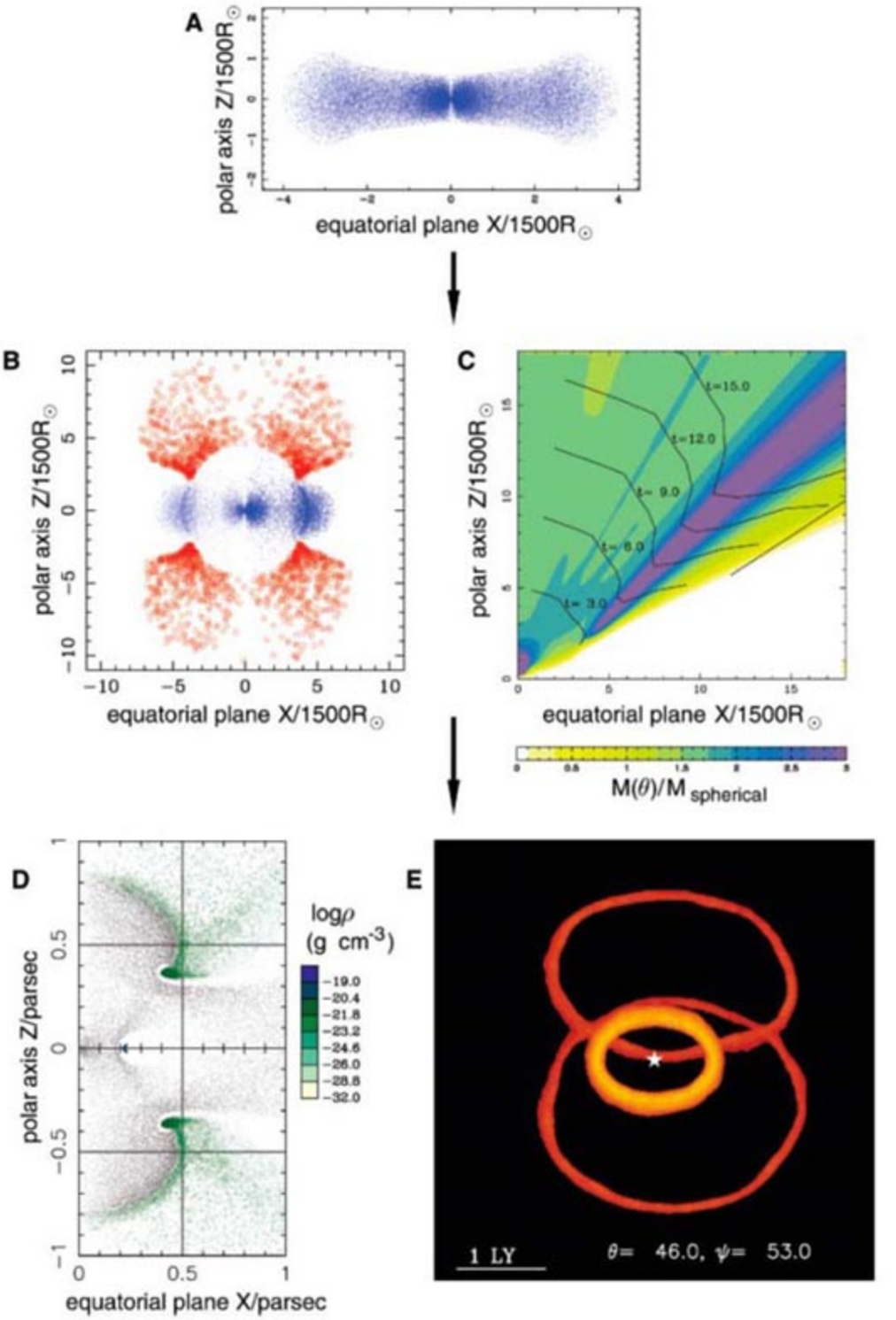

Fig. 2. Three-dimensional hydrodynamical (SPH) simulations to model the various phases shown in Fig. 1. (**A**) Cross-section of the rapidly rotating red-supergiant envelope, containing 2×10^5 SPH particles, following the spin-up in the initial common-envelope phase (Fig. 1B) after a total amount of orbital angular momentum of $L = 8 \times 10^{54}$ erg s has been deposited in the envelope. In these units, the red supergiant had an initial radius of 1. (**B**) Image of particles in the meridional plane approximately 3 years after the orbital energy has been injected in the central part of the common envelope (Fig. 1C), showing the formation of the enhancement at mid-latitudes. Red particles are unbound. (**C**) The mass enhancement in the ejecta plotted as a function of time (contours) and distance from the center of mass, as a function of latitude. The horizontal axis shows the equatorial plane where no mass is ejected, and the color scale beneath the plot shows the increase of ejected mass over the value expected in spherical symmetry. The contours show the mean radius of the ejected material at the time shown, in units of 0.8 years (*21*). The axes are in the same unit system as those of (A) and (B). (**D**) The final particle distribution (10^6 particles) plotted in the meridional plane at an age of 20,000 years. The density and mean velocity of the material in the equatorial ring is $\sim 2 \times 10^4$ cm^{-3} and 10.3 km s^{-1}, respectively. The density and mean velocity of the material in the outer rings is 10^3 cm^{-3} and 31 km s^{-1}, respectively. Wind particles are shown in black and the nebula particles are shown in dark blue through pale green based on a logarithmic density scale as indicated. The axes are in units of 3×10^{18} cm. (**E**) Simulated emission measure at ~2000 days after the supernova in the 656-nm Hα line for our best model. The total flux from the outer rings is 4×10^{45} photons s^{-1}, comparable to the observed flux (*4*). LY, light year; θ, the inclination of the symmetry axis with respect to the observer; ψ, the direction of the velocity kick measured in the equatorial plane. The star indicates the location of the supernova. Simulations are available online (movies S1 and S2).

all of the orbital energy released was transported to the surface, where it was radiated away. Ultimately, the secondary star inside the envelope merged with the core, and in doing so dredged up core material from the primary star core (*10*). The whole merger process is expected to have taken a few hundred years. Afterward, the star was initially an oversized red supergiant, but it shrank over the course of a few thousand years—the time scale on which the envelope lost its excess thermal energy—and became a blue supergiant. In this phase, the fast, energetic wind from the blue supergiant swept up the ejecta associated with the merger and shaped the whole nebula.

To simulate the mass ejection during the merger and the subsequent evolution of the ejecta (Fig. 2), we used GADGET (*19*), a three-dimensional, particle-based hydrodynamics code that uses the smooth-particle hydrodynamics (SPH) method. We split the simulations into two parts. First, we simulated the mass ejection associated with the merger, and then we took the output from this model to start a second calculation to simulate the subsequent evolution of the ejecta as they are being swept up by the blue-supergiant wind.

We modeled the red supergiant as a polytrope with a central point source of 8 $M_{\odot}$, representing the compact core of the star and the immersed companion, and an envelope mass of 12 $M_{\odot}$; the initial radius of the star was taken to be 1500 $R_{\odot}$. We then mimicked the initial spin-up phase by adding angular momentum to the envelope over a period of ~6 years until all of the angular momentum from the initial binary was deposited in the envelope (*20*). Because of this spin-up, the envelope became highly nonspherical and took on a disklike shape (Fig. 2A). Most of the orbital energy was injected impulsively when the orbital energy released was comparable to the binding energy of the envelope (*21*). This produced an inner region of overpressure that started to expand and drive a shock in the overlying layers, ejecting some of the outer layers in the process. Because of the highly flattened envelope structure, mass ejection was easiest in the polar direction and occurred there first. Whether mass was ejected in the equatorial direction depended on the amount of energy injected. If it was less than about one-third the binding energy of the envelope, the large mass concentration in the equatorial plane inhibited equatorial mass ejection (*20*); particles that tried to escape in the equatorial direction were deflected by the large equatorial mass concentration toward higher latitudes (Fig. 2C). This produced a large density enhancement in the ejecta at roughly 45°. Indeed, it is the overdensity at mid-latitude that would ultimately be swept up to form the outer rings in the SN 1987A nebula.

In our best model, no matter was ejected in the equatorial direction. However, because the merged object has much more angular momentum than a more compact blue supergiant could have, the merged object has to lose this excess angular momentum, most likely in the form of a slow equatorial outflow (*22*), as it shrinks to become a blue supergiant. We estimated that, for typical parameters, most likely several solar masses would need to be lost in this transition phase (*21*). Once the merged object has become a blue supergiant, its energetic blue-supergiant wind will start to sweep up all the structures ejected previously.

To model the blue-supergiant phase, we started a second SPH calculation in which we only simulated the ejecta. For the initial model of this calculation, we took the output from the first simulation once the ejecta expanded freely. This gives the mass and the velocity of the ejecta as a function of latitude. We then ballistically extrapolated the evolution of the ejecta for 4000 years, the assumed time of the red-blue transition. We modeled the equatorial mass shedding by including an equatorial outflow, lasting for 2000 years (*21*). We then introduced a spherically symmetric blue-supergiant wind (with a mass-loss rate of $\dot{M} = 2 \times 10^{-7}\ M_{\odot}\ \mathrm{year}^{-1}$ and wind velocity $v_w = 500\ \mathrm{km\ s}^{-1}$) and observed the subsequent evolution.

In a typical simulation, after ~20,000 years (Fig. 2D), the density enhancement at mid-latitude had been swept up into two well-defined rings, which together with the swept-up equatorial outflow produced the main features of the triple-ring nebula when observed at an inclination of ~45° (Fig. 2E). The Hubble Space Telescope image (*4*) of the nebula shows that the symmetry center of the outer rings is slightly displaced from the symmetry axis of the central ring. This asymmetry can be easily explained if the ejecta associated with the merger are given a small velocity kick of ~2 $\mathrm{km\ s}^{-1}$ in a direction to the northwest of the nebula, at an angle of 11° out of the equatorial ring plane. This was done to produce the model shown in Fig. 2E, which almost perfectly reproduces not only the main features of the triple-ring nebula but also the small asymmetries of the outer rings (such as their deviations from perfect ellipses and their displacement from the central symmetry axis). To generate this emission model (*21*), we assumed that the nebula was fully ionized by the supernova explosion and that the emission was optically thin. This best model also reproduces the kinematics of both the inner ring (*23*) and the outer rings (*4*). In this particular model, the inner ring contains 0.4 $M_{\odot}$ of mass, whereas the outer rings contain a total of 0.02 $M_{\odot}$ each.

The physical origin of this small kick is not entirely clear. It could be associated with a nonradial pulsational mode excited during the early spiral-in phase; alternatively, it could be due to the orbital motion caused by a more distant low-mass third star in the system.

In addition to the three rings, the model predicts several other structures. The outer rings form the ends of two bipolar lobes that, combined with the bow-shock structure around the inner ring, are reminiscent of an hourglass nebula (Fig. 2D). This structure is presumably the origin of the hourglass structure that has been inferred from light-echo studies (*24*). Further light echoes have also been detected from beyond the triple-ring structure (*25*); these were most likely formed during the earlier red-supergiant phase of the primary star before the merger or in the phase immediately preceding the merger, where accretion on the companion may produce a bipolar outflow (*26*). These phases were not included in our simulations.

The hydrodynamical model we present here provides an excellent fit to the observed triple-ring nebula around SN 1987A. Notably, this model does not require any physically ad hoc assumptions, and all of the input parameters are compatible with the values expected from simple modeling of the various phases of the merger (apart from the physical origin of the small kick given to the ejecta, which is presently not explained).

The model also makes several predictions, specifically about the mass in the different rings and other structures. These may ultimately become visible when the supernova ejecta begin destroying the nebula or when the emergent x-ray flux resulting from the supernova-ring interaction re-ionizes the nebula. In our favored model, the outer rings are ejected before the core material is dredged up, whereas the inner ring is ejected afterward. This distinction suggests some chemical differences between the inner ring and the outer rings—namely, that the inner ring should show a larger helium enhancement and more evidence for CNO processing than the outer rings. This may already have been observed (*27*) but needs to be confirmed in a more detailed comparative study.

References and Notes

1. G. Sonneborn *et al.*, *Astrophys. J.* **477**, 848 (1997).
2. H. Saio, K. Nomoto, M. Kato, *Astrophys. J.* **331**, 388 (1988).
3. E. J. Wampler *et al.*, *Astrophys. J.* **362**, L13 (1990).
4. C. Burrows *et al.*, *Astrophys. J.* **452**, 680 (1995).
5. R. McCray, *Nature* **386**, 438 (1997).
6. R. A. Chevalier, N. Soker, *Astrophys. J.* **341**, 867 (1989).
7. Ph. Podsiadlowski, P. C. Joss, S. Rappaport, *Astron. Astrophys.* **227**, L9 (1990).
8. W. Hillebrandt, F. Meyer, *Astron. Astrophys.* **219**, L3 (1989).
9. Ph. Podsiadlowski, *Publ. Astron. Soc. Pac.* **104**, 717 (1992).
10. N. Ivanova, Ph. Podsiadlowski, in *From Twilight to Highlight: The Physics of Supernovae*, W. Hillebrandt, B. Leibundgut, Ed. (Springer, Berlin, 2003), pp. 19–22.
11. D. Luo, R. McCray, *Astrophys. J.* **379**, 659 (1991).
12. P. Lundqvist, C. Fransson, *Astrophys. J.* **380**, 575 (1991).
13. C. Martin, D. Arnett, *Astrophys. J.* **447**, 378 (1995).
14. Ph. Podsiadlowski, A. C. Fabian, I. R. Stevens, *Nature* **354**, 43 (1991).
15. M. Lloyd, T. O'Brien, F. Kahn, *Mon. Not. R. Astron. Soc.* **273**, L19 (1995).
16. F. Meyer, *Mon. Not. R. Astron. Soc.* **285**, L11 (1997).
17. N. Soker, *Mon. Not. R. Astron. Soc.* **303**, 611 (1999).
18. T. Tanaka, H. Washimi, *Science* **296**, 321 (2002).
19. V. Springel, N. Yoshida, S. White, *N. Astron.* **6**, 51 (2001).
20. T. Morris, Ph. Podsiadlowski, *Mon. Not. R. Astron. Soc.* **365**, 2 (2006).

21. Materials and methods are available as supporting material on *Science* Online.
22. A. Heger, N. Langer, *Astron. Astrophys.* **334**, 210 (1998).
23. A. P. Crotts, S. R. Heathcote, *Nature* **350**, 683 (1991).
24. J. Xu, A. Crotts, W. Kunkel, *Astrophys. J.* **451**, 806 (1995).
25. B. Sugerman, A. Crotts, W. Kunkel, S. Heathcote, S. Lawrence, *Astrophys. J.* **627**, 888 (2005).
26. N. Soker, *Astrophys. J.*, in press; preprint available online (http://xxx.lanl.gov/abs/astro-ph/0610655)
27. N. Panagia *et al.*, *Astrophys. J.* **459**, L17 (1996).
28. The authors would like to thank L. Nelson for providing access to the Bishop/Sherbrooke Beowulf cluster (Elix3) which was used to perform the interacting winds calculations. The binary merger calculations were performed on the UK Astrophysical Fluids Facility. T.M. acknowledges support from the Research Training Network "Gamma-Ray Bursts: An Enigma and a Tool" during part of this work.

Supporting Online Material
www.sciencemag.org/cgi/content/full/315/5815/1103/DC1
Materials and Methods
SOM Text
Tables S1 and S2
References
Movies S1 and S2

16 October 2006; accepted 15 January 2007
10.1126/science.1136351

Decagonal and Quasi-Crystalline Tilings in Medieval Islamic Architecture

Peter J. Lu[1]* and Paul J. Steinhardt[2]

The conventional view holds that girih (geometric star-and-polygon, or strapwork) patterns in medieval Islamic architecture were conceived by their designers as a network of zigzagging lines, where the lines were drafted directly with a straightedge and a compass. We show that by 1200 C.E. a conceptual breakthrough occurred in which girih patterns were reconceived as tessellations of a special set of equilateral polygons ("girih tiles") decorated with lines. These tiles enabled the creation of increasingly complex periodic girih patterns, and by the 15th century, the tessellation approach was combined with self-similar transformations to construct nearly perfect quasi-crystalline Penrose patterns, five centuries before their discovery in the West.

Girih patterns constitute a wide-ranging decorative idiom throughout Islamic art and architecture (*1*–*6*). Previous studies of medieval Islamic documents describing applications of mathematics in architecture suggest that these girih patterns were constructed by drafting directly a network of zigzagging lines (sometimes called strapwork) with the use of a compass and straightedge (*3*, *7*). The visual impact of these girih patterns is typically enhanced by rotational symmetry. However, periodic patterns created by the repetition of a single "unit cell" motif can have only a limited set of rotational symmetries, which western mathematicians first proved rigorously in the 19th century C.E.: Only two-fold, three-fold, four-fold, and six-fold rotational symmetries are allowed. In particular, five-fold and 10-fold symmetries are expressly forbidden (*8*). Thus, although pentagonal and decagonal motifs appear frequently in Islamic architectural tilings, they typically adorn a unit cell repeated in a pattern with crystallographically allowed symmetry (*3*–*6*).

Although simple periodic girih patterns incorporating decagonal motifs can be constructed using a "direct strapwork method" with a straightedge and a compass (as illustrated in Fig. 1, A to D), far more complex decagonal patterns also occur in medieval Islamic architecture. These complex patterns can have unit cells containing hundreds of decagons and may repeat the same decagonal motifs on several length scales. Individually placing and drafting hundreds of such decagons with straightedge and compass would have been both exceedingly cumbersome and likely to accumulate geometric distortions, which are not observed.

On the basis of our examination of a large number of girih patterns decorating medieval Islamic buildings, architectural scrolls, and other forms of medieval Islamic art, we suggest that by 1200 C.E. there was an important breakthrough in Islamic mathematics and design: the discovery of an entirely new way to conceptualize and construct girih line patterns as decorated tessellations using a set of five tile types, which we call "girih tiles." Each girih tile is decorated with lines and is sufficiently simple to be drawn using only mathematical tools documented in medieval Islamic sources. By laying the tiles edge-to-edge, the decorating lines connect to form a continuous network across the entire tiling. We further show how the girih-tile approach opened the path to creating new types of extraordinarily complex patterns, including a nearly perfect quasi-crystalline Penrose pattern on the Darb-i Imam shrine (Isfahan, Iran, 1453 C.E.), whose underlying mathematics were not understood for another five centuries in the West.

As an illustration of the two approaches, consider the pattern in Fig. 1E from the shrine of Khwaja Abdullah Ansari at Gazargah in Herat, Afghanistan (1425 to 1429 C.E.) (*3*, *9*), based on a periodic array of unit cells containing a common decagonal motif in medieval Islamic architecture, the 10/3 star shown in Fig. 1A (see fig. S1 for additional examples) (*1*, *3*–*5*, *10*). Using techniques documented by medieval Islamic mathematicians (*3*, *7*), each motif can be drawn using the direct strapwork method (Fig. 1, A to D). However, an alternative geometric construction can generate the same pattern (Fig. 1E, right). At the intersections between all pairs of line segments not within a 10/3 star, bisecting the larger 108° angle yields line segments (dotted red in the figure) that, when extended until they intersect, form three distinct polygons: the decagon decorated with a 10/3 star line pattern, an elongated hexagon decorated with a bat-shaped line pattern, and a bowtie decorated by two opposite-facing quadrilaterals. Applying the same procedure to a ~15th-century pattern from the Great Mosque of Nayriz, Iran (fig. S2) (*11*) yields two additional polygons, a pentagon with a pentagonal star pattern, and a rhombus with a bowtie line pattern. These five polygons (Fig. 1F), which we term "girih tiles," were used to construct a wide range of patterns with decagonal motifs (fig. S3) (*12*). The outlines of the five girih tiles were also drawn in ink by medieval Islamic architects in scrolls drafted to transmit architectural practices, such as a 15th-century Timurid-Turkmen scroll now held by the Topkapi Palace Museum in Istanbul (Fig. 1G and fig. S4) (*2*, *13*), providing direct historical documentation of their use.

The five girih tiles in Fig. 1F share several geometric features. Every edge of each polygon has the same length, and two decorating lines intersect the midpoint of every edge at 72° and 108° angles. This ensures that when the edges of two tiles are aligned in a tessellation, decorating lines will continue across the common boundary without changing direction (*14*). Because both line intersections and tiles only contain angles that are multiples of 36°, all line segments in the final girih strapwork pattern formed by girih-tile decorating lines will be parallel to the sides of the regular pentagon; decagonal geometry is thus enforced in a girih pattern formed by the tessellation of any combination of girih tiles. The tile decorations have different internal rotational symmetries: the decagon, 10-fold symmetry; the pentagon, five-fold; and the hexagon, bowtie, and rhombus, two-fold.

Tessellating these girih tiles provides several practical advantages over the direct strapwork method, allowing simpler, faster, and more accurate execution by artisans unfamiliar with their mathematical properties. A few full-size girih tiles could serve as templates to help position decorating lines on a building surface, allowing rapid, exact pattern generation. More-

[1]Department of Physics, Harvard University, Cambridge, MA 02138, USA. [2]Department of Physics and Princeton Center for Theoretical Physics, Princeton University, Princeton, NJ 08544, USA.

*To whom correspondence should be addressed. E-mail: plu@fas.harvard.edu

over, girih tiles minimize the accumulation of angular distortions expected in the manual drafting of individual 10/3 stars, with concomitant errors in sizing, position, and orientation.

Girih tiles further enable the construction of periodic decagonal-motif patterns that do not arise naturally from the direct strapwork method. One class of such patterns repeats pentagonal motifs but entirely lacks the 10/3 stars that establish the initial decagonal angles needed for direct drafting with straightedge and compass. Patterns of this type appear around 1200 C.E. on Seljuk buildings, such as the Mama Hatun Mausoleum in Tercan, Turkey (1200 C.E.; Fig. 2A) (*5*, *15*, *16*), and can be created easily by tessellating bowtie and hexagon girih tiles to create perfect pentagonal motifs, even in the absence of a decagon star (i.e., lacking decagon girih tiles; see fig. S5). Even more compelling evidence for the use of girih tiles occurs on the walls of the Gunbad-i Kabud in Maragha, Iran (1197 C.E.) (*11*, *17*, *18*), where seven of eight exterior wall panels on the octagonal tomb tower are filled with a tiling of decagons, hexagons, bowties, and rhombuses (Fig. 2, B and C). Within each wall panel, the decagonal pattern does not repeat; rather, the unit cell of this periodic tiling spans the length of two complete panels (fig. S6). The main decorative raised brick pattern follows the girih-tile decorating lines of Fig. 1F. However, a second set of smaller decorative lines conforms to the internal rotational symmetry of each individual girih tile without adhering to pentagonal angles (Fig. 2, C and D): Within each region occupied by a hexagon, bowtie, or rhombus, the smaller line decoration has a two-fold, not five-fold, rotational symmetry, and therefore could not have been generated using the direct strapwork method. By contrast, constructing both patterns is straightforward with girih tiles. Two sets of line decoration were applied to each girih tile: the standard line decoration of Fig. 1F, and a second, nonpentagonal set of motifs with an overall two-fold symmetry (Fig. 2, C and D). The girih tiles were then tessellated, with the regular line pattern expressed in large raised brick on the tower and the second set of lines expressed in smaller bricks. The dual-layer nature of line patterns on the Maragha tower thus adds strong evidence that the pattern was generated by tessellating with the girih tiles in Fig. 1F.

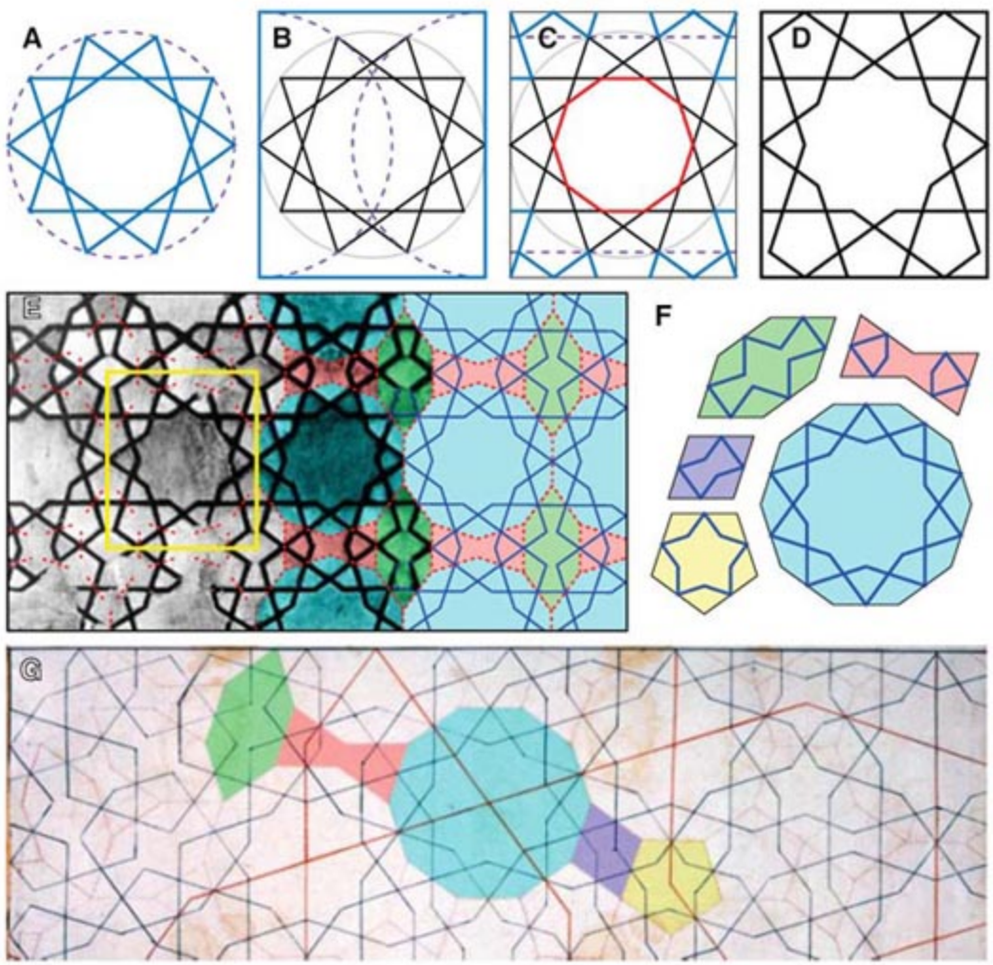

Fig. 1. Direct strapwork and girih-tile construction of 10/3 decagonal patterns. (**A** to **D**) Generation of a common 10/3 star pattern by the direct strapwork method. (A) A circle is divided equally into 10, and every third vertex is connected by a straight line to create the 10/3 star that (B) is centered in a rectangle whose width is the circle's diameter. In each step, new lines drafted are indicated in blue, lines to be deleted are in red, and purple construction lines not in the final pattern are in dashed purple. (**E**) Periodic pattern at the Timurid shrine of Khwaja Abdullah Ansari at Gazargah in Herat, Afghanistan (1425 to 1429 C.E.), where the unit cell pattern (D) is indicated by the yellow rectangle. The same pattern can be obtained by tessellating girih tiles (overlaid at right). (**F**) The complete set of girih tiles: decagon, pentagon, hexagon, bowtie, and rhombus. (**G**) Ink outlines for these five girih tiles appear in panel 28 of the Topkapi scroll, where we have colored one of each girih tile according to the color scheme in (F).

Perhaps the most striking innovation arising from the application of girih tiles was the use of self-similarity transformation (the subdivision of large girih tiles into smaller ones) to create overlapping patterns at two different length scales, in which each pattern is generated by the same girih tile shapes. Examples of subdivision can be found in the Topkapi scroll (e.g., Fig. 1G; see also fig. S4A) and on the Friday Mosque (*17*) and Darb-i Imam shrine (1453 C.E.) (*2*, *9*, *19*) in Isfahan, Iran. A spandrel from the Darb-i Imam shrine is shown in Fig. 3A. The large, thick, black line pattern consisting of a handful of decagons and bowties (Fig. 3C) is subdivided into the smaller pattern, which can also be perfectly generated by a tessellation of 231 girih tiles (Fig. 3B; line decoration of Fig. 1F filled in with solid color here). We have identified the subdivision rule used to generate the Darb-i Imam spandrel pattern (Fig. 3, D and E), which was also used on other patterns on the Darb-i Imam shrine and Isfahan Friday Mosque (fig. S7).

A subdivision rule, combined with decagonal symmetry, is sufficient to construct perfect quasi-crystalline tilings—patterns with infinite perfect quasi-periodic translational order and crystallographically forbidden rotational symmetries, such as pentagonal or decagonal—which mathematicians and physicists have come to understand only in the past 30 years (*20*, *21*). Quasi-periodic order means that distinct tile shapes repeat with frequencies that are incommensurate; that is, the ratio of the frequencies cannot be expressed as a ratio of integers. By having quasi-periodicity rather than periodicity, the symmetry constraints of conventional crystallography can be violated, and it is possible to have pentagonal motifs that join together in a pattern with overall pentagonal and decagonal symmetry (*21*).

The most famous example of a quasi-crystalline tiling is the Penrose tiling (*20*, *22*), a two-tile tessellation with long-range quasi-periodic translational order and five-fold symmetry. The Penrose tiles can have various shapes. A convenient choice for comparison with medieval Islamic architectural decoration is the kite and dart shown on the left side of Fig. 4, A and B. As originally conceived by Penrose in the 1970s, the tilings can be constructed either by "matching rules" or by self-similar subdivisions. For the matching rules, the kite and dart can each be decorated with red and blue stripes (Fig. 4, A and B); when tiles are placed so that

the stripes continue uninterrupted, the only possible close-packed arrangement is a five-fold symmetric quasi-crystalline pattern in which the kites and darts repeat with frequencies whose ratio is irrational, namely, the golden ratio $\tau \equiv (1 + \sqrt{5})/2 \approx 1.618$. We see no evidence that Islamic designers used the matching-rule approach. The second approach is to repeatedly subdivide kites and darts into smaller kites and darts, according to the rules shown in Fig. 4, A and B. This self-similar subdivision of large tiles into small tiles can be expressed in terms of a transformation matrix whose eigenvalues are irrational, a signature of quasi-periodicity; the eigenvalues represent the ratio of tile frequencies in the limit of an infinite tiling (*23*).

Our analysis indicates that Islamic designers had all the conceptual elements necessary to produce quasi-crystalline girih patterns using the self-similar transformation method: girih tiles, decagonal symmetry, and subdivision. The pattern on the Darb-i Imam shrine is a remarkable example of how these principles were applied. Using the self-similar subdivision of large girih tiles into small ones shown in Fig. 3, D and E, an arbitrarily large Darb-i Imam pattern can be constructed. The asymptotic ratio of hexagons to bowties approaches the golden ratio τ (the same ratio as kites to darts in a Penrose tiling), an irrational ratio that shows explicitly that the pattern is quasi-periodic.

Moreover, the Darb-i Imam tile pattern can be mapped directly into Penrose tiles following the prescription for the hexagon, bowtie (*22*), and decagon given in Fig. 4, C to E. Using these substitutions, both the large (Fig. 3C) and small (Fig. 3B) girih-tile patterns on the Darb-i Imam can be mapped completely into Penrose tiles (fig. S8). Note that the mapping shown in Fig. 4, C to E, breaks the bilateral symmetries of the girih tiles; as a result, for an individual tile, there is a discrete number of choices for the mapping: 10 for the decagon, two each for hexagon and bowtie. Therefore, the mapping is completed by using this freedom to eliminate Penrose tile edge mismatches to the maximum degree possible. Note that, unlike previous comparisons in the literature between Islamic designs with decagonal motifs and Penrose tiles (*18*, *24*), the Darb-i Imam tessellation is not embedded in a periodic framework and can, in principle, be extended into an infinite quasi-periodic pattern.

Although the Darb-i Imam pattern illustrates that Islamic designers had all the elements needed to construct perfect quasi-crystalline patterns, we nonetheless find indications that the designers had an incomplete understanding of these elements. First, we have no evidence that they ever developed the alternative matching-rule approach. Second, there are a small number of tile mismatches, local imperfections in the Darb-i Imam tiling. These can be visualized by mapping the tiling into the Penrose tiles and identifying the mismatches. However, there are only a few of them—11 mismatches out of 3700 Penrose tiles—and every mismatch is point-like, removable with a local rearrangement of a few tiles without affecting the rest of the pattern (Fig. 4F and fig. S8). This is the kind of defect that an artisan could have made inadvertently in constructing or repairing a complex pattern. Third, the designers did not begin with a single girih tile, but rather with a small arrangement of large tiles that does not appear in the subdivided pattern. This arbitrary and unnecessary choice means that, strictly speaking, the tiling is not self-similar, although repeated application of the subdivision rule would nonetheless lead to the same irrational τ ratio of hexagons to bowties.

Our work suggests several avenues for further investigation. Although the examples we have studied thus far fall just short of being perfect quasi-crystals, there may be more interesting examples yet to be discovered, including perfectly quasi-periodic decagonal patterns. The subdivision analysis outlined above establishes a procedure for identifying quasi-periodic patterns

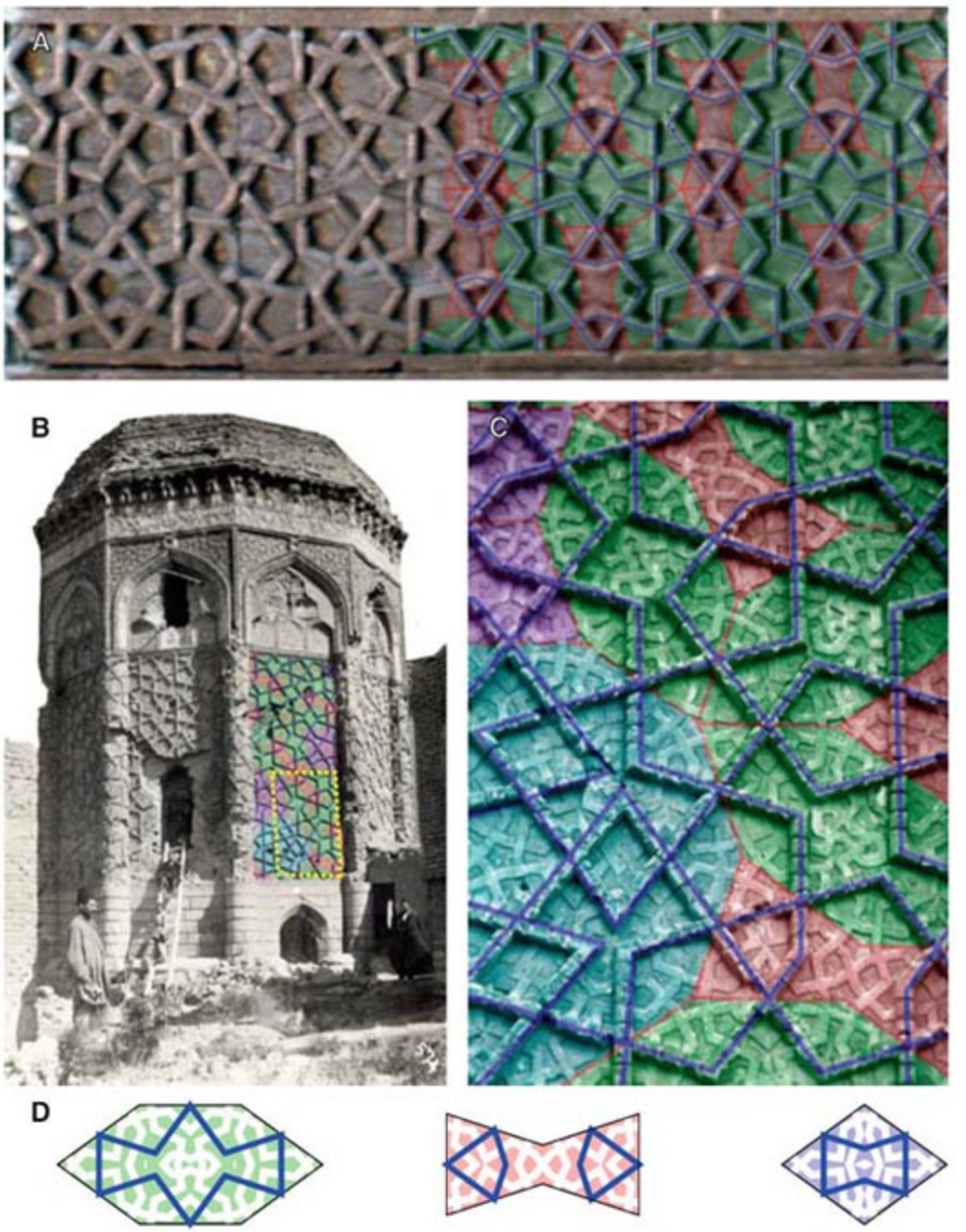

Fig. 2. (**A**) Periodic girih pattern from the Seljuk Mama Hatun Mausoleum in Tercan, Turkey (~1200 C.E.), where all lines are parallel to the sides of a regular pentagon, even though no decagon star is present; reconstruction overlaid at right with the hexagon and bowtie girih tiles of Fig. 1F. (**B**) Photograph by A. Sevruguin (~1870s) of the octagonal Gunbad-i Kabud tomb tower in Maragha, Iran (1197 C.E.), with the girih-tile reconstruction of one panel overlaid. (**C**) Close-up of the area marked by the dotted yellow rectangle in (B). (**D**) Hexagon, bowtie, and rhombus girih tiles with additional small-brick pattern reconstruction (indicated in white) that conforms not to the pentagonal geometry of the overall pattern, but to the internal two-fold rotational symmetry of the individual girih tiles.

and measuring their degree of perfection. Also, analogous girih tiles may exist for other non-crystallographic symmetries, and similar dotted tile outlines for nondecagonal patterns appear in the Topkapi scroll. Finally, although our analysis shows that complex decagonal tilings were being made by 1200 C.E., exactly when the shift from the direct strapwork to the girih-tile paradigm first occurred is an open question, as is the identity of the designers of these complex Islamic patterns, whose geometrical sophistication led the medieval world.

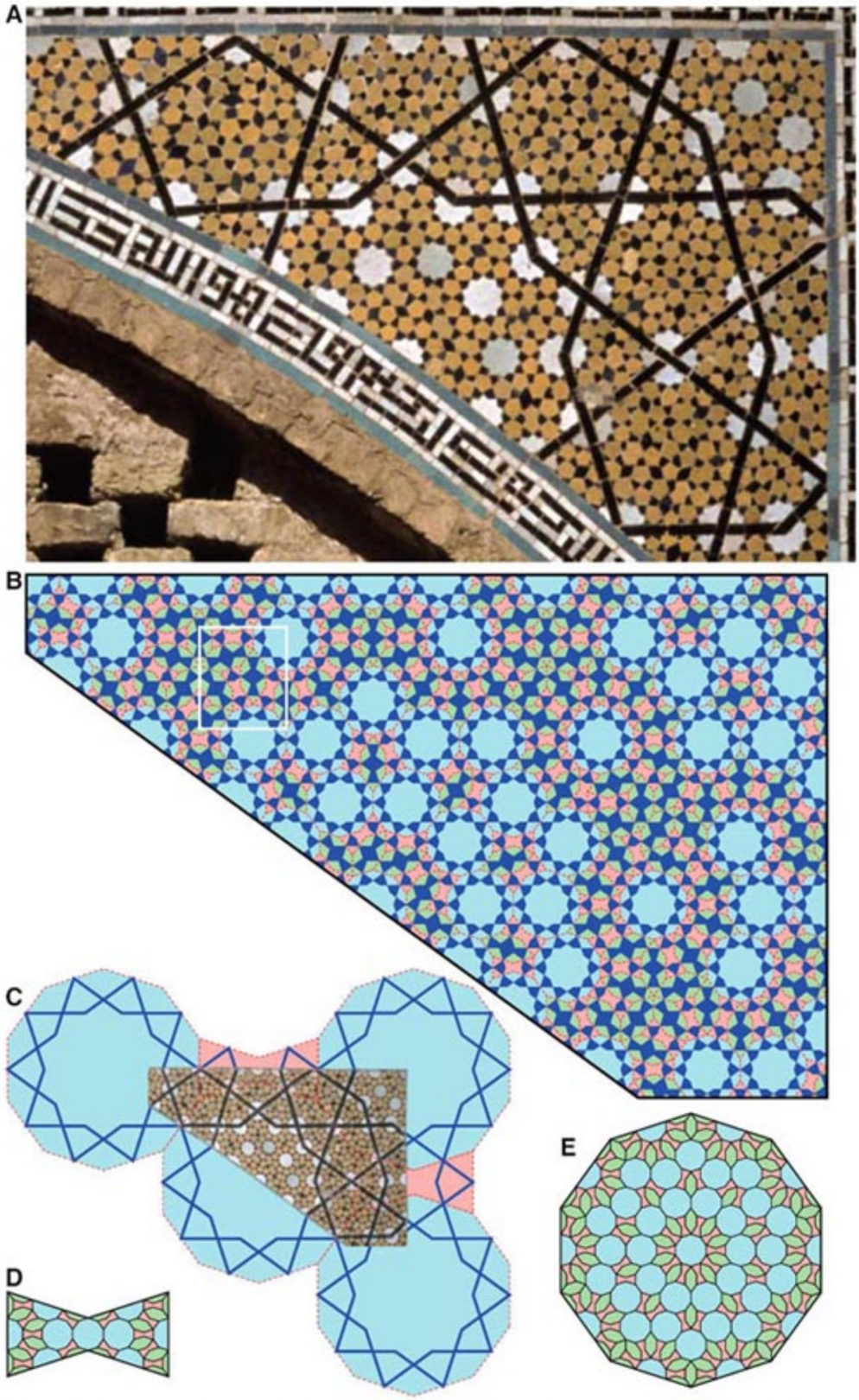

Fig. 3. Girih-tile subdivision found in the decagonal girih pattern on a spandrel from the Darb-i Imam shrine, Isfahan, Iran (1453 C.E.). (**A**) Photograph of the right half of the spandrel. (**B**) Reconstruction of the smaller-scale pattern using girih tiles where the blue-line decoration in Fig. 1F has been filled in with solid color. (**C**) Reconstruction of the larger-scale thick line pattern with larger girih tiles, overlaid on the building photograph. (**D** and **E**) Graphical depiction of the subdivision rules transforming the large bowtie (D) and decagon (E) girih-tile pattern into the small girih-tile pattern on tilings from the Darb-i Imam shrine and Friday Mosque of Isfahan.

References and Notes

1. J. Bourgoin, in *Les elements de l'art arabe; le trait des entrelacs* (Firmin-Didot, Paris, 1879), p. 176.
2. G. Necipoglu, *The Topkapi Scroll: Geometry and Ornament in Islamic Architecture* (Getty Center for the History of Art and the Humanities, Santa Monica, CA, 1995).
3. I. El-Said, A. Parman, in *Geometric Concepts in Islamic Art* (World of Islam Festival, London, 1976), pp. 85–87.
4. S. J. Abas, A. S. Salman, in *Symmetries of Islamic Geometrical Patterns* (World Scientific, Singapore, 1995), p. 95.
5. Y. Demiriz, in *Islam Sanatinda Geometrik Susleme* (Lebib Yalkin, Istanbul, 2000), pp. 27, 128–129.
6. G. Schneider, in *Geometrische Bauornamente der Seldschuken in Kleinasien* (Reichert, Wiesbaden, Germany, 1980), pp. 136–139, plate 3.
7. Abu'l-Wafa al-Buzjani's (940–998 C.E.) treatise *On the Geometric Constructions Necessary for the Artisan*, and an anonymous manuscript appended to a Persian translation of al-Buzjani and likely dating from the 13th century, *On Interlocks of Similar or Corresponding Figures* (*2*), document specific techniques for architecturally related mathematical constructions (*2*, *25*). The mathematical tools needed to construct the girih tiles are entirely contained in these two manuscripts—specifically, bisection, division of a circle into five equal parts, and cutting and rearrangement of paper tiles to create geometric patterns.
8. A. Bravais, *J. Ec. Polytech.* **33**, 1 (1850).
9. L. Golombek, D. Wilber, in *The Timurid Architecture of Iran and Turan* (Princeton Univ. Press, Princeton, NJ, 1988), pp. 246–250, 308–309, 384–386, 389, color plates IV, IXb, plates 46, 374.
10. Additional examples of this particular 10/3 decagonal pattern, shown in fig. S1: the Seljuk Congregational Mosque in Ardistan, Iran (~1160 C.E.) (*16*); the Timurid Tuman Aqa Mausoleum in the Shah-i Zinda complex in Samarkand, Uzbekistan (1405 C.E.) (*9*, *16*); the Darb-i Kushk shrine in Isfahan, Iran (1496 C.E.) (*2*, *9*, *17*); and the Mughal I'timad al-Daula Mausoleum in Agra, India (~1622 C.E.) (*28*).
11. R. Ettinghausen, O. Grabar, M. Jenkins-Madina, in *Islamic Art and Architecture 650–1250* (Yale Univ. Press, New Haven, CT, 2001), p. 109.
12. Additional architectural examples of patterns that can be reconstructed with girih tiles, shown in fig. S3: the Abbasid Al-Mustansiriyya Madrasa in Baghdad, Iraq (1227 to 1234 C.E.) (*26*); the Ilkhanid Uljaytu Mausoleum in Sultaniya, Iran (1304 C.E.) (*17*); the Ottoman Green Mosque in Bursa, Turkey (1424 C.E.) (*27*); and the Mughal I'timad al-Daula Mausoleum in Agra, India (~1622 C.E.) (*28*). Similar patterns also appear in the Mamluk Qurans of Sandal (1306 to 1315 C.E.) and of Aydughdi ibn Abdallah al-Badri (1313 C.E.) (*29*). Note that the girih-tile paradigm can make pattern design structure more clear. For example, all of the spandrels with decagonal girih patterns we have thus far examined (including Fig. 3C and figs. S2 and S3A) follow the same prescription to place decagons: Partial decagons are centered at the four external corners and on the top edge directly above the apex of the arch.
13. A similar convention was used to mark the same girih tiles in other panels (e.g., 28, 50, 52, and 62) in the Topkapi scroll (fig. S4) (*2*).
14. E. H. Hankin, *The Drawing of Geometric Patterns in Saracenic Art* (Government of India Central Publications Branch, Calcutta, 1925), p. 4.
15. This pattern type also occurs on the Great Mosque in Malatya, Turkey (~1200 C.E.) (*6*), and the madrasa in

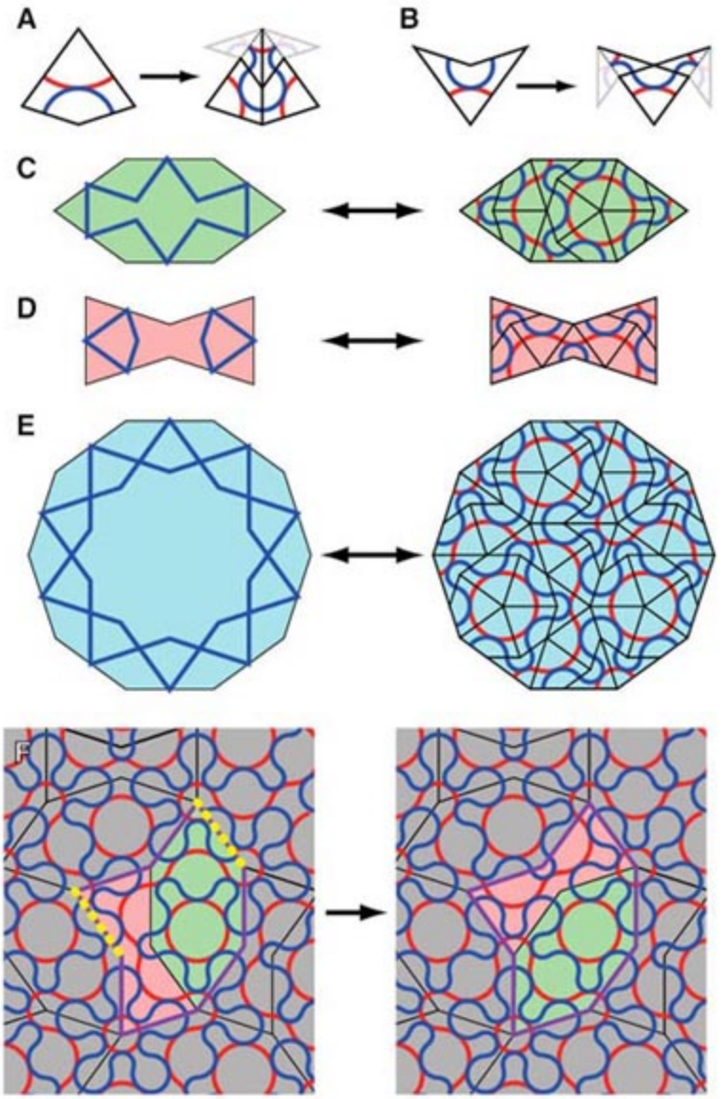

Fig. 4. (**A** and **B**) The kite (A) and dart (B) Penrose tile shapes are shown at the left of the arrows with red and blue ribbons that match continuously across the edges in a perfect Penrose tiling. Given a finite tiling fragment, each tile can be subdivided according to the "inflation rules" into smaller kites and darts (at the right of the arrows) that join together to form a perfect fragment with more tiles. (**C** to **E**) Mappings between girih tiles and Penrose tiles for elongated hexagon (C), bowtie (D), and decagon (E). (**F**) Mapping of a region of small girih tiles to Penrose tiles, corresponding to the area marked by the white rectangle in Fig. 3B, from the Darb-i Imam shrine. At the left is a region mapped to Penrose tiles following the rules in (C) to (E). The pair of colored tiles outlined in purple have a point defect (the Penrose edge mismatches are indicated with yellow dotted lines) that can be removed by flipping positions of the bowtie and hexagon, as shown on the right, yielding a perfect, defect-free Penrose tiling.

Zuzan, Iran (1219 C.E.) (*30*) (fig. S5), as well as on a carved wooden double door from a Seljuk building in Konya (~13th century C.E.), in the Museum of Islamic Art in Berlin (Inv. Nr. 1.2672).

16. D. Hill, O. Grabar, in *Islamic Architecture and Its Decoration, A.D. 800–1500* (Univ. of Chicago Press, Chicago, 1964), pp. 53, 62, 65, plates 38, 276, 346, 348.
17. S. P. Seherr-Thoss, *Design and Color in Islamic Architecture* (Smithsonian Institution, Washington, DC, 1968), plates 34–36, 40, 84, 90.
18. E. Makovicky, in *Fivefold Symmetry*, I. Hargittai, Ed. (World Scientific, Singapore, 1992), pp. 67–86.
19. J. F. Bonner, in *ISAMA/Bridges Conference Proceedings*, R. Sarhangi, N. Friedman, Eds. (Univ. of Granada, Granada, Spain, 2003), pp. 1–12.
20. R. Penrose, *Bull. Inst. Math. Appl.* **10**, 266 (1974).
21. D. Levine, P. J. Steinhardt, *Phys. Rev. Lett.* **53**, 2477 (1984).
22. M. Gardner, in *Penrose Tiles to Trapdoor Ciphers* (Freeman, New York, 1989), pp. 1–29.
23. D. Levine, P. J. Steinhardt, *Phys. Rev. B* **34**, 596 (1986).
24. A single figure, part of a geometric proof from *On Interlocks of Similar or Corresponding Figures*, has been related to the outlines of individual Penrose tiles, but there is no evidence whatsoever for tessellation (*31*). Makovicky has connected the Maragha Gunbad-i Kabud pattern in Fig. 2 with the Penrose tiling (*18*), but explicitly states (as we show in fig. S6) that the pattern is periodic, so by definition it cannot be a properly quasi-periodic Penrose tiling.
25. A. Ozdural, *Hist. Math.* **27**, 171 (2000).
26. H. Schmid, *Die Madrasa des Kalifen Al-Mustansir in Baghdad* (Zabern, Mainz, Germany, 1980), plates 15, 87.
27. G. Goodwin, *A History of Ottoman Architecture* (Thames and Hudson, London, 1971), pp. 58–65.
28. Y. Ishimoto, *Islam: Space and Design* (Shinshindo, Kyoto, 1980), plates 378, 380, 382.
29. D. James, *Qur'ans of the Mamluks* (Thames and Hudson, New York, 1988), pp. 54, 57–59.
30. R. Hillenbrand, *Islamic Architecture* (Columbia Univ. Press, New York, 1994), pp. 182–183.
31. W. K. Chorbachi, *Comp. Math. Appl.* **17**, 751 (1989).

32. We thank G. Necipoglu and J. Spurr, without whose multifaceted assistance this paper would not have been possible. We also thank R. Holod and K. Dudley/M. Eniff for permission to reproduce their photographs in Figs. 2C and 3A, respectively; C. Tam and E. Simon-Brown for logistical assistance in Uzbekistan; S. Siavoshi and A. Tafvizi for motivating the exploration of Isfahan's sights; and S. Blair, J. Bloom, C. Eisenmann, T. Lentz, and I. Winter for manuscript comments. Photographs in Fig. 2, A and B, and in the online figures courtesy of the Fine Arts Library, Harvard College Library. Supported by C. and F. Lu and by the Aga Khan Program for Islamic Architecture at Harvard University.

Supporting Online Material
www.sciencemag.org/cgi/content/full/315/5815/1106/DC1
Figs. S1 to S8

25 September 2006; accepted 22 December 2006
10.1126/science.1135491

Ex Situ NMR in Highly Homogeneous Fields: ^{1}H Spectroscopy

Juan Perlo, Federico Casanova, Bernhard Blümich*

Portable single-sided nuclear magnetic resonance (NMR) magnets used for nondestructive studies of large samples are believed to generate inherently inhomogeneous magnetic fields. We demonstrated experimentally that the field of an open magnet can be shimmed to high homogeneity in a large volume external to the sensor. This technique allowed us to measure localized high-resolution proton spectra outside a portable open magnet with a spectral resolution of 0.25 part per million. The generation of these experimental conditions also simplifies the implementation of such powerful methodologies as multidimensional NMR spectroscopy and imaging.

Single-sided nuclear magnetic resonance (NMR) sensors have been used for over two decades to characterize arbitrarily large samples (*1*). In contrast to conventional NMR apparatus, where the sample must be adapted to fit into the bore of large superconducting magnets, single-sided NMR experiments use portable open magnets placed on one side of an object to detect NMR signals ex situ. This configuration is convenient for the nondestructive inspection of valuable objects from which fragmentary samples cannot be drawn, but it does not allow generation of the high and homogeneous magnetic fields that afford spectral resolution in conventional NMR studies. Given these detrimental conditions, the standard techniques of conventional NMR do not work, and new strategies need to be developed in order to extract valuable information from the NMR signal (*2*–*8*).

Starting from simple relaxation-time measurements, more sophisticated methods of ex situ NMR have been developed, such as Fourier imaging (*5*), velocity imaging (*6*), and multi-

Institut für Technische Chemie und Makromolekulare Chemie, Rheinisch-Westfälische Technische Hochschule–Aachen, D-52056, Germany.

*To whom correspondence should be addressed. E-mail: bluemich@mc.rwth-aachen.de

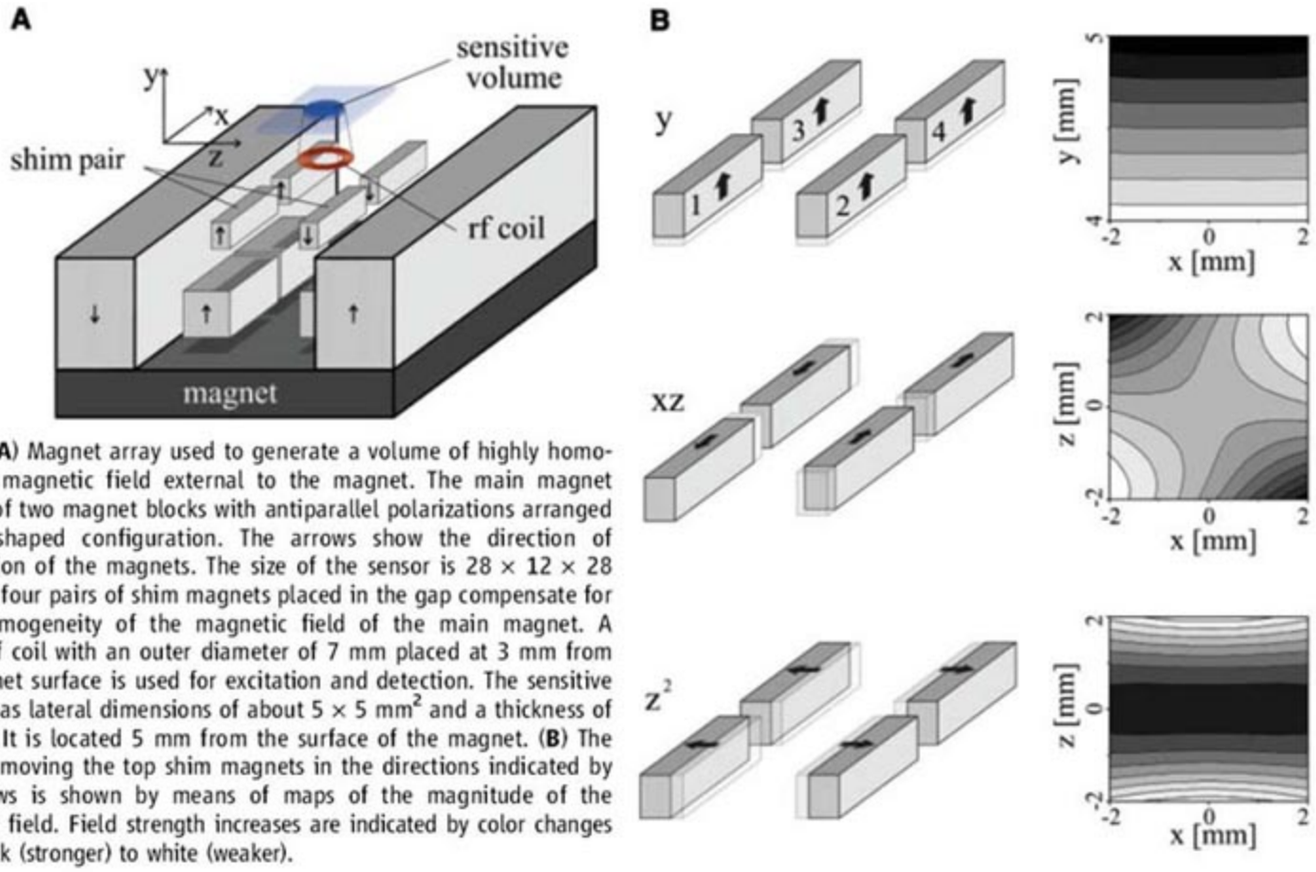

Fig. 1. (**A**) Magnet array used to generate a volume of highly homogeneous magnetic field external to the magnet. The main magnet consists of two magnet blocks with antiparallel polarizations arranged in a U-shaped configuration. The arrows show the direction of polarization of the magnets. The size of the sensor is 28 × 12 × 28 cm^3. The four pairs of shim magnets placed in the gap compensate for the inhomogeneity of the magnetic field of the main magnet. A surface rf coil with an outer diameter of 7 mm placed at 3 mm from the magnet surface is used for excitation and detection. The sensitive volume has lateral dimensions of about 5 × 5 mm^2 and a thickness of 0.5 mm. It is located 5 mm from the surface of the magnet. (**B**) The effect of moving the top shim magnets in the directions indicated by the arrows is shown by means of maps of the magnitude of the magnetic field. Field strength increases are indicated by color changes from black (stronger) to white (weaker).

dimensional relaxation and diffusion correlation/exchange maps (*7*). A remarkable achievement is the use of nutation echoes generated by a combination of static and radio-frequency (rf) magnetic fields with matched inhomogeneities to resolve the chemical shift in inhomogeneous fields. Proposed in 2001 (*8*), this approach was recently implemented using a portable single-sided sensor (*9*).

Magnetic fields generated by open magnets are believed to be inherently inhomogeneous, precluding the acquisition of chemical-shift resolved NMR spectra. This perception is the reason for designing such ingenious tricks as nutation echoes (*8*) and shim pulses (*10*, *11*) to measure the chemical shift ex situ. We broke with that assumption and demonstrated experimentally that highly homogeneous magnetic fields (the degree of homogeneity is of a few parts in 10^7) can be generated external to the magnet in a very simple way. Conventional NMR magnets, which enclose the sample, are equipped with shim coils to tune the shape of the polarizing magnetic field to extreme homogeneity for narrow lines in the NMR spectrum. The straightforward adaptation of this approach to shim the stray field of an ex situ sensor must be discarded because of excessive requirements for the shim currents. However, a current loop of 1000 A can be replaced by an approximately 1-mm-thick NdFeB permanent magnet block, and single-sided shimming can be achieved simply by a suitable arrangement of such blocks. We found that the current distribution needed for electrical single-sided shims can be replaced by pairs of magnet blocks with opposite polarization, suitably arranged with respect to the main magnet.

We used this strategy to shim the field of a conventional U-shaped single-sided magnet (*5*) (Fig. 1A). The shim unit consists of four magnet block pairs placed inside the gap of the main magnet. Two pairs are fixed at the bottom and produce a strong gradient along the depth direction *y*; and two further pairs on the top are movable. Together they generate a total of eight shim components. The first-order shim components *x*, *y*, and *z* are generated by displacing the two movable pairs along the *x*, *y*, and *z* directions, respectively. The second-order terms x^2 and z^2 are adjusted by varying the distance between the pairs while keeping their centers fixed with respect to the main magnet. Moreover, cross terms *xy*, *xz*, and *yz* can also be generated by displacing the magnets as described in Table 1. An important issue to be taken into account when magnets are built from small permanent magnet blocks is the inaccuracy in their fabrication. Although the size of the magnet pieces can be defined with good precision, their remnant polarization varies typically on the order of a few percent [>10,000 parts per million (ppm)], which is orders of magnitude larger than the desired homogeneity (<1 ppm). In spite of this source of uncertainty, the effect of these imperfections can be eliminated by setting the shim unit in a configuration that cancels the unwanted field variations. The shim unit also includes three single-sided coils generating *x*, *y*, and *z* gradient fields used for fine tuning of the field (not shown in Fig. 1).

Table 1. Shim components and required magnet displacements.

Shim component	Magnet			
	1	2	3	4
x	Δx	Δx	Δx	Δx
y	Δy	Δy	Δy	Δy
z	Δz	Δz	Δz	Δz
x^2	Δx	Δx	$-\Delta x$	$-\Delta x$
z^2	Δz	$-\Delta z$	Δz	$-\Delta z$
xy	$-\Delta y$	$-\Delta y$	Δy	Δy
zy	Δy	$-\Delta y$	Δy	$-\Delta y$
xz	Δx	$-\Delta x$	Δx	$-\Delta x$

The magnetic fields generated either by conventional closed magnets or by the open sensor presented here possess the required degree of homogeneity only in a limited volume. In conventional NMR, this limitation is often not important because the sample size is restricted to fit into this volume, but the main motivation for ex situ NMR is to investigate arbitrarily large samples. Hence, the sensitivity of the sensor must be limited to the region of homogeneous field. We achieved this spatial selection by combing a 90° soft pulse for excitation with the natural lateral selection of a surface rf coil (Fig. 1A). The selected volume was 5 × 5 mm^2 along the lateral directions and 0.5 mm across, and it was situated 2 mm above the rf coil surface (*12*). Figure 2

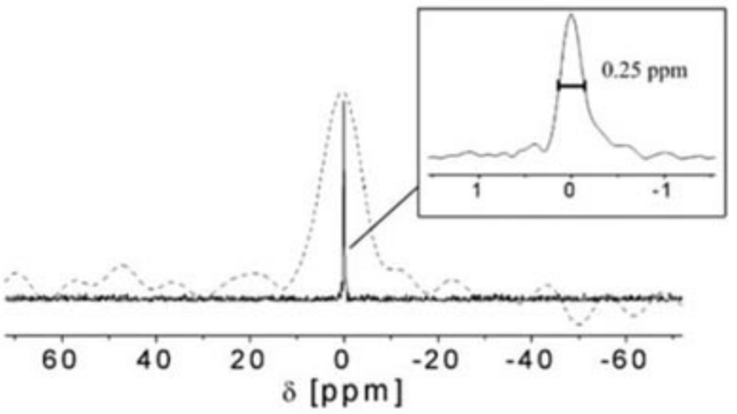

Fig. 2. ^{1}H NMR spectra of water. Solid line: magnitude spectrum of a water sample much larger than the sensitive volume, placed on top of the rf coil. The spectrum is the Fourier transform of the Hahn echo signal from 64 scans acquired with a repetition time of 5 s to improve the SNR. The full width at medium height of the line (inset) is 0.25 ppm at a proton resonance frequency of 8.33 MHz. Dashed line: best spectrum obtained by ex situ spectroscopy following the nutation-echo method. The linewidth is 8 ppm (*9*). Both data sets were obtained in the same measuring time, using sensors of the same size and working at comparable depths. Therefore, spectral resolution and sensitivity can be compared quantitatively.

shows the spectrum of a water sample much larger than the sensitive volume (an arbitrarily large sample) placed on top of the sensor. The linewidth is 2.2 Hz, corresponding to a spectral resolution of about 0.25 ppm (*13*). For comparison, the state-of-the-art spectrum for single-sided NMR, measured recently by nutation echoes in the presence of spatially matched static and rf fields (*9*), is shown as well. The spectral resolution has been improved by a factor of about 30 with a concomitant fivefold extension of the excited volume. Together with a sensitivity-optimized surface rf coil, the increased size of the sensitive volume leads to an appreciably higher signal-to-noise ratio (SNR).

The sub–part per million resolution achieved in this work allowed us to resolve different molecular structures, such as toluene and acetic acid (Fig. 3) (*14*). The toluene ^{1}H spectrum exhibits two lines at 7.0 and 2.1 ppm, with relative intensities of about 5:3, corresponding to the aromatic and the methyl protons, respectively (Fig. 3A). In the case of acetic acid, the two lines correspond to methyl and carboxylic protons, which appear at 2.3 and 11.3 ppm, with intensity ratios of 3:1 (Fig. 3B). These results prove that ex situ NMR can be used to determine the molecular composition of liquids by ^{1}H NMR spectroscopy. Figure 3C shows the ^{1}H spectrum of a mixture of water and crude oil. From the line integrals, the water/oil ratio can be quantified, a result of interest for well logging in the oil industry.

The generation of highly homogeneous fields with single-sided magnets considerably expands the methodologies available for open NMR sensors. Ex situ ^{1}H spectroscopy can be used for noninvasive screening for molecular composition, the control of chemical reactions, and the identification of target compounds. The most important advantage of having high field homogeneity available for ex situ NMR is that the established techniques of multidimensional NMR spectroscopy and imaging can now be implemented in a straightforward way for the nondestructive testing of large objects.

An important limitation on the field use of such a mobile sensor concerns the strong temperature dependence of the remnant polarization of permanent magnets. This property imposes a large resonance frequency drift of up to –1200 ppm/°C for NdFeB magnets. Conventional solutions to this problem combine the use of large thermal insulation chambers with NMR field-frequency locks. However, these solutions are far too complicated to be of practical use for mobile open sensors. An ideal solution would be the construction of a temperature-compensated magnet. We addressed this issue by combining materials with different temperature coefficients, κ_a and κ_b, chosen to fulfill the condition $B_a/B_b = -\kappa_b/\kappa_a$, where B_a and B_b are the contributions of each material to the total field. In the case of the magnet presented here (Fig. 1), the field B_a generated by the main magnet and the field B_b by the shim unit oppose each other with an amplitude proportion of $B_a/B_b = -4.2$. A ratio of 4.0 of the temperature coefficients can be achieved by building the main magnet from SmCo and the shim unit from NdFeB. The combination of these two materials would reduce the temperature drift in the present magnet geometry from –1200 ppm/°C to –17 ppm/°C. This performance can be further improved by slightly modifying the size of the shim unit.

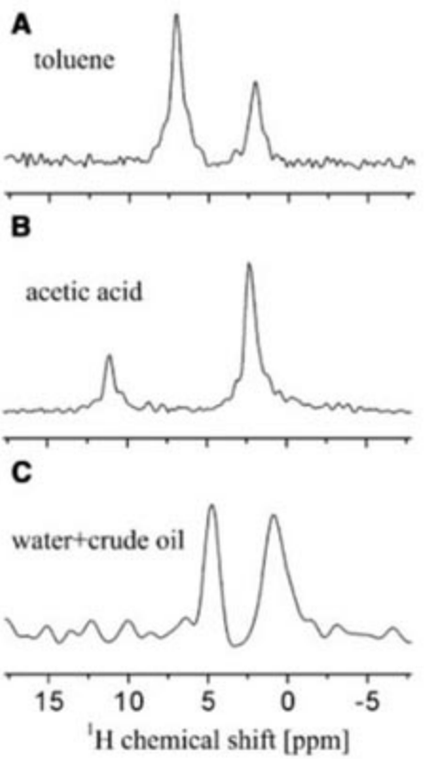

Fig. 3. ^{1}H NMR spectra of different liquid samples obtained within a measuring time of 1 min. The chemical-shift differences and the relative peak intensities are in good agreement with the results obtained using conventional high-resolution NMR spectrometers. The spectra of toluene (**A**) and acetic acid (**B**) were obtained from the echo signal, whereas in the case of the water/oil mixture (**C**), the free induction decay was acquired because of the relatively short relaxation time of the oil.

References and Notes

1. B. Blümich, *NMR Imaging of Materials* (Oxford Univ. Press, Oxford, 2000).
2. Y.-Q. Song, S. Ryu, P. N. Sen, *Nature* **406**, 178 (2000).
3. T. M. Brill *et al.*, *Science* **297**, 369 (2002).
4. S. Appelt, H. Kühn, F. Wolfgang, B. Blümich, *Nat. Phys.* **2**, 105 (2006).
5. J. Perlo, F. Casanova, B. Blümich, *J. Magn. Reson.* **166**, 228 (2004).
6. J. Perlo, F. Casanova, B. Blümich, *J. Magn. Reson.* **173**, 254 (2005).
7. M. D. Hürlimann, L. Venkataramanan, *J. Magn. Reson.* **157**, 31 (2002).
8. C. A. Meriles, D. Sakellariou, H. Heise, A. J. Moulé, A. Pines, *Science* **293**, 82 (2001).
9. J. Perlo *et al.*, *Science* **308**, 1279 (2005).
10. B. Shapira, L. Frydman, *J. Am. Chem. Soc.* **126**, 7184 (2004).
11. D. Topgaard, R. Martin, D. Sakellariou, C. A. Meriles, A. Pines, *Proc. Natl. Acad. Sci. U.S.A.* **101**, 17576 (2004).
12. The maximum depth attainable with the present magnet geometry is 5 mm. It would be achieved by placing the rf coil at the surface of the magnet; however, when this is done, a decrease in SNR is expected because of the loss of sensitivity of the rf coil with depth.
13. The final shim configuration is obtained in two stages. First, the total magnetic field is scanned via measurement of the resonance frequency of a tiny water sample (~1 mm^3). Subsequently, the position of the magnet pairs for shimming is adjusted for maximum compensation of the field variations. This procedure is repeated several times until the deviations from the average field are less than 10 ppm. In a second stage, and to further improve the resolution, the shim magnets remain fixed, but the current through three single-sided shim coils is optimized by maximizing the signal peak (of a large sample) in the frequency domain.
14. The experiments were carried out in the lab without the need of a temperature chamber. The insulation given by a 1-cm-thick polystyrene foam layer, added to the large thermal inertia of the magnet, allowed us to average the signal over 1 min without appreciable frequency drift.

15. This project was supported by Deutsche Forschungsgemeinschaft grant CA660/1-1, "Development of methodologies and portable sensors for high-resolution NMR spectroscopy in inhomogeneous fields." We thank K. Kupferschläger for technical support.

25 September 2006; accepted 19 December 2006
Published online 11 January 2007;
10.1126/science.1135499
Include this information when citing this paper.

Structure of the Polycrystalline Zeolite Catalyst IM-5 Solved by Enhanced Charge Flipping

Christian Baerlocher,[1] Fabian Gramm,[1] Lars Massüger,[1] Lynne B. McCusker,[1]* Zhanbing He,[2] Sven Hovmöller,[2] Xiaodong Zou[2]

Despite substantial advances in crystal structure determination methodology for polycrystalline materials, some problems have remained intractable. A case in point is the zeolite catalyst IM-5, whose structure has eluded determination for almost 10 years. Here we present a charge-flipping structure-solution algorithm, extended to facilitate the combined use of powder diffraction and electron microscopy data. With this algorithm, we have elucidated the complex structure of IM-5, with 24 topologically distinct silicon atoms and an unusual two-dimensional medium-pore channel system. This powerful approach to structure solution can be applied without modification to any type of polycrystalline material (e.g., catalysts, ceramics, pharmaceuticals, complex metal alloys) and is therefore pertinent to a diverse range of scientific disciplines.

As a result of impressive methodological advances in recent years, the determination of a crystal structure from powder diffraction data is no longer a rarity (*1*, *2*). However, some problems have remained intractable. The prospect of dealing successfully with such cases has been improved recently by two developments. First, the charge-flipping structure-solution algorithm introduced by Oszlányi and Sütő in 2004 for single-crystal data (*3*, *4*) has been adapted to accommodate powder diffraction data (*5*). The resulting powder charge-flipping (pCF) algorithm implemented in the program Superflip (*6*) has been shown to work well with both organic and inorganic materials of varying complexities. The second advance involves the inclusion of crystallographic phases obtained from high-resolution transmission electron microscopy (HRTEM) images in the input to the zeolite-specific program FOCUS (*7*). This approach led to the solution of the extremely complex structure of the polycrystalline zeolite TNU-9 (*8*). We reasoned that by including crystallographic phases from HRTEM images in the pCF algorithm, a powerful and generally applicable approach to structure solution for polycrystalline materials could be developed. We were particularly eager to apply this method to the polycrystalline zeolite catalyst IM-5, whose structure has eluded determination for almost 10 years.

The synthesis of the high-silica zeolite IM-5 was reported in 1998 (*9*), and the general features of its pore system were deduced from catalytic test reactions in 2000 (*10*). Although the material has proven to be an important thermally stable catalyst for hydrocarbon cracking and NO reduction (*11*–*16*), its properties cannot be fully understood without detailed crystal structure information. Like many zeolitic materials, IM-5 is polycrystalline, but this alone does not account for the particular challenge posed by its structure analysis. It has an unusually large unit cell (*C*-centered orthorhombic with a = 14.299 Å, b = 57.413 Å, and c = 20.143 Å) with a volume almost triple that of ZSM-5 (*17*), one of the more complex known zeolites. There are also approximate relationships between the axes ($b \sim 4a$ and $c \sim \sqrt{2}a$), which means that symmetrically unrelated reflections (e.g., 200 and 080 or 022 and 060) have very similar d spacings. These factors result in an enormous degree of reflection overlap, which is the key hindrance to structure solution from powder diffraction data (*1*). Furthermore, impurities, which complicate any powder diffraction data analysis, are common in IM-5 syntheses. We overcame these difficulties by combining powder diffraction and electron microscopy techniques in a charge-flipping structure-solution algorithm.

This study builds on our prior adaptation of the charge-flipping algorithm to accommodate powder diffraction data (*5*). The algorithm itself is a deceptively simple one. Structure factor amplitudes ($|F_{hkl}|$), derived from the measured diffraction intensities (I_{hkl}), are assigned random crystallographic phases (ϕ_{hkl}), and the corresponding (random) electron density map [$\rho(xyz)$] is generated with the equation

$$\rho(xyz) = \frac{1}{V}\sum_{hkl}|F_{hkl}|\cos(2\pi(hx + ky + lz) - \phi_{hkl}) \quad (1)$$

Then the signs of all electron density pixels below a user-defined threshold value δ (a small positive number close to zero) are reversed (hence "charge flipping") to produce a modified electron density map. Essentially, all negative electron densities (which are not physically meaningful) are made positive. From this map, a new set of structure factor amplitudes and phases is calculated. The new phases are then combined with the measured amplitudes to produce a new electron density map. This cycle is repeated until convergence (calculated amplitudes matching measured ones) is reached. An R value comparing the calculated and measured amplitudes provides an estimate of the reliability of the final map.

In a powder diffraction pattern, reflections with similar d spacings (or diffraction angle 2θ) overlap, obscuring their individual intensities. To improve the initial estimate of these intensities (usually a simple equipartitioning) during the course of a pCF run, we introduced a periodic repartitioning within each overlap group. In our implementation, this repartitioning procedure involves an additional density modification based on histogram matching (*18*) and is performed after a user-defined number of cycles of charge flipping. Wu and co-workers use the charge-flipping modification itself for this repartitioning step (*19*). The advantages of the charge-flipping algorithm are twofold. First, all calculations are performed without any assumptions about the symmetry, thereby side-stepping space group ambiguities, common in powder diffraction data. Second, no chemical information (e.g., bond distances, bond angles, atom connectivity) is required, so the technique can be applied to any class of material. The question was whether or not this algorithm could handle a problem as complex as the structure of IM-5.

In parallel to the development of the pCF algorithm, we were exploring ways of combining the complementary aspects of powder diffraction and electron microscopy techniques for structure determination. In the case of TNU-9 (*8*) mentioned earlier, intensities extracted from high-resolution powder diffraction data were combined with crystallographic phases obtained from HRTEM images in the zeolite-specific program FOCUS (*7*). We reasoned that a similar approach could be used for IM-5, except that the information from the two techniques would be combined in the pCF algorithm rather than in FOCUS. Because the pCF algorithm operates in both real (electron density) and reciprocal (phase) space, it is relatively easy to add supplementary information in either realm. For example, a partial or approximate model can be introduced in real space as a starting electron density map, instead of the usual random phase map; a (partial) pore system in a zeolite can be defined in real space in terms of a structure envelope (*20*); or phase information from HRTEM images can be added in reciprocal space.

High-resolution powder diffraction data were collected from several different samples of IM-5 at the Swiss-Norwegian Beamlines (SNBL) at the European Synchrotron Radiation Facility in Grenoble, France, and the Swiss Light Source (SLS) in Villigen. None of the samples were ideal. All contained impurities, none had particularly sharp peaks, and diffraction intensity decreased rapidly with diffraction angle. Indeed, the main difference between IM-5 and TNU-9 in

[1]Laboratory of Crystallography, ETH Zurich, CH-8093 Zurich, Switzerland. [2]Structural Chemistry, Stockholm University, SE-106 91 Stockholm, Sweden.

*To whom correspondence should be addressed. E-mail: mccusker@mat.ethz.ch

terms of the difficulty of the structure determination lies in the inferior quality of the IM-5 powder diffraction data. Nonetheless, by comparing the different IM-5 patterns, the peaks corresponding to the IM-5 phase could be distinguished from those of the various impurities, and a tentative indexing of the patterns achieved. In some patterns, the impurity peaks could be assigned to known materials, but in others they remained unidentified. Because of the relationships between the axes mentioned earlier and the quality of the data, the indexing was uncertain and the cell difficult to refine. Generally, determining the unit cell from a powder diffraction pattern is a straightforward and accurate procedure. However, when reflection overlap is extreme and/or when unidentified impurities are present, electron diffraction is a valuable complementary technique. Because electrons interact much more strongly with atoms than do x-rays, a single-crystal electron diffraction pattern can be obtained from a very tiny crystallite (dimensions of ~20 nm versus ~20 μm for x-rays). Unfortunately, this strong interaction generally results in intensities that are difficult or impossible to interpret directly. However, the single-crystal nature of the diffraction patterns allows impurities to be discriminated from the main phase and reflections with similar d spacings to be distinguished from one another.

We therefore collected series of selected area electron diffraction (SAED) patterns on different crystallites of IM-5 as they were tilted around various axes. The SAED patterns from each tilt series were combined with the programs ELD (*21*) and Trice (*22*) to construct a three-dimensional (3D) reciprocal lattice, from which approximate lattice parameters could be determined. These results confirmed the powder indexing. The systematic absences in the SAED patterns indicated that the most probable space groups were $Cmc2_1$, $C2cm$, and $Cmcm$.

The powder diffraction pattern exhibiting the sharpest peaks and the largest range in d spacings (2θ) was selected for further analysis. First, the analcime impurity peaks were subtracted from this pattern, and then a set of reflection intensities were extracted assuming the space group $Cmcm$. Of the 4120 reflections in the pattern (d_{min} = 1.05 Å), 3499 were within 0.2 × FWHM (full width at half maximum) of another reflection, forming 862 overlap groups. To optimize the relative intensities within the overlap groups, the FIPS (fast iterative Patterson squaring) routine was applied (*23*). These intensities were expanded to the space group $P1$ (no symmetry within the unit cell) and used as input to the pCF program. Although some of the resulting electron density maps showed feasible pore systems, none could be interpreted to a level sufficient for structure determination. There were indications in these maps that the assignment of a mirror plane perpendicular to the a axis (in $Cmcm$) might be erroneous.

To resolve this issue, we took high-quality HRTEM images of IM-5 along the three main zone axes at 300 kV on a JEM-3010 transmission electron microscope (Fig. 1). A Fourier transform was calculated from a thin area near the crystal edge in each image, and structure factor amplitudes and phases were extracted with the program CRISP (*24*). Note that crystallographic phases, which are lost in diffraction experiments, can be retrieved from HRTEM images. These phases were analyzed to determine the symmetry of each projection, and the combination of the three different projections supported the assignment of the noncentrosymmetric space group $C2cm$ (standard setting $Ama2$). Consequently, the phase relations and phase restrictions of the space group $C2cm$ were imposed on the amplitudes and phases extracted from the HRTEM images of each projection. The contrast transfer function was determined from the Fourier transform of each image and compensated with the program CRISP, after which the projected potential maps (insets in Fig. 1) were calculated.

The structure factor amplitudes and phases from the three HRTEM projections were combined to produce a 3D set of 95 structure factors. Common reflections were used to scale the amplitudes and to determine the common origin of the different projections (*25*). A 3D potential map was then calculated by inverse Fourier transformation with the program eMap (*26*). In this potential map, 36 unique Si-atom positions were located and then adjusted to produce a four-connected framework structure. Oxygen bridges were added between the connected Si atoms, and the geometry was optimized with the distance least-squares program DLS-76 (*27*). However, the R value of the optimization (comparison of calculated and ideal distances) indicated that the framework was highly strained. Furthermore, the powder diffraction pattern generated from this model did not fit the measured one very well, even after structure refinement.

The 95 phases derived from the HRTEM images were then included in the pCF routine, along with a structure envelope (*20*) defining the channels along [100] and [001] (Fig. 1, A and B). The structure envelope was used to eliminate electron density within the channels. However,

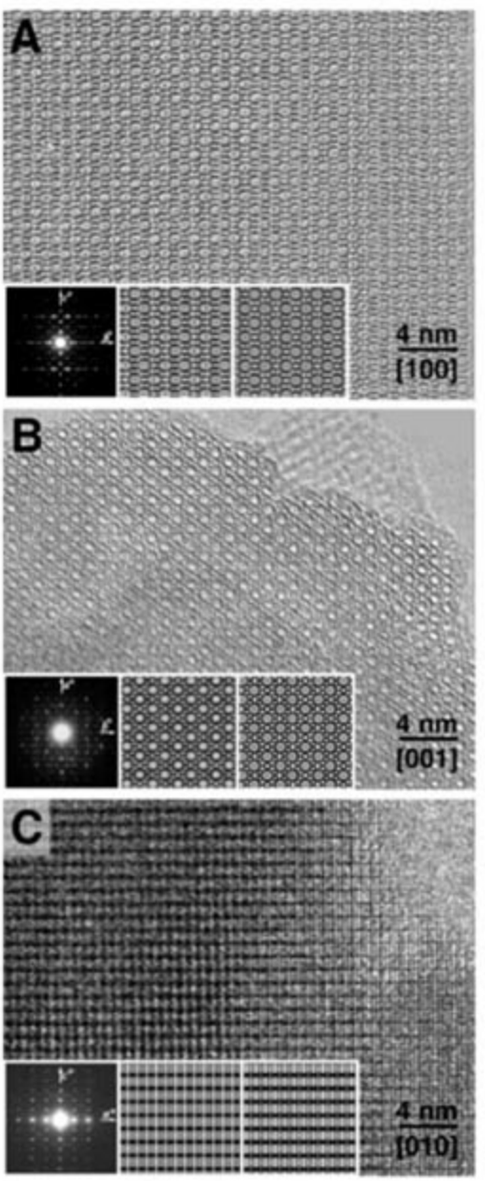

Fig. 1. HRTEM images taken along different zone axes of IM-5. (**A**) [100], (**B**) [001], and (**C**) [010]. Insets show the corresponding selected-area electron diffraction patterns (left), the symmetry-averaged images (middle), and the simulated images from the structural model (right). The crystal thicknesses for the simulations were 50, 50, and 750 Å, and the defocus values were −500, −400, and +1500 Å, respectively.

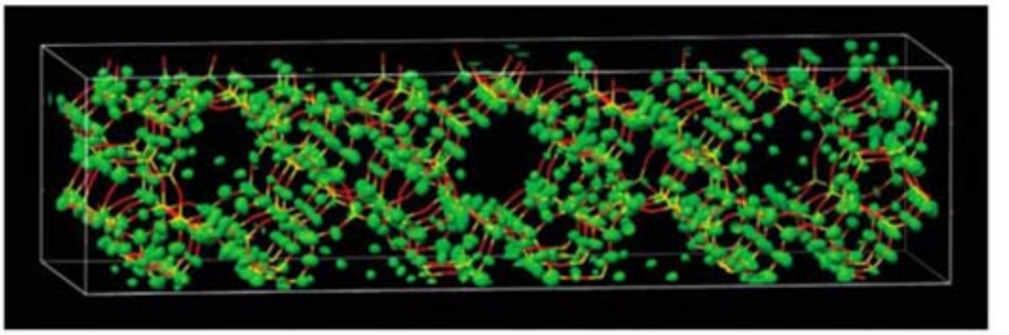

Fig. 2. Electron density map from pCF that was used to derive the structure of IM-5. A stick model of the final refined structure of IM-5 has been superimposed for comparison. The image was produced with the UCSF Chimera package (*30*).

the resulting electron density maps were not improved sufficiently over the earlier ones for meaningful interpretation. Speculating that the model derived from the HRTEM data was probably partially correct, we used it to calculate alternative starting electron density maps to replace the initial map generated by the use of random phases. The phase of each reflection calculated from the structure was varied by up to 25% in random fashion, thereby generating 1000 different starting points for 1000 distinct pCF runs. During the course of each run, the channel system was enforced periodically by applying the structure envelope restriction. The resulting maps were symmetry averaged assuming the space group *C*2*cm*, and then the five best maps (lowest pCF *R* values) were combined to yield the one shown in Fig. 2.

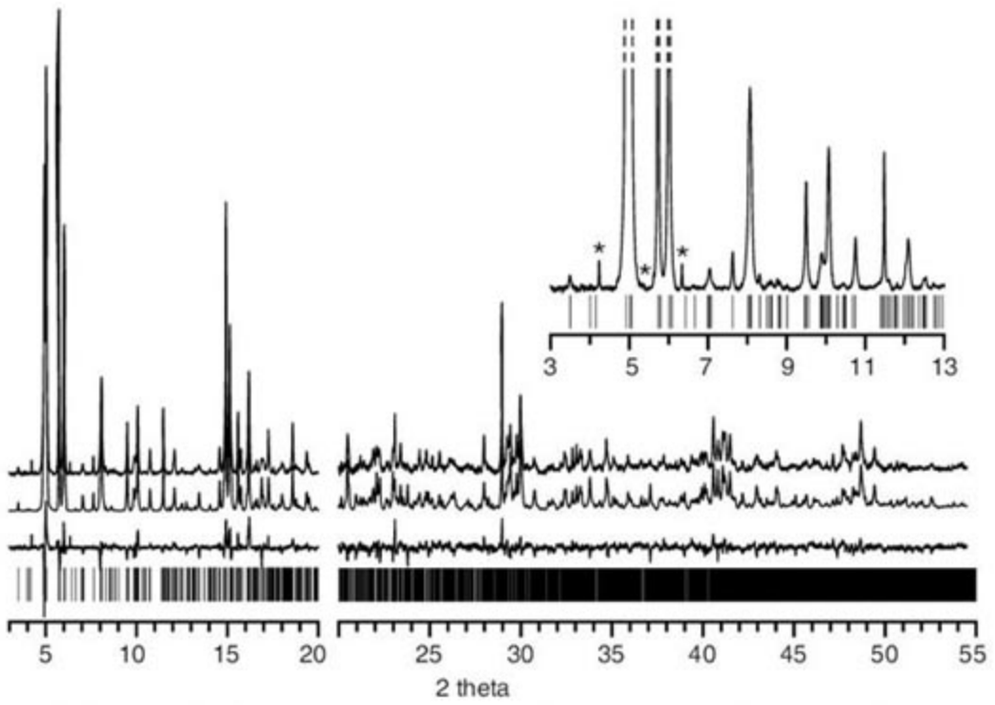

Fig. 3. Observed (**top**), calculated (**middle**), and difference (**bottom**) diffraction profiles for the Rietveld refinement of calcined IM-5 (λ = 0.99995 Å). The higher-angle data have been scaled up by a factor of 4 to show more detail. Tick marks indicate the positions of the reflections. A small section of the low-angle data has been expanded in the inset to illustrate the high degree of reflection overlap even in the large *d*-spacing range. Three clearly separated impurity peaks are marked with asterisks.

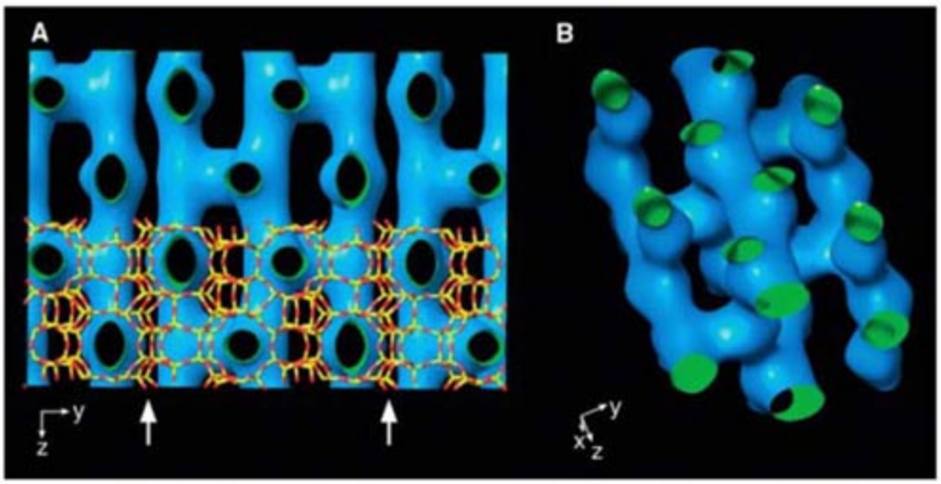

Fig. 4. The unusual 2D 10-ring channel system of IM-5. (**A**) Projection along [100], showing the connections between the channels running parallel to [001]. The walls between channel systems are marked with arrows. (**B**) A single 2D channel system [between the walls marked in (A)], showing more detail of the connectivity. The details of the shape and size of the structure envelope (generated from 21 reflections) used to depict the channel system are only approximate and should not be overinterpreted. The envelope is only meant to indicate the approximate arrangement of the channels within the framework structure. The image was produced with the UCSF Chimera package (*30*).

Interpretation of this map was almost trivial. The positions of 35 of the 36 Si atoms and 61 of the 79 O atoms could be located directly in the top 106 peaks. The position of the missing Si atom could be deduced quite easily from the four surrounding Si atoms. Two of the other Si atoms had to be shifted by ~0.1 Å along the *c* axis to complete the four-connected framework structure. The positions of the missing oxygen bridges were then generated, and the geometry was optimized with DLS-76 (*27*). This time, the DLS *R* value was indicative of an unstrained geometry, and the calculated powder diffraction pattern matched the main features of the measured one.

The framework structure appeared to be consistent with the centrosymmetric space group *Cmcm*, so we began Rietveld refinement of the structure assuming this symmetry. To simplify the refinement, we used data collected on a calcined sample (i.e., one in which the organic molecules in the pores had been removed by heat treatment) [*a* = 14.2088(3) Å, *b* = 57.2368(13) Å, *c* = 19.9940(2) Å], even though the peaks were not as sharp as those in the pattern used for the structure determination. Soft geometric restraints were placed on the bond distances and angles of the atoms of the framework, and the refinement converged with the structure factor, weighted profile (R_{wp}), and statistically expected *R* values 0.075, 0.188, and 0.142, respectively (Fig. 3). Strong anisotropic peak broadening along two crystallographic directions (e.g., peak widths of 0.026, 0.060, and 0.068°2θ for reflections with similar 2θ values, but orthogonal orientations) was observed and could only be modeled approximately. The high R_{wp} value stems mainly from this complication, as well as a particularly irregular background that was difficult to estimate and the presence of an unidentified impurity. Nonetheless, the refinement of the structure itself was extremely stable. Although 12 of the 24 Si atoms in the asymmetric unit lie on the mirror plane perpendicular to the *a* axis, the geometry remained reasonable, with the possible exception of the 180° Si-O-Si angle at O(25), which lies on a center of symmetry. Reducing the symmetry to one of the noncentrosymmetric *C*-centered subgroups of *Cmcm* (*C*2*cm*, *C*222$_1$, or *Cmc*2$_1$) did not result in any substantial improvement in either the profile fit or the geometry, so the higher space group *Cmcm* was retained. It is possible that the calcined form of IM-5, which was used for the refinement, adopts a symmetry higher than that of the as-synthesized form, which was used for all the other analyses.

With 24 topologically distinct Si atoms, the framework structure of IM-5 (see data file S1 for IM-5 crystallographic information) is as complex as that of TNU-9, the most complex zeolite hitherto solved (*8*). For comparison, the next most complex zeolite, ITQ-22 (*28*), has only 16 topologically distinct (Si,Ge) atoms. The [001]

projection (Fig. 1B) of IM-5 is very similar to one found in several other high-silica zeolites [Ferrierite, ZSM-5, ZSM-11, ZSM-57, SUZ-4, Theta-1, and TNU-9 (*29*)]. However, the connectivity along [001] is different and leads to an unusual pore system (Fig. 4). As suggested by the catalytic tests (*10*), IM-5 has a 2D 10-ring (10 Si atoms and 10 O atoms in the ring describing the pore opening) channel system with effective pore widths ranging from 4.8 to 5.5 Å. What is unusual is that this channel system also has a limited third dimension. Three 2D channel systems running perpendicular to the *b* axis are connected to one another to form a ~2.5-nm-thick pore system. Single walls of four, five, and six rings (Fig. 4A) separate these nanoslabs from one another. This distinctive pore structure (Fig. 4B) gives IM-5 the character of a 3D channel system with complex channel intersections that can accommodate bulky intermediates in a catalytic reaction, while retaining the overall effect of a 2D one with long-range diffusion restricted to just two dimensions.

Because no symmetry is assumed, the number of atoms per unit cell rather than the number per asymmetric unit is the prime limitation of the pCF algorithm. For IM-5, this number is 864 (288 Si atoms + 576 O atoms). Therefore, the structures of other polycrystalline materials with similar numbers of atoms per unit cell, whether they be other catalysts, ceramics, pharmaceuticals, or complex metal alloys, should also be accessible via a similar route, provided that HRTEM images can be obtained. All of the enhancements to the charge-flipping approach discussed here have been implemented in the freely available program Superflip (Superflip input file for IM-5 is given in data file S2) (*6*).

References and Notes

1. W. I. F. David, K. Shankland, L. B. McCusker, Ch. Baerlocher, Eds., *Structure Determination from Powder Diffraction Data* (Oxford Univ. Press, Oxford, 2002).
2. Ch. Baerlocher, L. B. McCusker, Eds., *Z. Kristallogr.* **219** (Spec. Iss.), 782 (2004).
3. G. Oszlányi, A. Sütő, *Acta Crystallogr. A* **60**, 134 (2004).
4. G. Oszlányi, A. Sütő, *Acta Crystallogr. A* **61**, 147 (2005).
5. Ch. Baerlocher, L. B. McCusker, L. Palatinus, *Z. Kristallogr* **222**, 47 (2007).
6. L. Palatinus, G. Chapuis, http://superspace.epfl.ch/superflip (2006).
7. R. W. Grosse-Kunstleve, L. B. McCusker, Ch. Baerlocher, *J. Appl. Cryst.* **30**, 985 (1997).
8. F. Gramm *et al.*, *Nature* **444**, 79 (2006).
9. E. Benazzi, J. L. Guth, L. Rouleau, PCT Gazette WO 98/17581 (1998).
10. A. Corma *et al.*, *J. Catal.* **189**, 382 (2000).
11. A. Corma, J. Martínez-Triguero, S. Valencia, E. Benazzi, S. Lacombe, *J. Catal.* **206**, 125 (2002).
12. S.-H. Lee *et al.*, *J. Catal.* **215**, 151 (2003).
13. E. Benazzi, S. Kasztelan, U.S. Patent 6667267 (2003).
14. J. M. Serra, E. Guillon, A. Corma, *J. Catal.* **227**, 459 (2004).
15. J. M. Serra, E. Guillon, A. Corma, in *Molecular Sieves: From Basic Research to Industrial Applications*, J. Cejka, N. Zilkova, P. Nachtigall, Eds. (Elsevier, Amsterdam, 2005), vol. 158, p. 1757.
16. J.-L. Duplan, J. Bayle, S. Lacombe, C. Thomazeau, U.S. Patent application 20050222475.
17. G. T. Kokotailo, S. L. Lawton, D. H. Olson, W. M. Meier, *Nature* **272**, 437 (1978).
18. K. Y. J. Zhang, P. Main, *Acta Crystallogr. A* **46**, 41 (1990).
19. J. Wu, K. Leinenweber, J. C. H. Spence, M. O'Keeffe, *Nat. Mater.* **5**, 647 (2006).
20. S. Brenner, L. B. McCusker, Ch. Baerlocher, *J. Appl. Cryst.* **35**, 243 (2002).
21. X. D. Zou, Y. Sukharev, S. Hovmöller, *Ultramicroscopy* **52**, 436 (1993).
22. X. D. Zou, A. Hovmöller, S. Hovmöller, *Ultramicroscopy* **98**, 187 (2004).
23. M. A. Estermann, V. Gramlich, *J. Appl. Cryst.* **26**, 396 (1993).
24. S. Hovmöller, *Ultramicroscopy* **41**, 121 (1992).
25. X. D. Zou, Z. M. Mo, S. Hovmöller, X. Z. Li, K. H. Kuo, *Acta Crystallogr. A* **59**, 526 (2003).
26. P. Oleynikov, X. D. Zou, S. Hovmöller, www.analitex.com/Index.html (2006).
27. Ch. Baerlocher, A. Hepp, W. M. Meier, *DLS-76. Distance Least Squares Refinement Program* (Institut für Kristallographie, ETH Zurich, 1977).
28. A. Corma, F. Rey, S. Valencia, J. L. Jorda, J. Rius, *Nat. Mater.* **2**, 493 (2003).
29. Ch. Baerlocher, W. M. Meier, D. H. Olson, *Atlas of Zeolite Framework Types* (Elsevier, Amsterdam, 2001); and www.iza-structure.org/databases/.
30. E. F. Pettersen *et al.*, *J. Comput. Chem.* **25**, 1605 (2004).

31. We thank H. Kessler (Université de Haute-Alsace, Mulhouse) and S. Lacombe and L. Rouleau (Institut Français du Pétrole) for providing samples of IM-5. Special thanks to L. Palatinus (EPF Lausanne) for developing the program Superflip to suit our needs. Experimental assistance from the staff at SNBL and SLS is gratefully acknowledged. This work was supported in part by the Swiss National Science Foundation, the Swedish Research Council, and Carl-Trygger's Foundation.

Supporting Online Material

www.sciencemag.org/cgi/content/full/315/5815/1113/DC1
Data files S1 and S2

22 November 2006; accepted 18 January 2007
10.1126/science.1137920

Shaping of Elastic Sheets by Prescription of Non-Euclidean Metrics

Yael Klein, Efi Efrati, Eran Sharon*

The connection between a surface's metric and its Gaussian curvature (Gauss theorem) provides the base for a shaping principle of locally growing or shrinking elastic sheets. We constructed thin gel sheets that undergo laterally nonuniform shrinkage. This differential shrinkage prescribes non-Euclidean metrics on the sheets. To minimize their elastic energy, the free sheets form three-dimensional structures that follow the imposed metric. We show how both large-scale buckling and multiscale wrinkling structures appeared, depending on the nature of possible embeddings of the prescribed metrics. We further suggest guidelines for how to generate each type of feature.

Thin sheets are common in natural and man-made structures, are shaped to a huge variety of diverse three-dimensional (3D) structures, and span many length scales (*1*). Natural slender structures, such as flowers, lichens, and marine invertebrates, attain elaborate configurations during their unconfined (free) growth. One wonders what mechanisms lead to shaping of free sheets and whether they can be implemented with artificial materials. Thin sheets can form nontrivial 3D structures in many different ways. Confinement of flat sheets can lead to buckling (*2*), wrinkling (*3*), and crumpling (*4*). The construction of layered material can result in both bending (*5*, *6*) and wrinkling (*7*, *8*). Recent studies of wavy patterns along edges of torn plastic sheets (*9*–*11*) have shown that 3D wavy patterns can result from inplane deformations. Mathematically, a structure made of a thin sheet can be viewed as a two-dimensional (2D) surface in a 3D Euclidean space. Intrinsically, a surface is characterized by its metric, a tensor that specifies the local distances between points across the surface (*12*). The shape of a surface, its configuration in space, is a realization, an embedding, of the metric in space. In many cases, there would be many possible embeddings of a given 2D surface (metric) in space; that is, the metric alone does not determine a configuration. To select a specific shape (a specific embedding), one needs to determine, in addition to the metric, the local curvatures on the surface (*13*).

We present a shape selection principle based on two main ideas: The first is Gauss theorem (Theorema Egregium), which states that the metric tensor of a surface locally determines its Gaussian curvature $K(x,y)$. The second principle, known from the study of crumpling (*14*–*16*), shell collapse (*17*), and wrinkling (*18*), states that equilibria of thin elastic sheets involve only small amount of inplane strain. Combined, these two principles lead to a novel shaping mechanism: Rather than aiming at a specific embedding, one prescribes on the sheet only a 2D metric, the "target metric" g_{tar}, one that results in a nonzero Gaussian curvature (a non-Euclidean metric). A sheet adopting a configuration (embedding) satisfying g_{tar} would have been completely free of inplane strain, that is, stretching energy. The free sheet will settle to a 3D configuration that minimizes its elastic energy. In this mechanism, the selected configuration is set by the competition between bending and stretching energies, and its metric will be close to (but

Racah Institute of Physics, Hebrew University of Jerusalem, Jerusalem, Israel.

*To whom correspondence should be addressed. E-mail: erans@vms.huji.ac.il

different from) g_{tar}. We show that the construction of elastic sheets with various target metrics is possible and results in spontaneous formation of 3D structures. These structures exist in both large-scale buckling and small-scale wrinkling forms. We further suggest guidelines for how to generate each type of feature. Being free in space and not locked onto a specific embedding, these sheets undergo morphological transitions, driven by global constraints on possible embeddings of their target metrics.

We used *N*-isopropylacrylamide (NIPA) gels to construct sheets with inducible non-Euclidean g_{tar}. The gels are produced by mixing NIPA monomers with bisacrylamide (BIS) (6% by weight of NIPA) cross-linker in water. The addition of catalysts initiates polymerization of a cross-linked elastic hydrogel [Supporting Online Material (SOM) text]. This gel undergoes a sharp, reversible, volume reduction transition at T_c = 33°C (*19*), above which its equilibrium volume decreases considerably. Calibration experiments (fig. S1) using various homogeneous (each of a different fixed NIPA concentration) gel discs provide the relation between the monomer concentration and η, the shrinkage ratio of the "activated" gel. These measurements show that dilute gels shrink a lot, whereas gels with high monomer concentrations undergo moderate shrinking.

To impose nontrivial target metrics, we constructed sheets with internal lateral gradients in NIPA concentration, i.e., $\eta = \eta(\mathbf{r})$. We used programmable actuated valves to inject solutions with gradients in monomer concentration into a mold (Fig. 1). Polymerization takes place within a minute, and the imposed gradients are thus frozen within the gel. The constructed sheets are flat below T_c but are programmed to shrink differentially, with ratio $\eta(\mathbf{r})$, upon activation at $T > T_c$. Indeed, the sheets adopted a non-Euclidean metric and underwent large reversible shape transformations (Movie S1). To cast radially symmetric discs, we used a Hele-Shaw cell configuration. The solution is injected into the gap between two flat glass plates through a central hole in one of them (Fig. 1). Gel tubes were cast by injecting the solution into the gap between two concentric glass tubes.

The differential shrinking changes distances between points on the surface; that is, it defines a new target metric on the disc. Because the system is radially symmetric, we consider a closed circle of radius r on the cold disc. After the shrinking, both perimeter and radius of the circle are modified. The perimeter is now $2\pi r\eta$, and the radius is $\rho(r) = \int_0^r \eta(r')dr'$. Thus, the perimeter of a circle of radius ρ on the shrunk disc is now $f(\rho)2\pi\rho$, where $f(\rho)$ is determined by $\eta(\rho)$. With use of a radial coordinate system (ρ, θ), the linear element determined by g_{tar} is $dl^2 = d\rho^2 + \rho^2 f(\rho)^2 d\theta^2$, and the prescribed target Gaussian curvature reads

$$K_{tar}(\rho) = -\frac{[\rho f'(\rho)]_{\rho\rho}}{\rho f(\rho)} \qquad (1)$$

The ρ-dependent monomer concentration is thus a knob with which we can set $[\rho f(\rho)]_{\rho\rho}$ and determine a target Gaussian curvature. When $[\rho f(\rho)]_{\rho\rho}$ does not equal 0, K_{tar} also does not equal 0, implying that any embedding of g_{tar} cannot be flat. This is demonstrated in Fig. 2A, where increasing and decreasing monomer concentrations result in $K_{tar} < 0$ and $K_{tar} > 0$, respectively. The resultant configurations of the sheets are nonflat, corresponding to g_{tar} (Fig. 2A insets).

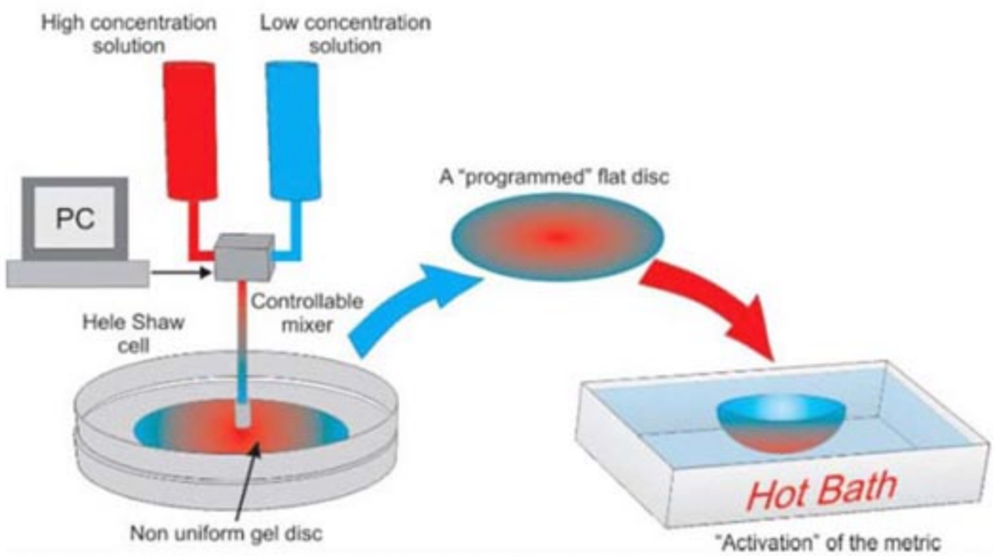

Fig. 1. The experimental system. High (~ 30%) and low (~ 10%) monomer concentration solutions are mixed in a programmable mixer and injected into a Hele-Shaw cell (**left**). Polymerization leads to the generation of a flat disc having internal lateral gradients in monomer concentration (**center**). Once this programmed disc is activated in a hot bath of temperature $T > T_c$ = 33°C, it shrinks differentially, adopting a new, non-Euclidean target metric (**right**). As a result, it attains a 3D configuration. Illustrated is a surface of positive Gaussian curvature, generated by increasing monomer concentration during the injection.

The sheets are not ideal 2D surfaces, and their equilibrium configurations are determined by balancing stretching and bending energies: The stretching energy, which vanishes only in embeddings that fully follow g_{tar}, scales linearly with the sheet thickness, t (*20*). The bending energy, which is 0 only in flat configurations (because the sheets are uniform across their thickness), leads to deviations from g_{tar} and scales as t^3. Thus, as $t \to 0$ the stretching term dominates, and, therefore, a sheet will be willing to bend a lot in order to reduce its inplane strain. Therefore, equilibrium configurations will involve only small amounts of inplane strain, and the metric of the selected configuration g is expected to approach g_{tar}. To check this conjecture, we compared the metrics of curved discs to their target metrics. The topography of the discs $z(x,y)$ was measured by using an optical profilometer (Conoscan 3000, Optimet, Jerusalem, Israel) (SOM text). Radial geodesics (the equivalent of radial lines on a curved disc) were plotted for azimuthal angles θ (Fig. 2B, insets), enabling the identification of circles of radius ρ on the curved surface (in general, the projections of these curves are not circles in the x,y plane). We measured the perimeter of such circles and compared it to $f(\rho)2\pi\rho$, the perimeter set by g_{tar}. This comparison is shown for two types of discs of positive and of negative target Gaussian curvature (Fig. 2B). In both cases, the perimeter at ρ closely follows the prescribed one, and indeed the sheets' metric (averaged over θ) is very close to their target metric.

When averaged over θ, the two types of discs follow g_{tar}; however, they present two qualitatively different physical behaviors. The surfaces of $K_{tar} > 0$ preserve the radial symmetry of g_{tar}, generating surfaces of revolution (Fig. 2, lower insets). The surfaces of $K_{tar} < 0$ break this symmetry, forming wavy structures (Fig. 2 upper insets). To understand the nature of this qualitative difference, we compared the magnitude and the distribution of bending and stretching energy densities across the sheets. The stretching energy density results from inplane strain, that is, differences between g and g_{tar}. Thus (according to Gauss' theorem), local differences between $K(\rho,\theta)$ and $K_{tar}(\rho)$ indicate a nonzero stretching energy density. The bending energy density is $E_b(\rho,\theta) = DB(\rho,\theta)$, where D is the bending stiffness of the sheet (SOM text) and $B(\rho,\theta) = 4H^2(\rho,\theta) - K(\rho,\theta)$, with $H(\rho,\theta)$ the local mean curvature. Thus, the bending energy density can be studied by analyzing $B(\rho,\theta)$.

The distributions of $H^2(\rho,\theta)$ and $K(\rho,\theta)$ are presented in Fig. 3. For discs of $K_{tar} > 0$ (Fig. 3, A and B, left), both K and H^2 are distributed in a radially symmetric manner and are of the same magnitude. The symmetric distribution of K indicates that g_{tar} is obeyed locally and not just on average (Fig. 2). This indicates that the surfaces' configuration is very close to an embedding of g_{tar}, and thus its stretching energy is close to 0. $H^2(\rho,\theta) \approx K(\rho,\theta)$ implies that B is

close to its minimal locally possible value, $B = 3K$ (SOM text). Thus, the bending energy density is minimal as well. The selected configuration locally minimizes both bending and stretching energy densities, thus forming a very low energy solution. In contrast, for surfaces with $K_{tar} < 0$ (Fig. 3, A and B, right), H^2 attains large values (larger than $|K_{tar}|$), and the condition for minimal bending energy density [$H(\rho,\theta) = 0$] is far from being fulfilled, resulting in high bending energy. Indeed, the average of $B(\rho,\theta)$ over this surface is twice as large as that of the surface of $K_{tar} > 0$ (whereas its minimally possible value, $B = K$, is three times smaller than that of the surface of $K_{tar} > 0$).

A more surprising observation is the asymmetric distribution of the Gaussian curvature. Instead of the negative, rotationally symmetric K_{tar} (Eq. 1), $K(\rho,\theta)$ varies periodically in θ, attaining positive and negative values (Fig. 3B, right). The comparison with K_{tar} at a fixed ρ (Fig. 3C) shows that K oscillates, with amplitudes larger than its mean (K_{tar}). These fluctuations imply a periodic deviation from g_{tar}, i.e., significant modulations in stretching energy density. Compared with the case of $K_{tar} > 0$, the selected configuration is not successful in reducing both bending and stretching energies.

Intrinsically, the discs in Fig. 2 differ only by the sign of K_{tar}. What is the mechanism that causes the disc with $K_{tar} < 0$ to break the symmetry, bend a lot, and localize inplane strain? Because the discs are free in space and energy is minimized globally over the entire disc, limitations on possible global embeddings of g_{tar} play a central role in setting the shape of the disc.

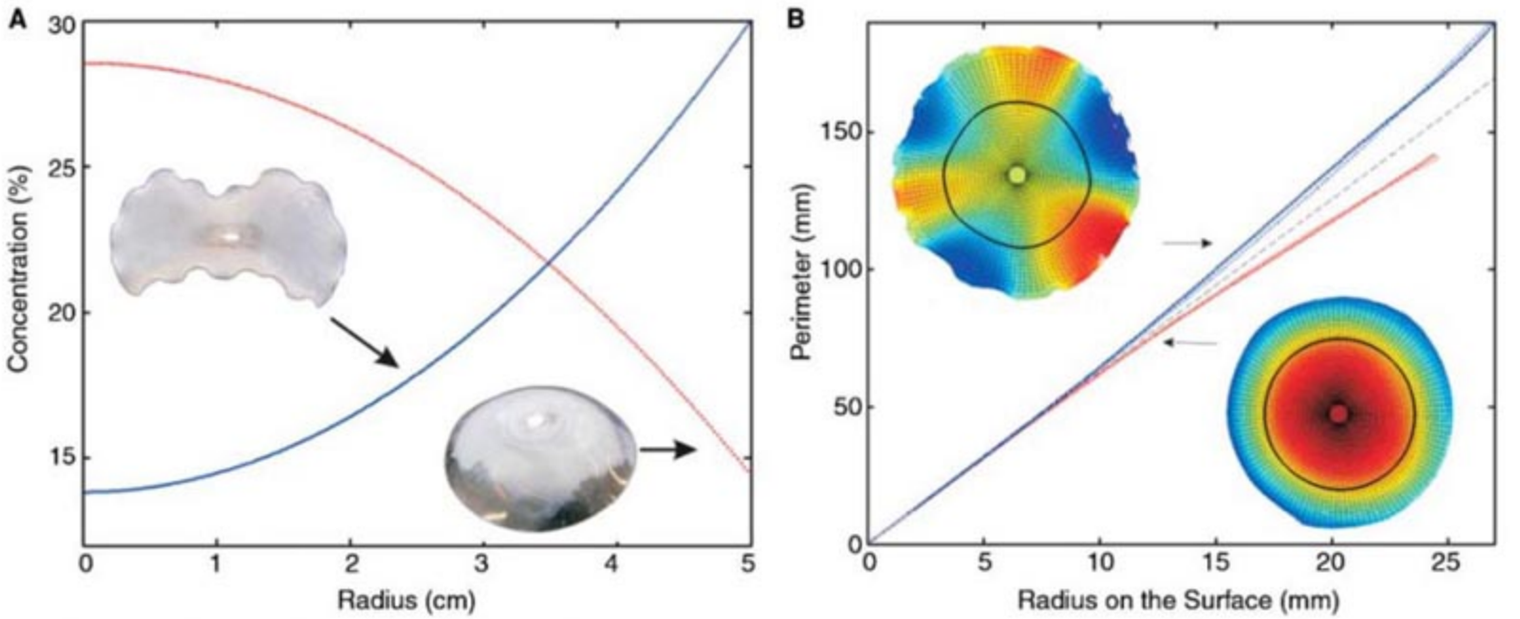

Fig. 2. Shaping of non-Euclidean elastic discs. (**A**) A radially decreasing monomer concentration (red line) prescribes a positive Gaussian curvature on the disc, which adopts a dome shape (lower image). When the monomer concentration profile is inverted (blue line), it prescribes a negative Gaussian curvature, leading to an azimuthally oscillating shape (upper image). Discs' initial thickness $t_0 = 0.5$ mm. (**B**) Disc perimeter as a function of ρ (solid lines) compared to the perimeter prescribed by g_{tar} (dashed lines). Both positive (red) and negative (blue) Gaussian curvature discs follow, on average, g_{tar}. The dashed black line indicates a flat disc for which the perimeter equals to $2\pi\rho$. (Images) Measured disc topography $z(x,y)$ with a semigeodesic coordinate system. Lines of constant radius $\rho = 15$ mm on the curved discs are highlighted in bold.

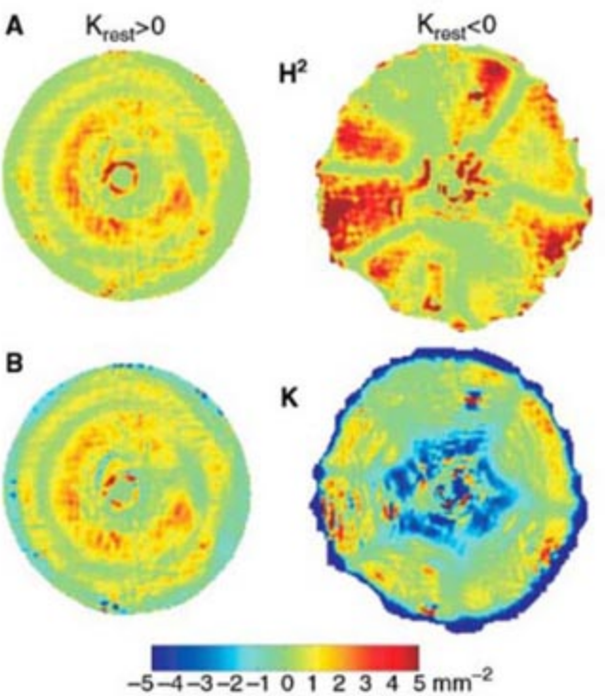

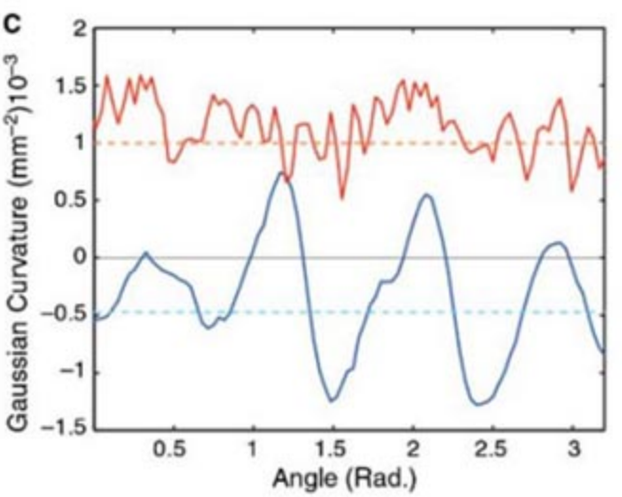

Fig. 3. Distribution of Gaussian and mean curvatures on the discs. (**A**) The squared local mean curvature on discs of $K_{tar} > 0$ (left) and $K_{tar} < 0$ (right). The first is radially symmetric (except for few defects), whereas the other oscillates. (**B**) The measured Gaussian curvature on the positive curvature disc (left) is radially symmetric and of magnitude similar to that of H^2. In the case of $K_{tar} < 0$, the Gaussian curvature oscillates, breaking the radial symmetry. (**C**) The local Gaussian curvature along a line of $\rho = 15$ mm is plotted versus the angle for the discs with $K_{tar} > 0$ (red) and $K_{tar} < 0$ (blue). The dashed lines indicate K_{tar} at $\rho = 15$ mm. For the disc of $K_{tar} > 0$, the generated Gaussian curvature is positive and closely distributed around its mean. In contrast, the Gaussian curvature of the disc of $K_{tar} < 0$ oscillates with amplitudes larger than its mean, in correlation with surface undulations.

For metrics with $K_{tar}(\rho) > 0$, radially symmetric global embeddings with small bending do exist (*21*). Such theoretical configurations are good minimizers of the sheet's energy; they fully follow g_{tar} (are free of stretching) and would possess low bending energy. The physical sheets select such embeddings as a basis for their equilibrium configurations. The finite thickness of the sheets will lead to configuration that are close to the mathematical (2D) ones, with both bending and stretching energies small, as we have shown. In contrast, embeddings of radially symmetric metrics, with $K_{tar} < 0$ (hyperbolic metrics) are nontrivial, do not preserve the radial symmetry of the metric, and must include small-scale structure (*22*, *23*). The larger the sheet is, the smaller this scale gets. Such embeddings of a physical sheet would have large (bending) energy and thus are not candidates for sheets' equilibrium shapes. Indeed, the substantial localized stretching energy, together with the large bending energy (Fig. 3, A and B, right), indicates that the sheets do not select an embedding of g_{tar} as a basis for their equilibrium configuration but follow a wrinkling-type behavior. In wrinkling, stressed small-scale (*18*) and multiscale (*24*) wavy structures are formed because of the inability to facilitate stretch-free configurations with low bending energy. Our experiments show that such conditions can occur with free sheets, depending on their target metric.

The prescription of smooth symmetric metrics can thus lead to the formation of both symmetric large-scale and oscillating small-scale structures. This tool can be used as a basis for a shaping principle. Different types of shapes are constructed (Fig. 4) by combining regions of different curvatures and controlling sheet thickness and sheet topology. In contrast to the disc topology, in cylindrical topology, symmetric, low bending embeddings of $K_{tar} < 0$ do exist (*22*, *25*) in a trumpet form. A physical sheet will thus be able to select such an embedding as a basis for its equilibrium configuration, resulting (Fig. 4 E) in a configuration that is symmetric and feature-free. However, such a symmetric surface can accommodate only up to -2π negative Gaussian curvature (*22*, *25*). Beyond this limit, the symmetric solution no longer exists. This is seen in Fig. 4, F to H, where cylindrical sheets with $K_{tar} < 0$ adopt wavy configurations, as with the radial discs.

We suggest that large-scale buckling of unconstrained elastic sheets occurs when a non-Euclidean target metric g_{tar} can be symmetrically embedded, with low associated bending energy. When no such embedding exists, energy minimization of the sheet is achieved via a wrinkling-type behavior. This shaping principle might play a role during developmental processes in naturally growing tissues, where the local nature of the growth provides a mechanism for the formation of non-Euclidean metrics. In our experimental system, g_{tar} can be turned "on" and "off" by environmental conditions, having an applicative potential. This approach can be implemented by using other artificial materials that undergo large volume reduction. Such new materials are being developed to respond to different external stimuli, such as light (*26*), pH (*27*), glucose level (*28*), and other chemical signals (*29*). Further study of the principles of shaping by metric prescription can extend the types and variety of structures that can be formed by using thin sheets, as well as improve our understanding of developmental processes.

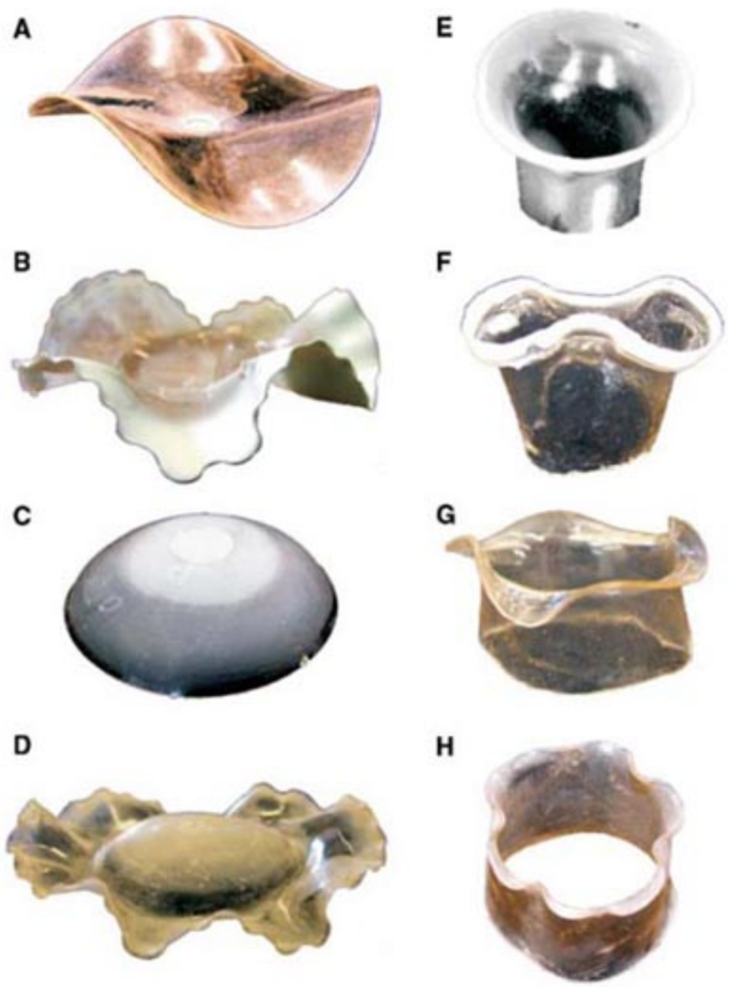

Fig. 4. Different structures of sheets with radially symmetric target metrics. (**A**) A thick sheet (t = 0.75 mm) with relatively flat hyperbolic metric adopts a configuration with only three waves. Thinner (t = 0.3 mm) sheets with larger gradients in monomer concentration form two generations of waves (**B**). Symmetric surfaces of positive curvature, such as in (**C**), can be combined with negative curvature margins to obtain a wavy sombrero-like structure (**D**). Axially symmetric metrics can be applied to cylindrical sheets. (**E**) A tube with $K < 0$ preserves the radial symmetry because the amount of Gaussian curvature integrated over the tube is less than -2π. When too much negative curvature is accumulated over a tube, it develops a wavy edge. Tubes with two (**F**), four (**G**), and six (**H**) waves are obtained, depending on the sheet thickness and the metric profile.

References and Notes

1. D. W. Thompson, *On Growth and Form* (Cambridge Univ. Press, Cambridge, 1942).
2. B. Roman, A. Pocheau, *Europhys. Lett.* **46**, 602 (1999).
3. E. Cerda, K. Ravi-Chandar, L. Mahadevan, *Nature* **419**, 579 (2002).
4. E. Kramer, T. Witten, *Phys. Rev. Lett.* **78**, 1303 (1997).
5. Z. Hu, X. Zhang, Y. Li, *Science* **269**, 525 (1995).
6. Y. Yu, M. Nakano, T. Ikeda, *Pure Appl. Chem.* **76**, 1467 (2004).
7. N. Bowden, S. Brittain, A. Evans, J. W. Hutchinson, G. M. Whitesides, *Nature* **393**, 146 (1998).
8. T. Mora, A. Boudaoud, *Eur. Phys. J. E* **20**, 119 (2006).
9. E. Sharon, B. Roman, M. Marder, H. Swinney, *Nature* **419**, 579 (2002).
10. M. Marder, E. Sharon, B. Roman, S. Smith, *Europhys. Lett.* **62**, 498 (2003).
11. B. Audoly, A. Boudaoud, *Phys. Rev. Lett.* **91**, 086105 (2003).
12. M. Spivak, *A Comprehensive Introduction to Differential Geometry* (Publish or Perish, Berkeley, CA, ed. 2, 1979), vol. I.
13. M. Spivak, *A Comprehensive Introduction to Differential Geometry* (Publish or Perish, Berkeley, CA, ed. 2, 1979), vol. III.
14. A. Lobkovsky, I. Witten, *Phys. Rev. E* **55**, 1577 (1997).
15. M. Ben Amar, Y. Pomeau, *Proc. R. Soc. London Ser. A* **453**, 729 (1997).
16. A. Boudaoud, P. Patricio, Y. Couder, M. Ben Amar, *Nature* **407**, 718 (2000).
17. Y. Pomeau, S. Rica, *C. R. Acad. Sci. Paris Sér. II* **325**, 181 (1997).
18. E. Cerda, L. Mahadevan, *Phys. Rev. Lett.* **90**, 074302 (2003).
19. Y. Hirokawa, T. Tanaka, *J. Chem. Phys.* **81**, 6379 (1984).
20. A. Föppel, *Vorlesungen ü. technische Mechanik* (B.G. Teubner, Leipzig, Germany, ed. 5, 1907).
21. B. O'Neill, *Elementary Differential Geometry* (Academic Press, New York, 1966).
22. E. Poznyak, E. Shikin, *Am. Math. Soc. Transl.* **176**, 151 (1996).
23. E. Rozendorn, in *Encyclopaedia of Mathematical Sciences: Geometry III* (Springer-Verlag, Berlin, 1992), vol. 48, p. 89.
24. K. Efimenko *et al.*, *Nat. Mater.* **4**, 293 (2005).
25. M. Marder, N. Papanicolaou, *J. Stat. Phys.* **125**, 1069 (2005).
26. A. Lendlein, H. Jiang, O. Junger, R. Langer, *Nature* **434**, 879 (2005).
27. O. Philippova, D. Hourdet, R. Audebert, A. Khokhlov, *Macromolecules* **30**, 8278 (1997).
28. K. Kataoka, H. Miyazaki, M. Bunya, T. Okano, Y. Sakurai, *J. Am. Chem. Soc.* **120**, 12694 (1998).

29. T. Tanaka, *Phys. Rev. Lett.* **40**, 820 (1978).
30. We thank G. Cohen for help in writing this manuscript. This work was supported by Israel Science Foundation Bikura program (no. 1437/04), German-Israeli Foundation, United States–Israel Binational Foundation (grant no. 2004037), and the MechPlant project of European Union's New and Emerging Science and Technology program.

Supporting Online Material
www.sciencemag.org/cgi/content/full/315/5815/1116/DC1
Materials and Methods
Fig. S1
Movie S1

6 October 2006; accepted 18 January 2007
10.1126/science.1135994

Focusing Beyond the Diffraction Limit with Far-Field Time Reversal

Geoffroy Lerosey, Julien de Rosny, Arnaud Tourin, Mathias Fink*

We present an approach for subwavelength focusing of microwaves using both a time-reversal mirror placed in the far field and a random distribution of scatterers placed in the near field of the focusing point. The far-field time-reversal mirror is used to build the time-reversed wave field, which interacts with the random medium to regenerate not only the propagating waves but also the evanescent waves required to refocus below the diffraction limit. Focal spots as small as one-thirtieth of a wavelength are described. We present one example of an application to telecommunications, which shows enhancement of the information transmission rate by a factor of 3.

Subwavelength information about an object is carried by evanescent waves. As they decay exponentially, these evanescent waves are generally lost before reaching the far-field image plane, which is the origin of the diffraction limit. One approach to recover evanescent waves in near-field microscopy is to place a subwavelength scatterer in the near field of the object to be imaged. By diffracting off the scatterer, evanescent waves can convert into propagating waves, which can then be detected in the far field. In the past decade, several schemes for detecting evanescent waves were introduced (*1*, *2*). They use either a subwavelength-sized aperture or a sharp stylus that samples the field very close ($<\lambda$) to the specimen to be imaged.

More recently, superlenses have been proposed for imaging beyond the diffraction limit (*3*–*5*). These discoveries followed the original descriptions of negative refraction and perfect imaging of quasistatic line sources (*6*, *7*). Such superlenses consist of thin slabs of materials with negative permittivity, permeability, or both (*4*, *5*, *8*–*11*). Recently a cylindrical lens relying on anisotropic metamaterials has also been theoretically proposed (*12*). Superlenses transmit evanescent waves with enhanced amplitude, in contrast to conventional materials. Thus, evanescent components radiated by an object can be recovered in the image plane. In contrast with near-field microscopy, which requires a point-by-point scanning, superlenses form the whole image at once. One drawback is that in all existing experimental verifications, the image still forms in the near-field zone of the superlens and a scanning near-field microscopy technique must be used to create the far-field image (*13*).

Our approach for subwavelength focusing uses a focusing aperture placed in the far field. The idea is to build a microstructured medium in the near field of the point where one intends to focus and to use a time-reversal mirror (TRM) placed in the far field to build the time-reversed wave field that will focus at the target without being subject to the diffraction limit.

The time-reversal technique is well known in acoustics and has led to a number of applications in ultrasound and underwater acoustics, such as brain therapy, lithotripsy, and nondestructive testing, as well as in telecommunications (*14*). In a typical time-reversal experiment, an acoustic source is placed at the location where one intends to focus. First, this source sends out a short pulse. The wave field propagates and is recorded with a set of transducers located on a surface. Second, the recorded signals are flipped in time. Third, the flipped signals are transmitted back by the same set of transducers acting as transmitters. The resulting wave is found to converge back to its initial source. At best, if the transducers are located on a closed surface surrounding the original source, forming a closed TRM, the time-reversed wave converges from all directions. However, even if the original source is pointlike, the focal spot is not. Indeed, as the amplitude of the evanescent waves decays

Laboratoire Ondes et Acoustique, École Supérieure de Physique et de Chimie Industrielles, Université Paris VII, Centre National de la Recherche Scientifique, UMR 7587, 10 rue Vauquelin, 75005 Paris, France.

*To whom correspondence should be addressed. E-mail: mathias.fink@espci.fr

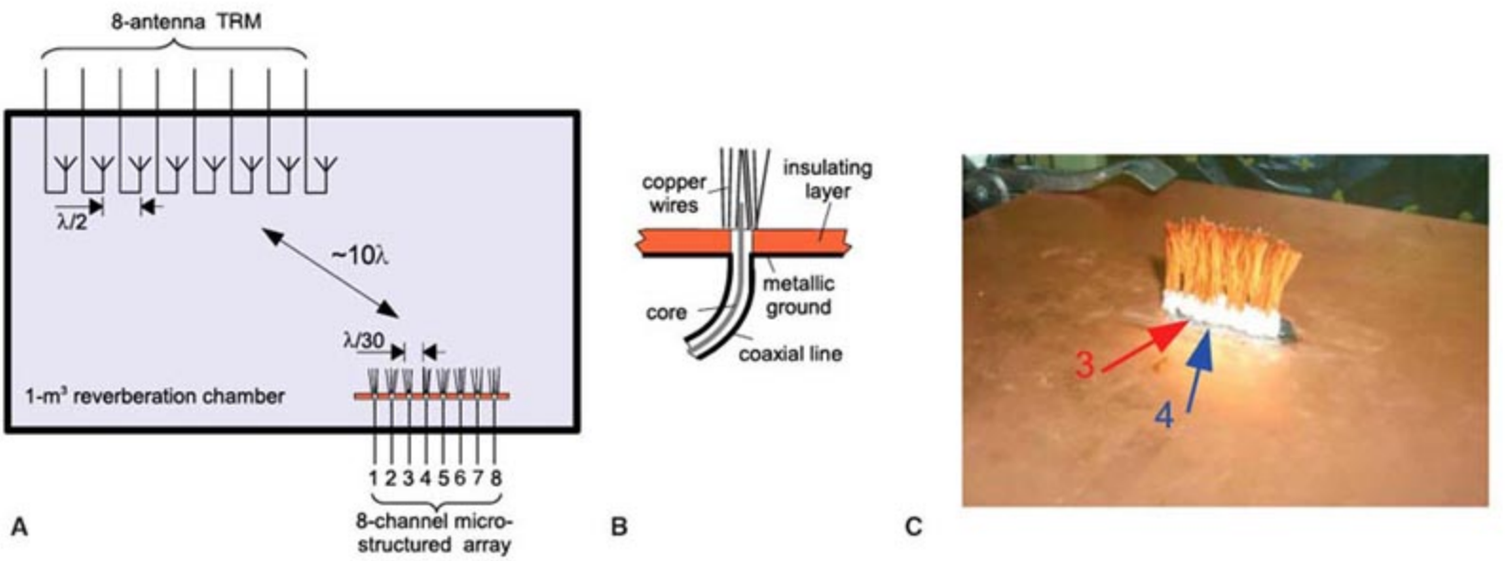

Fig. 1. Experimental setup. (**A**) A TRM made of eight commercial dipolar antennas operating at 2.45 GHz (i.e., λ = 12 cm) is placed in a 1-m^3 reverberating chamber. Ten wavelengths away from the TRM is placed a subwavelength receiving array consisting of eight microstructured antennas λ/30 apart from one another. (**B**) Details of one microstructured antenna. It consists of the core of a coaxial line that comes out 2 mm from an insulating layer and is surrounded by a microstructure consisting of a random distribution of thin copper wires. (**C**) Photo of the eight-element subwavelength array surrounded by the random distribution of copper wires. Antennas 3 and 4 are indicated by the red and blue arrows.

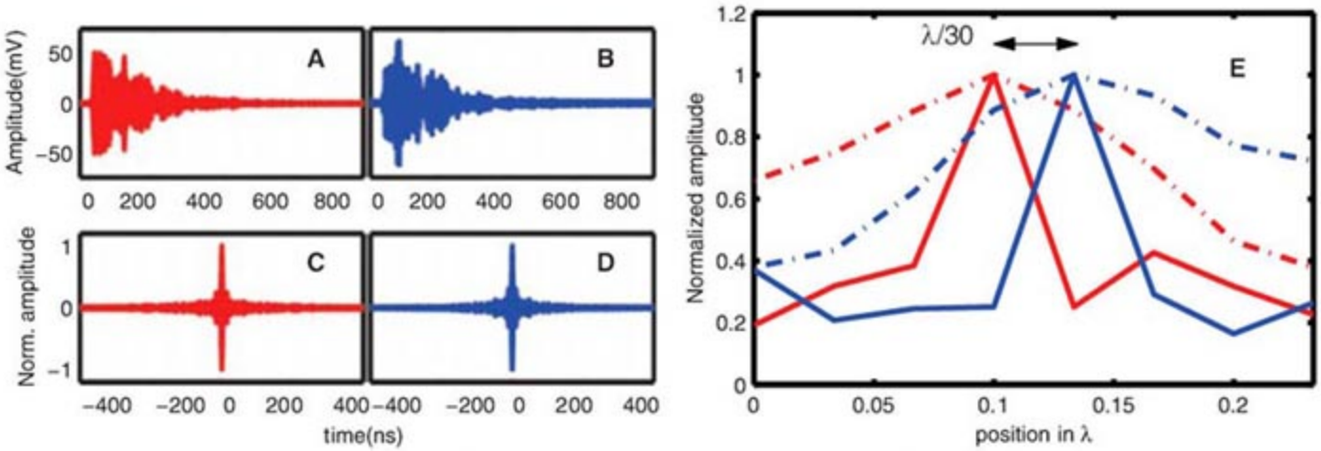

Fig. 2. Focusing beyond the diffraction limit. (**A** and **B**) show the signal received at one antenna of the TRM when a 10-ns pulse is sent from antennas 3 and 4, respectively, of the microstructured array. The signals in (A) and (B) look considerably different, although antennas 3 and 4 are only λ/30 apart. (**C** and **D**) show the time compression obtained at antennas 3 and 4, respectively, when the eight signals coming from antennas 3 and 4 are time-reversed and sent back from the TRM. (**E**) In full line are shown the focusing spots obtained around antennas 3 and 4. Their typical width is λ/30. Thus, antennas 3 and 4 can be addressed independently. The focal spots obtained when there are no copper wires are shown for comparison (dashed-dotted line). All maxima have been normalized by scaling factors in the ratios: 1 (red and blue dashed-dotted lines), 2.2 (red full line), 2.5 (blue full line).

exponentially, a closed TRM located in the far field cannot sense and retransmit the evanescent components. Therefore, the time-reversed field produces a λ/2 focal spot in agreement with the diffraction limit.

In practice, a closed TRM is difficult to realize. The time-reversal operation is usually performed on a limited angular area, but if the time-reversal experiment is conducted inside a reverberant chamber, the diffraction limit can actually be reached, even with a small-aperture TRM (*15*). In this case, the time-reversed wave focuses from all directions because of reverberation off boundaries. Recently, experimental demonstrations of phase conjugation and broadband time reversal were reported for microwaves (*16*–*18*). In our microwave time-reversal experiments, a TRM made of eight antennas operating at a central frequency of 2.45 GHz with a bandwidth of 150 MHz was able to focus on a λ/2 focal spot inside a reverberant chamber.

Our approach to recover evanescent waves is to place a random distribution of subwavelength scatterers in the near field of the source. By diffracting off the scatterers, evanescent waves can convert into propagating waves, which can then be detected by the far-field time-reversal mirror. These propagating waves are time-reversed in the far field and transmitted back. Because of the theorem of generalized reciprocity between evanescent waves and propagating waves (*19*), the part of the far-field time-reversed wave originating from the evanescent waves of the source is converted back into the initial evanescent components, which thus participate in the refocusing process. In contrast to superlenses, evanescent waves are not enhanced here but, as a result of reciprocity, are recovered in the back-propagation step of the time-reversal process.

We have applied this idea to microwaves. A source consists of a wire antenna operating at a central frequency of 2.45 GHz (i.e., λ = 12 cm).

Fig. 3. Transmission of a color image. Transmission of a color image between a three-antenna TRM and a three-antenna receiving array. The original image is encoded on three RGB channels, and the three corresponding bitstreams are sent from the three antennas of the TRM. With a classical receiving array, the image is gray after decoding (**A**) because the three antennas coding for the red, green, and blue channels receive the same signal. With a microstructured receiving array, the red, green, and blue signals are focused independently on the three receiving antennas, although these latter are λ/30 apart from each other. The relative weights between the RGB channels are thus preserved and the color image is restored (**B**).

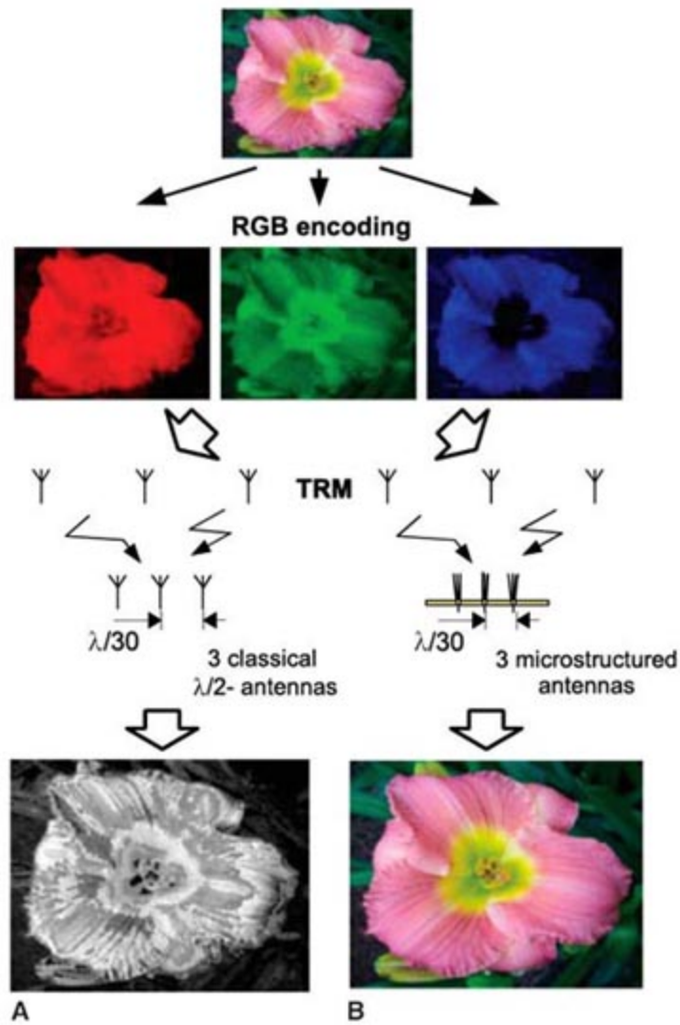

To convert the evanescent waves into propagating waves, the antenna is surrounded by a microstructure consisting of a random distribution of thin copper wires located in the near field of the antenna (see details of one antenna in Fig. 1, B and C). In our experiment, we consider eight possible focusing points placed in a strongly reverberating chamber (Fig. 1A). Eight microwave sources surrounded by a random microstructure are placed at these eight locations so that they can be used in the initial step of the time-reversal process. The distance between two adjacent antennas is λ/30. These eight antennas form an array that will be referred to as the re-

ceiving array. A TRM made of eight commercial dipolar antennas is placed in the far field, 10 wavelengths away from the receiving array. (The electronic part of the setup is described in fig. S1.) When antenna 3 sends a short pulse (10 ns), the eight signals received at the TRM are much longer than the initial pulse because of strong reverberation in the chamber (typically 500 ns). An example of the signal received at one of the antennas of the TRM is shown in Fig. 2A. When antenna 4 is used as a source, the signal received at the same antenna in the TRM (shown in Fig. 2B) is considerably different, although sources 3 and 4 are $\lambda/30$ apart. When these signals are time-reversed and transmitted back, the resulting waves converge respectively to antennas 3 and 4, where they recreate pulses as short as the initial ones (Fig. 2, C and D). Measuring the signal received at the other antennas of the receiving array gives access to the spatial focusing around antennas 3 and 4 (Fig. 2E). The two antennas can now be addressed independently, because the focusing spots created around them are much smaller than the wavelength (typically $\lambda/30$). The diffraction limit is overcome, although the focusing points are in the far field of the TRM.

The origin of the diffraction limit, and the way to overcome it, can be revisited by using the time-reversal concept and the Green's function formalism, without the explicit use of the evanescent wave concept (*20*–*22*). The time-reversed wave, generated by a closed TRM, which converges to its source, is always followed by a spatially diverging wave due to energy flux conservation. Because the focal spot results from the interference of these two waves, the time-reversed field can always be expressed (for a monochromatic wave) as the imaginary part of the Green's function (*22*). In a homogeneous medium, the imaginary part of the Green's function oscillates typically on a wavelength scale. To create focal spots much smaller than the wavelength, one introduces subwavelength scatterers in the near field of the source. Therefore, the spatial dependence of the imaginary part of the Green's function is modified to oscillate on scales much smaller than the wavelength.

A promising application of time-reversal subwavelength focusing is telecommunications. One way that has been proposed to increase the data rate of a communication system is to use multiantenna arrays at both transmitter and receiver (*23*); different bitstreams sent from each antenna of the transmitting array can be decoded at the receiving array under the condition that the medium creates sufficient scattering. It is also generally stated that the spacing between the receiving antennas must be larger than $\lambda/2$ (*23*). If these two conditions are fulfilled, the global maximum error-free data rate, or "Shannon Capacity," is at best multiplied by the number of transmitting antennas. Such methods are referred to as MIMO (multiple input–multiple output). However, from a practical perspective, it is difficult to ensure that the distance between antennas can be made large enough for this requirement to be satisfied. This difficulty is typically encountered when antennas are placed in a laptop and the telecommunication wavelengths are on the centimeter scale (e.g., Bluetooth or Wi-Fi). An illustration of the benefit of time-reversal subwavelength focusing to overcome this difficulty is given in Fig. 3. A three-antenna TRM is used to transmit a color picture to a three-antenna receiving array. The original picture is encoded onto three RGB (red-green-blue) color channels. Each corresponding figure is represented by a bit series giving the gray levels of each pixel on that particular channel. Then the simplest modulation is used (a positive pulse for bit 1, a negative one for bit 0) to create three bitstreams with a data rate of 50 Mbit/s each. The intended global data rate is thus 150 Mbit/s. Time reversal is used to focus each bitstream onto one of the antennas (one antenna for each color) of the receiving array. Then the three bitstreams are decoded and mixed to reconstruct the color image. The communication is performed with two kinds of receiving arrays. The first is "classical"; it consists of three dipolar antennas with a $\lambda/30$ spacing. The second is a microstructured antenna array analogous to the one previously described (Fig. 1). It turns out that the image reconstructed with the classical array is gray-scaled: Its colors are lost. Indeed, subwavelength spaced antennas are strongly coupled, that is, they essentially receive the same signal. Hence, each transmitted pixel is gray because the three different antennas corresponding to the three different color channels receive the same gray levels. However, when the microstructured receiving array is used, each color stream focuses independently at each antenna. Consequently, the relative weights of the RGB components of each pixel are preserved and the image is transmitted without major losses. This experiment shows that our approach allows one to increase the information transfer rate to a given volume of space.

References and Notes

1. E. Betzig, J. K. Trautman, *Science* **257**, 189 (1992).
2. F. Zenhausern, Y. Martin, H. K. Wickramasinghe, *Science* **269**, 1083 (1995).
3. J. B. Pendry, *Phys. Rev. Lett.* **85**, 3966 (2000).
4. D. R. Smith, J. B. Pendry, M. C. K. Wiltshire, *Science* **305**, 788 (2004).
5. D. R. Smith, *Science* **308**, 502 (2005).
6. V. G. Veselago, *Sov. Phys. Usp.* **10**, 509 (1968).
7. N. A. Nicorovici, R. C. McPhedran, G. W. Milton, *Phys. Rev. B* **49**, 8479 (1994).
8. R. Shelby, D. R. Smith, S. Schultz, *Science* **292**, 77 (2001).
9. M. C. K. Wiltshire *et al.*, *Science* **291**, 849 (2001).
10. N. Fang, H. Lee, C. Sun, X. Zhang, *Science* **308**, 534 (2005).
11. D. O. S. Melville, R. J. Blaikie, *Opt. Exp.* **13**, 2127 (2005).
12. Z. Jacob, L. V. Alekseyev, E. Narimanov, *Opt. Exp.* **14**, 8247 (2006).
13. T. Taubner *et al.*, *Science* **313**, 1595 (2006).
14. M. Fink, *Phys. Today* **50**, 34 (1997).
15. C. Draeger, M. Fink, *Phys. Rev. Lett.* **79**, 407 (1997).
16. B. E. Henty, D. D. Stancil, *Phys. Rev. Lett.* **93**, 243904 (2004).
17. G. Lerosey, J. de Rosny, A. Tourin, A. Derode, M. Fink, *Phys. Rev. Lett.* **92**, 193904 (2004).
18. G. Lerosey, J. de Rosny, A. Tourin, A. Derode, M. Fink, *App. Phys. Lett.* **88**, 154101 (2006).
19. R. Carminati, J. J. Saenz, J.-J. Greffet, M. Nieto-Vesperinas, *Phys. Rev. A* **62**, 012712 (2000).
20. D. Cassereau, M. Fink, *IEEE Trans. Ultrason. Ferroelectr. Freq. Control* **39**, 579 (1992).
21. J. de Rosny, M. Fink, *Phys. Rev. Lett.* **89**, 124301 (2002).
22. Further details are available as supporting material on *Science* Online.
23. A. L. Moustakas, H. U. Baranger, L. Balents, A. M. Sengupta, S. H. Simon, *Science* **287**, 287 (2000).

24. This work was partially funded by the Agence Nationale de la Recherche under grant ANR-05-BLAN-0054-01.

Supporting Online Material

www.sciencemag.org/cgi/content/full/315/5815/1120/DC1
SOM Text
Fig. S1
References

7 September 2006; accepted 19 December 2006
10.1126/science.1134824

Redefining the Age of Clovis: Implications for the Peopling of the Americas

Michael R. Waters[1]* and Thomas W. Stafford Jr.[2]

The Clovis complex is considered to be the oldest unequivocal evidence of humans in the Americas, dating between 11,500 and 10,900 radiocarbon years before the present (^{14}C yr B.P.). Adjusted ^{14}C dates and a reevaluation of the existing Clovis date record revise the Clovis time range to 11,050 to 10,800 ^{14}C yr B.P. In as few as 200 calendar years, Clovis technology originated and spread throughout North America. The revised age range for Clovis overlaps non-Clovis sites in North and South America. This and other evidence imply that humans already lived in the Americas before Clovis.

For nearly 50 years, it has been generally thought that small bands of humans carrying a generalized Upper Paleolithic tool kit entered the Americas around 11,500 radiocarbon years before the present (^{14}C yr B.P.) and that these first immigrants traveled southward through the ice-free corridor separating the Laurentide and Cordilleran Ice Sheets (*1*). These people developed the distinctive lithic, bone, and ivory tools of Clovis (*2*, *3*) and then quickly populated

the contiguous United States. Clovis humans and their descendants then rapidly populated Central America and reached southernmost South America by 10,500 ^{14}C yr B.P. (*1*).

Identifying when the Clovis complex first appeared and knowing the complex's duration is critical to explaining the origin of Clovis, evaluating the Clovis-first model of colonization of the Americas, determining the role of humans in the extinction of late Pleistocene megafauna, and assessing whether people inhabited the Americas before Clovis. We determined a more accurate time span for Clovis by analyzing the revised existing Clovis ^{14}C date record and reporting high-precision accelerator mass spectrometry (AMS) ^{14}C ages from previously dated Clovis sites. Our AMS ^{14}C dates are on culturally specific organic matter—bone, ivory, and seeds—that accelerator mass spectrometers can date accurately (*4*, *5*) to precisions of ±30 years at 11,000 ^{14}C yr B.P.

Clovis technology has strong Old World antecedents, but Clovis-specific traits (e.g., fluted lanceolate projectile points) probably originated in the New World, south of the continental ice sheets (*3*). Clovis tools and debitage identify and unify archaeological sites over a broad geographic range. Clovis sites and artifacts cluster in North America, especially in the contiguous United States (*1*). A small number of Clovis artifacts have been recovered from Mexico and possibly as far south as Venezuela (*6*). Even though Clovis covers a broad geographic range, only 22 Clovis sites in North America have been directly ^{14}C-dated (Fig. 1, Table 1, and table S1). The ^{14}C dates from these sites traditionally place Clovis between 11,500 and 10,900 ^{14}C yr B.P. (*1*, *7*, *8*). However, the ^{14}C dates from 11 of these sites are problematic and do not provide accurate or precise chronological information to determine the age of Clovis (*5*).

Three sites (East Wenatchee, Washington; Blackwater Draw, New Mexico; and Cactus Hill, Virginia) have Clovis diagnostic artifacts but lack precise ages (*5*). Three sites (Lubbock Lake, Texas; Kanorado, Kansas; and Indian Creek, Montana) fall within the Clovis age range but lack diagnostic Clovis artifacts (*5*). The site of Sheriden Cave, Ohio, provides only bracketing ages for Clovis artifacts (*5*). Questions exist about the accuracy of the ^{14}C dates from Aubrey, Texas (*5*), where diagnostic Clovis artifacts were found. We obtained three dates from the Sheaman site, Wyoming, that averaged 10,305 ± 15 ^{14}C yr B.P. These dates indicate that the Clovis context at Sheaman is mixed with younger cultural materials (*5*). Finally, associations between Clovis artifacts and ^{14}C-dated faunal remains at two sites (Wally's Beach, Canada; and Union Pacific, Colorado) are unresolved (*5*). Because of these problems, we excluded the dates from these sites in assessing the age of Clovis.

This leaves 11 sites with a total of 43 ^{14}C dates (Table 1 and table S1) (*5*). These sites have assemblages of Clovis artifacts in secure geological contexts. Existing ages from five sites (Anzick, Montana; Paleo Crossing, Ohio; Lehner, Arizona; Murray Springs, Arizona; and Jake Bluff, Oklahoma) already have high-precision ^{14}C dates on credible materials. We obtained nine new ages from seeds and highly purified bone and ivory collagen for five imprecisely dated sites (Lange-Ferguson, South Dakota; Dent, Colorado; Domebo, Oklahoma; Shawnee-Minisink, Pennsylvania; and Colby, Wyoming) (*4*, *5*). In addition, we obtained five ages on human remains from the Anzick site, Montana (*5*). We attempted to date samples from Sloth Hole, Florida, but the samples contained no collagen.

These 43 ^{14}C dates place the beginning of Clovis at ~11,050 ^{14}C yr B.P. (reducing former estimates by 450 ^{14}C years) and its end at ~10,800 ^{14}C yr B.P. (younger than previous estimates by 100 ^{14}C years). Accurate calendar correlation of ^{14}C ages from the Clovis time period is not currently possible because of correlation uncertainties (*9*). The Clovis-period segment of the INTCAL04 calibration is based on ^{14}C-dated marine foraminifera and is not accurate for the Clovis time period (*10*). The most accurate calibration for this time period is provided by a floating European tree-ring chronology that is provisionally anchored to INTCAL04 (*11*). Using this tentative calibration (*11*), we estimated that Clovis has a maximum possible date range of 13,250 to 12,800 calendar yr B.P.—a span of 450 calendar years (Fig. 2). By taking the youngest possible calibrated age for the oldest Clovis site and the oldest possible calibrated age for the youngest Clovis site, a minimum range for Clovis is calculated as 13,125 to 12,925 calendar yr B.P.—a span of

Fig. 1. Map showing the location of Clovis and other early sites. The numbers correspond to those found in Table 1. Other sites are 31, Monte Verde, Chile; 32, Nenana Complex sites, Alaska; and 33, Broken Mammoth, Alaska.

[1]Departments of Anthropology and Geography, Center for the Study of the First Americans, Texas A&M University, 4352 TAMU, College Station, TX 77843-4352, USA. [2]Stafford Research Laboratories, 200 Acadia Avenue, Lafayette, CO 80026, USA.

*To whom correspondence should be addressed. E-mail: mwaters@tamu.edu

200 calendar years. The ages for all Clovis sites overlap within this 200-year period, and this time span probably represents the true range of Clovis. However, the absolute calendar placement of the floating tree-ring record is disputed (*12*). By an alternative calibration (*12*), the maximum time range for Clovis is 13,110 to 12,660 calendar yr B.P., and the minimum time range is 12,920 to 12,760 calendar yr B.P. (Fig. 3). Regardless of the exact calendar dates, the 200-year duration for Clovis remains secure because the floating dendrochronological sequence provides calendar-year separations between two ^{14}C-dated sites.

The oldest Clovis sites (n = 3 sites) are located in Montana, South Dakota, and Florida; younger Clovis sites are located in the interior (n = 5) of the United States and in the Southwest (n = 2) and East (n = 1). The distribution of dated sites shows no clear indication of north-south or east-west age differences that would indicate movement of people in one direction or another. Instead, Clovis technology seems to have appeared synchronously across the United States at ~11,050 ^{14}C yr B.P. This pattern of ^{14}C dates is compatible with two contrasting hypotheses.

First, this pattern could support the idea that there was a rapid spread of Clovis people across an empty continent. Demographic models suggest that people exiting the ice-free corridor could have occupied the contiguous United States within 100 years or less (*13*). Although there is much speculation about a coastal migration of the first Americans from both Asia and Europe (*14*, *15*), the revised date range for Clovis reopens the possibility of a Late Glacial migration through the ice-free corridor that separated the Laurentide and Cordilleran Ice Sheets. People could have easily traveled through the ice-free corridor after ~11,500 ^{14}C yr B.P. (*1*)—at least 200 calendar years before the oldest known Clovis date. The biface and blade industry of Nenana (*16*) was well established at the Broken Mammoth site, Alaska, to 11,770 ± 210 ^{14}C yr B.P. (WSU-4351)—at least 300 calendar years before our oldest recalibrated Clovis date. The Nenana lithic assemblage shows strong similarities to the Clovis lithic assemblage (*17*). It is possible that either Nenana people or others with a biface and blade industry traveled through the corridor, and once south of the ice sheets, they developed the technological hallmarks characteristic of Clovis and spread rapidly across the continent.

An alternative interpretation is that the instantaneous appearance of Clovis across North America represents the rapid spread of Clovis technology through a preexisting but culturally and genetically undefined human population in North America (*18*). In this case, Clovis technology could have been introduced to this population through a Late Glacial migration of Clovis or Clovis progenitors or developed in situ from a pre-Clovis technology already in the Americas. Regardless of which hypothesis is correct, our revised chronology indicates that Clovis technology spread rapidly.

Faunal remains associated with dated Clovis sites constrain the timing of the extinction of Proboscideans at the end of the Pleistocene. Mammoths and mastodons were an important source of food and raw materials used to manufacture bone and ivory tools (*3*), as well as perishable items from soft tissues. Proboscidean remains are associated with seven of the well-dated Clovis sites (Lange-Ferguson, Sloth Hole, Dent, Domebo, Lehner, Murray Springs, and Colby), and the last occurrence of mammoth in the United States is dated at ~10,900 ^{14}C yr B.P. After this time, Clovis and sites of other complexes (e.g., Goshen and Folsom) contained only bison and other extant species. The extinction of mammoth and mastodon coincides with the main florescence of Clovis.

Our revised ages for Clovis overlap dates from a number of North American sites that are technologically or culturally not Clovis. The earliest dated sites of the Goshen complex (Mill Iron, Montana; and Hell Gap, Wyoming) (*19*) overlap the age range of Clovis (Figs. 2 and 3, and Table 1, and table S1). This indicates that Goshen is either coeval with the entire range of Clovis or briefly overlaps the later stages of the Clovis time period. Clovis also overlaps the date for the Arlington Springs human skeleton from Santa Rosa Island, California (Figs. 2 and 3 and Table 1) (*20*). No artifacts were found with the Arlington Springs human remains, and his cultural affiliation is unknown. The presence of human remains on Santa Rosa

Table 1. Summary of ^{14}C dates from Clovis and Clovis-age sites. Single ^{14}C dates, date ranges, and averaged dates are reported. If multiple ^{14}C dates were available from a single-component site, the dates were averaged with the method in (*28*). All dates are given at 1σ SD. *n*, number of dates.

Site	Date (^{14}C yr B.P.)
Clovis sites (credible ages and Clovis diagnostics)	
1. Lange-Ferguson, SD (n = 3)	11,080 ± 40
2. Sloth Hole, FL (n = 1)	11,050 ± 50
3. Anzick, MT (foreshaft ages) (n = 2)	11,040 ± 35
4. Dent, CO (n = 3)	10,990 ± 25
5. Paleo Crossing, OH (n = 3)	10,980 ± 75
6. Domebo, OK (n = 1)	10,960 ± 30
7. Lehner, AZ (n = 12)	10,950 ± 40
8. Shawnee-Minisink, PA (n = 5)	10,935 ± 15
9. Murray Springs, AZ (n = 8)	10,885 ± 50
10. Colby, WY (n = 2)	10,870 ± 20
11. Jake Bluff, OK (n = 3)	10,765 ± 25
Clovis sites (indirectly dated and Clovis diagnostics)	
12. East Wenatchee, WA (n = 1)	<11,125 ± 130
Clovis-age sites (credible ages but no Clovis diagnostics)	
13. Indian Creek, MT (n = 1)	10,980 ± 110
14. Lubbock Lake, TX (n = 2)	11,100 ± 60
15. Bonneville Estates, NV (n = 1)	11,010 ± 40
16. Kanorado, KS (n = 2)	10,980 ± 40
17. Arlington Springs, CA (n = 1)	10,960 ± 80
Problematic Clovis and Clovis-age sites	
18. Sheriden Cave, OH (above artifacts, n = 5)	10,600 ± 30
Sheriden Cave, OH (below artifacts, n = 2)	10,920 ± 50
19. Blackwater Draw, NM (n = 3)	11,300 ± 235
20. Cactus Hill, VA (n = 1)	10,920 ± 250
21. Wally's Beach, Canada (n = 4)	11,350 ± 80 to 10,980 ± 80
22. Union Pacific, WY (n = 1)	11,280 ± 350
23. Aubrey, TX (n = 2)	11,570 ± 70
24. Sheaman, WY (n = 3)	10,305 ± 15
Ages from other early sites	
25. Mill Iron, MT (Goshen) (n = 4)	10,840 ± 60
26. Hell Gap, WY (Goshen) (n = 1)	10,955 ± 135
27. Cerro Tres Tetas, Argentina (pre-Fishtail, n = 5)	10,935 ± 35
28. Cuevas Casa del Minero, Argentina (pre-Fishtail, n = 2)	10,985 ± 40
29. Piedra Museo, Argentina (pre-Fishtail, n = 2)	10,960 ± 45
30. Fell's Cave, Chile (Fishtail, n = 1)	11,000 ± 170

Island is unequivocal evidence that water crafts were used during Clovis time and that a Pacific maritime-coastal adaptation was probably contemporaneous with Clovis. At Bonneville Estates Rockshelter, Nevada (*21*), the earliest date from a series of hearths is coeval with the Clovis time period and is associated with stone artifacts. Diagnostic artifacts have yet to be found at this level, and it is unknown whether this early horizon is associated with Clovis or stemmed points.

Several sites in South America have yielded ^{14}C dates that are coeval with Clovis (Figs. 2 and 3). These include the early archaeological horizons at Cerro Tres Tetas, Cueva Casa del Minero, and Piedra Museo, Argentina, and the earliest Fishtail point horizon at Fell's Cave, Chile (Fig. 1, Table 1, and table S1) (*8*, *22*). The actual calendar dates of these South American sites may be slightly more recent because Southern Hemisphere samples have a lower initial ^{14}C content than contemporaneous samples in the Northern Hemisphere. This latitudinal difference causes Southern Hemisphere terrestrial materials to be 5 to 80 ^{14}C years older than contemporaneous samples in North America (*23*). The extent of this interhemisphere offset in ^{14}C years for the Clovis time period is unknown, but it is probably less than 80 years. Even with an 80-year correction to the ^{14}C dates from these four sites, Clovis, Fishtail, and other early complexes in the Southern Cone of South America are still contemporaneous.

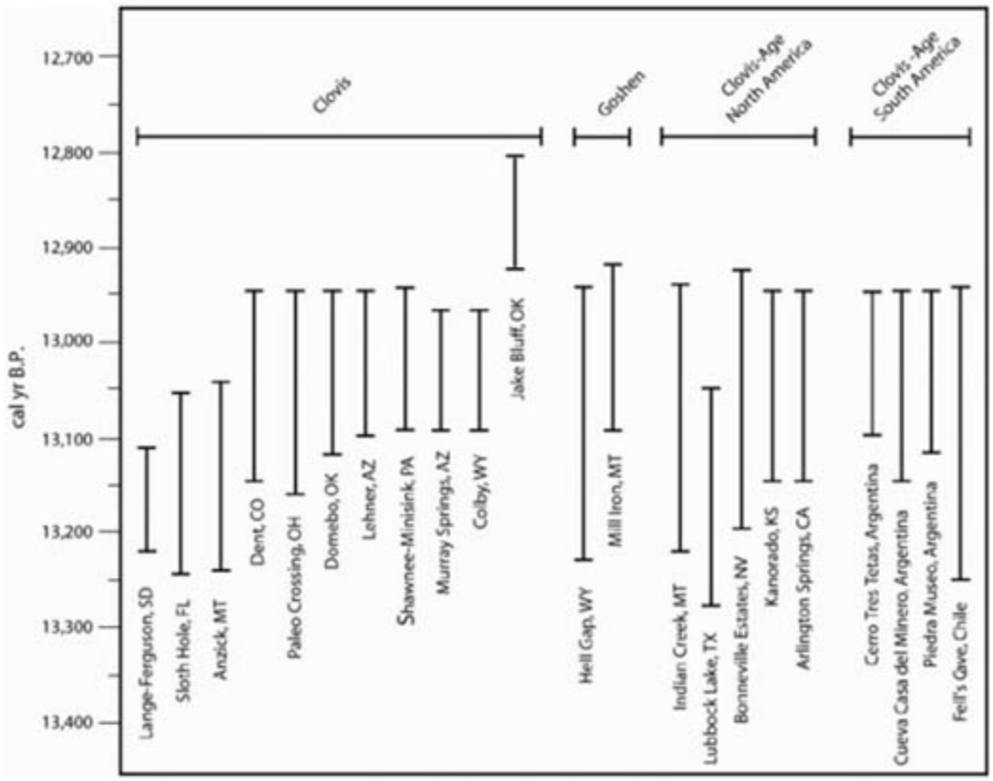

Fig. 2. Calendar-year age ranges for Clovis and other early sites based on the European dendrochonological calibration (*11*) at 1σ SD.

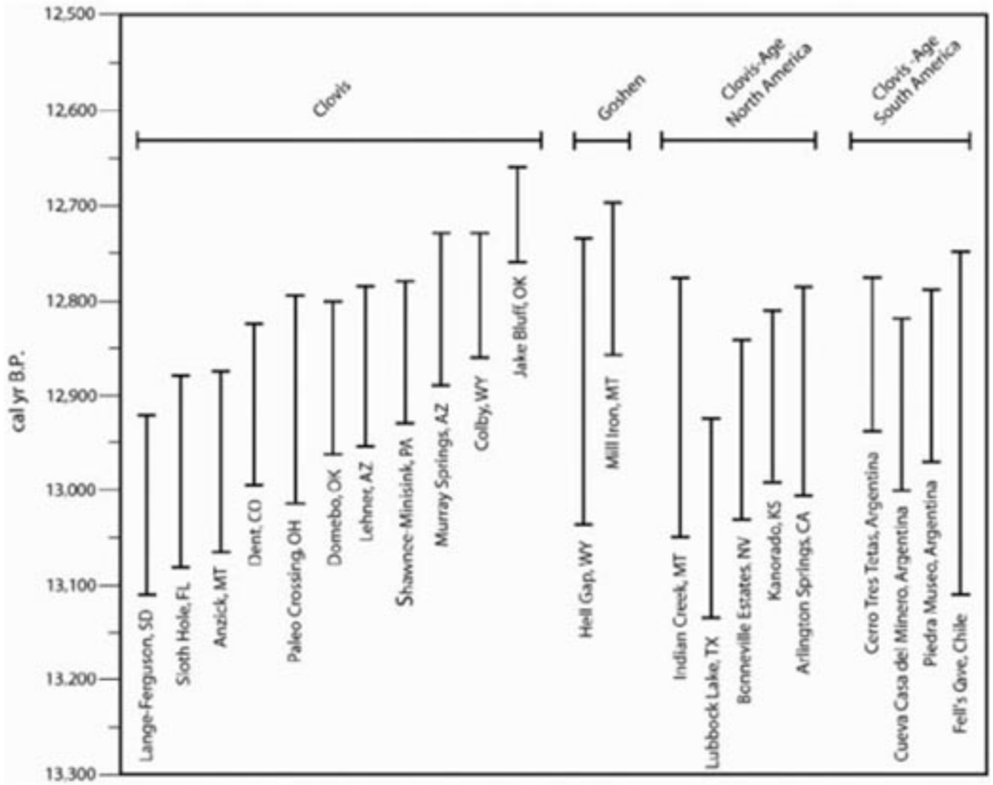

Fig. 3. Calendar-year age ranges for Clovis and other early sites based on the Fairbanks calibration (*12*) at 1σ SD.

The presence of non-Clovis sites that are contemporaneous with Clovis in both North and South America implies that Clovis does not represent the earliest occupation of the Americas. It would probably have taken a minimum of 600 to 1000 years for the first Paleoamericans and their descendents to travel by land from the southern limit of the ice-free corridor to Tierra del Fuego (*13*, *24*)—a distance of over 14,000 km (Fig. 1). However, at most 300 to 350 calendar years separate the oldest possible date for Clovis and the youngest possible ages from the well-dated unequivocal sites in southernmost South America (Figs. 2 and 3). The difference is reduced to 200 calendar years, when the minimum date for the beginning of Clovis in North America and the youngest dates for the sites in South America are considered. It is highly improbable that within 200 to 350 calendar years, people entered North America; adapted to biomes ranging from artic tundra to grasslands, deserts, and rainforests; increased in population; and reached the southern tip of South America within the span of 10 to 18 human generations. This suggests that human populations already existed in the New World before Clovis.

There is an emerging archaeological record that supports a pre-Clovis human occupation of the Americas. Stone tools and butchered mammoth remains dating to ~12,500 ^{14}C yr B.P. have been found at the Schaefer and Hebior sites in Wisconsin (*25*, *26*). Older butchered mammoth remains dating to ~13,500 ^{14}C yr B.P. have been recovered from the Mud Lake site, Wisconsin (*25*, *26*). In South America, humans appear to have been present at 12,500 ^{14}C yr B.P. at Monte Verde, Chile (*27*). The archaeological data now show that Clovis does not represent the earliest inhabitants of the Americas and that a new model is needed to explain the peopling of the Americas.

References and Notes

1. C. V. Haynes Jr., in *Paleoamerican Origins: Beyond Clovis*, R. Bonnichsen, B. T. Lepper, D. Stanford,

M. R. Waters, Eds. (Center for the Study of the First Americans, College Station, TX, 2005), pp. 113–132.
2. M. B. Collins, *Clovis Blade Technology* (Univ. of Texas Press, Austin, TX, 1999).
3. K. B. Tankersley, in *The Settlement of the American Continents: A Multidisciplinary Approach to Human Biogeography*, C. M. Barton, G. A. Clark, D. R. Yesner, G. A. Pearson, Eds. (Univ. of Arizona Press, Tucson, AZ, 2004), pp. 49–63.
4. T. W. Stafford Jr., P. E. Hare, L. Currie, A. J. T. Jull, D. J. Donahue, *J. Archaeol. Sci.* **18**, 35 (1991).
5. Materials and methods are available as supporting material on *Science* Online.
6. G. A. Pearson, in *The Settlement of the American Continents: A Multidisciplinary Approach to Human Biogeography*, C. M. Barton, G. A. Clark, D. R. Yesner, G. A. Pearson, Eds. (Univ. of Arizona Press, Tucson, AZ, 2004), pp. 85–102.
7. A. C. Roosevelt, J. Douglas, L. Brown, in *The First Americans: The Pleistocene Colonization of the New World*, no. 27 of *Memoirs of the California Academy of Sciences*, N. G. Jablonski, Ed. (California Academy of Sciences, San Francisco, CA, 2002), pp. 159–235.
8. C. V. Haynes Jr., in *Radiocarbon After Four Decades: An Interdisciplinary Perspective*, R. E. Taylor, A. Long, R. S. Kra, Eds. (Springer-Verlag, New York, 1992), pp. 355–374.
9. S. J. Fiedel, *Am. Antiq.* **64-1**, 95 (1999).
10. S. Bondevik, J. Mangerud, H. H. Birks, S. Gulliksen, P. Reimer, *Science* **312**, 1514 (2006).
11. B. Kromer *et al.*, *Radiocarbon* **46-3**, 1203 (2004).
12. R. G. Fairbanks *et al.*, *Quat. Sci. Rev.* **24**, 1781 (2005).
13. S. J. Fiedel, *J. Archaeol. Res.* **8-1**, 39 (2000).
14. C. A. S. Mandryk, H. Josenhans, D. W. Fedje, R. W. Mathewes, *Quat. Sci. Rev.* **20**, 301 (2001).
15. B. Bradley, D. Stanford, *World Archaeol.* **36**, 459 (2004).
16. T. D. Hamilton, T. Goebel, in *Ice Age Peoples of North America: Environments, Origins, and Adaptations of the First Americans*, R. Bonnichsen, K. L. Turnmire, Eds. (Oregon State Univ. Press, Corvallis, OR, 1999), pp. 156–199.
17. J. F. Hoffecker, W. R. Powers, T. Goebel, *Science* **259**, 46 (1993).
18. R. Bonnichsen, in *Clovis: Origins and Adaptations*, R. Bonnichsen, K. L. Turnmire, Eds. (Oregon State Univ. Press, Corvallis, OR, 1991), pp. 309–329.
19. G. C. Frison, Ed., *The Mill Iron Site* (Univ. of New Mexico Press, Albuquerque, NM, 1996).
20. J. R. Johnson, T. W. Stafford Jr., H. O. Ajie, D. P. Morris, in *Proceedings of the Fifth California Islands Symposium* (U.S. Department of the Interior, Minerals Management Service, Pacific Outer Continental Shelf Region, Washington, DC, 23 March to 1 April 1999), pp. 541–544.
21. T. Goebel, B. Hockett, K. Graf, D. Rhode, paper presented at the 30th Great Basin Anthropological Conference, Las Vegas, NV, 19 to 21 October 2006.
22. L. Miotti, M. C. Salemme, *Quat. Int.* **109-110**, 95 (2003).
23. M. Barbetti *et al.*, *Nucl. Instrum. Methods* **223-224B**, 366 (2004).
24. D. G. Anderson, J. C. Gillam, *Am. Antiq.* **65-1**, 43 (2000).
25. D. F. Overstreet, in *Paleoamerican Origins: Beyond Clovis*, R. Bonnichsen, B. T. Lepper, D. Stanford, M. R. Waters, Eds. (Center for the Study of the First Americans, College Station, TX, 2005), pp. 183–195.
26. D. J. Joyce, *Quat. Int.* **142-143**, 44 (2006).
27. T. D. Dillehay, Ed., *Monte Verde: A Late Pleistocene Settlement in Chile: Volume 2: The Archaeological Context and Interpretation* (Smithsonian Institution Press, Washington, DC, 1997).
28. G. K. Ward, S. R. Wilson, *Archaeometry* **20**, 19 (1978).
29. We thank A. Hannus, C. V. Haynes, J. Gingerich, G. Frison, and A. Hemmings for providing samples for dating; M. Payn and the North Star Archaeological Research Program established by J. Cramer and R. Cramer for providing funding; P. Reimer and J. Southon for providing advice on ^{14}C calibration; D. Carlson, T. Goebel, J. Southon, S. Forman, and three anonymous reviewers for offering useful comments to improve this paper; and L. Lind, C. Pevny, J. Halligan, and P. Johnson for helping in the preparation of the text and illustrations.

Supporting Online Material

www.sciencemag.org/cgi/content/full/315/5815/1122/DC1
Materials and Methods
SOM Text
Table S1
References

3 November 2006; accepted 12 January 2007
10.1126/science.1137166

Quantitative Phylogenetic Assessment of Microbial Communities in Diverse Environments

C. von Mering,[1]* P. Hugenholtz,[2] J. Raes,[1] S. G. Tringe,[2] T. Doerks,[1] L. J. Jensen,[1] N. Ward,[3] P. Bork[1]†

The taxonomic composition of environmental communities is an important indicator of their ecology and function. We used a set of protein-coding marker genes, extracted from large-scale environmental shotgun sequencing data, to provide a more direct, quantitative, and accurate picture of community composition than that provided by traditional ribosomal RNA–based approaches depending on the polymerase chain reaction. Mapping marker genes from four diverse environmental data sets onto a reference species phylogeny shows that certain communities evolve faster than others. The method also enables determination of preferred habitats for entire microbial clades and provides evidence that such habitat preferences are often remarkably stable over time.

Microorganisms are estimated to make up more than one-third of Earth's biomass (*1*). They play essential roles in the cycling of nutrients, interact intimately with animals and plants, and directly influence Earth's climate. Yet our molecular and physiological knowledge of microbes remains surprisingly fragmentary, largely because most naturally occurring microbes cannot be cultivated in the laboratory (*2*).

For characterizing this "unseen majority" of cellular life, the first step is to provide a taxonomic census of microbes in their environments (*3*–*6*). This is usually achieved by cloning and sequencing their ribosomal RNA (rRNA) genes (most notably the 16*S*/18*S* small subunit rRNA). This approach has been extremely successful in revealing the overwhelming diversity of microbial life (*7*), but it also has some limitations due to quantitative errors: The polymerase chain reaction (PCR) step introduces amplification bias, and it generates chimeric and otherwise erroneous molecules that hamper phylogenetic analysis (*8*, *9*).

Shotgun sequencing of community DNA ("metagenomics") provides a more direct and unbiased access to uncultured organisms (*10*–*13*): No PCR amplification step is involved, and because no specific primers or sequence anchors are needed, even very unusual organisms can be captured by this technique. Although current metagenomics data are still not entirely free of quantitative distortions (mostly due to sample preparation), remaining biases are bound to diminish further with the optimization of yield and reproducibility of DNA extraction protocols (*14*–*16*).

To make use of metagenomics data for taxonomic profiling, we analyzed 31 protein-coding marker genes previously shown to provide sufficient information for phylogenetic analysis [they are universal, occur only once per genome, and are rarely transferred horizontally (*17*)]. We extracted these marker genes from metagenomics sequence data (*9*), aligned them to a set of hand-curated reference proteins, and used maximum likelihood to map each sequence to an externally provided phylogeny of completely sequenced organisms [tree of life; we used the tree from (*17*), although any reference tree can be used as long as the marker genes have been sequenced for all its taxa]. Our procedure provides branch length information and confidence ranges for each placement (*18*) (Fig. 1), allowing statements such as "This unknown sequence evolves relatively fast, is from a proteobacterium (95% confidence), and more specifically, probably from a novel clade related to the Campylobacterales (65% confidence)." The procedure weighs the number of informative residues that are found on each sequence fragment, then adjusts the spread and confidence of its placement

[1]European Molecular Biology Laboratory, Meyerhofstrasse 1, 69117 Heidelberg, Germany. [2]DOE Joint Genome Institute, 2800 Mitchell Drive, Walnut Creek, CA 94598, USA. [3]The Institute for Genomic Research, Rockville, MD 20850, USA.
*Present address: University of Zurich, Winterthurerstrasse 190, 8057 Zurich, Switzerland.
†To whom correspondence should be addressed. E-mail: peer.bork@embl.de

in the tree accordingly [after alignment, concatenation, and gap removal, the number of remaining informative residues ranges from 80 to more than 3000 per sequence fragment (*9*)]. We have implemented the entire phylogenetic assignment protocol as an automated software pipeline with a Web interface that allows submission of sequences online (http://MLtreemap.embl.de).

Jackknife validation of our method [i.e., leaving out various parts of the reference tree and measuring the consequences on placement accuracy (*9*)] showed that the performance of our method depends on the completeness and balance of the reference tree: The larger the phylogenetic distance to any known relative of an environmental sequence, the less precise is its placement. Overall, the mapping precision is remarkably good, as long as each sequence has some relative from the same phylum among the reference genomes (fig. S2). In contrast, BLAST-based assignments of taxonomy based on "best hit," a frequently used method, are more error-prone: For example, more than 10% of the sequences change to a different domain of life (e.g., changing assignment from Bacteria to Archaea) upon removal of the phylum to which they originally mapped; with our method, such changes are reduced to 0.19% (fig. S2). Moreover, because the best BLAST match always assigns a single organism as the most likely phylogenetic neighbor, it does not specify the level of relatedness (e.g., class-, order-, or phylum-level), which is needed to trace organisms in their preferred habitats and through time.

In one of the recent, large-scale metagenomics sequencing projects (*12*), traditional PCR-based assessment of 16*S* rRNA molecules was executed in parallel to the shotgun sequencing. This enabled us to compare our approach to this currently most widely used experimental method for phylogenetic profiling of environments. Overall, the relative abundances of phyla as reported by both methods were broadly similar, although the metagenomics approach appears quantitatively closer to the truth, as can be measured by comparison to rRNAs that are contained directly in the PCR-independent shotgun reads (*9*). The PCR-based approach presumably suffers from amplification biases and from copy number variations among rRNA genes in bacteria (*19*) but benefits from an exhaustive coverage of phyla among known rRNA sequences. In contrast, the approach we present here requires far more resources in terms of sequencing and computation, but, at least for phyla already represented among fully sequenced genomes, it is noticeably more quantitative. Our approach should essentially be seen as a by-product of metagenomics sequencing projects, which are usually conducted for functional purposes [see (*9*) for a discussion of the strengths, weaknesses, and complementarities of both approaches].

We applied our procedure to four large, heterogeneous data sets of microbial community sequences derived from distinct and geographically separate environments (*11*–*13*). The consistent treatment of the data allowed us to quantitatively compare habitat preferences in the context of the tree of life (Fig. 2 and fig. S1; see also fig. S3 for robustness estimates).

Overall, we observed a remarkably uneven representation of previously sequenced genomes in naturally occurring communities. Some parts of the tree of life (such as the Streptococci or the Enterobacteriales) are well covered by published genome sequencing projects, but they represent only a small fraction of naturally occurring microbes. Conversely, entire phyla such as the Acidobacteria or the Chloroflexi are poorly represented among the sequenced genomes but are widely abundant in natural communities.

In agreement with (*20*), we found Proteobacteria to be the most dominant phylum of microbial life in both marine and soil environments (Fig. 2). However, as is the case with other phyla, marked differences within the Proteobacteria were apparent: relatives of the Rickettsiales, for example [including the marine genus *Pelagibacter* (*21*)], were mostly found in the surface-water sample, whereas relatives of Rhizobiales or Burkholderiales were mostly found in the soil sample. We observed surprisingly few endospore-forming organisms in the community sequences: Both Bacilli and Clostridia were quite rare; their largest combined abundance was a mere 1% (in soil). Similarly, Actinobacteria (many of which have a spore stage) ranged from being virtually absent in the acidic mine drainage biofilm to only 6.2% in the soil sample. It is conceivable that spores are underrepresented in the data (they may withstand the DNA extraction protocols), but, at least among the vegetative, actively growing cells, spore-formers appear to be a minority.

Quantitative analyses of relatively rare phyla—as, for example, in the case of the spore-formers mentioned above—can potentially suffer from limited sampling. Although our approach used 31 marker genes with a total of about 7500 amino acid residues per genome, low-abundance organisms might be represented by only a few of these (the total number of sufficiently complete marker genes usable for our approach ranged from 247 for the smallest data set to 15,741 for the largest data set). We quantified the potential undersampling errors by jackknife and bootstrap analysis (fig. S3). These tests showed that, for the worst case of a low-abundance clade in the smallest data set, the quantitative error due to undersampling was on the order of 50% (fig. S3). However, such errors are bound to decrease with the expected rise in sequencing depth facilitated by technological advances. In addition, even for a low estimate such as the 1% abundance mentioned above for Bacilli and Clostridia, the current data support a 95% confidence interval of 0.995 to 2.153%, meaning that endospore-formers are indeed rare in soil and are not just undersampled. Generally, none of the results reported here would change much if all data sets had as many as 15,000 marker genes sampled (in particular because we do not comment on diversity, and because we discuss entire clades, not individual species).

Almost all placements of environmental sequences occurred at relatively deep, internal nodes in the reference tree; only a few could be placed toward the tips as close relatives of the cultured and sequenced genomes. Indeed, the average sequence similarity of the "best hits" of environmental sequences to sequenced genomes was usually less than 60% (for soil, the median identity was only 47%). This dissimilarity was

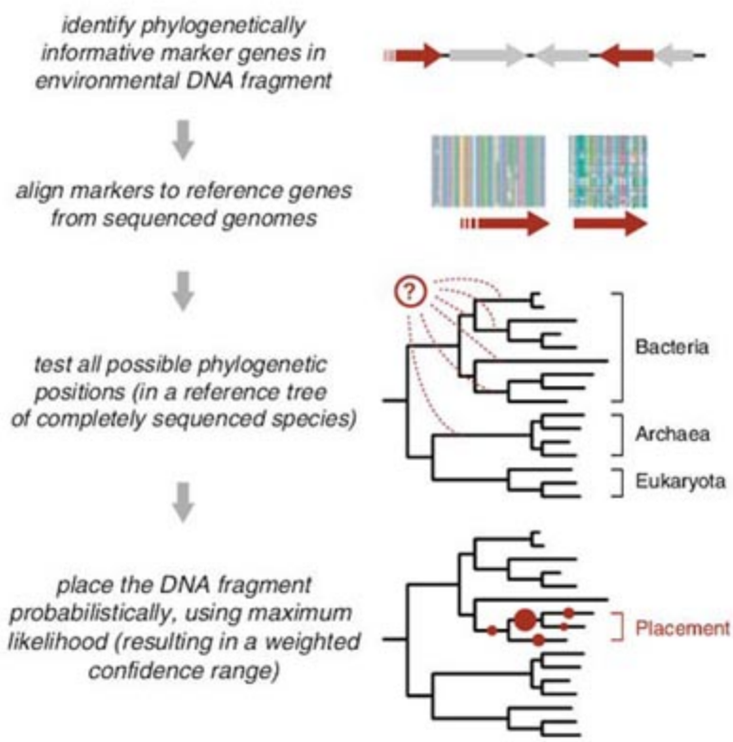

Fig. 1. Assessing community taxonomy from metagenomics sequence data. The diagram depicts how a restricted set of marker genes can be used for phylogenetic characterization of community microbes from poorly assembled sequence data. Instances of the marker genes are sought in the sequences and assessed relative to an external tree-of-life phylogeny with the use of maximum likelihood scoring. A central step in the mapping procedure is the assignment of a confidence range for each placement, thereby avoiding overconfident placement of sequence fragments that are short or otherwise uninformative.

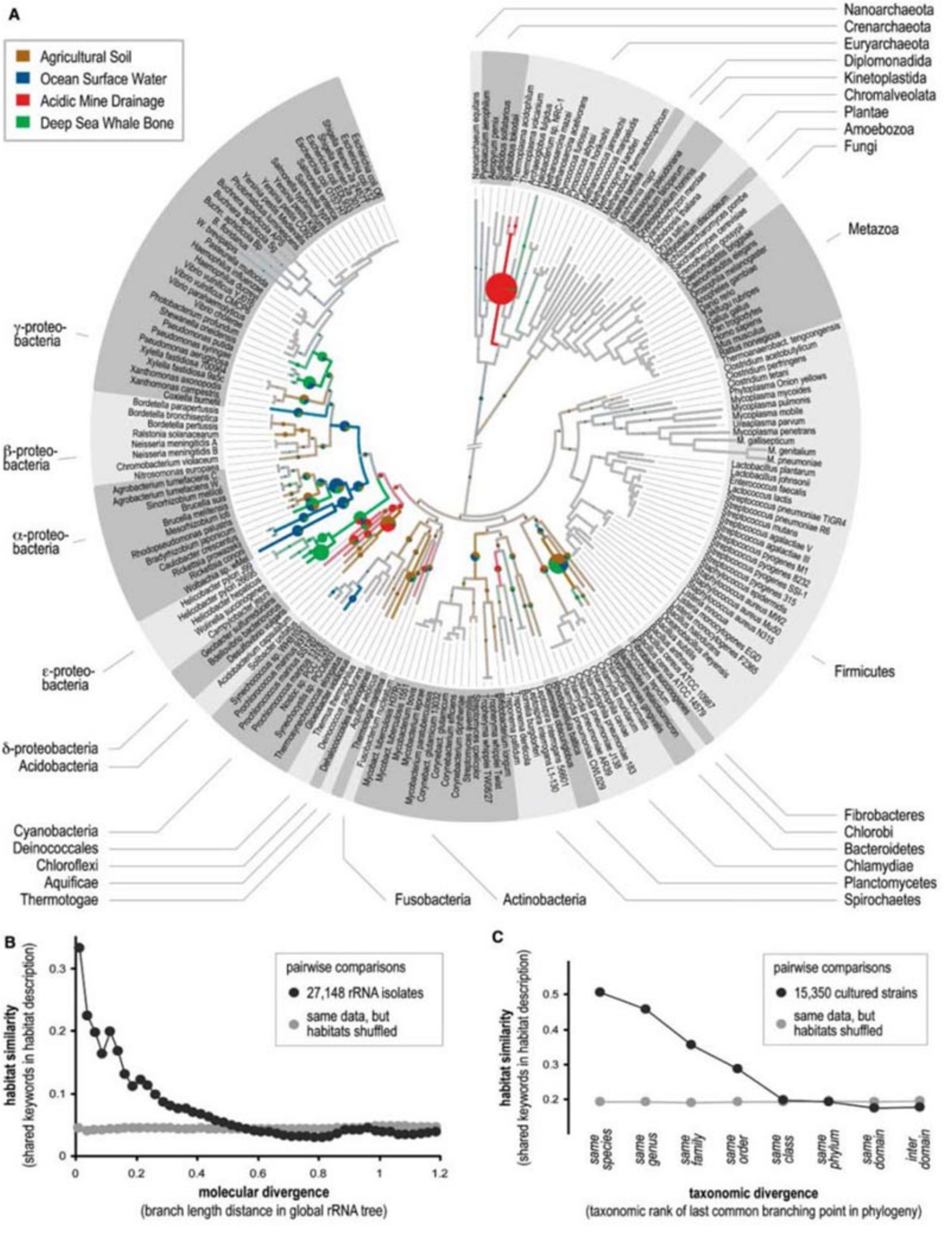
A
Agricultural Soil
Ocean Surface Water
Acidic Mine Drainage
Deep Sea Whale Bone
Nanoarchaeota
Crenarchaeota
Euryarchaeota
Diplomonadida
Kinetoplastida
Chromalveolata
Plantae
Amoebozoa
Fungi
Metazoa
γ-proteo-bacteria
β-proteo-bacteria
α-proteo-bacteria
ε-proteo-bacteria
δ-proteobacteria
Acidobacteria
Cyanobacteria
Deinococcales
Chloroflexi
Aquificae
Thermotogae
Fusobacteria
Actinobacteria
Firmicutes
Fibrobacteres
Chlorobi
Bacteroidetes
Chlamydiae
Planctomycetes
Spirochaetes
B
habitat similarity
(shared keywords in habitat description)
pairwise comparisons
27,148 rRNA isolates
same data, but habitats shuffled
molecular divergence
(branch length distance in global rRNA tree)
C
habitat similarity
(shared keywords in habitat description)
pairwise comparisons
15,350 cultured strains
same data, but habitats shuffled
same species
same genus
same family
same order
same class
same phylum
same domain
inter domain
taxonomic divergence
(taxonomic rank of last common branching point in phylogeny)

Fig. 2. Habitat-phylotype associations and their stability in time. (**A**) Four microbial communities are mapped onto the same reference tree. Pie charts represent the various environments in which a particular tree clade has been observed. If there is a clearly preferred habitat, lines are colored accordingly (*9*). (**B** and **C**) Habitat preference over time. (B) Comparison of rRNA sequences from public databases, indicating the similarity of habitats from which they were sampled. (C) Comparison of cultured microbial strains, plotting habitat similarity against their level of relatedness in the NCBI taxonomy. For the taxonomic level of order, and all closer relations, the difference is highly significant ($P < 10^{-6}$). The tree-drawing algorithm is implemented for public use at (*34*).

reflected in the maximum likelihood branch lengths: On average, more than 0.3 substitutions per site have occurred since the branching from the reference tree. This corresponds roughly to the sequence divergence between β- and γ-proteobacteria, which has been tentatively dated at more than 500 million years ago (*22*–*24*), clearly enough time for functional capabilities and lifestyles to have changed. Thus, the closest sequenced relative of an environmental microbe should generally not be considered as a reliable guide for its phenotypes and functions.

The environments we analyzed contained a few sequences that were placed unusually deep in the tree (i.e., basal to the three known domains of life: Archaea, Bacteria, and Eukaryota). Upon closer inspection, we determined that most of these deep placements in fact originated from lineages not yet represented among sequenced genomes. Therefore, it is likely that the remaining deep placements will also find a home as soon as more lineages are included in the reference tree, rather than belonging to a hypothetical "fourth domain" of life.

The maximum likelihood branch lengths, as measured by our method, provide detailed information on the community-wide distribution of evolutionary rates (that is, the rates at which mutations occur and are fixed). We therefore assessed, for each sequence fragment placed into the tree, the cumulative branch length from the tip of its branch down to the base of the corresponding phylum, and compared these to the branch lengths of all known reference organisms in that same phylum, measured for the very gene families found on the fragment (Fig. 3; very deeply placed fragments are compared to all phyla in their sister clade). Although not all 31 of the marker genes were present for each organism in the metagenomics data, the measurements of relative rates in each gene family revealed distinct branch length distributions for the four environmental communities tested. These indicate that organisms at the ocean surface evolve the fastest, whereas organisms in the soil evolve the slowest (Fig. 3). Large-scale trends like this, involving entire communities, were previously observed mainly for multicellular organisms [e.g., a dependency between latitudinal geographic location and mutation rates in plants (*25*)]. In the case of microbes, fast-evolving species were previously known in the context of symbiotic or pathogenic settings or in cases of extreme genome "streamlining" (*21*, *26*). The more subtle, global variations in mutation rates reported here may be caused by differences in population sizes or generation times, or by the abundance of external mutagens (such as the strong fluxes of ultraviolet light in ocean surface water). Notably, the ocean surface community is not only evolving the fastest, it is also the one with the smallest genomes (*27*). In the case of soil, the apparent evolutionary stability at the sequence level is also consistent with intermittent periods of dormancy (for example, during winter and/or under desiccation).

Our tree-based mapping (with an implicit molecular clock) also allowed us to trace the habitat preference of microbial organisms through time, and thus enabled us to estimate how frequently lineages change their preferred environment. At short to intermediate evolutionary time scales, we observed a noticeable stability of habitats: Many of the closer relatives in the tree showed the same environmental preference, indicating that microbial lineages do not very often change (or specialize) their lifestyles and habitats (Fig. 2). Conversely, at longer time scales, we did observe notable changes of preferred habitats—for example, within diverse lineages of at least two phyla, namely Proteobacteria and Cyanobacteria; this is consistent with the observed morphological and ecological variability of cultured isolates from most phyla. In the case of Cyanobacteria, we identified relatives of the fast-evolving and widespread Prochlorococci in the ocean sample, whereas more basal, slower-evolving Cyanobacteria such as *Gloeobacter* were mostly found in the soil sample.

Even though molecular methods tend to find most phyla ubiquitously, Baas-Becking and Beyerinck postulated decades ago that microbial taxa have preferred environments: "for microbial taxa, everything is everywhere—but the environment selects" [(*28*) and references therein]. The hypothesis posits that microorganisms are frequently dispersed globally, and that they are only subsequently selected by the environments on the basis of their functional capacities. Existing communities would thus constantly be challenged by intruders from nonspecialist phyla that may occasionally survive simply by chance, acquiring the necessary functionality through horizontal gene transfer (*29*–*31*). Our observations provide quantitative support for this hypothesis, showing strong environmental preference along lineages, but with a time-dependent decay. We confirmed and extended this finding by also analyzing habitat information available for cultivated strains in culture collections, as well as the large body of publicly available rRNA sequence data. Both data sets provide information about hundreds of habitats and allow an approximate ranking of lineage separation events in time. In the case of rRNA sequence data, branch length information can be analyzed using a global phylogeny of small subunit RNA sequences, whereas in the case of cultivated strains, taxonomic assignments can be parsed for the last taxonomic rank still shared (*9*). Indeed, we observe a remarkable time-dependent stability of

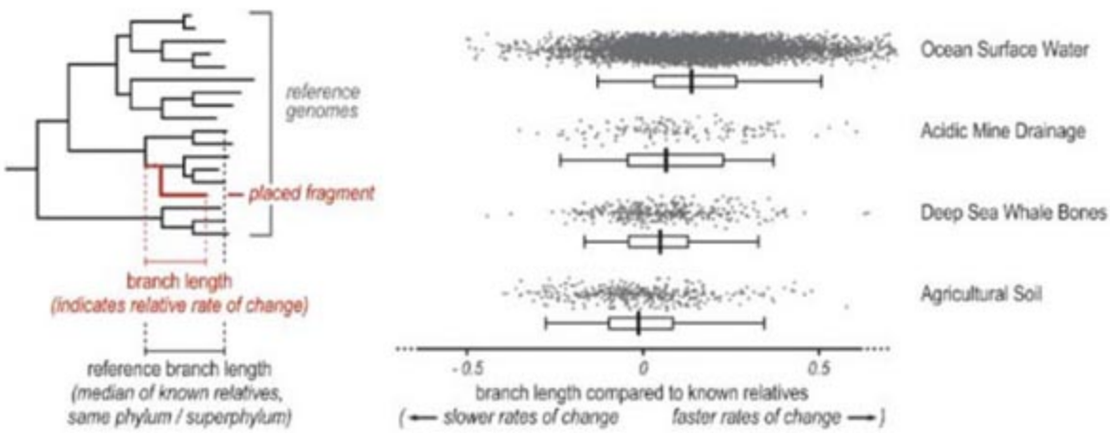

Fig. 3. Distinct evolutionary rates of environmental communities. Organisms found in the surface waters of the Sargasso Sea have accumulated, on average, the largest number of mutations (i.e., evolved fastest), those in the agricultural soil the fewest. For each data set, the branch lengths of the placements are plotted as dots. Each branch length is expressed relative to the median of branch lengths of known genomes in the same phylum, or against all phyla in the sister clade in the case of very deep placements. The quantiles 5%, 25%, 50% (median), 75%, and 95% are indicated. All data sets differ highly significantly (two-sided Kolmogorov-Smirnov tests, $P \leq 10^{-5}$, except for the comparison of acidic mine drainage with whale bone: $P < 0.05$). The number of data points underlying each distribution is as follows: ocean surface water, 15,741 genes on 9,286 contigs; acidic mine drainage, 275 genes on 148 contigs; deep-sea whale bones (three subsamples pooled), 630 genes on 362 contigs; agricultural soil, 598 genes on 395 contigs.

habitats and show that for any two microbial isolates, the similarity of their annotated habitat (as measured by automated keyword comparisons) is strongly correlated to their evolutionary relatedness (Fig. 2, B and C). We observe such common habitat preferences surprisingly far back in time: Even strains related only at the level of taxonomic order are still significantly more frequently found in the same environment than a random pair of isolates (Fig. 2C). Thus, most microbial lineages remain associated with a certain environment for extended time periods, and successful competition in a new environment seems to be a rare event. The latter might require more than just the acquisition of a few essential functions; probably only a limited number of functionalities are self-sufficient enough, and provide sufficient advantage, to be pervasively transferred (*32*). For most other adaptations, fine-tuned regulation and/or subtle changes in the majority of proteins may be needed. Because this is difficult to achieve, well-adapted specialists might in fact rarely be challenged in their environment. This does not rule out the presence of a "long tail" of rare, atypical organisms in each environment (*33*), but most microbial clades do seem to have a preferred habitat.

Taken together, our alternative approach of taxonomic profiling of complex communities has sufficient resolution to uncover differences in evolutionary rates of entire communities, as well as long-lasting habitat preferences for bacterial clades. The latter raises the question of how many distinct environmental habitats there are on Earth—a factor that might ultimately determine the true extent of microbial biodiversity.

References and Notes

1. W. B. Whitman, D. C. Coleman, W. J. Wiebe, *Proc. Natl. Acad. Sci. U.S.A.* **95**, 6578 (1998).
2. J. T. Staley, A. Konopka, *Annu. Rev. Microbiol.* **39**, 321 (1985).
3. S. J. Giovannoni, T. B. Britschgi, C. L. Moyer, K. G. Field, *Nature* **345**, 60 (1990).
4. D. M. Ward, R. Weller, M. M. Bateson, *Nature* **345**, 63 (1990).
5. T. M. Schmidt, E. F. DeLong, N. R. Pace, *J. Bacteriol.* **173**, 4371 (1991).
6. N. R. Pace, *Science* **276**, 734 (1997).
7. P. Hugenholtz, B. M. Goebel, N. R. Pace, *J. Bacteriol.* **180**, 4765 (1998).
8. F. von Wintzingerode, U. B. Gobel, E. Stackebrandt, *FEMS Microbiol. Rev.* **21**, 213 (1997).
9. See supporting material on *Science* Online.
10. C. S. Riesenfeld, P. D. Schloss, J. Handelsman, *Annu. Rev. Genet.* **38**, 525 (2004).
11. J. C. Venter *et al.*, *Science* **304**, 66 (2004); published online 4 March 2004 (10.1126/science.1093857).
12. S. G. Tringe *et al.*, *Science* **308**, 554 (2005).
13. G. W. Tyson *et al.*, *Nature* **428**, 37 (2004).
14. G. M. Luna, A. Dell'Anno, R. Danovaro, *Environ. Microbiol.* **8**, 308 (2006).
15. H. A. Barton, N. M. Taylor, B. R. Lubbers, A. C. Pemberton, *J. Microbiol. Methods* **66**, 21 (2006).
16. I. M. Kauffmann, J. Schmitt, R. D. Schmid, *Appl. Microbiol. Biotechnol.* **64**, 665 (2004).
17. F. D. Ciccarelli *et al.*, *Science* **311**, 1283 (2006).
18. K. Strimmer, A. Rambaut, *Proc. Biol. Sci.* **269**, 137 (2002).
19. J. A. Klappenbach, P. R. Saxman, J. R. Cole, T. M. Schmidt, *Nucleic Acids Res.* **29**, 181 (2001).
20. M. S. Rappe, S. J. Giovannoni, *Annu. Rev. Microbiol.* **57**, 369 (2003).
21. S. J. Giovannoni *et al.*, *Science* **309**, 1242 (2005).
22. F. U. Battistuzzi, A. Feijao, S. B. Hedges, *BMC Evol. Biol.* **4**, 44 (2004).
23. D. F. Feng, G. Cho, R. F. Doolittle, *Proc. Natl. Acad. Sci. U.S.A.* **94**, 13028 (1997).
24. H. Ochman, S. Elwyn, N. A. Moran, *Proc. Natl. Acad. Sci. U.S.A.* **96**, 12638 (1999).
25. S. Wright, J. Keeling, L. Gillman, *Proc. Natl. Acad. Sci. U.S.A.* **103**, 7718 (2006).
26. A. Dufresne, L. Garczarek, F. Partensky, *Genome Biol.* **6**, R14 (2005).
27. J. Raes *et al.*, *Genome Biol.* **8**, R10 (2007).
28. J. B. Martiny *et al.*, *Nat. Rev. Microbiol.* **4**, 102 (2006).
29. W. F. Doolittle, *Trends Cell Biol.* **9**, M5 (1999).
30. R. F. Doolittle, *Curr. Opin. Struct. Biol.* **15**, 248 (2005).
31. I. Chen, P. J. Christie, D. Dubnau, *Science* **310**, 1456 (2005).
32. N. U. Frigaard, A. Martinez, T. J. Mincer, E. F. DeLong, *Nature* **439**, 847 (2006).
33. C. Pedros-Alio, *Trends Microbiol.* **14**, 257 (2006).
34. I. Letunic *et al.*, *Bioinformatics* **23**, 127 (2007).

35. We thank P. Dawyndt for providing an early version of his integrated strain database (www.straininfo.net), and members of the Bork team for insightful discussions. Supported by the European Union through its BioSapiens and GeneFun networks, by the University of Zurich through its Research Priority Program Systems Biology and Functional Genomics, by the NSF Assembling the Tree of Life and Microbial Genome Sequencing programs, and by the German Federal Government through its National Genome Research Network.

Supporting Online Material

www.sciencemag.org/cgi/content/full/1133420/DC1
SOM Text
Figs. S1 to S4
Tables S1 to S3
References

3 August 2006; accepted 19 January 2007
Published online 1 February 2007;
10.1126/science.1133420
Include this information when citing this paper.

Staphylococcus aureus Panton-Valentine Leukocidin Causes Necrotizing Pneumonia

Maria Labandeira-Rey,[1] Florence Couzon,[2–5] Sandrine Boisset,[2–5] Eric L. Brown,[1]* Michele Bes,[2–5] Yvonne Benito,[2–5] Elena M. Barbu,[1] Vanessa Vazquez,[1] Magnus Höök,[1] Jerome Etienne,[2–5] François Vandenesch,[2–5]†‡ M. Gabriela Bowden[1]†‡

The *Staphylococcus aureus* Panton-Valentine leukocidin (PVL) is a pore-forming toxin secreted by strains epidemiologically associated with the current outbreak of community-associated methicillin-resistant *Staphylococcus aureus* (CA-MRSA) and with the often-lethal necrotizing pneumonia. To investigate the role of PVL in pulmonary disease, we tested the pathogenicity of clinical isolates, isogenic PVL-negative and PVL-positive *S. aureus* strains, as well as purified PVL, in a mouse acute pneumonia model. Here we show that PVL is sufficient to cause pneumonia and that the expression of this leukotoxin induces global changes in transcriptional levels of genes encoding secreted and cell wall–anchored staphylococcal proteins, including the lung inflammatory factor staphylococcal protein A (Spa).

The combined actions of many virulence factors enable *Staphylococcus aureus* to cause disease (*1*, *2*). Depending on these factors and on the immune status of the host, staphylococci can cause diseases ranging from superficial skin infections to deep-seated and systemic conditions such as osteomyelitis, septic shock, and necrotizing pneumonia. Staphylococcal necrotizing pneumonia can affect young, immunocompetent patients. This disease, characterized by leukopenia, hemoptysis, and extensive necrosis of the lung tissue, is caused by *S. aureus* strains that produce Panton-Valentine leukocidin (PVL) (*3*). *S. aureus* PVL-positive strains are often methicillin-resistant (MRSA) and, in the USA, they are the predominant cause of community-associated infections (*4*).

PVL is a bi-component, pore-forming exotoxin (*5*) that targets cells of the immune system such as polymorphonuclear neutrophils (PMNs). The active form of PVL requires the assembly of two polypeptides, LukS-PV and LukF-PV, into a heterooligomeric pore. Although PVL has potent cytolytic and inflammatory activities in vitro (*6*, *7*), its role in necrotizing pneumonia has not been demonstrated. To analyze the molecular pathogenesis of PVL-expressing *S. aureus* strains, we have established a murine model of acute primary pneumonia.

We infected mice with strains isolated from necrotizing (PVL-positive) or nonnecrotizing

[1]Center for Extracellular Matrix Biology, Institute of Biosciences and Technology, The Texas A&M University System Health Science Center, Houston, TX 77030, USA. [2]Université de Lyon, Lyon, F-69008, France. [3]Université de Lyon 1, Faculté Laennec, Lyon, F-69008, France. [4]INSERM E0230, Centre National de référence des staphylocoques, Lyon, F-69008, France. [5]Hospices Civils de Lyon, Hôpital Edouard Herriot, Lyon, F-69003, France.

*Present address: University of Texas School of Public Health, Houston, TX 77030, USA.
†These authors contributed equally to this work.
‡To whom correspondence should be addressed. E-mail: gbowden@ibt.tamhsc.edu and denesch@univ-lyon1.fr

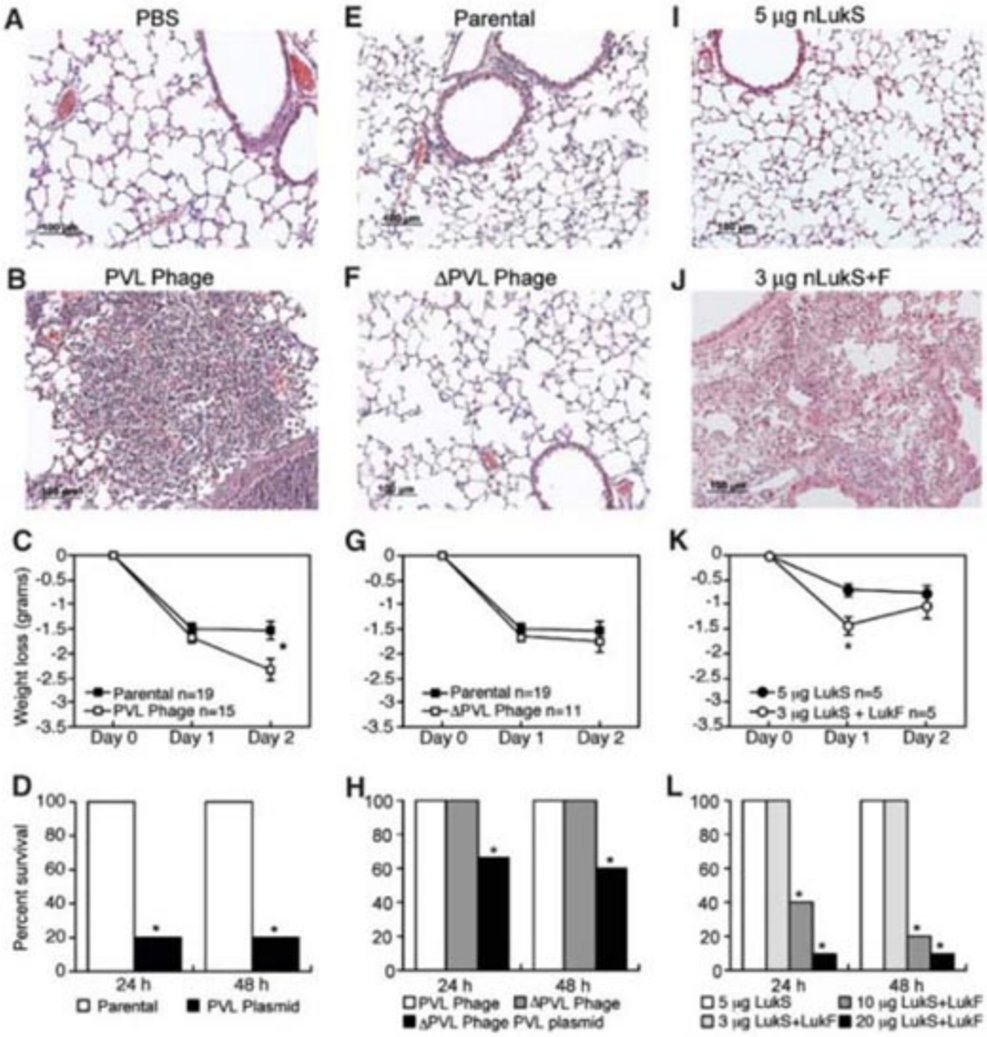

Fig. 1. Expression of PVL enhances the virulence of isogenic *S. aureus* strains. (**A**, **B**, **E**, **F**, **I**, and **J**) Lung histology of mice infected with PVL-positive and PVL-negative strains or inoculated with PVL toxin. The sections are representative of at least three separate experiments. Scale bar, 100 μm. (**C**, **G**, and **K**) Line graphs indicate weight loss in grams. (C) Parental versus PVL phage; $^*P < 0.001$. (G) Parental versus ΔPVL phage; no statistical difference observed. (K) Animals inoculated with 3 μg of LukS+F-PV versus 5 μg LukS-PV; $^*P < 0.01$ on day 1. (**D**, **H**, and **L**) Mouse survival. (D) Parental and PVL plasmid; (H) PVL phage, ΔPVL phage, and ΔPVL phage PVL plasmid; (L) 20 μg or 10 μg of LukS+LukF-PV versus 3 μg LukS+LukF-PV or 5 μg LukS-PV, $^*P < 0.0001$.

(PVL-negative) staphylococcal pneumonia patients (table S1). PVL-positive strains caused murine necrotizing pneumonia with manifestations resembling human disease (fig. S1). In the PVL-positive strains, the *lukS-PV* and *lukF-PV* genes are organized as an operon within a phage (ϕSLT, or other similar phages) that could potentially contribute to the virulence of these strains. To define the role of PVL, we developed several isogenic strains (*8*). A PVL-negative, transformable *S. aureus* strain was lysogenized with ϕSLT or with a mutated ϕSLT in which the PVL operon (*luk-PV*) was deleted. We complemented the PVL-negative strains with a plasmid containing the *luk-PV* operon under the control of its own promoter (table S1).

Mice infected with PVL-positive strains showed symptoms of severe illness: lethargy, hunched posture, ruffled fur, and significant weight loss. Lungs from infected mice were examined 48 hours postinoculation. Tissue sections from lungs infected with PVL-positive strains revealed a strong recruitment of neutrophils and significant inflammation in the lung parenchyma, bronchial epithelial damage, tissue necrosis, and hemorrhage (Fig. 1 and table S2). The lungs infected with PVL-negative strains showed normal lung structures, despite some leukocyte infiltration. By contrast, when the PVL-negative strains were complemented with a plasmid encoding PVL, we observed massive tissue damage and 35 to 80% mortality within 24 hours after inoculation (Fig. 1 and fig. S2). We stained lung sections using antibodies against LukS-PV (fig. S3) and showed that the toxin was detected in tissues infected with PVL-positive bacteria.

Administration of increasing equimolar amounts of native LukS-PV and LukF-PV resulted in concentration-dependent localized lesions, weight loss, and, at concentrations higher than 3 μg, high rates of mortality (Fig. 1). The protein-inoculated mice recovered the lost weight after 24 hours, whereas those infected with PVL-positive bacteria were still ill at 48 hours (Fig. 1C compared with Fig. 1K); these findings demonstrated that an active bacterial infection is required to cause severe morbidity.

Previous studies have demonstrated that PVL-positive strains had increased adherence to injured airway epithelium (*3*, 9). To examine the expression of surface proteins in these strains, we examined by SDS–polyacrylamide electrophoresis (SDS-PAGE) cell wall extracts and supernatants from cultures taken at both the exponential growth phase and the stationary growth phase (Fig. 2). Samples from a PVL-positive strain showed an enhanced expression of at least two cell wall–anchored polypeptides identified as SdrD and protein A (Spa) by N-terminal sequencing and Western analysis (Fig. 2, C to E, and fig. S4). The SdrD and Spa overexpression was not observed in a strain carrying the phage with the deleted *luk-PV* operon, which indicated that this effect was not mediated by products encoded by other phage genes or by its insertion in the chromosome of *S. aureus*. PVL-negative strains complemented with the *luk-PV* operon in a multicopy plasmid (table S1) also showed an increased expression of Spa during both logarithmic and stationary growth phases (Fig. 2F). A group of polypeptides with apparent molecular masses between 32 and 47.5 kD (Fig. 2B, dots) were present in the supernatants from the PVL-negative, but not the PVL-positive, strains. Some of the secreted polypeptides were identified as proteases by using zymograms (Fig. 2G). Thus, expression of the *luk-PV* operon resulted in an altered regulation of cell wall–anchored and secreted protein production.

Spa is a known virulence factor in mouse models of *S. aureus* infections, including pneumonia (*10*, *11*); therefore, we examined the role of Spa in necrotizing pneumonia. Animals infected with the *spa*-deleted isogenic strains had less severe symptoms of disease (Fig. 3A). However, the lungs from animals infected with *spa*-deleted, PVL-positive strains showed localized lesions with massive leukocyte infiltration (fig. S5), which demonstrated that PVL alone was sufficient to cause pneumonia. Complementation of Spa-positive strains with PVL rendered them lethal, whereas the Spa-negative, PVL-plasmid strains did not cause mortality (Fig. 3B). These data suggested that PVL and Spa may act together to cause the overwhelming inflammation and tissue damage that are seen in necrotizing pneumonia.

PVL-positive strains expressed Spa during both exponential and stationary growth phases (Fig. 2). To analyze the effect of PVL on *spa* transcription, PVL was introduced into mutants deficient in *spa* regulators. The Spa production was abolished in a *sarS*-deletion mutant (fig. S6), whether PVL was present or not, which indicated that PVL acts upstream of SarS. To evaluate the transcriptional profile of a PVL-positive strain

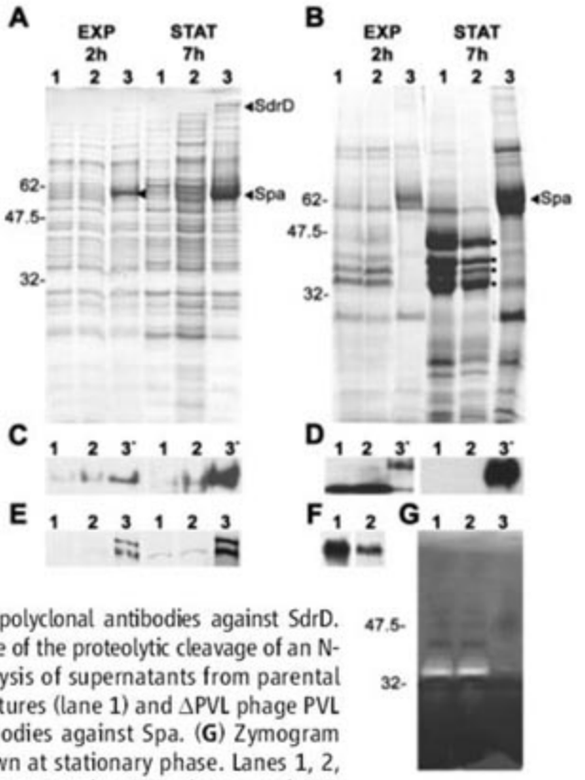

Fig. 2. PVL alters the expression pattern of cell wall–anchored and secreted proteins. (**A** to **E**) Lanes 1, 2, and 3 represent extracts from parental, ΔPVL phage, and PVL phage strains respectively; samples were isolated from bacterial cultures grown at exponential (EXP) and stationary (STAT) phases of growth. (A) Lysostaphin extracts analyzed by SDS-PAGE. The arrows point to overexpressed proteins. (B) Exoproteins from culture supernatants harvested from bacterial cultures analyzed by SDS-PAGE. Arrows point to overexpressed proteins; dots indicate exoproteins reduced or absent in PVL-positive strains. (C and D) Western blot analysis of lysostaphin extracts and supernatants using a monoclonal antibody against Spa. Complete gels shown in fig. S4 (*8*). *Samples were diluted 1:100. (E) Western blot analysis of lysostaphin extracts using polyclonal antibodies against SdrD. SdrD is detected as two polypeptides because of the proteolytic cleavage of an N-terminal subdomain. (**F**) Western blot analysis of supernatants from parental PVL plasmid stationary phase (7-hour) cultures (lane 1) and ΔPVL phage PVL plasmid (lane 2) using monoclonal antibodies against Spa. (**G**) Zymogram analysis of exoproteins from cultures grown at stationary phase. Lanes 1, 2, and 3 represent proteins extracted from parental, ΔPVL phage, and PVL phage, respectively.

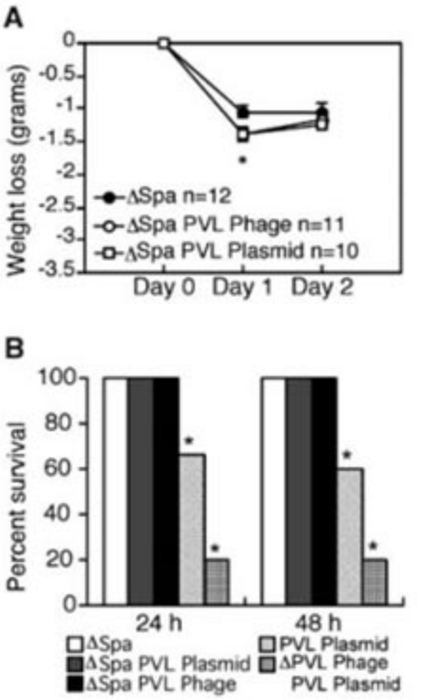

Fig. 3. Spa enhances the virulence of PVL-positive strains. (**A**) Line graph indicates weight loss in grams, *$P < 0.01$ ΔSpa versus ΔSpa PVL phage or ΔSpa PVL plasmid. (**B**) Percent survival of animals infected with ΔSpa, ΔSpa PVL plasmid, ΔSpa PVL phage, PVL plasmid, and ΔPVL phage PVL plasmid, *$P < 0.001$ ΔSpa, ΔSpa PVL phage and ΔSpa PVL plasmid versus PVL plasmid or ΔPVL phage PVL plasmid.

compared with the PVL-negative strain, we used microarray analysis: 28 genes showed a distinct expression pattern during exponential growth (table S3), whereas, during the stationary phase, 133 genes showed differential expression (table S4). The *agr* transcripts and several exoproteins were repressed, whereas genes encoding for cell wall–anchored proteins and the *spa* activator *sarS* (*12*) were up-regulated (Fig. 4A). Elevated expression of the *spa* and *sdrD* transcripts correlated with the enhanced production of Spa and SdrD observed in Western blot analysis (Fig. 2 and fig. S4). The repression of exoprotein transcripts paralleled the absence of the 32- to 47.5-kD exoproteins in the supernatants of PVL-positive strains (Fig. 2). This pattern of transcription implicated PVL in an interaction with a factor (or factors) that controls gene expression during the transition from the logarithmic growth to stationary phase.

The regulatory model proposed here was inferred by using strains derived from RN6390, a strain harboring a deletion in *rsbU*, which encodes a regulator necessary for the activity of the stress sigma factor σ^B. Strains with a reduced σ^B (*13*) activity display, among other traits, a decreased production of cell wall–anchored proteins and an increased production of exoproteins. We subsequently generated isogenic PVL-positive and PVL-negative strains in the SH1000 (*14*) *rsbU+* background and observed overexpression of Spa during the stationary phase of growth (fig. S7A). The SH1000-derived PVL-positive strain was more virulent than its PVL-negative isogenic pair (fig. S7, C and D). When compared with RN6390, the SH1000 lineage showed an increased expression of Spa, but produced ≥20% PVL, although some variability was seen (fig. S7A) (*15*). This suggested that RsbU/σ^B partially regulates PVL.

We show here that PVL is a significant *S. aureus* virulence factor and that PVL-positive strains can cause murine necrotizing pneumonia with manifestations that resemble those observed in human patients. Our results demonstrate that the expression of the genes that encode PVL (*lukS-PV* and *lukF-PV*) or direct inoculation with native toxin is sufficient to induce pneumonia in mice. The expression of the *luk-PV* operon also resulted in an altered expression of multiple proteins, including the tightly regulated (*16*, *17*) proinflammatory factor Spa.

In PVL-positive strains, many secreted proteins are down-regulated (Fig. 4B), similarly to data reported by Vojtov *et. al.* (*18*), who demonstrated that two staphylococcal superantigens, toxic shock syndrome toxin-1 (TSST-1) and enterotoxin B (SEB), strongly repressed production of secreted proteins. It is possible that these toxins act similarly to PVL, interacting with unknown factors that interfere with regulatory networks.

Several genes encoding putative and known microbial surface components recognizing adhesive matrix molecules (MSCRAMMs) (including SdrD) are up-regulated in the PVL-positive strains (Fig. 4A). The up-regulation of MSCRAMMs may lead to enhanced tissue adherence and colonization of PVL-expressing strains, thereby contributing to the virulence potential of these strains (*19*, *20*).

Spa is highly expressed in PVL-positive strains. Our in vivo data underscore the documented role of Spa as a proinflammatory factor in pneumonia (*11*). Increased production of Spa, coupled with the ability of PVL to lyse PMNs and macrophages (*6*), could lead to a vicious cycle of cell recruitment, lysis, and release of inflammatory mediators (*7*), resulting in overwhelming tissue inflammation and necrosis.

Here, we show not only that PVL is a key virulence factor in pulmonary infections but also that expression of the *luk-PV* genes interferes with global regulatory networks, which may also enhance virulence. A detailed analysis of such dysregulation will be useful to identify targets for the potential development of novel therapies to treat *S. aureus* infections.

References and Notes

1. T. J. Foster, M. Höök, *Trends Microbiol.* **6**, 484 (1998).
2. T. J. Foster, *Nat. Rev. Microbiol.* **3**, 948 (2005).
3. Y. Gillet *et al.*, *Lancet* **359**, 753 (2002).
4. H. F. Chambers, *N. Engl. J. Med.* **352**, 1485 (2005).
5. P. N. Panton, M. C. Camb, F. C. O. Valentine, M. R. C. P. Lond, *Lancet* **1**, 506 (1932).
6. A. L. Genestier *et al.*, *J. Clin. Invest.* **115**, 3117 (2005).
7. B. Konig, G. Prevost, Y. Piemont, W. Konig, *J. Infect. Dis.* **171**, 607 (1995).
8. Materials and methods are available as supporting materials on *Science* Online.

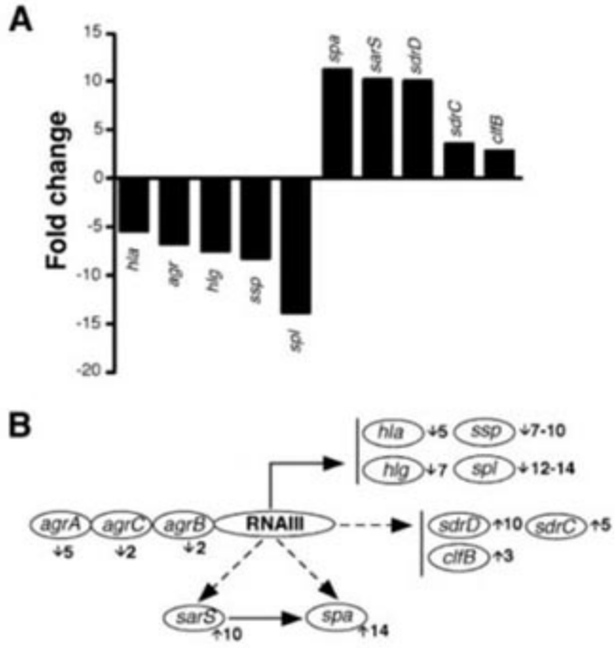

Fig. 4. *S. aureus* PVL-positive strains show an altered transcriptional profile. (**A**) Fold increase or decrease levels of transcript from selected genes. Total RNA extracted from cultures grown to stationary phase. Genes were considered to be induced or repressed in the PVL phage if they were transcribed at least twice or half as much as those of ΔPVL phage. The shown transcripts encode *agrA-C*, accessory gene regulator system; *sar*S, staphylococcal accessory regulator S; *spa*, staphylococcal protein A; *sdr*D, serine-aspartate repeat protein D; *sdr*C, serine-aspartate repeat protein C; *clf*B, clumping factor B; *hla*, alpha toxin; *ssp*, a representative of serine proteases *ssp*B and *ssp*C; *spl*, a representative of *splA-F* proteases. (**B**) A schematic overview of the interactions between regulators involved in cell wall–anchored and secreted protein genes (full and broken lines indicate positive and negative regulation, respectively) based on previously published data. Numbers next to the gene name indicate fold change based on microarray analysis (upward arrow indicates up-regulation, downward arrow indicates down-regulation). The down-regulation of RNAIII (the effector of the *agr* system) results in the down-regulation of secreted protein genes (*hla*, *hlg*C, *hlg*B, and proteases) and the up-regulation of *sar*S and cell wall–anchored proteins (*spa*, *sdr*D, *sdr*C, *clf*B). In addition, the up-regulation of *sar*S results in the up-regulation of *spa*.

9. S. de Bentzmann *et al.*, *J. Infect. Dis.* **190**, 1506 (2004).
10. N. Palmqvist, T. Foster, A. Tarkowski, E. Josefsson, *Microb. Pathog.* **33**, 239 (2002).
11. M. I. Gomez *et al.*, *Nat. Med.* **10**, 842 (2004).
12. J. Oscarsson, C. Harlos, S. Arvidson, *Int. J. Med. Microbiol.* **295**, 253 (2005).
13. I. Kullic, P. Giachino, T. Fuchs, *J. Bacteriol.* **180**, 4814 (1998).
14. M. J. Horsburgh *et al.*, *J. Bacteriol.* **184**, 5457 (2002).
15. B. Said-Salim *et al.*, *J. Clin. Microbiol.* **43**, 3373 (2005).
16. A. L. Cheung, K. Eberhardt, J. H. Heinrichs, *Infect. Immun.* **65**, 2243 (1997).
17. E. Huntzinger *et al.*, *EMBO J.* **24**, 824 (2005).
18. N. Vojtov, H. F. Ross, R. P. Novick, *Proc. Natl. Acad. Sci. U.S.A.* **99**, 10102 (2002).
19. P. Thomas, M. Riffelmann, B. Schweiger, S. Dominik, C. H. von Konig, *Pediatr. Infect. Dis. J.* **22**, 201 (2003).
20. L. O'Brien *et al.*, *Mol. Microbiol.* **44**, 1033 (2002).

21. We thank S. L. Mueller-Ortiz and S. M. Drouin for their invaluable help establishing the animal model; Z. Chroneos for his input in the interpretation of histological samples; C. Badiou for technical assistance; G. Lina for scientific advice; and S. Foster, T. Foster, B. Fournier, R. Novick, and P. McNamara for providing strains. This work was supported by grants from the TAMUS HSC to M.G.B., from the French Ministry of Research to F.V. and NIH AI020624 to M.H. Support from the Neva and Wesley West and the Hamill Foundations were awarded to M.H. The authors declare that they have no competing financial interests. Microarray data are deposited in the GEO database (http://www.ncbi.nlm.nih.gov/projects/geo/) under the accession number GPL4653.

Supporting Online Material

www.sciencemag.org/cgi/content/full/1137165/DC1
Materials and Methods
Figures S1 to S8
Tables S1 to S5
References

3 November 2006; accepted 19 December 2006
Published online 18 January 2007;
10.1126/science.1137165
Include this information when citing this paper.

Regulation of *Drosophila* Life Span by Olfaction and Food-Derived Odors

Sergiy Libert,[1,2] Jessica Zwiener,[1] Xiaowen Chu,[1] Wayne VanVoorhies,[3] Gregg Roman,[4] Scott D. Pletcher[1,2,5]*

Smell is an ancient sensory system present in organisms from bacteria to humans. In the nematode *Caenorhabditis elegans*, gustatory and olfactory neurons regulate aging and longevity. Using the fruit fly, *Drosophila melanogaster*, we showed that exposure to nutrient-derived odorants can modulate life span and partially reverse the longevity-extending effects of dietary restriction. Furthermore, mutation of odorant receptor *Or83b* resulted in severe olfactory defects, altered adult metabolism, enhanced stress resistance, and extended life span. Our findings indicate that olfaction affects adult physiology and aging in *Drosophila*, possibly through the perceived availability of nutritional resources, and that olfactory regulation of life span is evolutionarily conserved.

As in many species, reduced nutrient availability (dietary restriction) increases life span in the fruit fly, *Drosophila melanogaster*, and leads to alterations in age-dependent patterns of gene expression, physiology, and behavior (*1*–*4*). Acute nutrient manipulation causes sudden and rapid changes in age-specific mortality (*5*, *6*). Whole-genome expression data, containing age-dependent patterns of gene expression in diet-restricted long-lived flies and fully fed control flies (*1*), revealed that expression of genes encoding odorant-binding proteins was strongly affected by both age and nutrient availability (fig. S1).

To determine whether detection of food-related odors is sufficient to affect fly life span, we measured the life spans of flies in the presence and absence of odorants from live yeast. Yeast odorants were used because demographic and gene-expression data suggested that yeast availability is a major component of the longevity response to diet in *Drosophila* (*7*–*9*). Exposure to yeast odorants reduced life span in long-lived flies from two laboratory fly strains (Canton-S and yw) that had been subjected to dietary restriction (Fig. 1, A and C). Life span was further reduced when flies were allowed to consume yeast paste. The magnitude of the odorant effect was variable and usually small, relative to that caused by the consumption of yeast paste; odorant-mediated life-span reductions ranged from 6 to 18% in Canton-S flies and from 7 to 8% in yw flies (Fig. 1C). Such variability is reminiscent of the dietary-restriction response in flies, which depends on genetic background (*8*). Odorants are therefore sufficient to modulate life span, and currently unidentified odors may alter longevity with greater potency.

We tested whether diet-restricted flies might exhibit altered feeding behavior or altered in-

[1]Huffington Center on Aging, Baylor College of Medicine, One Baylor Plaza, Houston, TX 77030, USA. [2]Interdepartmental Program in Cellular and Molecular Biology, Baylor College of Medicine, One Baylor Plaza, Houston, TX 77030, USA. [3]Molecular Biology Program, New Mexico State University, Post Office Box 30001, Department 3C, Las Cruces, NM 88003, USA. [4]Biology and Biochemistry Department, University of Houston, Houston, TX 77024, USA. [5]Department of Molecular and Human Genetics, Baylor College of Medicine, One Baylor Plaza, Houston, TX 77030, USA.

*To whom correspondence should be addressed. E-mail: pletcher@bcm.tmc.edu

vestment in reproduction when exposed to nutrient-related odors, thereby accounting for the longevity effect. Increases in the intensity of either of these behaviors would reduce life span by compensating for our diet-restriction procedure or by augmenting the costs of reproduction, respectively. In our experiments, neither food consumption (as measured by the rate of dye ingestion, proboscis extension, and fecal output) nor fecundity was affected by yeast odorants (Fig. 1D and figs. S2 and S3). Behavioral alterations leading to increased nutrient intake or reproductive effort are therefore not responsible for reduced longevity upon exposure to yeast odorants.

The effects of yeast odorants on fly life span depend on nutrient availability. Longevity was not affected by yeast odorants when flies were fully fed (Fig. 1, B and C). Thus, the odor effect is a regulated biological response, and yeast odorants are not a generalized toxin that shortens life span. Our data support the hypotheses that diet- and odorant-mediated regulation of aging act at least partly through the same molecular pathway and that nutrient-related odors can rescue, albeit incompletely, the extension of longevity through dietary restriction. Consequently, the beneficial effects of dietary restriction may be due in part to the decreased perception of nutrient availability.

We next asked whether the loss of olfactory function is sufficient to increase life span. In vertebrates and insects, each olfactory neuron ex-

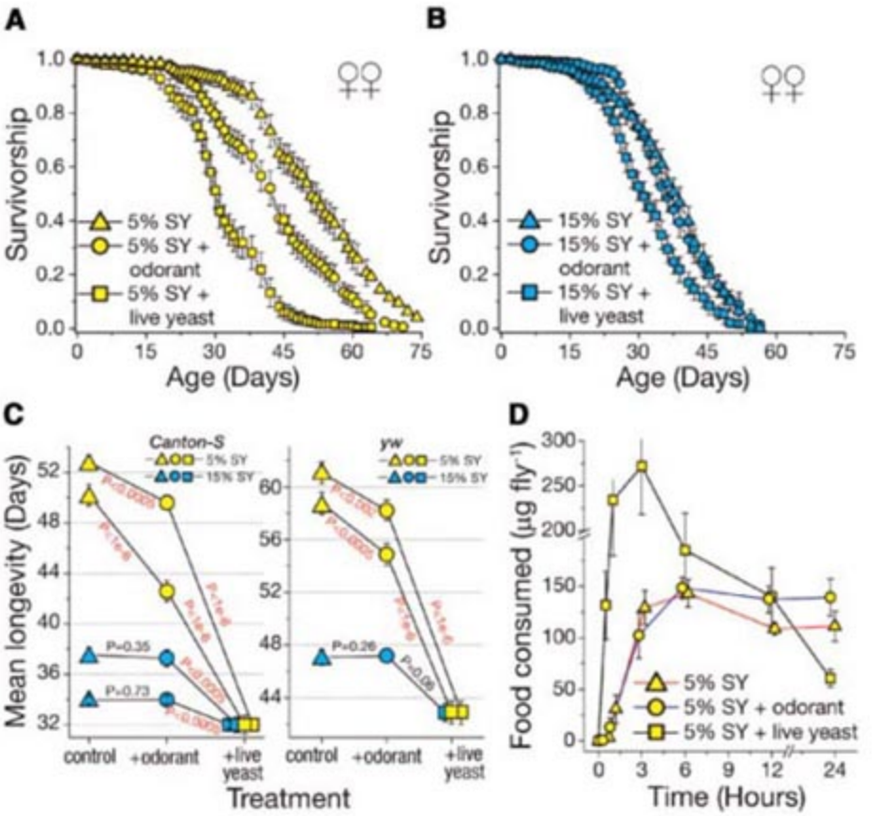

Fig. 1. Exposure to yeast odorants alters life span in *Drosophila*. (**A**) Canton-S female flies were maintained under dietary restriction (5% SY medium) (triangles), with the addition of odorants from live yeast (circles) or yeast for consumption (squares). Sample sizes: control, $n = 206$; + odorant, $n = 247$; + live yeast, $n = 193$. (**B**) Canton-S female flies were unaffected by yeast odorants when fully fed (15% SY medium). Sample sizes: control, $n = 269$; + odorant, $n = 267$; + live yeast, $n = 266$. Error bars in (A) and (B) represent 95% confidence intervals on observed survivorship. (**C**) The effect of yeast odorants on longevity is repeatable and depends on diet. Replicate experiments showing mean life span (and SEM) for female *Drosophila* maintained under dietary restriction (5% SY, yellow symbols) and fully fed conditions (15% SY, blue symbols). Yeast odorants had no effect when flies were maintained in fully fed conditions ($P > 0.05$ in all cases). Each point represents life spans of 5 to 10 cohorts and a minimum of 206 (maximum of 403) animals. (**D**) Food consumption is unaffected by yeast odorants. Mean food consumption (and SEM) as measured by dye uptake (see the supporting online material) is shown. Multivariate profile analysis reveals no significant treatment effects ($P > 0.05$). The decline in dye uptake at later time points is a consistent finding that may reflect diurnal patterns of feeding and the dynamics of dye uptake and excretion. For survival data, block effects were adjusted for by analysis of variance (based on yeast paste treatments) to allow for comparisons across multiple experiments. *P* values were determined by means of a log-rank test.

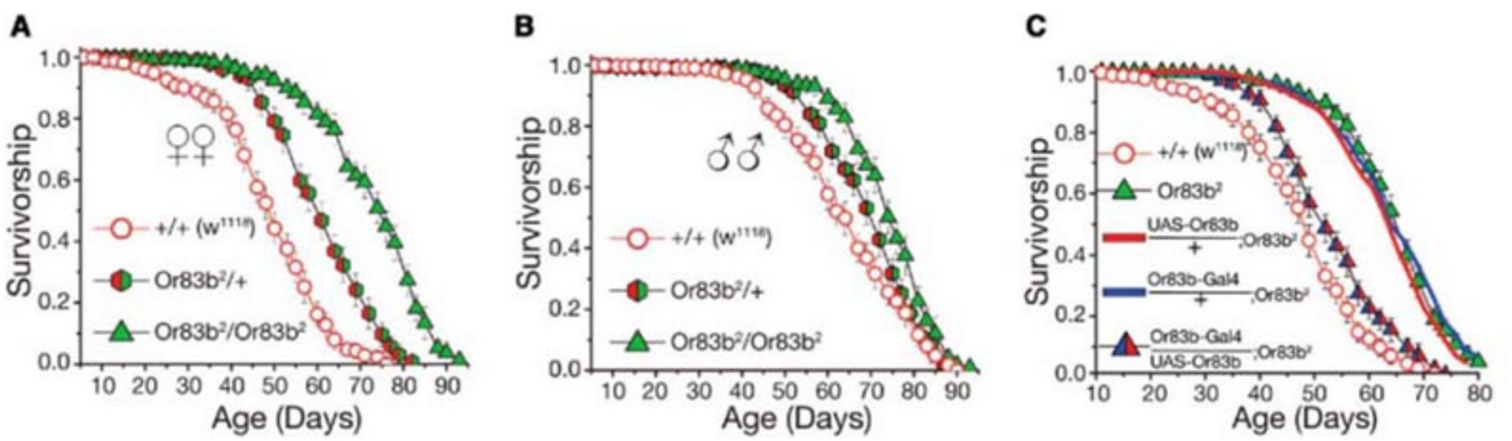

Fig. 2. Mutation of *Or83b* increases life span. (**A** and **B**) Both female and male flies carrying the $Or83b^2$ mutation are long-lived. Sample sizes (females): +/+, $n = 326$; +/–, $n = 314$; –/–, $n = 320$. Sample sizes (males): +/+, $n = 317$; +/–, $n = 346$; –/–, $n = 305$. Error bars represent 95% confidence intervals, and statistical comparisons by means of a log-rank test and Cox regression yielded $P < 1 \times 10^{-6}$ for all paired comparisons except (B) (males) where $P = 0.001$ for +/+ versus +/–. (**C**) $Or83b^2$ homozygous mutant flies expressing *UAS-GFP:Or83b* under control of the Or83b-Gal4 driver (bicolor triangles) have comparable life spans to those of background control animals (w^{1118}, open circles). Controls for the transgenic constructs had no effect on life span (compare solid red and blue lines to green triangles). Data are presented for females and are qualitatively similar for males (fig. S7). Experiments were carried out with the use of 15% SY media and were repeated by means of independent transgenic insertions with identical results. Error bars represent 95% confidence intervals on observed survivorship.

presses a small number of odorant receptors that impart response characteristics of the neuron to specific odors (*10*–*13*). Of the 62 putative odorant receptors in *Drosophila*, *Or83b* is atypical in that it is broadly expressed throughout olfactory tissues (*14*, *15*). *Or83b* interacts with conventional odorant receptors and is required for their localization to the neuronal dendrite (*14*–*16*). Loss-of-function mutations in *Or83b* limit spontaneous activity in many odorant-receptor neurons and severely reduce physiological and behavioral responses to a wide range of odorants (*14*, *16*), including nutrient-related odors (fig. S4).

Table 1. Life-span data for female *Or83b* mutant *Drosophila*. Mean life spans of $Or83b^2$ homozygous mutant and wild-type control females. The $Or83b^2$ allele was backcrossed into each of three genetic backgrounds. For all comparisons, longevity extension in the mutant was calculated with respect to the wild-type background to which it had been backcrossed. All increases are statistically significant ($P < 1 \times 10^{-6}$), determined by means of a log-rank test and Cox regression. *YP represents live yeast paste added to the vials.

Genetic background	Nutrient level (% SY)	Control longevity			*Or83b* longevity			Absolute change	% Increase
		n	Mean	(SE)	*n*	Mean	(SE)		
Canton-S									
	3%	319	50.1	(0.77)	311	61.6	(0.86)	11.5	23.0%
	5%	319	50.1	(0.81)	304	62.5	(0.78)	12.3	24.6%
	7.5%	324	43.9	(0.80)	315	58.9	(0.83)	15.0	34.1%
	10%	313	44.8	(0.82)	318	58.6	(0.92)	13.8	30.7%
	15%	314	41.6	(0.69)	329	55.6	(0.76)	14.0	33.7%
yw									
	3%	249	58.0	(0.85)	234	76.1	(0.63)	18.1	31.2%
	5%	244	60.0	(0.83)	239	76.5	(0.60)	16.5	27.6%
	7.5%	254	62.0	(0.74)	236	76.0	(0.76)	14.0	22.6%
	10%	241	61.9	(0.74)	238	75.6	(0.81)	13.7	22.1%
	15%	242	50.5	(0.57)	246	69.4	(0.60)	18.9	37.4%
	YP*	237	42.9	(0.84)	243	65.7	(0.73)	22.8	53.1%
w^{1118}									
	3%	315	51.9	(0.89)	318	75.6	(0.86)	23.7	45.6%
	5%	326	53.2	(0.90)	320	76.0	(0.81)	22.8	43.0%
	7.5%	333	49.6	(0.83)	319	78.0	(0.77)	28.4	57.3%
	10%	316	51.1	(0.79)	317	77.6	(0.84)	26.5	51.9%
	15%	314	49.3	(0.79)	319	72.7	(0.78)	23.4	47.3%

Table 2. Life-span data for male *Or83b* mutant *Drosophila*. Mean life spans of $Or83b^2$ homozygous mutant and wild-type control males. The $Or83b^2$ allele was backcrossed into each of three genetic backgrounds. For all comparisons, longevity extension in the mutant was calculated with respect to the wild-type background to which it had been backcrossed. All increases are statistically significant ($P < 1 \times 10^{-6}$), determined by means of a log-rank test and Cox regression.

Genetic background	Nutrient level (% SY)	Control longevity			*Or83b* longevity			Absolute change	% Increase
		n	Mean	(SE)	*n*	Mean	(SE)		
Canton-S									
	3%	322	52.1	(0.83)	317	66.8	(0.75)	14.7	28.2%
	5%	315	53.2	(0.67)	282	66.3	(0.80)	13.1	24.6%
	7.5%	331	52.3	(0.71)	313	68.7	(0.77)	16.4	31.3%
	10%	330	52.0	(0.76)	296	67.5	(0.82)	15.6	30.0%
	15%	325	47.2	(0.74)	301	67.1	(0.85)	19.9	42.1%
yw									
	3%	257	63.6	(0.81)	238	73.8	(0.57)	10.3	16.2%
	5%	242	63.9	(0.89)	243	75.2	(0.57)	11.4	17.8%
	7.5%	251	64.4	(0.75)	240	74.3	(0.72)	9.9	15.4%
	10%	246	65.3	(0.92)	246	75.8	(0.67)	10.5	16.0%
	15%	244	60.1	(0.73)	222	70.3	(0.69)	10.1	16.8%
w^{1118}									
	3%	317	63.2	(0.80)	328	69.1	(0.72)	6.0	9.5%
	5%	314	63.9	(0.77)	322	69.5	(0.77)	5.6	8.7%
	7.5%	322	63.6	(0.80)	324	73.6	(0.74)	10.0	15.7%
	10%	317	65.2	(0.77)	310	74.6	(0.77)	9.4	14.5%
	15%	317	64.4	(0.80)	305	73.8	(0.71)	9.4	14.5%

We measured the life span of flies carrying the $Or83b^2$ allele, in which the first five of seven transmembrane domains were replaced with the w^+ marker (*14*) (fig. S6). $Or83b^2$ homozygous flies lack detectable levels of *Or83b* mRNA and protein, which suggests that it is a null allele (*14*). Fully fed female $Or83b^2$ mutant flies exhibited a 56% increase in median life span when compared to appropriate wild-type animals (Fig. 2A). Males were also significantly long-lived, but the magnitude of the extension was generally smaller (Fig. 2B). Heterozygous flies exhibited intermediate longevity in both sexes, and heterozygous adult females showed a similar deficiency in attraction to live yeast paste (fig. S4, B and C). We found no evidence of such impairment in heterozygous mutant males (fig. S4D). It may be that odor-evoked behaviors are less affected or that different classes of odorants are critical for male longevity. Longevity was also extended when olfactory signaling was suppressed in *Or83b*-expressing neurons through the disruption of guanine nucleotide–binding protein (G protein) signaling (fig. S5). Because the *Or83b* mutant also disrupts G protein activity, it is possible that G protein function in olfactory neurons, rather than perception per se, influences life span.

To verify that the extended life span of $Or83b^2$ flies was not due to heterosis or to comparison against a relatively weak control stock, we backcrossed the $Or83b^2$ allele into two additional laboratory stocks (Canton-S and yw). In all cases, the longevity of mutant flies was considerably greater than that of their wild-type controls (Tables 1 and 2). The degree of life-span extension was independent of the longevity of the corresponding wild-type stock, establishing that loss of *Or83b* function extends life span in healthy animals (*17*).

Expression of a rescuing *Or83b* transgene (*15*) under the control of an Or83b-Gal driver (*14*) restored normal life span to the $Or83b^2$ mutant flies (Fig. 2C). The effectiveness of this construct was verified by genomic polymerase chain reaction and visually (fig. S6), and it rescues most (but not all) olfactory phenotypes (*14*, *15*). The Or83b-Gal4 driver and the upstream activating sequence–green fluorescent protein *Or83b* transgene (*UAS-GFP:Or83b*) were inserted into different genomic positions and none affected life span on their own (Fig. 2C and fig. S7). These rescue data and the persistence of the longevity phenotype through extensive backcrossing to three different genetic backgrounds provide compelling evidence that loss of function in *Or83b* is the cause of increased life span in these animals.

Olfactory signaling modulates life span primarily by altering the onset of demographic senescence (Fig. 3). Mortality analysis suggests that olfaction shifts the mortality curve to earlier (in the case of yeast odorants) or later (in

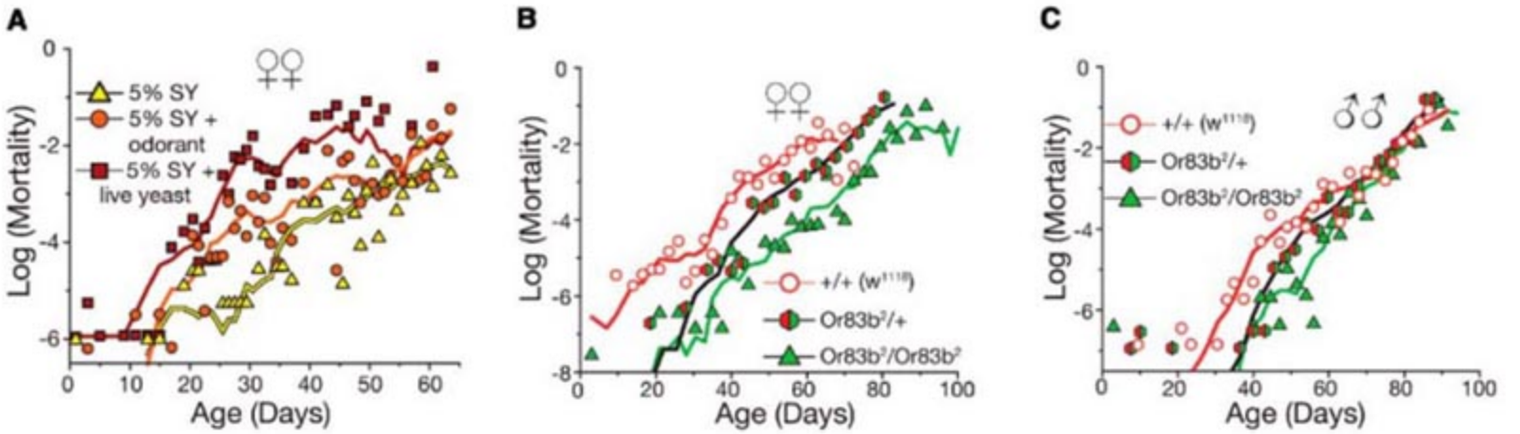

Fig. 3. Olfaction modulates the onset of demographic senescence. (**A**) Age-specific mortality rates for flies exposed to yeast odorants expressed on the natural log scale. Corresponding survival data are presented in Fig. 1A. (**B** and **C**) Age-specific mortality rates for *Or83b* mutant (B) females and (C) males and their controls (see also fig. S8). Corresponding survival data are presented in Fig. 2, A and B. Points represent observed mortality rates. Lines are obtained by smoothing hazard rates (3-day window) by means of a kernel smoother prior to log transformation.

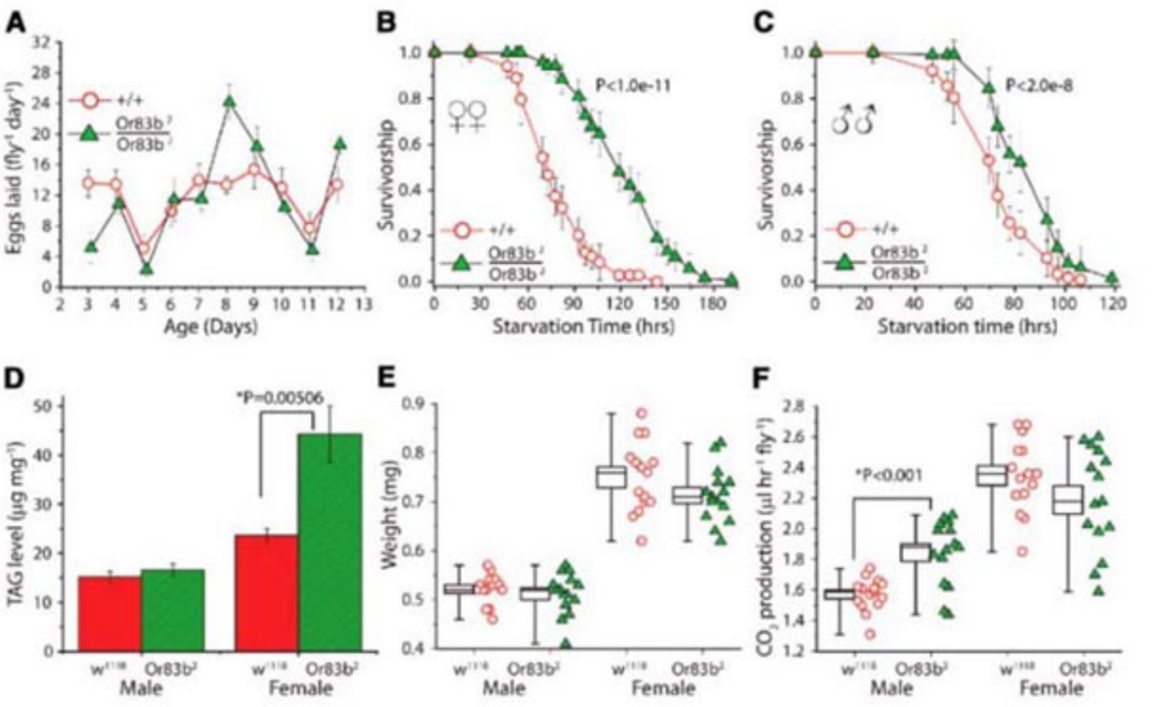

Fig. 4. *Or83b*^{2} flies exhibited altered physiology and enhanced stress resistance. (**A**) Total reproductive output through day 14 is not different between *Or83b* mutant and control females. Data represent average daily egg production per female (n = 60 females per genotype). Error bars represent 95% confidence intervals on the mean. *Or83b*^{2} mutants had significantly lower egg production over the first observation period (two-tailed Student's t test, $P = 0.0005$) and higher levels of egg production at age 8 and 12 days (two-tailed Student's t test, $P = 5.7 \times 10^{-5}$ and $P = 0.009$, respectively). (**B** and **C**) *Or83b*^{2} homozygous mutant flies are starvation resistant. Sample sizes (females): +/+, n = 79; –/–, n = 79. Sample sizes (males): +/+, n = 100; +/– n = 94. Statistical comparisons and P values were determined by means of a log-rank test. Error bars represent 95% confidence intervals on observed survivorship. (**D**) *Or83b*^{2} homozygous mutant flies have increased triglyceride levels. Triglyceride levels are presented after normalization to total weight. Error bars represent 95% confidence intervals. TAG, triacylglycerol. (**E** and **F**) Weight and CO_2 production for *Or83b*^{2} homozygous mutant and wild-type flies. Each point represents one fly (n = 15 for each sex and genotype). Box plots represent the median (horizontal line), 95% confidence intervals (box), and range (whiskers) of the data.

the case of *Or83b* mutation) ages. In females, the rate of increase in mortality with age was largely unaffected (Fig. 3, A and B, and fig. S8), an effect that is similar to diet restriction (*1*, *5*). In males, the impact of olfaction on mortality rate was reduced later in life; mortality trajectories converge at the oldest ages (Fig. 3C).

We next investigated whether olfactory function was required for longevity extension through diet manipulation. We measured male and female life span in different nutritional regimes ranging from severe nutrient restriction [3% sugar/yeast (SY) media] to nutrient-replete conditions (15% SY media). Flies homozygous for the *Or83b*^{2} mutation were consistently longer-lived than those of appropriate control stocks (Tables 1 and 2). Despite their exceptional longevity, life span was further increased in the *Or83b*^{2} mutants by dietary restriction. *Or83b* is therefore not required for diet-mediated longevity. Consistent with the yeast odorant results, however, we do find evidence for interaction between the olfactory and diet pathways. The relative increase in median and mean longevity in *Or83b*^{2} flies was significantly greater when flies were maintained in well-fed conditions (Tables 1 and 2), and mutant animals were partially resistant to changes in diet (fig. S9). Thus, the *Or83b* mutation extends longevity largely, but not exclusively, through a diet-independent pathway.

Reduced early reproductive output is not required for extended longevity in *Or83b*^{2} mutants. We observed the largest life-span extension in very high nutrient conditions where flies were provided access to live yeast paste (see Table 1), and, under these conditions, homo-

zygous *Or83b*^{2} mutant females had equal or greater reproductive output than control females (Fig. 4A). We consistently observed that *Or83b*^{2} mutants showed moderately reduced egg production from 24 to 48 hours post-eclosion, but the reason for this is unclear. Feeding rates are not reduced in mature flies (fig. S10), but reduced reproduction may be due to a delay in the onset of adult feeding, because the chemotaxis ability of mutant flies is compromised.

Or83b^2 flies exhibited a range of phenotypes indicative of altered physiology and enhanced stress resistance. Females were more resistant to hyperoxia (mean longevity = 110 ± 2.04 hours and 123 ± 1.0 hours for control and *Or83b*^{2} mutant females, respectively; $P < 1 \times 10^{-6}$, determined by means of a log-rank test). Mutants are resistant to starvation (Fig. 4, B and C), and females have significantly elevated levels of triglyceride, the primary lipid-storage molecule in *Drosophila* (Fig. 4D), despite their similar overall size and weight (Fig. 4E). Mutant males have higher but statistically indistinguishable levels of triglyceride, which suggests that life span and fat content are separable in this sex. The observed increases in longevity and stress resistance do not result from decreased metabolic rate (Fig. 4F).

Aging and longevity in *Caenorhabditis elegans* are regulated by sensory function through antagonistic effects of specific gustatory and olfactory neurons (*18*, *19*). Although the specific environmental cues that regulate longevity in *C. elegans* are unknown, sensory regulation of aging largely involves insulin/IGF (insulin-like growth factor) signaling (*18*). Modulation of aging by gustatory neurons is entirely insulin signaling (i.e., *daf-16*)–dependent, whereas longevity extension by the ablation of olfactory neurons has a large *daf-16*–independent component (*18*).

Sensory systems and insulin-mediated longevity regulation are evolutionarily conserved (*20*, *21*). Thus, as in *C. elegans*, olfaction may affect aging in *Drosophila* through altered insulin signaling and subsequent modulation of transcription factor dFOXO (the fly ortholog to *daf-16*). However, expression levels of *Drosophila* insulin-like peptides show no consistent differences in *Or83b*^{2} mutant flies (fig. S11). Consistent with normal levels of insulin signaling, we found that expression of *Thor*—the *Drosophila* homolog of mammalian *4E-BP* and a primary target of dFOXO (*22*)—is not elevated in the body of mutant animals (fig. S11). Olfactory regulation of aging in *Drosophila* may therefore contain a substantial component that is independent of insulin signaling.

We have identified a nutrient-related olfactory cue (odorants from live yeast) and a gene involved in olfaction (*Or83b*) that limit fly life span. Olfactory-receptor function constrains the beneficial effects of dietary restriction, indicating that consumption is not the only way that nutrient availability modulates longevity (*4*). Genetic dissection of the roles of conventional odorant receptors in the life span of *Drosophila* may reveal additional candidate odors and neural circuits for longevity regulation.

References and Notes

1. S. D. Pletcher *et al.*, *Curr. Biol.* **12**, 712 (2002).
2. J. Zheng, R. Mutcherson II, S. L. Helfand, *Aging Cell* **4**, 209 (2005).
3. T. G. Bross, B. Rogina, S. L. Helfand, *Aging Cell* **4**, 309 (2005).
4. G. B. Carvalho, P. Kapahi, S. Benzer, *Nat. Methods* **2**, 813 (2005).
5. W. Mair, P. Goymer, S. D. Pletcher, L. Partridge, *Science* **301**, 1731 (2003).
6. T. P. Good, M. Tatar, *J. Insect Physiol.* **47**, 1467 (2001).
7. W. Mair, M. D. W. Piper, L. Partridge, *PLoS Biol.* **3**, e223 (2005).
8. S. D. Pletcher, S. Libert, D. Skorupa, *Aging Res. Rev.* **4**, 451 (2005).
9. A. K. Chippindale, A. Leroi, S. B. Kim, M. R. Rose, *J. Evol. Biol.* **6**, 171 (1993).
10. L. B. Vosshall, A. M. Wong, R. Axel, *Cell* **102**, 147 (2000).
11. T. Elmore, R. Ignell, J. R. Carlson, D. P. Smith, *J. Neurosci.* **23**, 9906 (2003).
12. E. A. Hallem, M. G. Ho, J. R. Carlson, *Cell* **117**, 965 (2004).
13. S. A. Kreher, J. Y. Kwon, J. R. Carlson, *Neuron* **46**, 445 (2005).
14. M. C. Larsson *et al.*, *Neuron* **43**, 703 (2004).
15. R. Benton, S. Sachse, S. W. Michnick, L. B. Vosshall, *PLoS Biol.* **4**, e20 (2006).
16. E. M. Neuhaus *et al.*, *Nat. Neurosci.* **8**, 15 (2005).
17. W. C. Orr, R. S. Sohal, *Exp. Gerontol.* **38**, 227 (2003).
18. J. Alcedo, C. Kenyon, *Neuron* **41**, 45 (2004).
19. J. Apfeld, C. Kenyon, *Nature* **402**, 804 (1999).
20. A. Dahanukar, E. A. Hallem, J. R. Carlson, *Curr. Opin. Neurobiol.* **15**, 423 (2005).
21. M. Tatar, A. Bartke, A. Antebi, *Science* **299**, 1346 (2003).
22. M. Miron *et al.*, *Nat. Cell Biol.* **3**, 596 (2001).

23. We thank S. Lou, D. Skorupa, M. Tierney, and the Pletcher laboratory for help with *Drosophila* husbandry and metabolic assays; and J. Ferris for his technical assistance in the behavioral assays. C. Gendron, M. Tatar, three anonymous reviewers, and members of the Antebi laboratory provided comments on the manuscript. The research is supported by NIH (R01AG023166), Glenn Foundation, the Ellison Medical Foundation to S.D.P., and the American Federation for Aging Research to S.L. and S.D.P.

Supporting Online Material

www.sciencemag.org/cgi/content/full/1136610/DC1
Materials and Methods
Figs. S1 to S11
References

23 October 2006; accepted 23 January 2007
Published online 1 February 2007;
10.1126/science.1136610
Include this information when citing this paper.

Redirection of Silencing Targets by Adenosine-to-Inosine Editing of miRNAs

Yukio Kawahara,[1]*† Boris Zinshteyn,[1]† Praveen Sethupathy,[2] Hisashi Iizasa,[1] Artemis G. Hatzigeorgiou,[2,3] Kazuko Nishikura[1]*

Primary transcripts of certain microRNA (miRNA) genes are subject to RNA editing that converts adenosine to inosine. However, the importance of miRNA editing remains largely undetermined. Here we report that tissue-specific adenosine-to-inosine editing of miR-376 cluster transcripts leads to predominant expression of edited miR-376 isoform RNAs. One highly edited site is positioned in the middle of the 5′-proximal half "seed" region critical for the hybridization of miRNAs to targets. We provide evidence that the edited miR-376 RNA silences specifically a different set of genes. Repression of phosphoribosyl pyrophosphate synthetase 1, a target of the edited miR-376 RNA and an enzyme involved in the uric-acid synthesis pathway, contributes to tight and tissue-specific regulation of uric-acid levels, revealing a previously unknown role for RNA editing in miRNA-mediated gene silencing.

Many developmental and cellular processes are regulated by microRNA (miRNA)–mediated RNA interference (RNAi) (*1*–*4*). After incorporation into the RNA-induced silencing complex, miRNAs guide the RNAi machinery to their target genes by forming RNA duplexes, resulting in sequence-specific mRNA degradation or translational repression (*1*, *2*, *4*). The generation of mature miRNAs requires the processing of primary transcripts (pri-miRNAs) (*5*), and A → I RNA editing occurs to certain pri-miRNAs (*6*–*8*).

Human chromosome 14 and syntenic regions of the distal end of mouse chromosome 12 harbor the miR-376 cluster of miRNA genes (*9*).

[1]The Wistar Institute, 3601 Spruce Street, Philadelphia, PA 19104, USA. [2]Department of Genetics, School of Medicine, University of Pennsylvania, Philadelphia, PA 19104, USA. [3]Department of Computer and Information Science, School of Engineering and Applied Sciences, University of Pennsylvania, Philadelphia, PA 19104, USA.

*To whom correspondence should be addressed. E-mail: ykawahara@wistar.org (Y.K.); kazuko@wistar.org (K.N.)
†These authors contributed equally to this work.

The six human miR-376 RNAs (miR-376a2, -376b, -368, -B1, and -B2) (Fig. 1A) and three mouse miR-376a-c RNAs (fig. S1A) have highly similar sequences (fig. S2). Expression of miR-376 RNAs is detected in the placenta, developing embryos, and adult tissues (*9*, *10*).

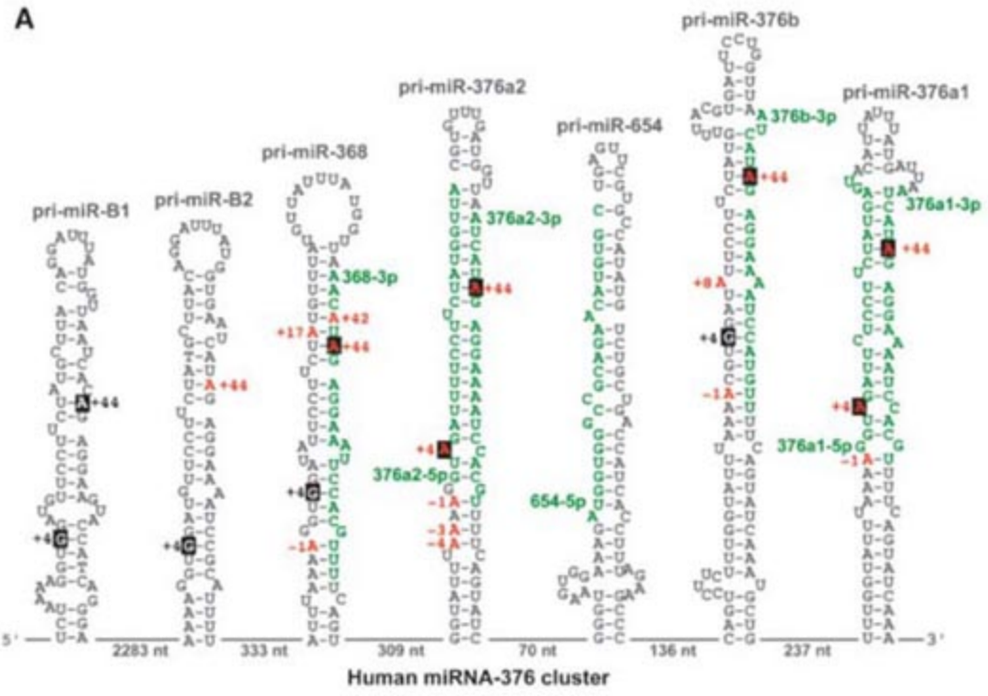

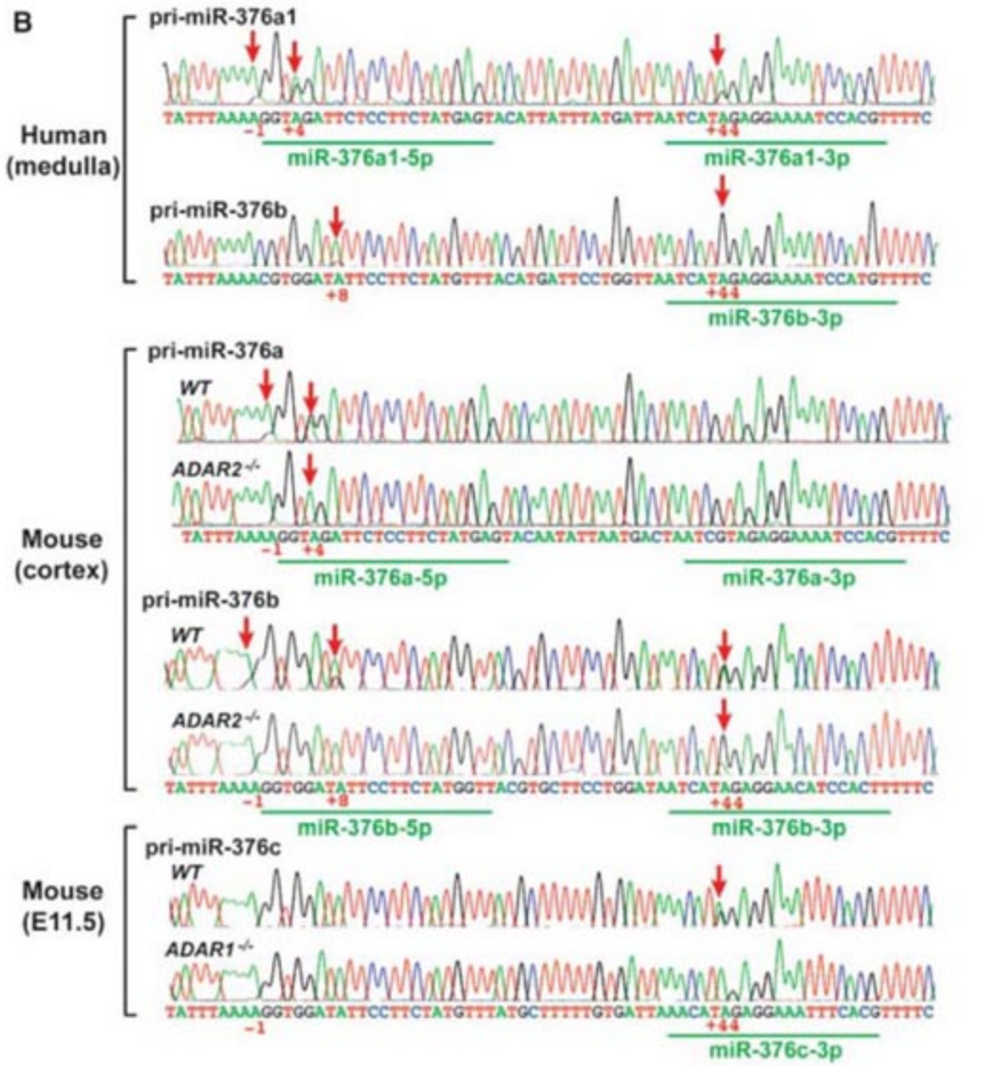

All of the miR-376 RNA cluster members are transcribed into a long primary transcript encompassing the entire region and (except human miR-B1) undergo extensive and simultaneous A → I editing at one or both of two specific sites (+4 and +44) in select human and mouse tissues and specific subregions of the brain (Fig. 2 and table S1) (*11*). The +4 site of some pri–miR-376 cluster genes (e.g., human -376b and -368) is genomically encoded as G and thus not subject to A → I editing (Fig. 1A). Certain miR-376 members, such as pri–miR-376a2, -376b, and -368, are nearly 100% edited at the +44 site in the human cortex and medulla (Figs. 1B and 2 and table S1), whereas no editing was detected in other tissues (e.g., the +4 site of human pri–miR-376a1 in liver and the +44 site of mouse pri–miR-376a in all tissues). In select members of the cluster, substantial editing (~20 to 55%) occurs at the –1 site, and infrequent editing occurs at several additional sites (table S1). In contrast, no editing was detected in human pri–miR-654 and mouse pri–miR-300. Although these two pri-miRNAs are located within the miR-376 cluster, their sequences are very different from those of miR-376 family members (fig. S2), indicating the strict selectivity of the editing machinery for pri–miR-376 family members and for specific A residues (+4 or +44 sites) within their foldback hairpin structures.

Two adenosine deaminases acting on RNA (ADARs), ADAR1 and ADAR2, are known to be involved in A → I editing (*12*–*15*). *ADAR2*$^{-/-}$ mice are viable (*16*), whereas *ADAR1*$^{-/-}$ mouse embryos die at embryonic day 12.0 (E12.0) (*17*, *18*). Analysis of RNA extracted from the brain cortices of *ADAR2*$^{-/-}$ mice and *ADAR1*$^{-/-}$ mouse E11.5 embryos revealed differences in the pri–miR-376 sites edited by ADAR1 and ADAR2. Editing of the –1 site of pri–miR-376a, pri–miR-376b, and pri–miR-376c, as well as the +4 site of pri–miR-376a, is almost eliminated in

Fig. 1. A → I RNA editing of pri–miR-376 RNAs. (**A**) Hairpin structures of six human pri–miR-376 RNAs are shown. Editing sites (red A's) are numbered with the 5′ end of the human miR-376a1-5p sequence counted as +1. Regions processed into mature miRNAs are highlighted in green. The two most highly edited A's (+4 and +44 sites, red As) are highlighted in black. The genomically encoded G at +4 is also highlighted in black. The genomic distance between miRNA genes is indicated by the numbers at the bottom. (**B**) Analysis of pri–miR-376a1 and pri–miR-376b RNAs in human and mouse brains (wild-type and *ADAR2*$^{-/-}$) and pri–miR-376c RNAs in mouse E11.5 embryos (wild-type and *ADAR1*$^{-/-}$) by sequencing of reverse transcription polymerase chain reaction (RT-PCR) products. Thus, an A → I RNA editing site is detected as an A → G change in the cDNA sequencing chromatogram. Editing of human pri–miR-376b at the +44 site is almost 100%, as seen by the presence of a sole G peak without an A peak. Editing sites are indicated by red arrows.

the cortex of *ADAR2*$^{-/-}$ mice. In contrast, the frequency of editing at the +44 site of pri–miR-376b and -376c is higher in *ADAR2*$^{-/-}$ mice, whereas editing of the +44 site was eliminated in *ADAR1*$^{-/-}$ embryos (Fig. 1B and table S1). The results indicate that the –1 and +4 sites are mainly edited by ADAR2. The +44 site is selectively edited by ADAR1. ADAR2, if coexpressed with ADAR1, appears to suppress ADAR1 activity.

Editing of pri-miRNAs could be biologically important by virtue of an effect on either the level of expression or on the function of miRNAs (*6*–*8*, *13*). Characterization of complementary DNA (cDNA) sequences corresponding to miR-376 cluster members revealed that the edited forms of mature miR-376 RNAs are highly expressed in certain tissues (Fig. 2). For instance, 41% of the miR-376a1-5p and 92% of the miR-368-3p molecules were edited at the +4 site and at the +44 site, respectively, in human medulla oblongata. In wild-type mouse cortex, 56% of miR-376c-3p molecules were edited at the +44 site, whereas 54% of the miR-376a-5p molecules were edited at the +4 site in wild-type mouse kidney. As expected from the editing frequency of pri–miR-376a2 RNA (98%), only the edited version of mature miR-376a2-5p was detected in the human medulla. Thus, editing does not affect the processing steps required for expression of mature miR-376 RNAs (Fig. 2).

Both of the major editing sites in pri–miR-376 RNAs (+4 and +44) are located within the functionally critical 5′-proximal "seed" sequences of miR-376-5p and -3p, suggesting that edited mature miR-376 RNAs may target genes different from those targeted by the unedited miR-376 RNAs. To investigate whether a single A → I base change at the +4 site of miR-376a-5p (which has identical human and mouse forms) would affect the selection of its target genes, we used an in-house computational algorithm, Diana-MicroT2, that predicts miRNA-to-target interactions, followed by the application of a species-conservation filter. We further filtered the predictions to retain only genes with multiple 3′ untranslated-region (UTR) target sites, with at least one of the sites being conserved. This filter yielded 78 target genes for unedited miR-376a-5p and 82 target genes for edited miR-376a-5p (conserved between human and mouse), with only two in common (fig. S3A and table S2). We randomly selected three unedited-version targets [SFRS11 (arginine/serine-rich splicing factor 11), SLC16A1 (solute carrier family 16-A1), and TTK (threonine and tyrosine kinase)] and three targets of the edited version [PRPS1 (phosphoribosyl pyrophosphate synthetase 1), ZNF513 (zinc finger protein 513), and SNX19 (sorting nexin 19)] for experimental verification (fig. S3B).

Luciferase expression was examined in HeLa cells cotransfected with reporter constructs containing the target sites for unedited or edited miR-376a-5p in their 3′UTRs (fig. S3C), together with unedited or edited miR-376a-5p RNAs. First, we used the edited miR-376a-5p RNA that had a G residue substituted for A at the +4 site. Specific repression of the edited-version and unedited-version target genes by edited and unedited miR-376a-5p RNAs, respectively, was observed (Fig. 3A). This selective silencing must be due to binding of edited (or unedited) miR-376a-5p RNAs specifically to their predicted target sites, because reciprocal cotransfection experiments resulted in no significant silencing (Fig. 3A). Experiments with the edited miR-376a-5p RNA that had an I residue at the +4 site again resulted in specific repression of the edited-version targets (Fig. 3B), revealing an equivalent contribution of I:C and G:C base pairs for hybridization of miRNAs to their targets. The A residue at the +4 site of unedited miR-376a-5p pairs with U residues of the unedited-version targets, whereas the I residue of the edited isoform pairs with C residues of the edited-version targets (fig. S3B). Our results suggest that a single A → I base change is sufficient to redirect silencing miRNAs to a new set of targets.

To confirm the in vivo effects of miR-376 RNA editing, we measured endogenous expression levels of unedited-version (TTK) and edited-version (PRPS1) miR-376a-5p target genes in wild-type and *ADAR2*$^{-/-}$ mouse cortices. The +4 site of miR-376a-5p is edited by ADAR2 almost exclusively (Fig. 1B). No edited mature miR-376a-5p is expressed in *ADAR2*$^{-/-}$ mice, whereas both unedited and edited miR-376a-5p is expressed in the brain cortex, heart, and kidney of wild-type mice (Fig. 2A). Only unedited mature miR-376a-5p RNAs were detected in the liver of wild-type mice because of an almost total lack of pri-miR376a RNA editing in this tissue (Fig. 2A and table S1). PRPS1, which contains multiple target sites for the edited version of miR-376a-5p within its 3′UTR, had levels that were almost two times lower in the wild-type mouse cortex than in the *ADAR2*$^{-/-}$ mouse cortex. In contrast, no difference in PRPS1 expression was detected between the wild-type and *ADAR2*$^{-/-}$ liver (Fig. 3C). We also confirmed that the expression level of total miR-376a-5p is not significantly different between wild-type and *ADAR2*$^{-/-}$ tissues by primer-extension analysis. Thus, the edited miR-376a-5p, expressed only in select tissues of wild-type mice, does indeed repress this target gene in a tissue-specific manner (Fig. 3C). No significant difference in TTK expression was detected between wild-type and *ADAR2*$^{-/-}$ corti-

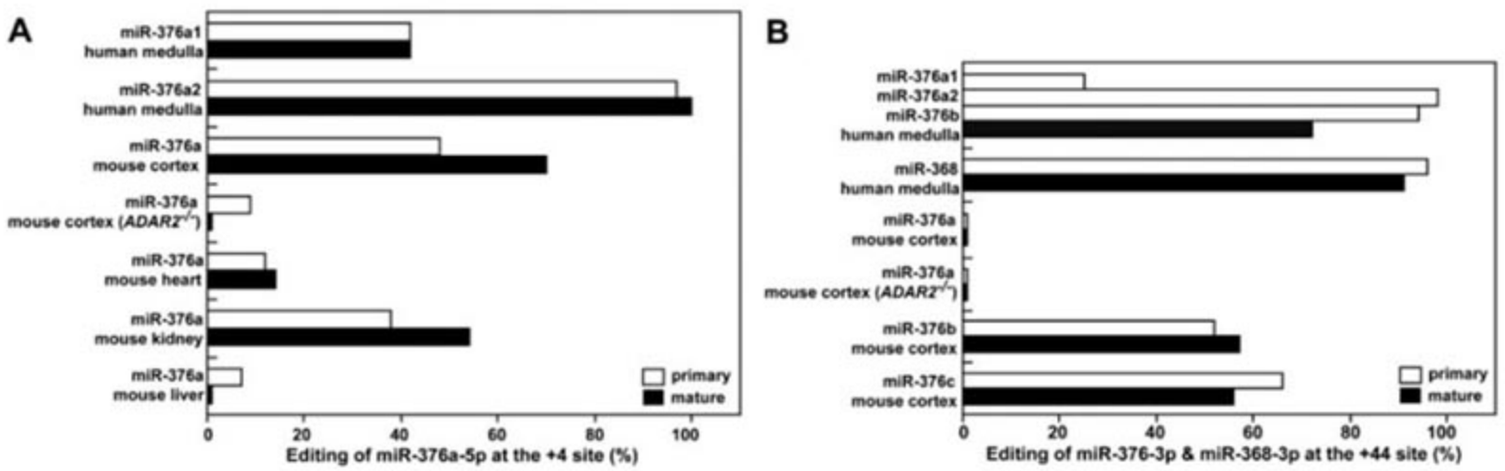

Fig. 2. Characterization of edited pri– and mature miR-376 RNAs in various tissues. (**A**) Editing frequency of pri– and mature miR-376a RNAs (5p strand) at the +4 site from various human and mouse tissues. (**B**) Editing frequency of pri– and mature miR-376a-c and miR-368 RNAs (3p strand) at the +44 site from subregions of human and mouse brains. The human mature miR-376a1-3p, miR-376a2-3p, and miR-376b-3p are not distinguishable in our assay, so the observed editing frequency represents the average of these three isoforms. [(A) and (B)] The editing frequency of pri-miRNAs is the ratio of the G peak over the sum of the G and A peaks of the sequencing chromatogram of RT-PCR products. Two separate measurements resulted in identical values. The editing frequency of mature miRNAs is a ratio of the cDNA clones containing the A → G change over the total cDNA clones examined (>50 isolates).

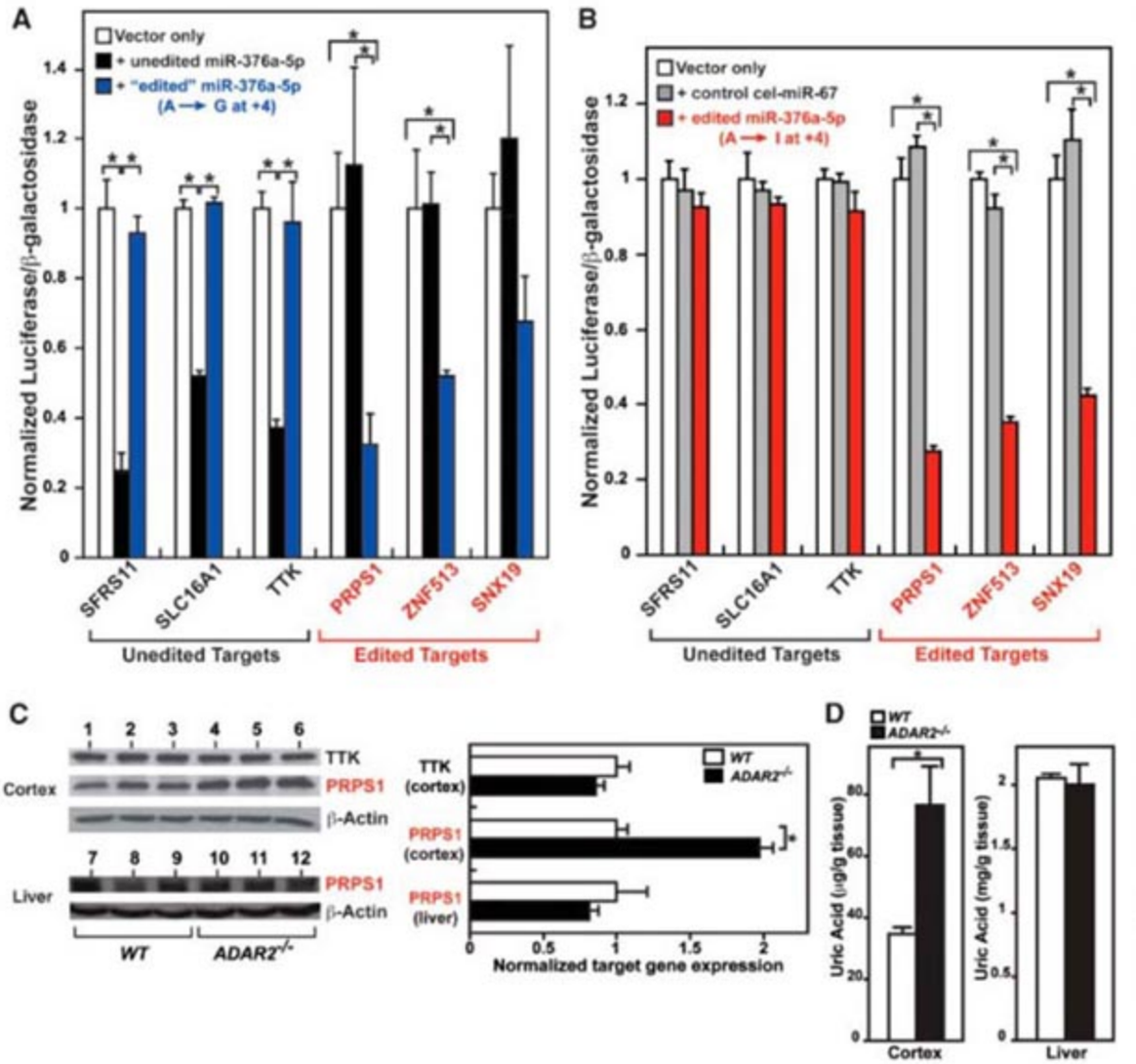

Fig. 3. Physiological effects of miR-376a RNA editing. (**A**) Confirmation of the edited miR-376a targets. Relative luciferase activities in HeLa cells cotransfected with unedited miR-376a-5p (black bars) and edited miR-376a-5p (A → G at the +4 site) (blue bars), respectively. Reciprocal experiments were also conducted; for example, miR-376a-5p edited-version target sites challenged by unedited miR-376a and vice versa. (**B**) Luciferase activities were examined in HeLa cells cotransfected with a negative control cel-miR-67 (gray bars) and edited miR-376a-5p (A → I at the +4 site) (red bars), respectively. [(A) and (B)] The luciferase activities were compared statistically by Mann-Whitney *U* tests. Significant differences are indicated by asterisks, $P < 0.05$. Error bars, SEM ($n = 3$, where n is the number of independent measurements taken). (**C**) Western blot analysis of TTK and PRPS1 expression levels in the wild-type and *ADAR2*$^{-/-}$ mouse cortex and liver. Significant differences are indicated by asterisks, $P < 0.05$. Error bars, SEM ($n = 3$). (**D**) Uric-acid levels in the wild-type and *ADAR2*$^{-/-}$ mouse cortex and liver. Significant difference is indicated by an asterisk, $P < 0.01$. Error bars, SEM ($n = 6$).

ces. The results indicate that unedited miR-376a-5p RNAs are sufficient to regulate this particular target gene, despite a threefold difference in expression between wild-type and *ADAR2*$^{-/-}$ mice (Fig. 2A).

PRPS1 is an essential housekeeping enzyme involved in purine metabolism and the uric-acid synthesis pathway. An X-chromosome–linked human disorder characterized by gout and neurodevelopmental impairment with hyperuricemia is caused by a two- to fourfold increase of PRPS1 levels, indicating the requirement for tight control of PRPS1 levels and activities (*19*). In order to confirm the biological importance of miR-376 editing, we examined uric-acid levels and found that tissue-specific repression of PRPS1 levels was indeed reflected in a twofold increase in uric-acid levels in *ADAR2*-null cortex (Fig. 3D). Thus, editing of miR-376a appears to be one of the mechanisms that ensure tight regulation of uric-acid levels in select tissues such as the brain cortex.

A systematic survey of human pri-miRNA sequences identified A → I editing sites in ~6% of all pri-miRNAs examined (*6*). However, this estimate may be too low (*6*): In vitro editing studies of randomly selected pri-miRNAs predict that as much as 50% of all pri-miRNAs may have specific A → I editing sites (*8*). Although expression of only one edited viral miRNA [miR-K12-10b (Kaposi sarcoma-associated virus miRNA)] has been reported previously (*20*), we predict that many additional edited isoforms of cellular miRNAs are likely to be identified in the future.

References and Notes

1. D. P. Bartel, *Cell* **116**, 281 (2004).
2. T. Du, P. D. Zamore, *Development* **132**, 4645 (2005).
3. S. M. Hammond, *Curr. Opin. Genet. Dev.* **16**, 4 (2006).
4. L. He, G. J. Hannon, *Nat. Rev. Genet.* **5**, 522 (2004).
5. V. N. Kim, *Nat. Rev. Mol. Cell Biol.* **6**, 376 (2005).
6. M. J. Blow *et al.*, *Genome Biol.* **7**, R27 (2006).
7. D. J. Luciano, H. Mirsky, N. J. Vendetti, S. Maas, *RNA* **10**, 1174 (2004).
8. W. Yang *et al.*, *Nat. Struct. Mol. Biol.* **13**, 13 (2006).
9. H. Seitz *et al.*, *Genome Res.* **14**, 1741 (2004).
10. M. N. Poy *et al.*, *Nature* **432**, 226 (2004).
11. Materials and methods are available as supporting material on *Science* Online.
12. B. L. Bass, *Annu. Rev. Biochem.* **71**, 817 (2002).
13. K. Nishikura, *Nat. Rev. Mol. Cell Biol.* **7**, 919 (2006).
14. R. A. Reenan, *Trends Genet.* **17**, 53 (2001).
15. P. H. Seeburg, *Neuron* **35**, 17 (2002).
16. M. Higuchi *et al.*, *Nature* **406**, 78 (2000).
17. J. C. Hartner *et al.*, *J. Biol. Chem.* **279**, 4894 (2004).
18. Q. Wang *et al.*, *J. Biol. Chem.* **279**, 4952 (2004).
19. M. Ahmed, W. Taylor, P. R. Smith, M. A. Becker, *J. Biol. Chem.* **274**, 7482 (1999).
20. S. Pfeffer *et al.*, *Nat. Methods* **2**, 269 (2005).

21. This work was supported in part by grants from NIH, the Juvenile Diabetes Research Foundation, the Commonwealth Universal Research Enhancement Program, and the Pennsylvania Department of Health (K.N.); and by a grant from NSF (AG.H.). P.S. is also supported by a predoctoral NIH training grant. We thank M. Higuchi and P. H. Seeburg for *ADAR2*$^{-/-}$ mice, Q. Wang for mouse embryo RNAs, Z. Mourelatos and J. M. Murray for reading and comments, and S. Lui and U. Samala for technical assistance.

Supporting Online Material

www.sciencemag/org/cgi/content/full/315/5815/1137/DC1
Materials and Methods
Fig. S1 to S3
Tables S1 to S3
References

28 November 2006; accepted 24 January 2007
10.1126/science.1138050

Gene Body–Specific Methylation on the Active X Chromosome

Asaf Hellman and Andrew Chess

Differential DNA methylation is important for the epigenetic regulation of gene expression. Allele-specific methylation of the inactive X chromosome has been demonstrated at promoter CpG islands, but the overall pattern of methylation on the active X (Xa) and inactive X (Xi) chromosomes is unknown. We performed allele-specific analysis of more than 1000 informative loci along the human X chromosome. The Xa displays more than two times as much allele-specific methylation as Xi. This methylation is concentrated at gene bodies, affecting multiple neighboring CpGs. Before X inactivation, all of these Xa gene body–methylated sites are biallelically methylated. Thus, a bipartite methylation-demethylation program results in Xa-specific hypomethylation at gene promoters and hypermethylation at gene bodies. These results suggest a relationship between global methylation and expression potentiality.

DNA methylation is essential for many developmental processes, including maintaining the silenced Xi state (*1*–*3*). Xi-specific methylation is seen at CpG islands (*4*–*9*), but the global distribution of Xi-specific methylation along the chromosome is unknown. Although silenced chromatin regions are usually hypermethylated, cytogenetic studies have suggested a global hypomethylation of the Xi (*10*); also, studies of mammalian hypoxanthine-guanine phosphoribosyltransferase (HPRT) genes have shown that at least one site within the transcribed region of the gene is methylated only on Xa in opposition to the Xi-specific methylation of the 5′ CpG island (*6*, *9*, *11*). This unexplained divergence led us to conduct a comprehensive analysis of the Xa and Xi allele–specific methylation patterns of the human X chromosome.

We modified the Affymetrix 500,000 (500K) single-nucleotide polymorphism (SNP) mapping array (*12*) to allow allele-specific analysis of DNA methylation (*13*). We digested genomic DNA with a cocktail of five methyl-sensitive restriction enzymes (MSREs) (*14*). Together, these frequent cutters recognize ~40% of all CG dinucleotides in the genome (*15*), allowing an efficient analysis of regions with both high and low GC content. After this pretreatment, fragments of 200 to 1100 base pairs containing the polymorphic sites were polymerase chain reaction (PCR) amplified, and the resulting amplicons were then labeled and hybridized to the array. Thus, an unmethylated MSRE site present on a given amplicon will lead to allele-specifically reduced intensity corresponding to the resident SNP (Fig. 1A). This allowed us to use either genotype calling or copy-number algorithms to identify transitions from a heterozygous state to a hemizygous state after the MSRE treatment. The assay is robust—replicate analyses of the same DNA never reveal allele-specific methylation status changing from one allele to the other [supporting online material (SOM) text 1]. Single locus validation included DNA sequencing of specific PCR products before and after MSRE treatment (table S1), and also bisulfite analyses (fig. S2).

Genotyping individuals from three generations of Centre d'Etude du Polymorphisme Humain (CEPH) pedigree 1332 (fig. S3) resolved the parental origins of 1948 heterozygous SNPs in the mother GM10849 and/or her daughter GM13130. Sequence analysis suggested that 1269 (65.1%) of them were suitable for our methylation assay, in that they had at least one methyl-sensitive restriction site on their respective amplicons (table S2). These informative SNPs were distributed along the chromosome (fig. S4) with an average distance of 120.1 kb between succeeding SNPs. Moreover, 351 SNPs mapped to 135 different genes (for an average of 2.6 SNPs per gene), representing ~9% of the known X-linked genes (table S2).

We resolved the active and inactive X copies in clones originated from single cells of GM10849

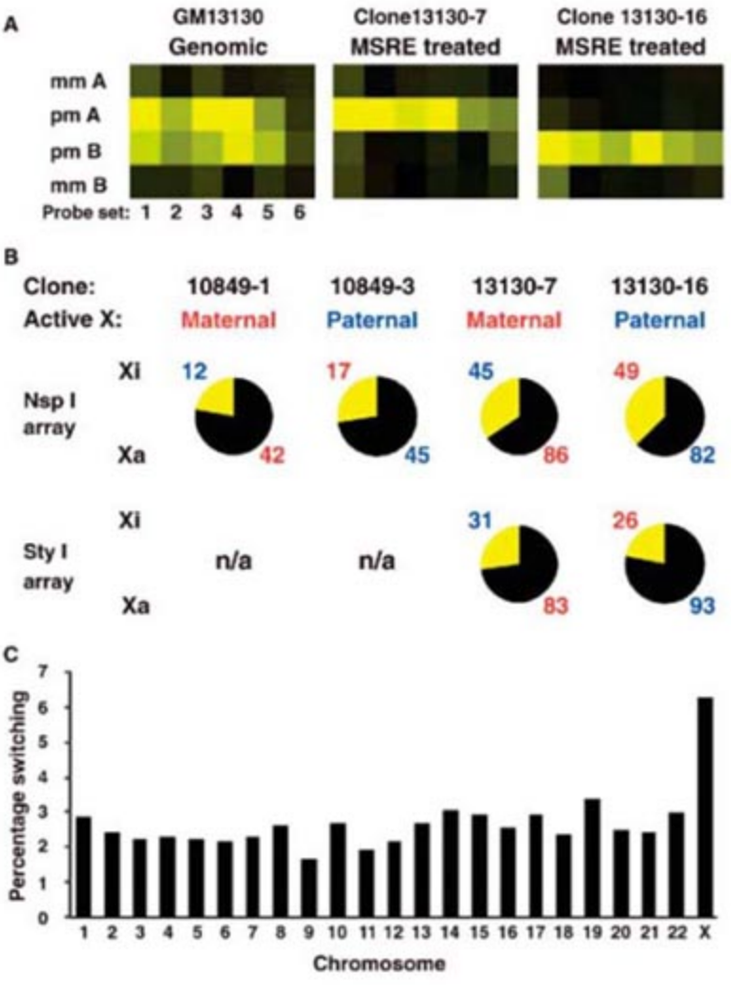

Fig. 1. Hypermethylation of the active X chromosome. (**A**) An example of hybridization intensities (brighter yellow indicates higher signal) for the six probe sets querying a particular SNP (rs16999756). When examining the perfect-match (pm) probes, one can observe both alleles in genomic DNA, but only one allele in each clone after MSRE treatment. This is due to methylation differences at an MSRE site present within the amplicon (fig. S1). Mismatch (mm) probes contain a single mismatch at a site distinct from the polymorphic site and serve as controls. (**B**) Presentations of Xa (black) and Xi (yellow) monoallelic methylation fractions in four clones from two individuals. The parental origin of Xa for each clone is indicated, and the numbers of occurrences of monoallelic methylation are marked blue (paternal) or red (maternal). Results from the Nsp I or the Sty I halves of the 500K array are presented. (**C**) Frequency of switching from heterozygous to hemizygous call after MSRE treatment for each chromosome. Data are presented for all informative 500K SNPs for GM13130 clone 7 and GM13130 clone 16. Potential monoallelic methylation at parentally imprinted regions, as well as technical artifacts resulting from MSRE site polymorphisms or allelic bias of the genotyping algorithm, were filtered out by requiring at least one clone switch from AB to A0, and one clone switch from AB to B0 per each SNP.

Center for Human Genetic Research and Department of Medicine, Massachusetts General Hospital, Harvard Medical School, 185 Cambridge Street, Boston, MA 02114, USA. E-mail: hellman@chgr.mgh.harvard.edu (A.H.); chess@chgr.mgh.harvard.edu (A.C.)

and GM13130 using reverse transcription (RT)–PCR to examine allele-specific mRNA expression (table S3). Replication timing analyses further confirmed the direction of X inactivation. We selected four clones, one paternal active (Xap) and one maternal active (Xam) from each individual, for further analysis. By definition, these clones must originate from four independent X inactivation events.

As a prelude to determining which heterozygous SNPs switch to a hemizygous state after digestion with the MSRE cocktail, we first filtered out SNPs that would show loss of heterozygosity as a result of polymorphism in their linked MSRE sites (fig. S1). We then analyzed the methylation status of the remaining 913 informative SNPs (table S4).

A pattern appeared when we related the SNPs to Xa and Xi: We always observed a significant excess of monoallelically methylated loci on the Xa. The average Xa:Xi ratio was 2.4 (Fig. 1B). The allele-specific methylation we observed is unique to the X chromosome, as shown by control analyses of autosomes, which show a vastly lower level of switching and no parent-of-origin effects (Fig. 1C and fig S5).

Because this global Xa hypermethylation is contrary to the reports of Xi-specific methylation at CpG islands, we sought to rule out the possibility that the clones we analyzed have unusual Xi methylation patterns. Two informative SNPs reside on amplicons that overlap with CpG islands: rs17139585 at phosphoglycerate kinase 1 and rs864570 at calcium/calmodulin-dependent serine protein kinase. As expected, these two SNPs are monoallelically methylated on their Xi alleles, indicating that our clones were not abnormal in their Xi methylation. Analysis of allele-specific methylation of the androgen receptor gene (*16*) further confirmed normal Xi promoter methylation (fig. S6).

To see if this methylation targets a unique set of loci, we analyzed overlapping among four clones by adding two more GM13130 clones (fig. S3). The extent of overlap among all combinations of three and four clones (table S5) was significantly higher than expected from a random distribution of Xa methylated amplicons along the chromosome ($P < 0.001$). Thus, a set of chromosomal locations are consistently Xa methylated.

We next examined whether these Xa-methylated sites related to genes. Out of the 116 SNPs that were Xa methylated in at least one Xam and one Xap clone, 57 (49.1%) were within known genes (Fig. 2 and table S6). This ratio is significantly higher ($P = 0.0009$) than the occurrence of gene SNPs in the entire informative set (251 out of 913 = 27.5%) (SOM text 2). Considering overlap in three and in four clones further highlighted gene exclusivity (table S7). All 17 amplicons displaying monoallelic Xa methylation in all four GM13130 clones were found either within genes or <50 kb from a gene (Fig. 2).

The CpG frequency in gene-body amplicons displaying Xa methylation is similar to the genome-wide average (table S8), well below the frequency seen in CpG islands. Nevertheless, nearby CpGs within different amplicons distantly present in the same gene (Fig. 2 and table S4), and neighboring CpGs within individual amplicons (fig. S7) tend to have the same Xa-specific methylation pattern.

Silencing tissue-specific genes does not explain Xa-specific gene-body methylation; indeed, mining public databases for tissue specificity and B cell line expression levels showed that both expressed and silenced genes undergo Xa-specific methylation (table S9). Furthermore, genes subject to Xa methylation do not share a common biological function or expression pattern (*17*). We cannot rule out a specific need for shutting down spurious transcription (e.g., from transposable elements) at active regions (i.e., genes), but the absence of a methylation bias toward repetitive elements embedded in genic amplicons (table S9) is a probable hint against this hypothesis. The list

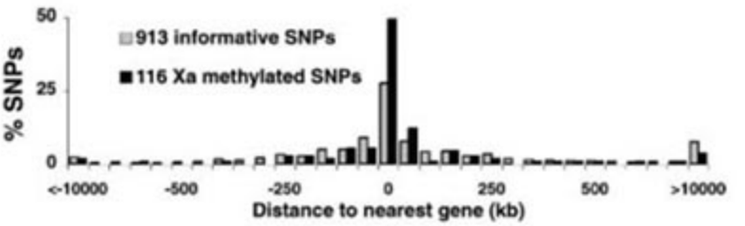

Fig. 2. Genes are preferable targets for Xa-specific methylation. (**Top**) Enrichment of Xa-methylated SNPs at gene regions. The distributions of Xa-methylated SNPs (black) and all informative SNPs (gray) are shown. SNPs were ranked according to distance from the nearest gene (table S6). (**Bottom**) The complete list of the SNPs showing Xa-specific methylations in all four clones from GM13130 is presented, with the methylated allele indicated for each clone (maternal in pink and paternal in blue).

SNP ID	Position	Gene	Gene relation (kb)	Clone 13130- 2	6	7	16
rs4826507	56693215	retro-UQCRB	upstream (46.2)	T	A	T	A
rs5931014	135698425	RBMX	upstream (10)	A	G	A	G
rs1638617	12576485	PRPS2	intron	C	G	C	G
rs2071211	21629701	MBTPS2	intron	C	T	C	T
rs5944690	24633379	POLA	intron	G	A	G	A
rs5972354	31036808	DMD	intron	C	T	C	T
rs17246798	37893629	RPGR	intron	G	A	G	A
rs6615850	95794852	DIAPH2	intron	T	A	T	A
rs5920651	96038343	DIAPH2	intron	T	G	T	G
rs5921728	96324533	DIAPH2	intron	A	G	A	G
rs5921827	96520713	DIAPH2	intron	G	A	G	A
rs42890	119360395	LAMP2	intron	T	G	T	G
rs209235	129073793	SUHW3	intron	T	C	T	C
rs5924843	149630958	CD99L2	intron	C	T	C	T
rs1212068	24323757	PDK3	downstream (11.6)	T	C	T	C
rs5951658	21699232	MBTPS2	downstream (38.7)	C	A	C	A
rs12557580	7900968	VCX2	downstream (46.8)	A	G	A	G

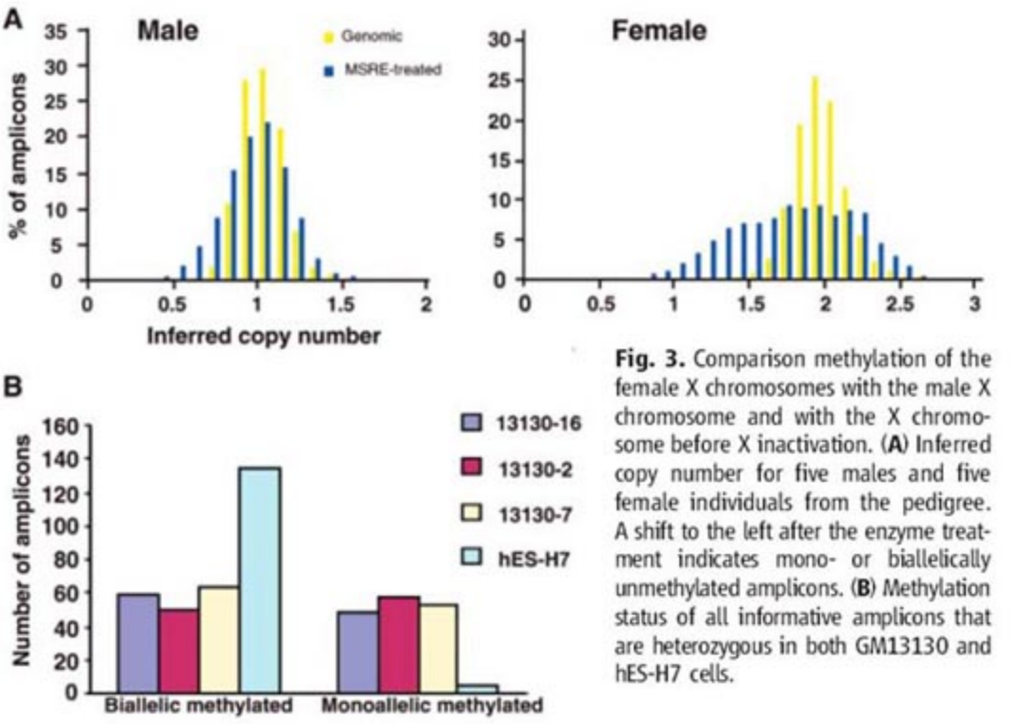

Fig. 3. Comparison methylation of the female X chromosomes with the male X chromosome and with the X chromosome before X inactivation. (**A**) Inferred copy number for five males and five female individuals from the pedigree. A shift to the left after the enzyme treatment indicates mono- or biallelically unmethylated amplicons. (**B**) Methylation status of all informative amplicons that are heterozygous in both GM13130 and hES-H7 cells.

of Xa-methylated genes contains several genes shown to escape X inactivation (*18*). However, given that these genes still have an elevated Xa expression level (*18*), the overall correlation between gene-body methylation and expression potentiality is maintained.

Male-to-female comparisons showed a more complete methylation level on the male X (Fig. 3A and fig. S8). Furthermore, the sites that are gene-body Xa-methylated in females are among the most highly methylated sites in males, highlighted even on the almost-complete methylation background of the male X chromosome (fig. S9).

An Xa-specific methylation present in somatic cells could reflect either methylation occurring only on Xa or demethylation occurring on Xi. The human embryonic stem (ES) cell line hES-H7 represents a stage of development just before X inactivation (*19*) and has been shown to stably maintain the appropriate characteristic methylation pattern for this stage, including allele-specific methylation (*20*). At this stage of development, the genome has presumably already undergone global demethylation and the wave of de novo methylation (*2*, *21*). Hence, we analyzed these cells using the 500K array. Out of the 116 amplicons shown to be gene-body Xa methylated, 50 also have a heterozygous genotype in H7 cells. We found that all 50 are biallelically methylated. When examining all 154 amplicons informative both for H7 and for 13130 clones, we observed that only five are monoallelically methylated in H7 cells, whereas the expected one-third are monoallelically methylated in the somatic clones (Fig. 3B). Bisulfite sequencing further verified biallelic methylation (fig. S10). Thus, given that biallelic methylation is the beginning state, demethylation of the Xi must account for the Xa-specific monoallelic pattern observed in somatic cells.

A simple model may explain both the Xa versus Xi and the gene versus intergenic differential methylation we observed: Constantly inactive regions, such as gene-poor regions and the entire Xi, may be more prone to loss of methylation maintenance (even if originally highly methylated). The resulting methylation decrease, for the entire Xi and for Xa intergenic regions, would thus highlight Xa gene body–specific methylation. At the same time, promoter CpG islands, which are protected from methylation on Xa, would remain more methylated on Xi.

In contrast to the widely held view that X chromosome allele-specific methylation is restricted to CpG islands on the inactive X, our global allele-specific methylation analyses uncovered extensive methylation specifically affecting transcribable regions (gene bodies) on the active X whether it is in the male or the female. One aspect of sex chromosome dosage compensation is the requirement for a chromosome-wide, likely epigenetic mechanism with the ability to double X-linked gene expression when necessary (i.e., in somatic cells but not in haploid germline cells). Indeed, such a phenomenon was recently described in mammals (*22*). Our finding of global elevation of methylation levels at gene bodies of both male and female active X chromosomes hints at such a chromosome-wide epigenetic control. Another example of a possible role for methylation in (potentially) active chromatin regions recently came from plants, in which extensive specific methylation of gene bodies was discovered (*23*). These results, together with the findings introduced here, should prompt reevaluation of the role of global DNA methylation that occurs away from gene promoters as well as the apparently complex relationship with chromatin activity.

Note added in proof. A second manuscript reporting gene body methylation in plants was recently published (*29*).

References and Notes

1. A. Bird, *Genes Dev.* **16**, 6 (2002).
2. T. Hashimshony, J. Zhang, I. Keshet, M. Bustin, H. Cedar, *Nat. Genet.* **34**, 187 (2003).
3. T. Mohandas, R. S. Sparkes, L. J. Shapiro, *Science* **211**, 393 (1981).
4. S. L. Gilbert, P. A. Sharp, *Proc. Natl. Acad. Sci. U.S.A.* **96**, 13825 (1999).
5. E. Heard, *Curr. Opin. Cell Biol.* **16**, 247 (2004).
6. L. F. Lock, D. W. Melton, C. T. Caskey, G. R. Martin, *Mol. Cell. Biol.* **6**, 914 (1986).
7. L. F. Lock, N. Takagi, G. R. Martin, *Cell* **48**, 39 (1987).
8. S. F. Wolf, D. J. Jolly, K. D. Lunnen, T. Friedmann, B. R. Migeon, *Proc. Natl. Acad. Sci. U.S.A.* **81**, 2806 (1984).
9. P. H. Yen, P. Patel, A. C. Chinault, T. Mohandas, L. J. Shapiro, *Proc. Natl. Acad. Sci. U.S.A.* **81**, 1759 (1984).
10. E. Viegas-Pequignot, B. Dutrillaux, G. Thomas, *Proc. Natl. Acad. Sci. U.S.A.* **85**, 7657 (1988).
11. Another recent study came to a conclusion that there is hypomethylation at gene-poor regions of the X chromosome, leading to an overall hypomethylation of Xi (*24*). Their conclusions are based entirely on the assumption that the single X chromosome of males is identical to Xa in female cells. In any case, our direct allele-specific analyses reveal only a modest hypomethylation of Xi in gene-poor regions, but a strong signature of Xi hypomethylation in gene bodies.
12. Details about the Affymetrix 500K SNP mapping array are available online (www.affymetrix.com).
13. A number of medium- to high-throughput assays have been described to analyze DNA methylation (*15*, *23*–*28*). Our methodology is most similar to the assay that used the 10K array (*28*).
14. The cocktail includes Aci I, BsaH I, Hha I, Hpa II, and HpyCH4 IV.
15. A. Schumacher *et al.*, *Nucleic Acids Res.* **34**, 528 (2006).
16. R. C. Allen, H. Y. Zoghbi, A. B. Moseley, H. M. Rosenblatt, J. W. Belmont, *Am. J. Hum. Genet.* **51**, 1229 (1992).
17. Materials and methods are available as supporting material on *Science* Online.
18. L. Carrel, H. F. Willard, *Nature* **434**, 400 (2005).
19. L. M. Hoffman *et al.*, *Stem Cells* **23**, 1468 (2005).
20. P. J. Rugg-Gunn, A. C. Ferguson-Smith, R. A. Pedersen, *Nat. Genet.* **37**, 585 (2005).
21. D. Frank *et al.*, *Nature* **351**, 239 (1991).
22. D. K. Nguyen, C. M. Disteche, *Nat. Genet.* **38**, 47 (2006).
23. X. Zhang *et al.*, *Cell* **126**, 1189 (2006).
24. M. Weber *et al.*, *Nat. Genet.* **37**, 853 (2005).
25. M. Bibikova *et al.*, *Genome Res.* **16**, 383 (2006).
26. I. Keshet *et al.*, *Nat. Genet.* **38**, 149 (2006).
27. C. M. Valley, H. F. Willard, *Curr. Opin. Genet. Dev.* **16**, 240 (2006).
28. E. Yuan *et al.*, *Cancer Res.* **66**, 3443 (2006).
29. D. Zilberman, M. Gehring, R. K. Tran, T. Ballinger, J. Henikoff, *Nat. Genet.* **39**, 61 (2007).

30. We thank H. Cedar, D. Housman, and J. Lee for discussions and comments and the staff of Harvard Medical School–Partners Healthcare Center for Genetics and Genomics Microarray Facility for Affymetrix array experiments. Support came from the NIH (to A.C.).

Supporting Online Material

www.sciencemag.org/cgi/content/full/315/5815/1141/DC1
Materials and Methods
SOM Text
Figs. S1 to S10
Tables S1 to S9

16 October 2006; accepted 22 January 2007
10.1126/science.1136352

Reversal of Neurological Defects in a Mouse Model of Rett Syndrome

Jacky Guy,[1] Jian Gan,[2] Jim Selfridge,[1] Stuart Cobb,[2] Adrian Bird[1]*

Rett syndrome is an autism spectrum disorder caused by mosaic expression of mutant copies of the X-linked *MECP2* gene in neurons. However, neurons do not die, which suggests that this is not a neurodegenerative disorder. An important question for future therapeutic approaches to this and related disorders concerns phenotypic reversibility. Can viable but defective neurons be repaired, or is the damage done during development without normal MeCP2 irrevocable? Using a mouse model, we demonstrate robust phenotypic reversal, as activation of MeCP2 expression leads to striking loss of advanced neurological symptoms in both immature and mature adult animals.

Mutations in the X-linked *MECP2* gene are the primary cause of Rett syndrome (RTT), a severe autism spectrum disorder with delayed onset that affects 1 in 10,000 girls (*1*). *MECP2* mutations are also found in patients with other neurological conditions, including learning disability, neonatal encephalopathy, autism, and X-linked mental

retardation (*2*). RTT patients show abnormal neuronal morphology, but not neuronal death (*3*), which implies that it is a neurodevelopmental rather than a neurodegenerative disorder. MeCP2 is expressed widely, but is most abundant in neurons of the mature nervous system (*4*). Conditional deletion and neuron-specific expression of *Mecp2* in mice showed that the mutant phenotype is specifically due to absence of MeCP2 in neurons (*5*–*7*). The persistent viability of mutant neurons in RTT patients raises the possibility that reexpression of MeCP2 might restore full function and, thereby, reverse RTT. Alternatively, MeCP2 may be essential for neuronal development during a specific time window, after which damage caused by its absence is irreversible. To distinguish these possibilities, we created a mouse in which the endogenous *Mecp2* gene is silenced by insertion of a *lox-Stop* cassette (*8*), but can be conditionally activated under the control of its own promoter and regulatory elements by cassette deletion (*9*) (fig. S1). Western blots (Fig. 1A) and in situ immunofluorescence (Fig. 1B) confirmed absence of detectable MeCP2 protein in $Mecp2^{lox\text{-}Stop/y}$ (*Stop/y*) animals. Like *Mecp2*-null mice (*6*), *Stop/y* males developed symptoms at ~6 weeks and survived for 11 weeks, on average, from birth (Fig. 1C). We concluded that the $Mecp2^{lox\text{-}Stop}$ allele behaves as a null mutation.

To control the activation of *Mecp2*, we combined a transgene expressing a fusion between Cre recombinase and a modified estrogen receptor (*cre-ER*) with the $Mecp2^{lox\text{-}Stop}$ allele (*10*). The Cre-ER protein remains in the cytoplasm unless exposed to the estrogen analog tamoxifen (TM), which causes it to translocate to the nucleus. To verify that the Cre-ER molecule did not spuriously enter the nucleus in the absence of TM and cause unscheduled deletion of the *lox-Stop* cassette, we looked for signs of *lox-Stop* deletion in $Mecp2^{lox\text{-}Stop/+}$,*cre-ER* (*Stop/+,cre*) females by Southern blotting. Even after 10 months in the presence of cytoplasmic Cre-ER, there was no sign of the deleted allele (Fig. 1D). The absence of spontaneous deletion of the *lox-Stop* cassette was independently confirmed by the finding that *Stop/y* males showed identical survival profiles in the presence or absence of Cre-ER (Fig. 1C). Therefore, in the absence of TM, the Cre-ER molecule does not cause detectable deletion of the *lox-Stop* cassette.

We next tested the ability of TM to delete the *lox-Stop* cassette in $Mecp2^{lox\text{-}Stop/y}$,*cre-ER* (*Stop/y,cre*) male mice. Five daily injections 3 to 4 weeks after birth caused 75 to 81% deletion of the cassette in brain (Fig. 1E, lanes 3, 4, and 6) and led to reexpression of the *Mecp2* gene as measured by Western blotting (Fig. 1A, lanes 4 and 5) and MeCP2 immunostaining of neurons (Fig. 1B). Activation of *Mecp2* in *Stop/y,cre* males at this stage [(Fig. 2A), bracket TM-1], before symptom onset, revealed toxicity associated with abrupt *Mecp2* reactivation, as 9 out of 17 mice developed neurological symptoms and died soon after the daily TM injection series (fig. S2). The remaining eight mice, however, did not develop any detectable symptoms, showed wild-type survival (fig. S2), and were able to breed. Four retained mice have survived for >15 months. Death of about half of animals was not due to intrinsic TM toxicity, because injected controls, including mice that had either the *Stop* allele or the *cre-ER* transgene (but not both), were unaffected. The toxic effects resembled those caused by overexpression of an *Mecp2* transgene in mice (*7*, *11*), although the reactivated *Mecp2* gene retains its native promoter. The data indicate that sudden widespread activation of the *Mecp2* gene leads to either rapid death or complete phenotypic rescue.

We found that a more gradual *Mecp2* activation induced by weekly TM injections followed by three daily booster treatments eliminated toxicity. Using this scheme, we asked whether *Stop/y,cre* male mice with advanced symptoms [(Fig. 2A), bracket TM-2] could be rescued by restoration of MeCP2. To monitor the specific features of the RTT-like mouse phenotype, we devised simple observational tests for inertia, gait, hind-limb clasping, tremor, irregular breathing, and poor general condition. Each symptom was scored weekly as absent, present, or severe (scores of 0, 1, and 2, respectively). Wild-type mice always scored zero (Fig. 2B), whereas *Stop/y* animals typically showed progression of aggregate symptom scores (e.g., from 3 to 10) during the last 4 weeks of life (Fig. 2, C and E). By contrast, five out of six symptomatic *Stop/y,cre* animals were rescued by TM treat-

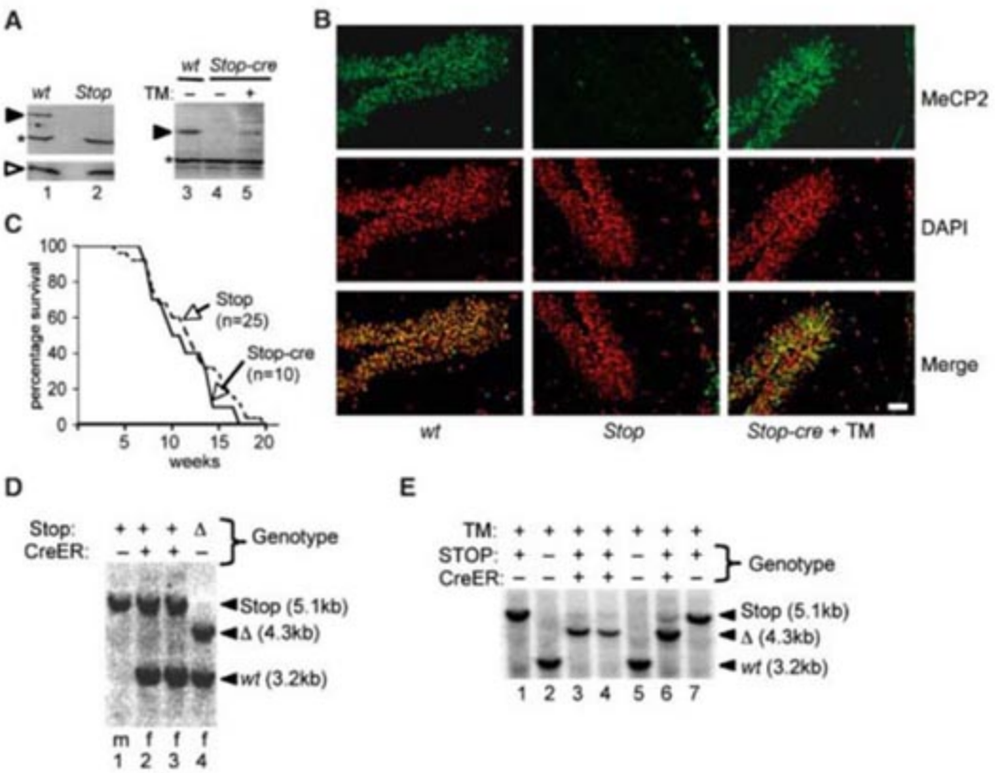

Fig. 1. Insertion of a *lox-Stop* cassette into intron 2 of the mouse *Mecp2* gene creates an allele that is effectively null, but can be activated by TM treatment. (**A**) Western blot analysis of MeCP2 protein (solid arrow) in brains of wild-type (*wt*), *Stop/y*, and *Stop/y,cre* mice before and after TM. Antibodies against MeCP2 were from J. Pevsner (left panel) and Upstate (right panel). Internal controls are nonspecific cross-reacting bands (asterisk) and bands generated by a histone H4–specific antibody (open arrow). (**B**) Detection of MeCP2 by in situ immunofluorescence in dentate gyrus of wild-type (*wt*), *Stop/y*, and TM-treated *Stop/y,cre* mice. White scale bar, 50 μm. Green cells that did not stain with DAPI (4′,6′-diamidino-2-phenylindole) in the upper *Stop* panel are nonnucleate erythrocytes showing background fluorescence. The DAPI channel was changed from blue to red using Adobe Photoshop to contrast with the green MeCP2 signal. (**C**) Comparison of the survival of *Stop/y* mice with and without the *cre-ER* transgene. (**D**) A Southern blot assay for deletion of the *lox-Stop* cassette in brains of heterozygous *Stop/+,cre* females (f) aged 10 months (lanes 2 and 3) that had not been exposed to TM. Restriction fragments from the *Mecp2 lox-Stop* (*Stop*; see male $Mecp2^{lox\text{-}Stop/y}$, lane 1), $Mecp2^{\Delta}$ with Stop deleted (Δ, see lane 4), and the wild-type (*wt*) alleles are indicated. (**E**) Southern blot assay for conversion of the *Stop* allele to the $Mecp2^{\Delta}$ allele (Δ) in male mouse brains after five daily TM injections. Lanes 2 and 5 show the *wt* allele.

[1]Wellcome Trust Centre for Cell Biology, Edinburgh University, The King's Buildings, Edinburgh EH9 3JR, UK. [2]Neuroscience and Biomedical Systems, Institute of Biomedical and Life Sciences, West Medical Building, University of Glasgow, Glasgow G12 8QQ, UK.

*To whom correspondence should be addressed. E-mail: a.bird@ed.ac.uk

ment. These animals initially had symptom scores of 2 or 3 and would be expected to survive for up to 4 weeks from the date of the first injection. Instead, they showed mild symptoms (see fig. S3 for examples of detailed scores) and survived well beyond the maximum-recorded life span of *Mecp2*$^{lox\text{-}Stop/y}$ animals (17 weeks) (Fig. 2, D to F, and fig. S4; see movies S1 and S2). The weekly TM injection regime, plus booster injections, gave the same level of *lox-Stop* cassette deletion as five daily TM injections (~80%) (Fig. 2G). The one animal that died had reduced *lox-Stop* cassette deletion (~50% compared with ~80%), which may explain failure to rescue.

RTT results from mosaic expression of mutant and wild-type *MECP2* alleles in the brain caused by the random inactivation of one X-linked *MECP2* allele during early female development. Heterozygous female mice may be the most appropriate model for human RTT (*12*), because both *Mecp2*$^{+/-}$ (*6*) and *Stop/+* females (Fig. 3, A, B, and E) develop RTT-like symptoms, including inertia, irregular breathing, abnormal gait, and hind-limb clasping, at 4 to 12 months of age. As in humans, the phenotype stabilizes, and the animals have an apparently normal life span. The mice often become obese, which is not a feature of the human condition. In an attempt to reverse the neurological phenotype in mature female heterozygotes, we TM-treated *Stop/+,cre* females with clear neurological symptoms. These mice progressively reverted to a phenotype that scored at or close to wild type (Fig. 3, C to E, and fig. S5 and movie S3; see fig. S3 for examples of detailed scores), including normalized weight (Fig. 3D and fig. S6). Mouse 5, for example, had a phenotypic score close to the usual plateau level and was obese at commencement of the weekly TM injection regime, but these features were both reversed (Fig. 3D). On the other hand, *Stop/+* females lacking Cre-ER did not respond to TM. Southern blots showed levels of cassette deletion in *Stop/+,cre* females that were consistently close to 50% (Fig. 3F). As the great majority of neurons became MeCP2-positive after TM treatment (fig. S7), we suspect that recombination predominantly occurs on the active X-chromosome (see legend to fig. S7). The results demonstrate that late-onset neurological symptoms in mature adult *Stop/+,cre* heterozygotes are reversible by de novo expression of MeCP2.

We also assessed the effect of *Mecp2* activation on neuronal signaling. Long-term potentiation (LTP) is reduced in the hippocampus of *Mecp2*-mutant male mice (*13*, *14*), but heterozygous females have not been tested. We performed electrophysiological analysis of *Mecp2*$^{+/-}$ heterozygous females (*6*) before and after onset of overt symptoms using both high-frequency stimulation and theta-burst (TBS) LTP induction protocols. Stimulation-response curves showed that the strength of basal synaptic transmission did not differ between symptomatic or presymptomatic *Mecp2*$^{+/-}$ female mice and wild-type littermate controls (Fig. 4A). In addition, no significant difference in hippocampal LTP between wild-type and presymptomatic females was detected. After symptom onset, however, LTP was significantly reduced in *Mecp2*$^{+/-}$ females with both protocols (Fig. 4, B and C). The magnitude of the defect was similar to that reported in *Mecp2*-null mice (*13*). To test for reversal of this effect, we measured LTP in six *Stop/+,cre* females that were TM-treated following the appearance of symptoms. LTP was measured 18 to 26 weeks after commencement of TM treatment. Control *Stop/+* and wild-type animals were also TM-treated and analyzed. The hippocampal LTP deficit was evident in symptomatic *Stop/+* mice lacking the *cre-ER* transgene, but in TM-treated *Stop/+,cre* mice, LTP was indistinguishable from wild type (Fig. 4D), which demonstrates that this pronounced electrophysiological defect is abolished in mature adults by restoration of MeCP2.

Our data show that developmental absence of MeCP2 does not irreversibly damage neurons, which suggests that RTT is not strictly a neurodevelopmental disorder. The delayed onset of behavioral and LTP phenotypes in *Mecp2*$^{+/-}$ females emphasizes the initial functional integrity of MeCP2-deficient neurons and fits with the proposal that MeCP2 is required to stabilize and maintain the mature neuronal state (*4*, *6*). Consistent with the maintenance hypothesis, the time taken for major symptoms to appear postnatally in females heterozygous for an *MECP2* mutation is similar in humans (6 to 18 months) and mice (4 to 12 months), despite fundamental interspecies differences in developmental maturity at this time. The restoration of neuronal function by late expression of MeCP2 suggests that the molecular preconditions for normal MeCP2 activity are preserved in its absence. To explain this, we propose that essential MeCP2 target sites in neuronal genomes are encoded solely by patterns of DNA methylation that are established and maintained normally in cells lacking the protein. According to this hypothesis, newly synthesized MeCP2 molecules home to their correct chromosomal positions as dictated by methyl-CpG patterns and, once in place, re-

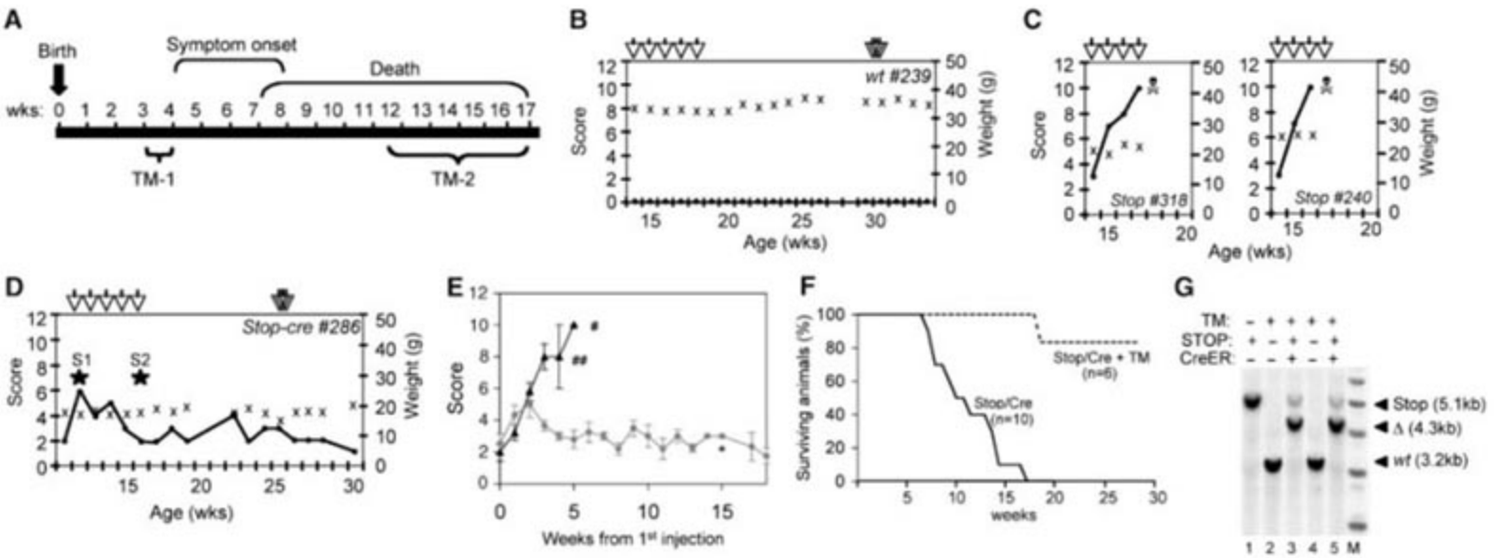

Fig. 2. Reversal of the neurological phenotype by activation of the *Mecp2* gene in *Stop/y,cre* males. (**A**) Time course of the *Stop/y* phenotype. (**B**, **C**, and **D**) Plots of the phenotypic scores (●) and weights (x) of individual wild-type (*wt*) (B), *Stop/y* (*Stop*) (C), and *Mecp2*$^{lox\text{-}Stop/y}$*,cre-ER* (*Stop-cre*) (D) animals after TM injections (vertical arrows). (See also fig. S2.) Stars in (D) indicate when the clips shown in movies S1 and S2 were recorded. (**E**) Aggregate symptom score profiles following TM injection of *Stop/y,cre* (○, n = 3 to 6, except *, which was a single animal) and *Stop/y* (▲, n = 4 to 5; except ## and #, which are 2 and 1 data points, respectively) mice. (**F**) Survival profiles of TM-treated *Stop/y,cre* mice and control *Stop/y* mice. (**G**) Southern blot showing deletion of the lox-Stop cassette (lanes 3 and 5) after a weekly TM injection regime + booster injections.

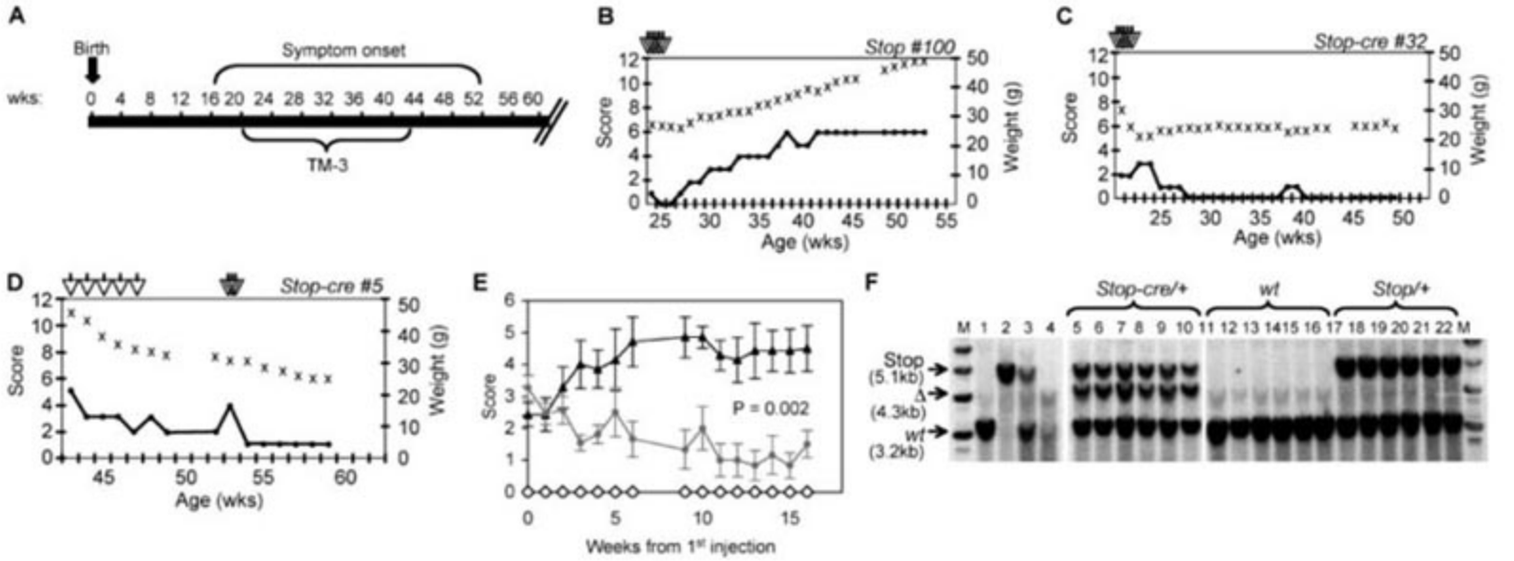

Fig. 3. Reversal of late-onset neurological symptoms by *Mecp2* gene induction in mature adult *Stop/+,cre* females. (**A**) Time course of symptom onset. TM administration began during the bracketed period (TM3). (**B**, **C**, and **D**) Phenotype (●) and weight (x) profiles for a *Stop/+* female (B) and two *Stop/+,cre* females (C and D). All animals shown were subjected to either five daily TM injections or five weekly plus three booster TM injections (vertical arrows). Animals subject to weekly injection regimes were scored blind as part of a mixed genotype cohort. (**E**) Plot of average symptom scores for females with *wt* (◇, $n = 5$ to 6), *Stop/+* (▲, $n = 6$ to 7), and *Stop,+,cre* (○, $n = 5$ to 11) genotypes. Repeated measures analysis of variance (ANOVA) compared *Stop/+* and *Stop/+,cre* female scores in weeks 11 to 16. (**F**) Southern blot analysis of the effects of TM treatment on a cohort including six *Stop/+,cre* (lanes 5 to 10), six *wt* (lanes 11 to 16) and six *Stop/+* (lanes 17 to 22) females. All three genotypes received TM. Restriction fragments derived from *Mecp2 lox-Stop* (Stop), deleted $Mecp2^{\Delta}$ (Δ) and wild type (*wt*) are marked with arrows. Brain DNA from animals 32 and 5 shown above are in lanes 9 and 6, respectively. Lanes 1 to 4 show blots of *wt* male, *Stop/y* male, *Stop/+* female, and $Mecp2^{\Delta/+}$ female, respectively.

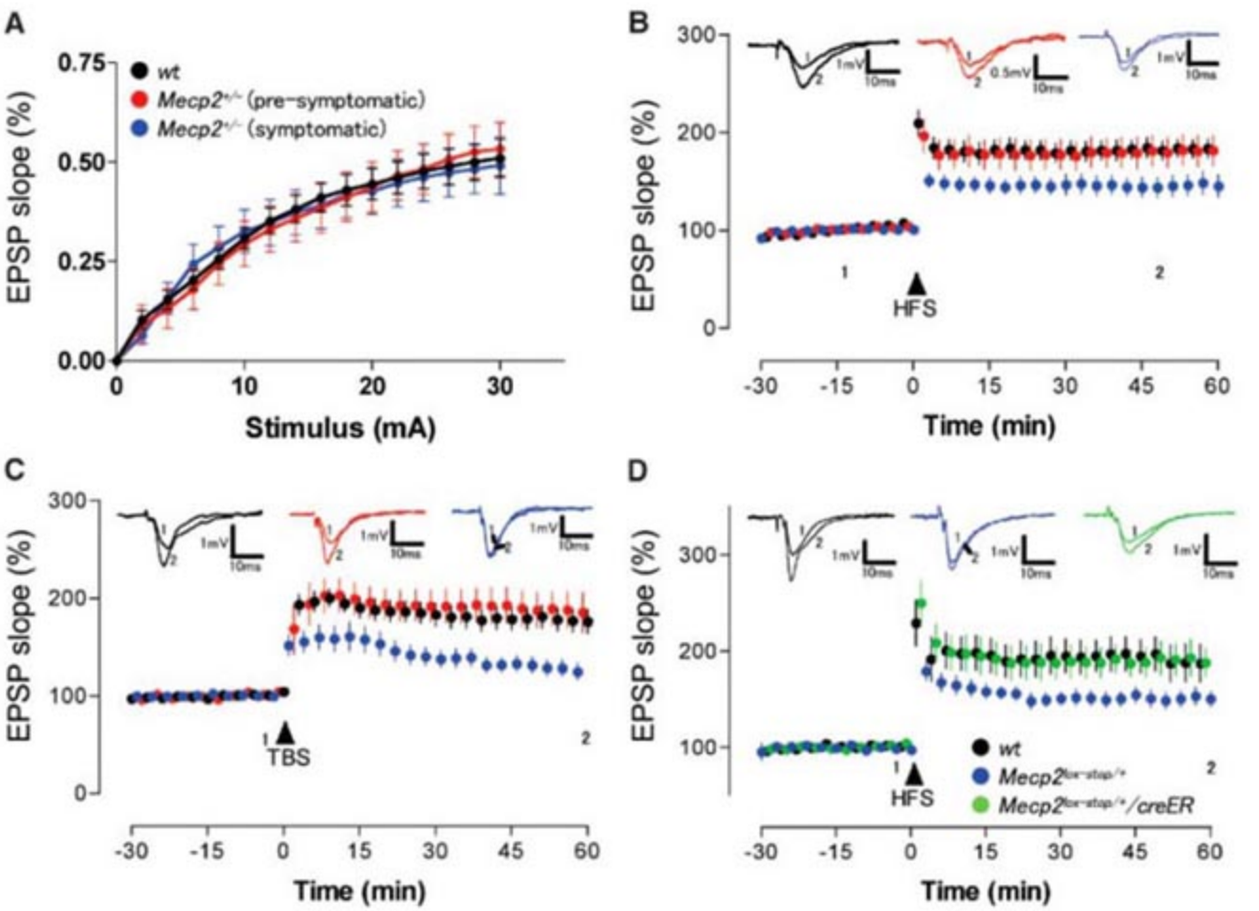

Fig. 4. A deficit in long-term potentiation (LTP) accompanies onset of symptoms in mature adult $Mecp2^{lox\text{-}Stop/+}$ heterozygous females and is reversed by *Mecp2* reactivation. (**A**) Stimulation-response curves in symptomatic (blue) or presymptomatic (red) $Mecp2^{+/-}$ female mice and *wt* littermate controls (black; all $P > 0.05$). (**B**) Measurements of LTP using a high-frequency stimulation (HFS) paradigm in presymptomatic ($n = 9$; $P > 0.05$), symptomatic ($n = 9$; $P < 0.05$) $Mecp2^{+/-}$ mice, and *wt* female littermate control groups ($n = 7$ and 8; pooled data plotted). (**C**) Measurements of LTP using theta-burst stimulation in presymptomatic ($n = 9$; $P > 0.05$), symptomatic ($n = 9$; $P < 0.05$) $Mecp2^{+/-}$ mice, and *wt* female littermate control groups ($n = 7$ and 8). (**D**) HFS-induced LTP measurements in TM-treated symptomatic *Stop/+* mice ($n = 11$; $P < 0.05$), *Stop/+,cre* mice ($n = 10$; $P > 0.05$), and *wt* mice ($n = 9$; $P > 0.05$). Recombination data are shown in Fig. 3F. Insets in (B) to (D) show representative voltage traces before (1) and after (2) LTP induction. Two-way repeated measures ANOVA was used to assess significance throughout.

sume their canonical role as interpreters of the DNA methylation signal (*15*, *16*).

Our study shows that RTT-like neurological defects due to absence of the mouse *Mecp2* gene can be rectified by delayed restoration of that gene. The experiments do not suggest an immediate therapeutic approach to RTT, but they establish the principle of reversibility in a mouse model and, therefore, raise the possibility that neurological defects seen in this and related human disorders are not irrevocable.

References and Notes

1. R. E. Amir *et al.*, *Nat. Genet.* **23**, 185 (1999).
2. J. L. Neul, H. Y. Zoghbi, *Neuroscientist* **10**, 118 (2004).
3. D. Armstrong, J. K. Dunn, B. Antalffy, R. Trivedi, *J. Neuropathol. Exp. Neurol.* **54**, 195 (1995).
4. N. Kishi, J. D. Macklis, *Mol. Cell. Neurosci.* **27**, 306 (2004).
5. R. Z. Chen, S. Akbarian, M. Tudor, R. Jaenisch, *Nat. Genet.* **27**, 327 (2001).
6. J. Guy, B. Hendrich, M. Holmes, J. E. Martin, A. Bird, *Nat. Genet.* **27**, 322 (2001).
7. S. Luikenhuis, E. Giacometti, C. F. Beard, R. Jaenisch, *Proc. Natl. Acad. Sci. U.S.A.* **101**, 6033 (2004).
8. I. Dragatsis, S. Zeitlin, *Nucleic Acids Res.* **29**, E10 (2001).
9. Materials and Methods are available as supporting material on *Science* Online.
10. S. Hayashi, A. P. McMahon, *Dev. Biol.* **244**, 305 (2002).
11. A. L. Collins *et al.*, *Hum. Mol. Genet.* **13**, 2679 (2004).
12. S. Kriaucionis, A. Bird, *Hum. Mol. Genet.* **12** (spec. issue 2), R221 (2003).
13. Y. Asaka, D. G. Jugloff, L. Zhang, J. H. Eubanks, R. M. Fitzsimonds, *Neurobiol. Dis.* **21**, 217 (2005).
14. P. Moretti *et al.*, *J. Neurosci.* **26**, 319 (2006).
15. X. Nan, J. Campoy, A. Bird, *Cell* **88**, 471 (1997).
16. J. D. Lewis *et al.*, *Cell* **69**, 905 (1992).

17. We are grateful to A. McClure and D. DeSousa for excellent technical assistance; to S. Zeitlin and J. Pevsner for reagents; and to D. Kleinjan, I. Vida, and R. Morris for comments on the manuscript. The work was funded by the Wellcome Trust, the Rett Syndrome Research Foundation (USA), and Rett Syndrome UK/Jeans for Genes.

Supporting Online Material

www.sciencemag.org/cgi/content/full/315/5815/1143/DC1
Materials and Methods
Figs. S1 to S7
References
Movies S1 to S3

4 December 2006; accepted 18 January 2007
10.1126/science.1138389

BIO-RAD

CLINICAL PROTEOMICS:

COMING TO TERMS WITH COMPLEXITY

Proteomics can explore what is going on (or going wrong) in a particular tissue at a particular time. Such knowledge can help to develop diagnostics and to select compounds and doses for clinical trials. But selecting the information to use is a conundrum. Protein content varies from cell to cell and minute to minute. Abundant proteins mask the presence of rare but key proteins. It is hard enough to find reliable differences between disease and health or between patients likely to be helped by a drug and those likely to be harmed by it. Even harder is homing in on the differences that really matter. **By Monya Baker**

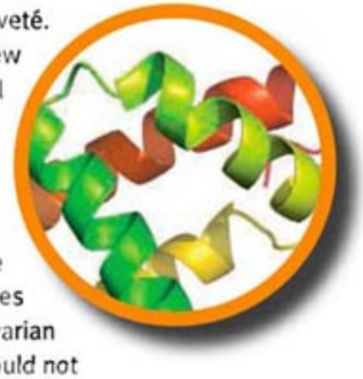

The early days of proteomics were characterized by optimistic naiveté. Large-scale study of the body's proteins promised to reveal new drug targets plus markers that would diagnose disease and reveal when and for whom a drug was working. The ease of generating data, paired with inconvenient or inadequate techniques for controlling variation, spawned poor experimental design.

Eventually, researchers looking for protein differences between experimental and disease groups began to realize that what they were finding either could not be replicated or could not be tied directly to diseases or drug mechanisms. In 2004, sales of an early proteomics test to detect ovarian cancer were halted following criticism that the protein profiling patterns could not be tied down to a consistent set of proteins. Just last year, the journal *Proteomics* issued a set of standards for submitted research and acknowledged that the rapid expansion of the field had led to publications of questionable quality (Wilkins, M.R. et al. Guidelines for the next 10 years of proteomics. *Proteomics* 6:4–8, 2006).

"There is a lot of exuberance when technologies do things that were previously not attainable," says Scot Weinberg, former head of proteomics at **Ciphergen** and now CEO of **GenNext Technologies**, a company that trains scientists for translational research. He thinks proteomics was harmed early on by "blinded enthusiasm" that has only recently started to listen to common sense.

For proteomics studies to yield applications for clinical research, companies must master the science of smart trade-offs. Researchers must simplify complex mixtures of proteins so that they can be analyzed reliably, but not so much that they eliminate the very differences they hope to find. Conversely, scientists must ensure techniques that collect data on hundreds of thousands of peptides don't pull out differences that don't actually exist. And once protein differences are identified, teams developing drugs and diagnostics must decide how, and how well, to characterize them.

> "There is a lot of exuberance when technologies do things that were previously not attainable."

Lowered Expectations

Proteomics advocates never tire of describing how a protein-level view of biology can reveal more than a survey of gene transcripts. "The mRNA levels might change, but not be consistent with the protein changes," says Yuqiao (Jerry) Shen, vice-president of research and development at **Applied Biomics**. He estimates that transcripts and proteins are correlated less than half the time. "Proteins are harder to analyze," he says, "but they give you more direct information."

continued ›

Look for these **Upcoming** Articles

Genomics — March 16
Cell Signaling — April 6
Stem Cells — April 20
RNAi — June 1

Ultimately, researchers often choose not the technique that enriches for a biologically interesting set of proteins but one that they can trust or afford.

The technology of proteomics is less mature than that of its cousin genomics. Commercially available DNA microarrays can interrogate the expression of every known human gene even in tiny samples, but the most optimistic advocates estimate that a proteomics survey will detect only one-fifth to one-third of the proteins in a sample. If researchers want to monitor a set of proteins from sample to sample, those fractions are even smaller.

One of the most significant advances in using proteomics to guide drug and diagnostics development is that researchers have stopped trying to be as complete as they can be with genomics, says Jenny Harry, deputy CEO of **Proteome Systems** in Sydney, Australia. "Initially, people used to try to make the technology display every protein in the proteome. That was an impossible task." Now, researchers tend to ask more limited, pertinent questions.

Clinical proteomics works best as a "practical science," says Howard Schulman, vice-president of biomarker discovery sciences at **PPD**, a large contract research organization. "You don't have to define the entire systems biology," he says. "You have to find enough things that change reproducibly that turn out to be useful." To do so, researchers must first imagine how protein profiles might be altered when a patient has a disease or when a drug affects a particular pathway. Then, they look for the samples and proteins that could reveal these differences.

Sample Collection and Protein Enrichment

Proteomics faces a strategic dilemma even before samples get near a mass spectrometer, the workhorse of proteomics research. In general, researchers must choose between less-informative samples from many patients or more-informative ones from fewer patients. Heart tissue might be ideal for studying cardiovascular disease, but collecting biopsies is difficult. Blood and urine are the most accessible but tend to be far removed from disease. Any proteins that leak from diseased tissue into the bloodstream are vastly diluted within a patient's body. Their presence will be masked further by much more abundant plasma proteins, and their characteristics modified by proteases and other substances in the blood or urine.

Even if diseased tissue can be sampled directly, as in a tumor biopsy, tissues are heterogenous mixtures of cells; a tumor may contain highly vascularized areas as well as other areas suffering from hypoxia. Consequently, the signal from the most relevant cells might be too faint to detect. Research teams can use a variety of tools to refine what they collect. Flow cytometry can select for certain cell types. In some techniques, healthy and cancerous cells taken from the same biopsy (and thus the same individual) can even be compared; or laser capture microdissection can pull specific organelles from cells, allowing researchers to focus on proteins associated with mitochondria, lysosomes, or other cellular fractions.

But these techniques are costly and time consuming. It can be difficult both to collect enough tissue from one patient and to collect samples from enough patients. Scott Patterson, executive director of medical sciences at **Amgen** and a co-author of the recently published proteomics guidelines (*Proteomics* 2006 as above), says that the difficulty of studying the individual cell types within tissues is the biggest barrier for using clinical samples in proteomics.

Researchers steeped in molecular biology don't always realize just how difficult it can be to find rare proteins with mass spectrometry (MS), says Ruth Vanbogelen, who is in charge of helping researchers at **Pfizer** incorporate proteomics studies into research programs across the company. Since no equivalent of PCR exists for proteins, they can only be detected if isolated in sufficient levels at the outset. The difference in concentration between the most and least abundant proteins in blood is around 10^{12}.

Researchers deplete abundant proteins to boost signal from less abundant proteins, but rare proteins are still hard to see. "If you remove 99 percent of the serum albumin, then most likely your most abundant species is still going to be albumin," observes Amgen's Patterson. Moreover, the affinity columns typically used to remove these abundant proteins introduce new sources of variation. Even if the amount of abundant proteins removed from different samples varies by only a fraction of a percent of the original amount, the concentrations left in the samples can vary by 50-fold. Worse, techniques to remove albumin and other abundant proteins tend to remove less abundant ones as well, often in irreproducible ways.

After depletion, researchers need to concentrate a particular class of proteins within a sample. Ideally, these techniques enrich proteins based on hypotheses of which proteins are likely to be biologically important. Techniques can pull out proteins that have been glycosylated, polyubiquitinated, or phosphorylated, with varying degrees of reliability and cost. Ultimately, researchers often choose not the technique that enriches for a biologically interesting set of proteins but one that they can trust or afford. Additional variation is introduced during the analysis stage, since mass spectrometry cannot simultaneously detect and identify every chemical species in a sample.

Bringing Proteomics to the Masses

Standardized techniques could reduce variation across experiments. So it's no surprise that kit and reagent companies are beefing up their offerings. David Smoller, vice-president of R&D at **Sigma-Aldrich**, estimates that his company's investment in proteomics has probably quadrupled over the past five years. **Bio-Rad** acquired the proteomics side of Ciphergen last year and hopes to "democratize" the technology so that biologists rather than MS specialists can run many of the experiments.

Part of Vanbogelen's job at Pfizer is to work with commercial suppliers and even competitors to disseminate proteomics tools. "Clinical proteomics is one area where intellectual property is not important and the freedom-to-operate concept is a key driver," she says. In addition to making benchwork easier for users, gold-standard kits and reagents would mean regulators are more likely to trust results from proteomics experiments. Amgen's Patterson continued ›

says that kits could be very useful, particularly for standardizing sample preparation, but that researchers have quite a wait before such products will be bought and trusted by drug companies.

Vanbogelen is more optimistic. "How much is available right now is limited," she admits, "but by 2010, we'll have seen that big shift." Still, she thinks it might take until 2050 before there's a way to measure 40,000 proteins, comparable to the number of transcripts that can be measured today on commercially available DNA microarrays.

Saved by Statistics

In the early days of proteomics, few researchers understood just how standardized studies needed to be during the discovery stage. Now, they are realizing that even rigorously standardizing techniques won't eliminate variation. That does not make analysis impossible, but it does mean that researchers must make sure that the biologic variation can still be seen despite variation introduced by experimental techniques.

To avoid finding artificial differences created by protein processing and analysis, researchers can label proteins in samples differently, then mix, process, and analyze them together. The ratios of the differentially labeled proteins should reveal biological variation between the samples. A variety of techniques exists. Applied Biomics, a certified service provider for **GE Healthcare**, labels proteins in samples with differently colored fluorescent dyes, and dissimilarities between samples show up readily in 2-dimensional difference gel electrophoresis (DIGE). Other techniques include **PerkinElmer's** ExacTag and **Proteome Sciences'** Chemical Mass Tags, Sigma's AQUA, and **Applied Biosystems'** ICAT, and can be used with gel or gel-free separation systems. Still other methods require heavy isotopes to be incorporated into proteins as they are produced, and so are not always practical for work on human samples.

Labeling samples can make statistical analysis possible, says Pfizer's Vanbogelen. Label-free methods, she says, tend to create what her team calls "holey spreadsheets," where information for thousands of different proteins is simply missing. With a label-free method, she says, you can run the same sample through a mass spectrometer six times, and only about 5 percent of the proteins will show up in all six runs, a rate too low to run a statistical analysis to find differences between groups. But if samples are labeled, several can be run at once, and this allows enough datapoints to be collected for multivariate statistics. However, better software to identify proteins from MS data is making label-free methods more useful, a development that will open up proteomics to broader groups of researchers.

In fact, the improvement of statistical techniques for both labeled and nonlabeled proteins is one of the most substantial advances the field has made, says Stephen Kingsmore, president of the National Center for Genome Resources in Santa Fe, New Mexico. Particularly useful are methods that can correct for the false discoveries that crop up whenever computers crunch through mounds of data. New enthusiasts don't always appreciate that they need to design experiments that collect the right data to answer their questions. "The idea that you can pull a mass spec into the room and have it magically deliver the goods is naive," says Kingsmore. "The error that people make all the time is they get their data set and then think, 'Now what am I going to do with it?'"

Bringing in Biology

PPD's Schulman says that he's seen research and development groups get more sophisticated over his years working for proteomics providers. Early on, he says, he would meet with protein chemists who knew how to separate components in a mixture but were unfamiliar with surveying large numbers of proteins within a sample. Now, says Schulman, he's more likely to meet with broader biomarker teams of experts who approach the problem from a clinical and biological vantage, not simply a technical one. They consider what kinds of samples can be collected and what classes of proteins should be enriched, not just how to generate the data.

Proteomic studies can indicate that a drug or disease has changed the concentrations of particular proteins, but not why. Ideally, additional literature and laboratory research will suggest biological reasons for these results along with further ideas for study. In any case, to translate proteomic studies into clinical decisions and other applications, most researchers believe they must shift from profiling proteins to validating the relevance of just a few.

That shift requires another exercise in trade-offs. Multiplexed antibody tests are relatively easy to perform, results vary little from test to test, and technologies to measure several proteins at once are improving. However, creating such tests can take several months, and cross-reactivity is a problem. On the other hand, a new advance in MS, multiplexed reaction monitoring, is more sensitive and less variable than other MS profiling techniques. Yet, it only works for abundant proteins and is still more variable than reagent-based tests.

But such debates are a sign of progress. Proteomics is littered with work that stopped at the discovery phase, says Peter Schulz-Knappe, chief scientific officer of Proteome Sciences. "The need is not just to do discovery but to commit yourself after discovery to do proper assays." In other words, proteomics research can become useful only when the study of the proteome shifts to the study of proteins.

Monya Baker is a freelance science writer based in San Francisco.

Featured Participants

Amgen
www.amgen.com

Applied Biomics
www.appliedbiomics.com

Applied Biosystems
www.appliedbiosystems.com

Bio-Rad
www.biorad.com

Ciphergen
www.ciphergen.com

GE Healthcare
www.gehealthcare.com

GenNext Technologies
www.gennexttech.com

National Center for Genome Resources
www.ncgr.org

PerkinElmer
www.perkinelmer.com

Pfizer
www.pfizer.com

PPD
www.ppdi.com

Proteome Sciences
www.proteome.co.uk

Proteome Systems Limited
www.proteomesystems.com

Sigma-Aldrich
www.SigmaAldrich.com

Sample Processing Platform

QIAcube is a compact platform that incorporates novel and proprietary technologies to allow users to fully automate the processing of almost all Qiagen consumable products. The platform can be used with more than 100 spin column–based protocols for DNA, RNA, and protein sample processing. The protocols are based on the same Qiagen consumable products that are used manually in more than 40,000 laboratories around the world, enabling effortless migration to the automated system. There are several hundred proprietary technologies incorporated into these Qiagen consumables, so by running them on the QIAcube, users can free up time and enjoy even higher levels of quality and performance. This compact system is designed for the low- to medium-throughput range for laboratories engaged in research, applied testing, and molecular diagnostics.
Qiagen For information +49-2103-29-11710
www.qiagen.com

Human Protein Microarray

The ProtoArray Human Protein Microarray version 4.0 enables rapid profiling of thousands of biochemical interactions in as little as one day. Users can screen biological samples or labeled probes against 8,000 unique human proteins from multiple gene families in a single, rapid experiment. Full-length, native human proteins from a broad range of protein classes are arrayed in duplicate on nitrocellulose-coated glass slides. These high-content protein microarrays can be used for identifying disease-specific protein biomarkers, mapping protein-protein interactions, profiling antibody specificity, and performing target discovery and validation.
Invitrogen For information 800-955-6288
www.invitrogen.com

Proteomics-Grade Detergents

The Variety packs are high-purity detergents suitable for membrane and total protein extraction. These proteomics-grade detergents are purified to reduce levels of peroxidases, aldehydes, carbonyls, heavy metals, and other contaminants. They are packed in a glass vial under inert gas to maintain quality. The Variety packs include 10 ml each of 10 nonionic, ready-to-use detergents.
G-Biosciences/Genotech For information 314-991-6034
www.GBiosciences.com

Proteomics Standard

The Universal Proteomics Standard is a complex mixture of 48 human proteins designed to enable researchers to better assess proteomics strategies, troubleshoot protocols, and normalize results from day to day and lab to lab. The protein mixture was evaluated by more than 100 independent proteomics laboratories worldwide.
Sigma-Aldrich For information 314-286-7616
www.SigmaAldrich.com

Gel Documentation System

The CSL MicroDOC is a compact, transportable, and inexpensive gel documentation system that produces high-quality images. Its integral 16-bit charge-coupled device digital camera provides resolution of 8.0 megapixels. A wide variety of images from agarose, other fluorescent gels, colorimetric gels, autoradiographic film, and blotting membranes can be viewed from the system's high-definition, 8-inch, thin-film transistor liquid crystal display. Files can be saved in a variety of formats, such as TIF, JPEG, RAW image, or QuickTime, ready for transfer to computer systems for storage and further analysis using the included USB cable. Images can also be printed directly from the MicroDOC. A 55-mm ethidium bromide filter includes a built-in safety switch to turn off the ultraviolet transilluminator when the door is open.
Cleaver Scientific For information +44 (0) 1788 565 300
www.cleaverscientific.com

Crystal Imaging for Protein Crystallography

Designed to fit on a lab bench, the Desktop Minstrel is a modular and expandable protein crystal imaging and analysis system. The Desktop Minstrel can be configured to meet a range of applications, from low throughput research to high throughput drug discovery programs. The system automatically images crystallization experiments and links images with crystallization conditions. The data are captured in CrystalTrak, a complete virtual crystallization laboratory that provides a chemical and crystallization database and data analysis tools. CrystalTrak provides a powerful interface for viewing images and conditions for evaluation and scoring. With a high-resolution imaging system that can visualize hanging drop, sitting drop, microbatch, and free interface diffusion experiments across most commercially available plate types, the Desktop Minstrel facilitates scoring and reporting as well as experimental design and project management. The instrument is cold-room compatible and expandable to a 160-plate capacity.
Rigaku For information 281-362-2300
www.Rigaku.com

Dual Channel Surface Plasmon Resonance

Introducing the SR7000DC Dual Channel SPR Instrument, a powerful, flexible and affordable instrument for determining biomolecular interactions. The SR7000DC provides real-time, label-free, simultaneous monitoring of sample and reference channels and is useful in proteomics, genomics, and antibody studies. Its modular design is easily configured to do customized research. Fluidic configurations range from manual to fully automated with an optional autosampler. It is able to do kinetic studies of small molecules up to 200 Daltons. Temperatures are programmable, micro or macro flow cells are available for different surface work, and flow rates can be run fast or slow.
Reichert For more information 888-849-8955
www.reichertai.com

POSITIONS OPEN

ASSOCIATE or FULL MEMBER
HIV Vaccine Trials Network

The Fred Hutchinson Cancer Research Center is currently recruiting a full-time faculty position at the Associate or Full Member level who will be a central figure in the leadership of the HIV Vaccine Trials Network (HVTN). This is an opportunity to help direct a global vaccine network, as well as build either a laboratory-based or infectious disease epidemiology research program in global health-related vaccines. This person will work with the HVTN leadership to facilitate interaction with other clinical research programs globally and locally.

The successful candidate will have an M.D. (Board-eligible/Board-certified) or a Ph.D. with experience as a clinical investigator in HIV medicine or viral vaccines. Experience with establishing an independently funded research program is desired.

Interested candidates may submit a letter of interest, curriculum vitae, and statement of research plans to:

Lawrence Corey, M.D.
HIV Vaccine Trials Network
Search Committee, Chair
Fred Hutchinson Cancer Research Center
1100 Fairview Avenue N., D3-100
P.O. Box 19024
Seattle, WA 98109-1024

Or by **e-mail: lcorey@u.washington.edu.** Application review will continue until the position is filled.

The Fred Hutchinson Cancer Research Center is an Affirmative Action, Equal Opportunity Employer. We are dedicated to the goal of building a culturally diverse and pluralistic faculty and staff committed to teaching and working in a multicultural environment and strongly encourage applications from women, minorities, individuals with disabilities, and covered veterans.

ASSISTANT/ASSOCIATE PROFESSOR
(Tenure Track)
Computer Science Morehouse College

The Division of Science and Mathematics at Morehouse College seeks candidates for tenure-track **ASSISTANT** and/or **ASSOCIATE PROFESSOR** positions in computer science. We seek an individual possessing a Ph.D. in computer science and a strong commitment to undergraduate teaching. The successful candidate is expected to establish a research program that involves undergraduates. Submit curriculum vitae, description of teaching experience and philosophy, description of research interests and career goals, and the names and contact information for three references to: **Dr. Kenneth R. Perry, Chair, Department of Computer Science, Morehouse College, 830 Westview Drive, S.W., Atlanta, GA 30314. E-mail: kperry@morehouse.edu.** Deadline March 15, 2007.

Morehouse is an Equal Opportunity/Affirmative Action Employer.

The College of William and Mary invites applications for a full-time, one-year teaching position at the **ASSISTANT PROFESSOR** level in microbiology. Previous teaching experience and/or postdoctoral experience would be advantageous. Teaching responsibilities will include one upper-level microbiology course with laboratories for one semester, and another course in an area of the candidate's expertise for the second semester. The individual selected will also be encouraged to supervise undergraduate student research. Review begins on February 23, 2007, and will continue until the appointment is made. Submit a letter of application, curriculum vitae, a statement of teaching experience, and three names of references to: **Dr. Patty Zwollo, Department of Biology, Millington Hall, The College of William and Mary, Williamsburg, VA 23187-8795.** *The College of William and Mary is an Equal Opportunity/Affirmative Action University. Members of underrepresented groups (including people of color, persons with disabilities, Vietnam veterans, and women) are encouraged to apply.*

POSITIONS OPEN

UNIVERSITY OF CALIFORNIA, DAVIS
School of Medicine
Department of Physiology and Membrane Biology

The Department of Physiology and Membrane Biology, at the University of California, Davis School of Medicine, is recruiting a mid-career faculty member for a state funded, tenure-track position at the **ASSOCIATE/FULL PROFESSOR** level as part of the Membrane Biology Initiative. The Department of Physiology and Membrane Biology has recently hired six junior faculty, one of whom was a joint hire with the newly formed Shriner's Hospital Institute for Pediatric Regenerative Medicine. Candidates must possess a Ph.D. and/or M.D. degree and have demonstrated academic leadership as evidenced from superior investigative accomplishment, sustained extramural funding, educational excellence, and effective mentoring and service. The individual selected for the position is expected to maintain a high quality research program and to participate in the teaching of medical and graduate students. The most important criteria in the consideration of applicants are: (1) a record of research excellence, creativity, and innovation; (2) a demonstrated ability to communicate effectively as an educator, and (3) a history of fostering collaborative research. The research interests of current departmental faculty are focused in the areas of cardiovascular physiology and neuroscience, with an emphasis on membrane phenomena. It is expected that the successful candidate will complement and extend the existing strengths of the Department and integrate with one or more of the School's strategic focus areas (cardiovascular, neuroscience, infectious disease, and cancer). Individuals that posses the potential to interface with and promote translational studies in partnership with clinical scientists are encouraged to apply. The Department web address is **website: http://www.ucdmc.ucdavis.edu/physiology/** and **website: http://www.physiology.ucdavis.edu/.**

Letters of interest, curriculum vitae, up to three representative reprints, synopsis of research plans (past, present, and future goals), summary of teaching experience/philosophy, and the names/addresses of five references should be forwarded to: **Martha E. O'Donnell, Ph.D., Chair, Search Committee, c/o Department of Physiology and Membrane Biology, 4136, Tupper Hall, East Health Sciences Drive, University of California, Davis, CA 95616.** The position will be open until filled; for full consideration, applications should be received by November 30, 2007. **Website: http://www.physiology.ucdavis.edu/.** *The University of California is an Equal Opportunity/Affirmative Action Employer.*

AVIAN RESEARCH ECOLOGIST
U.S. Geological Survey's
Patuxent Wildlife Research Center

The U.S. Geological Survey's Patuxent Wildlife Research Center in Laurel, Maryland, **website: http://www.pwrc.usgs.gov/,** seeks a full-time, GS-12/13, Research Ecologist with experience conducting research in avian biology, ecology, and conservation. As lead investigator the Ecologist designs, conducts, analyzes, and prepares reports on studies that respond to regional and national conservation goals, primarily in support of Department of Interior agencies missions. Applications must be completed online at **website: http://www.usgs.gov/ohr/oars/.** The Delegated Examining Unit announcement (*open to all qualified U.S. citizens*) will be vacancy announcement number ER-2007-0096; the MP announcement (open to current and former Federal employees) will be vacancy announcement number ER-2007-0107 Announcements will open on February 20, 2007, and close at midnight EST on March 19, 2007. Details on the position and application provided on the website.

Positions @ NIH

THE NATIONAL INSTITUTES OF HEALTH

DIRECTOR, PSI STRUCTURAL GENOMICS KNOWLEDGEBASE
National Institute of General Medical Sciences (NIGMS)

NIGMS is seeking an individual to serve as the Director of the PSI Structural Genomics Knowledgebase (SG-KB), a key component of the Protein Structure Initiative (PSI). The PSI is a national research program in the emerging field of structural genomics. The long-range goal of the PSI is to make the three-dimensional atomic-level structures of most proteins easily obtainable from knowledge of their corresponding DNA sequences. The PSI SG-KB will serve as a headquarters for scientific data and knowledge generated by the PSI-funded centers, so that they may be widely available to the scientific community. Information about the PSI may be found at: http://www.nigms.nih.gov/Initiatives/PSI.htm.

Requirements: The position will be a part-time temporary assignment for up to two years, with the possibility of an extension for up to two additional years. Individuals at an accredited U.S. public or private college or university, or technical institution of higher learning are eligible to apply. Students and employees from foreign universities are not eligible for consideration. Individuals detailed to the NIGMS remain employees of the outside organization, and may only serve in an advisory or consultative capacity.

Candidates must have a Ph.D. or equivalent degree in a field relevant to the position. The ideal candidate will have scientific knowledge and research experience in one or more of the following fields: molecular biophysics, structural biology, genomics, bioinformatics, and computational biology. In addition, candidates should possess experience in broad networking interactions and collaborations in the above research fields, a proven track record in directing and/or managing a large scientific database or large research project, as well as strong leadership ability and effective communication skills.

How to Apply: To be considered for this position, send to the e-mail address below a CV, bibliography, and a vision statement (not to exceed three pages) that presents your views on how to maximize the usefulness and impact of the Knowledgebase for the greater biological community.

NIGMSCV@mail.nih.gov

Applications must be received by the closing date: **March 30, 2007**. The National Institutes of Health inspires public confidence in our science by maintaining high ethical principles. Individuals detailed to NIH are subject to Federal government-wide regulations and statutes, as well as agency-specific regulations described at http://ethics.od.nih.gov. We encourage you to review this information. You may contact Kimberly Allen with questions regarding this announcement on 301-594-2755.

Staff Scientist
Pulmonary-Critical Care Medicine Branch

The Pulmonary Critical Care Medicine Branch (P-CCMB) of the National Heart, Lung, and Blood Institute, National Institutes of Health, Department of Health and Human Services is recruiting a Staff Scientist to work in the Laboratory of Dr. Stewart Levine. The Staff Scientist will play a lead role in conducting clinical, translational, and basic studies. Clinical and translational studies will investigate diagnostic and therapeutic approaches to inflammatory lung diseases, such as asthma. Basic studies are aimed at identifying and characterizing molecular mechanisms regulating the generation of soluble cytokine receptors, such as tumor necrosis factor receptors. The ideal candidate will have expertise in proteomics, cell biology, biochemistry, flow cytometry, and murine models of human disease. The successful candidate will work with minimal supervision to successfully complete projects that result in published manuscripts. Responsibilities will include performance of experiments, participation in clinical trials, training of students and post-doctoral fellows, and management of laboratory and branch activities.

Candidates should possess a Ph.D. (or equivalent) degree, have successfully completed postdoctoral training and have a strong publication record. The successful candidate will be offered a competitive salary commensurate with experience and qualifications. Appointees must be US citizens, resident aliens, or nonresident aliens with a valid employment visa. Applications must be received by **April 13, 2007**.

To apply, submit a curriculum vitae, statement of research interests and arrange to have at least three letters of recommendations sent to: **Vincent Manganiello, M.D., Ph.D., Chair, Search Committee, Pulmonary-Critical, Care Medicine Branch, NHLBI, Building 10, Room 5N307, MSC 1434, Bethesda, Maryland 20892-1434, Email: manganiv@nhlbi.nih.gov**.

Tenure/Tenure-Track Position
Laboratory of Persistent Viral Diseases
Rocky Mountain Laboratories, Hamilton, Montana

The Laboratory of Persistent Viral Diseases (LPVD), Rocky Mountain Laboratories, NIAID, NIH, DHHS, in Hamilton, Montana, seeks applicants for a tenured or tenure-track position (full to assistant professor equivalent) to conduct independent research on host immune or inflammatory responses in neuropathogenic viral diseases. Candidates with a background in adaptive or innate immunity, including neuroinflammation and gliosis are preferred; those interested in neurobiology, biochemistry or pathogenesis of CNS infections are also encouraged to apply. Candidates must hold a Ph.D., D.V.M, or M.D. degree and have a minimum of 3 years of relevant postdoctoral experience. Candidates must be able to develop an independent research program, supervise staff and fellows, and collaborate with other LPVD researchers working on CNS viral or prion diseases.

Rocky Mountain Laboratories' state-of-the-art facilities include an operational BSL-3 facility, a BSL-4 lab and animal facility nearing completion, and in-house core facilities for genomics, electron microscopy, and flow cytometry. Research programs focus on prions, murine retroviruses, HIV, flaviviruses, and numerous pathogenic prokaryotic organisms. The lab is located in the scenic Bitterroot Valley of western Montana with easy access to some of the finest outdoor recreational opportunities in North America. Additional information on the position may be obtained by contacting Dr. Bruce Chesebro at bchesebro@niaid.nih.gov.

Application Process: Salary depends on degree and qualifications. To apply, submit a curriculum vitae and bibliography, including a list of your five most significant papers, and a 2-3-page description of a proposed research program, via e-mail to **Ms. Felicia Braunstein at braunsteinf@niaid.nih.gov**. In addition, three letters of recommendation must be sent directly from the referees to **Ms. Felicia Braunstein, Committee Manager, NIAID/NIH; 10 Center Drive, Bldg. 10, Rm.4A31, MSC-1356; Bethesda, MD 20892-1356**. Applications must reference **AD #010** and must be received by **March 9, 2007**. Applicants will be notified when their applications are received and then completed. All information provided by applicants will remain confidential.

WWW.NIH.GOV

Senior Scientist, Vaccine Research Center
National Institute of Allergy and Infectious Diseases
National Institutes of Health (NIH)

The National Institute of Allergy and Infectious Diseases (NIAID), Vaccine Research Center (VRC) is recruiting for a Senior Scientist (non-tenure) to oversee preclinical research activities, investigate novel vaccine delivery methods, and serve as the head of the Laboratory of Animal Medicine. The NIAID is a major research component of the NIH and the Department of Health and Human Services (DHHS).

Due to the dual research and animal medicine functions of the position, the VRC is seeking candidates with a Ph.D. in virology, immunology or a related scientific field, and a Doctorate in veterinary medicine. The position involves a broad spectrum of scientific research, veterinary and business management skills encompassing laboratory animal medicine research, animal program management, ability to develop, manage and execute in-vivo animal research contracts for the VRC, financial oversight, and contract administration. The candidate will plan, manage and analyze data from animal studies evaluating immunogenicity of vaccine candidates. Board certification in either Veterinary Pathology or Laboratory Animal Medicine, and experience in financial oversight of a large program is preferred.

The ideal candidate will be experienced in vaccine development research, non-human primate studies, and good laboratory practices (GLP) animal studies, and will have a record of independent research and peer-reviewed publication.

The Senior Scientist selected for this position will have committed resources to support laboratory research, and an allocated annual budget to cover services, supplies and salaries. Salary will be based on the individual's qualifications and experience, in the range of $140-180k.

Interested candidates may contact **Dr. John Mascola via E-mail: VRC_Positions@mail.nih.gov** for additional information about the position. To apply for the position, candidates must submit a curriculum vitae, bibliography, three letters of reference, a detailed statement of research interests (limit to 3 pages) and reprints of up to three selected publications to: **National Institute of Allergy and Infectious Diseases, Vaccine Research Center, c/o Intramural Administrative Management Branch, Attn: Ms. Marie Hirsch; Building 40, Room 1118; 40 Convent Drive; Bethesda, MD 20892-3013 or email hirschm@niaid.nih.gov by April 12th, 2007.**

ARE YOU READY FOR AN EXCITING CAREER THAT COULD HELP IMPROVE MILLIONS OF LIVES AROUND THE WORLD?

The National Institute of Allergy and Infectious Diseases (NIAID), the second largest institute of the world-renowned National Institutes of Health (NIH), supports and conducts basic and applied research to better understand, treat, and prevent infectious, immunologic, and allergic diseases that threaten millions of lives around the world.

The Division of Intramural Research (DIR) conducts all of the in-house research undertaken by the NIAID and is involved in scientific research programs that cover a wide range of disciplines. The Laboratory of Viral Diseases (LVD), DIR carries out investigations on the molecular biology of viruses, the interactions of viruses with host cells, the pathogenesis of viral diseases and host defense mechanisms. Applied areas of research include the development of recombinant expression vectors, candidate vaccines and antiviral agents. LVD is seeking applications from exceptional candidates for the following position:

Scientific Operations Manager

The incumbent of this position serves as the principal advisor on scientific operational matters to the Laboratory Chief. The Scientific Operations Manager applies scientific expertise and knowledge of biomedical research methods and administrative procedures and concepts relative to health investigations in working closely with the Laboratory Chief to formulate and implement plans and procedures for the effective conduct of laboratory scientific programs and to develop, evaluate, and direct operational projects and activities including budget and human resources for the efficient and effective management and use of laboratory resources. This is an interface role that translates and interprets scientific requirements into administrative and operational processes.

Applicants must posses a bachelor's or higher degree that included a major field of study in the biological or health sciences. The understanding of and ability to provide management for Biomedical research and the ability to develop, evaluate, and direct operational projects and activities to enhance program productivity are required.

To apply to this vacancy, please visit:
http://usajobs.opm.gov/

Vacancy number: NIAID-07-166412-DE & NIAID-07-166412-MP; Salary: $79,397–$103,220; GS-601-13

Specific application procedures apply. Applications must be submitted to Human Resources by **March 14, 2007**.

We invite you to explore our Institute and view additional opportunities at:
http://healthresearch.niaid.nih.gov/som

DHHS and NIH are Proud to be Equal Opportunity Employers

HELP US HELP MILLIONS

National Institute of Allergy and Infectious Diseases

Executive Director, Dauphin Island Sea Lab (Alabama)

The Marine Environmental Sciences Consortium/Dauphin Island Sea Lab (DISL) provides the administrative framework for a significant portion of Alabama's marine research, education, and outreach activities from 21 colleges and universities. In addition to involvement in undergraduate and graduate academic programs funded by the state educational trust fund, DISL faculty members conduct a variety of research projects, funded in excess of 4 million dollars per year by competitive grants and contracts. The Sea Lab also delivers instruction in one of the largest K-12 marine programs in the country.

Responsibilities: This position reports to the Board of Directors, which includes the presidents of 21 Alabama colleges and universities, through an Executive Committee. The DISL Executive Director will administer all aspects of the Lab and its related facilities, and will advocate internally and externally for marine related research. Essential functions include facilitating marine related faculty and academic program development; overseeing K-12 educational programming; developing marine related research programs and projects; enhancing funding; providing general oversight for the DISL campus, vessels, and other physical facilities; coordinating state and endowment funds and overseeing budgets; supervising DISL administrative, vessel, and diving staff; increasing program visibility internally and externally; representing DISL on relevant regional and national groups and committees; establishing and administering policies on matters related to the programs; participating as a member on the DISL Executive Committee and Board of Directors. Effective state agency collaboration, and active promotion of support from the state legislature, is essential to the stability and success of the Lab.

Qualifications: Ph.D. in biology, life sciences, physical sciences, or engineering, with an emphasis on Marine Science. Ten years experience in marine related research and development. Demonstrated success in management of complex research and educational projects/programs at several levels. Excellent oral and written communication skills. Ability to work with a variety of constituencies including local, state, and federal agencies.

Salary: Competitive and commensurate with experience. This is a full time, 12-month position. Application Review begins May 1, 2007 and will continue until position is filled. Start date as early as September 1, 2007. Applicants should send a letter of intent, statement of administration philosophy, curriculum vitae, and the names, addresses, and phone numbers of 3 references (letters are not required at this time) by e-mail to: **G. David Johnson, djohnson@usouthal.edu**.

If electronic submission of applications is impractical, materials may be mailed to: **G. David Johnson, Chair Executive Director Search Committee, Dauphin Island Sea Lab, 101 Bienville Blvd., Dauphin Island, AL 36528**. Potential applicants are encouraged to visit the DISL website at: **www.disl.org**.

EOE/AA/M/F/D

synthetic genomics™

Careers

Synthetic Genomics, Inc. is a privately held company dedicated to developing and commercializing the latest advances in synthetic genomics for the production of clean and sustainable biofuels that alleviate our dependence on petroleum, enable carbon sequestration and reduce greenhouse gases.

We are currently seeking a talented and highly motivated scientist to join our metabolic engineering team in La Jolla, CA. Please send your CV and cover letter to **hr@syntheticgenomics.com** if you are interested in applying for the following position:

Senior Scientist - Microbial Metabolic Pathway Engineering

Successful candidate will conduct research applying the latest advances in synthetic genomics to the design and development of microbes for the production of novel biofuels. Candidate must have a Ph.D. in Microbiology, Molecular Biology, or Biochemical Engineering and demonstrated experience with microbial molecular genetics, bioinformatics analysis of metagenomic sequence data, gene synthesis, cloning and expression in a variety of microbial hosts, and biochemical and analytical characterization of engineered strains.

http://www.syntheticgenomics.com

Synthetic Genomics is an Equal Opportunity Employer.

MEKONG RIVER COMMISSION FOR SUSTAINABLE DEVELOPMENT — MRC

Mekong River Commission

The role of MRC is to co-ordinate and promote co-operation in all fields of sustainable development, utilisation, management and conservation of the water and related resources of the Mekong Basin. MRC is seeking an

ADVISOR, FISHERIES VALUATION

Fisheries Programme

Post level L-5

The Advisor, Fisheries Valuation will undertake a 3 year study to determine the economic value of inland capture fisheries and aquaculture in the Lower Mekong Basin (South East Asia).

For information, job description and application details, please visit MRC's web site at **www.mrcmekong.org** or send an email to **mrcs@mrcmekong.org**.

Closing date for applications: 12 March 2007

Hank Gardner and Marilyn Fiske Chair of Physiology

University of Wyoming

The Department of Zoology and Physiology at the University of Wyoming invites applications for a full-time, nine-month, tenured **FACULTY POSITION** at a senior level, starting 2008. We are seeking a biomedical physiologist who is conducting innovative research, and who will be able to complement and add to existing physiology research strengths (cell physiology, comparative physiology, neuroscience) in the department and university (cardiovascular physiology). The successful candidate will have a Ph.D., an externally funded research program, and be expected to teach in the department's physiology program which prepares students for further training in physiology and the health sciences. Start up and support for the chair is available. The department also has active research faculty in animal ecology and wildlife/fisheries biology. Outstanding microscopy and macromolecular facilities, an animal holding facility, the Nucleic Acid Exploration Facility, and the Red Buttes Environmental Research Laboratory are available.

Interested applicants should send a curriculum vitae, a statement of research and teaching interests, three publications that represent their best work, and the names of three referees to: **Gardner Physiology Chair Search Committee, Department of Zoology and Physiology, Dept. 3166, 1000 E. University Avenue, Laramie, WY 82071. Fax: 307-766-5625**. For further information by email: **zprequest@uwyo.edu** or by Website: **http://uwyo.edu/Zoology**. Applications should be submitted by **June 30, 2007**.

The University of Wyoming is a Carnegie Foundation Research/ Doctoral Extensive Institution, and is an AA/EEO Employer.

UNIVERSITÄT BAYREUTH

At the University of Bayreuth the following position is open for application at the Faculty of Biology, Chemistry and Earth Sciences:

Professorship (W2) Ecological Services

The position will be filled starting from 1st of July 2007, initially limited until 30th of September 2011. The continuation after that is subject to a positive evaluation.

This professorship will contribute to the research focus on Ecology and Environmental Science at the University of Bayreuth. The holder of the position is expected to cooperate closely with existing research groups (e.g. Bayreuth Center of Ecology and Environmental Research – BayCEER or Centre for Natural Risks and Development Bayreuth – ZENEB). Research topics that are expected address the services of ecological systems to mankind in the context of global change. The position is linking the field of ecology with interdisciplinary issues of human or social interests. The teaching will focus on the Elite Study Program "Global Change Ecology" (M.Sc.) within the Elite Network of Bavaria, but courses will also be offered for studies in Biology, Geoecology and Geography. Teaching language is English.

The successful candidate must hold a university degree; prove his/her potential for research and teaching skills. Documented activities in third-party funding are desired. Physically handicapped persons will be favoured, if equally qualified. To increase the number of women in science, women are explicitly encouraged to apply.

Applications including CV, university certificates, research projects, publications should be sent before **31st of March 2007** to the:

Dean of the Faculty of Biology, Chemistry and Geosciences
University of Bayreuth
D-95440 Bayreuth, Germany

UNIVERSITY of LOUISVILLE
Health Sciences Center

Tenure-Track Faculty Position
Developmental Neurobiology

http://www.louisville.edu/hsc/birthdefectscenter/index.htm

The University of Louisville Birth Defects Center, a NIH-funded Center for Biomedical Research Excellence, invites applications for tenure-track faculty appointment at the level of Assistant, Associate, or Full Professor in the area of Developmental Neurobiology. Candidates seeking appointment at the rank of Associate or Full Professor must have current extramural research funding. Candidates should have a research program in normal and/or abnormal mammalian pre/postnatal development with a focus on mechanisms of neurodevelopment and/or cognition utilizing contemporary molecular, genetic, electrophysiological and/or functional imaging approaches. Preference will be shown to applicants whose research program complements one or more of the Center's existing programs in craniofacial and CNS development; human neurocognition, behavior and learning; developmental toxicology; computational systems biology of the developing organism; and developmental regulation of gene expression. Candidates must have a Ph.D. degree or the equivalent, at least two years of postdoctoral training and a strong publication record. Successful candidates will be expected to maintain an independent and innovative research program that attracts extramural funding and participate in interdisciplinary research collaborations. Opportunities exist to collaborate with faculty in numerous Departments including the Departments of Psychological and Brain Science; Anatomical Sciences and Neurobiology; Psychiatry and Behavioral Sciences; and varied Centers/Institutes including the Center for Genetics and Molecular Medicine; the Spinal Cord Injury Research Center; the Early Childhood Research Center; the Center for Environmental Health Sciences; and the Institute for Public Health Research, among others. Salary and Rank at appointment will be commensurate with experience and qualifications.

Applicants must apply online at **www.louisville.edu/jobs** for Job 20998, at which time a *curriculum vitae* must be uploaded. In addition, a single PDF document containing a letter of intent with a brief description of current/planned research activities and the names of three references should be sent via e-mail directly to: Dr. M. Michele Pisano, Faculty Search Committee Chairman, at **Drmikeky@gmail.com**

The University of Louisville is an Affirmative Action, Equal Opportunity, Americans with Disabilities Employer, committed to diversity and in that spirit, seeks applications from a broad variety of candidates.

Lecturers in Animal Behaviour/ Behavioural Ecology (x2) (Ref: 4861)

School of Psychology

Exeter University is currently building an enthusiastic, integrative, interactive, and broad group in Animal Behaviour with the goal of making it an international centre of excellence. The new group is led by Prof. John A. Endler and the successful candidates will join him and three other colleagues, with at least one further appointment to follow. The following questions indicate the role: What is the behaviour's purpose in the sense of what are the problems that the behaviour solves? How does solving the environmental or social problem maintain or enhance fitness? Why and how does it evolve? We seek highly interactive individuals who do at least some work on natural populations of vertebrates or invertebrates.

We have a preference for those interested in animal signalling, mate choice, habitat choice, and prey choice related to anti-predation mechanisms. The successful applicant will show evidence of an original and independent research programme, high quality publications, and preferably some past research funding. She/he will develop teaching at the postgraduate or undergraduate level in his/her area of research expertise.

The appointment salary will be from £29,139 pa to £32,796 pa dependent upon qualifications, skills and achievements, with further progression available to £35,837 pa dependent upon performance. Appointment may be possible at a higher level for exceptionally well qualified individuals.

Application packs are available from www.exeter.ac.uk/jobs2007 e-mail j.e.orr@exeter.ac.uk or answerphone (01392) 263100, quoting reference number 4861. The closing date for completed applications is 16 March 2007.

Equal opportunities employer

UNIVERSITY OF EXETER

EMVI

STATENS SERUM INSTITUT

4 Vacancies at European Malaria Vaccine Initiative, EMVI

The European Malaria Vaccine Initiative, EMVI was established in order to address identified structural deficiencies in public funded malaria vaccine development.
The mission of EMVI is to provide a mechanism through which the development of experimental malaria vaccines can be accelerated within Europe and in developing countries. EMVI is facilitating and contributing financially and technically to nationally and internationally funded malaria vaccine research and development, and it provides a mechanism to see candidate molecules through to limited industrial production and early clinical development phase.

EMVI secretariat is hosted by Statens Serum Institut in Copenhagen, Denmark. EMVI is seeking a Product Manager, two Project Managers, and a Clinical Operations Manager. The positions are for 2 to 5 years.

Salary: commensurate with experience, within current "union/employer" agreements with the opportunity for a qualifications supplement.

To see detailed information, please visit EMVI website:
http://www.emvi.org/via20.html
Positions will remain open until viable candidates are selected.

University of Massachusetts
UMASS Lowell

Careers with **Mass Appeal**

Assistant/Associate Professor

Department of Biological Sciences

The University of Massachusetts Lowell Department in Biological Sciences invites applications for a full-time tenure-track position, rank negotiable, to start Fall 2007. The successful candidate will be expected to build a vigorous, externally funded research program, and collaboration within this and other departments is encouraged. Current faculty research interests include bioinformatics, genetics, plant science, neurobiology, cancer biology, invertebrate biology, developmental biology, virology, microbial ecology, and biogeochemistry. Our campus is located very near the vibrant academic and commercial biotechnology centers of Boston, Cambridge and Worcester.

We are seeking individuals with expertise in one or more of the following areas: Genetics, Population Genetics and/or Evolution. Teaching obligations include development of upper level undergraduate/graduate courses in his/her expertise and participation in the teaching of core undergraduate courses as needed.

MINIMUM QUALIFICATIONS:

- Earned doctorate
- Demonstrated ability teaching at the undergraduate and graduate levels
- Commitment to develop and sustain an externally funded research program
- Demonstrated potential for publications in scholarly journals
- Excellent communication and interpersonal skills
- Demonstrated ability working with diverse student and faculty population

Applicants should submit the following materials by both mail and electronic submission by March 16, 2007:

A curriculum vita, copies of several recent research publications, a statement of research and teaching interests, not to exceed three pages, and arrange for three letters of recommendation to be sent to:

Biological Sciences Faculty Search
Department of Biological Sciences
University of Massachusetts Lowell
One University Avenue
Lowell, MA 01854

Job Reference #FC04020701

Email materials to biology_search07@uml.edu.

Please include reference number in subject line of e-mail.

The University of Massachusetts is an Equal Opportunity/Affirmative Action Title IX, H/V, ADA 1990 Employer

Microbiology/Immunology Assistant Professor

The Department of Biology at the University of Tampa invites applications for a full-time tenure-track position beginning in August 2007, to teach microbiology and immunology for science majors and to participate in our introductory courses in Biology.

The department is interested in attracting a broadly trained microbiologist/immunologist to complement the existing faculty in biology. The candidate is expected to engage in research activities that involve undergraduates. Start-up funds are available.

PhD required, prior teaching and research experience with undergraduates desirable.

Please include a cover letter, current curriculum vitae, statement of teaching philosophy and a statement of research interests, copies of transcripts and name and contact information of three references.

To apply go to **jobs.ut.edu**.

Review of applications will begin March 1, 2007 and continue until the position is filled.

The University of Tampa
is an EO/AA employer.

The University Of
TAMPA

MSSM
MOUNT SINAI SCHOOL OF MEDICINE

www.mssm.edu

Statistical Genetics/Genetic Epidemiology Tenure Track Positions

The Department of Genetics and Genomic Sciences at The Mount Sinai School of Medicine of New York University seeks outstanding applicants for several tenure-track faculty positions in statistical genetics and genetic epidemiology as an Assistant, Associate or Full Professor. Successful candidates will join our new Center for Statistical Genetics and Genetic Epidemiology which was created to complement and collaborate with Mount Sinai's strong research programs in the genetics of complex traits in cancer, cardiovascular, metabolic, neurodegenerative, and psychiatric disorders. Outstanding opportunities are available for basic and clinical research as well as participation in educational activities.

Faculty positions include competitive salary/fringe benefits, generous startup package, and excellent office/laboratory space and computer facilities. Rank and salary are commensurate with experience and research accomplishments. Applicants should forward their curriculum vitae, statement of present and future research plans, letter of interest, and two to three references to: **Robert J. Desnick, PhD, MD, Department of Genetics and Genomic Sciences, Mount Sinai School of Medicine, Fifth Avenue at 100th Street, New York, NY 10029-6574. E-mail: robert.desnick@mssm.edu.** Mount Sinai is an equal opportunity employer.

RMIT University

RMIT University
School of Applied Sciences

TWO POSITIONS: $61,043 - $86,225 p.a. AUD

Lecturer/Senior Lecturer in Molecular Biology and Microbiology
Ref. No.50001876

Lecturer/Senior Lecturer in Ecotoxicology/Environmental Biology
Ref. No. 50021999

You will be expected to conduct collaborative high-quality research within the School of Applied Sciences at RMIT University relevant to existing school research strengths, to teach into relevant programs and to supervise research students in your area of expertise. You must possess a Ph.D. and preference will be given to those with post-doctoral research and teaching experience. This position will be based at modern facilities at the Bundoora campus but you will be required to travel to other local School locations.

For further information please contact:
A/Prof Ann Lawrie on **Tel: + 61 3 9925 7157/7100** or by **e-mail aclawrie@rmit.edu.au**
Closing date for applications is **16th March, 2007**.
To obtain application details and a position description please visit **www.rmit.edu.au/pc/jobs** and quote above ref no's applicable to position.

TaiGen Biotechnology

TaiGen Biotechnology is a research-based and product-driven pharmaceutical company focused on novel therapeutics for diseases of serious medical needs. We are seeking highly motivated and qualified individuals to serve for the following positions.

Director – Discovery Biology

The Director for Discovery Biology will provide leadership and direction in the area of molecular biology, biochemistry, in-vitro pharmacology and high/medium throughput screening. The successful candidate will have a strong track record in drug discovery, solid experience in assay design and development, and knowledge of infectious disease, cancer, and diabetic related disease. The candidate must be self-motivated, collaborative, and have excellent writing and verbal communication skills. Ability to communicate effectively in Taiwanese/Mandarin and English would be advantageous. A Ph.D. degree with a minimum of 8 years of relevant experience is required.

Manager – High Throughput Screening

The High Throughput Screening Manager will be expected to independently guide the day-to-day research activities of a research team dedicated to developing and executing cell-based assays for G-protein coupled receptors. The successful candidate will have strong managerial skills and will be able to communicate effectively in both Taiwanese/Mandarin and English. Occasional international travel, particularly to the United States, may be required. Experience in programming, operating and troubleshooting lab automation/robotics and liquid handling equipment would be advantageous. A Ph.D. degree with a minimum of 5 years of relevant experience or a Bachelor's/Master's degree with 8 years of relevant experience is required.

Please submit your curriculum vitae, bibliography, and contact information for three letters of reference to:

taigenrecruit@taigenbiotech.com.tw
URL: **http://www.taigenbiotech.com.tw/site/**

Texas A&M University Department of Wildlife and Fisheries Sciences Faculty Positions in Mammalogy and Ornithology

The Department of Wildlife and Fisheries Sciences at Texas A&M University seeks outstanding individuals to join our faculty as Assistant Professor of Ornithology and Assistant Professor of Mammalogy. These positions are charged with building successful teaching and research programs in their respective area of emphasis and will also serve as Curator of Birds and the Curator of Mammals for the Texas Cooperative Wildlife Collection. In this role, they will supervise and develop their respective collections, including frozen tissue collections. Successful candidates must have a PhD in an appropriate field and demonstrated research excellence in ecology, evolutionary biology, systematics, genetics, or conservation biology as evidenced by a record of peer reviewed publications. Records of extramural research funding and experience in teaching are desirable. Additional information on these positions, the department, and Texas A&M University can be found at **http://www.wfsc.tamu.edu**. To apply: Indicate clearly the position you are applying for (separate applications are necessary for each position) and submit an electronic CV, statements of teaching and research interests, and philosophy regarding collections management and curation, plus contact information for three references to: **Dr. Michael L. Morrison**, Search Committee Chair, **mlmorrison@ag.tamu.edu**. Electronic submission deadline is **31 March 2007**. *The Texas A&M University System is an Equal Opportunity Employer and strongly encourages women and minorities to apply.*

University of California San Francisco Department of Psychiatry Basic Scientist/Psychiatrist

THE DEPARTMENT OF PSYCHIATRY AT THE UNIVERSITY OF CALIFORNIA SAN FRANCISCO invites applications for a Psychiatrist with established skills in laboratory research in areas of basic science generally relevant to psychiatric problems. This state-funded position will be at an academic rank based on the applicant's qualifications and can begin on July 1, 2007 or thereafter. Applicants must be board eligible or certified in Psychiatry and have a California medical license at time of appointment and have a Ph.D. and/or postdoctoral training in a laboratory science. A joint appointment in the UCSF Neuroscience Program will be offered if appropriate.

Applicants should submit their CV, brief statement of research interest, three letters of reference and three representative journal articles to: **John Rubenstein, M.D., Ph.D., Search Committee Chair, c/o Susan Yu, Department of Psychiatry, Rock Hall, 1550 4th Street, 2nd Floor South, Room RH 284C, University of California, San Francisco, San Francisco, CA 94143-2611**. Review of applications is ongoing.

UCSF is an Affirmative Action/Equal Opportunity Employer. The University undertakes affirmative action to assure equal employment opportunity for underrepresented minorities and women, for persons with disabilities, and for covered veterans. UCSF seeks candidates whose experience, teaching, research, or community service has prepared them to contribute to our commitment to diversity and excellence.

University of California, Riverside UCR/UCLA Thomas Haider Program in Biomedical Sciences

Tenure Track Assistant Professor: Molecular Mechanisms of Pathogenesis

The Division of Biomedical Sciences at The University of California, Riverside (**www.biomed.ucr.edu**) is hiring to fill a Tenure Track position at the level of Assistant Professor. The Division seeks applicants with a strong research focus on molecular mechanisms of pathogenesis who employ interdisciplinary approaches that complement existing research strengths in the Division. The ideal applicant would have demonstrated ability to exploit mammalian models of human disease. The preferred areas of research interest include, but are not limited to:

- Mechanisms of host defense
- Emerging infectious diseases
- Mechanisms of inflammation and chronic disease

The Division of Biomedical Sciences is home to the UCR/UCLA Thomas Haider Medical Program. The Division has a strong commitment to graduate training; it sponsors the Graduate Program in Biomedical Sciences, which is developing an innovative graduate curriculum which integrates the core biomedical curriculum of the UCR/UCLA medical degree program with graduate training and research. At the University level, UCR has made the commitment to support and expand Biomedical research by recently launching the Health Sciences Research Institute (**www.hsi.ucr.edu**), and the UC Regents have approved planning for a proposed UCR School of Medicine, projected to open in the Fall of 2012 (**www.medschool.ucr.edu**). UC Riverside is centrally located in Southern California, within a 90 minute drive of all the major southern California biomedical research institutions in Los Angeles, Orange, and San Diego counties.

The tenure track position will include a State Health Sciences salary, laboratory space, and start-up funds, commensurate with experience. Applicants must have a Ph.D., M.D., or equivalent graduate degree and appropriate post-doctoral research experience. Participation in the graduate and medical curriculum will be expected but will be phased in over the first few years. Applications will be reviewed beginning **March 15, 2007**; the position will remain open until filled. Applicants should send Curriculum Vitae, statement of research interests, and at least 3 letters of reference to: **David D. Lo, M.D., Ph.D., Faculty Search, Committee Chair, Division of Biomedical Sciences, University of California, Riverside, CA 92521**.

The University of California, Riverside is an Equal Opportunity/Affirmative Action Employer.

The European Molecular Biology Organization (EMBO)
invites applications and nominations for the position of

Executive Director

The Executive Director is responsible for the execution of the scientific, financial and organisational aspects of EMBO's various activities. He/she reports to, and works with, the EMBO Council in conceiving and planning the long-term strategies of EMBO.

Responsibilities include maintaining and further developing EMBO's programmes, in particular the Fellowship Programme, the Courses, Workshops & Conferences Programme, and the publication of EMBO's scientific journals.

The Executive Director also maintains close interactions with the EMBO membership and partner organisations such as the European Molecular Biology Laboratory (EMBL); represents EMBO in dealing with other scientific and political bodies, in particular EMBO's intergovernmental funding body (EMBC); and acts as a major voice of EMBO in shaping European science policy.

Candidates should have a successful scientific track record (including research experience), scientific vision and political skills. Managerial expertise and the ability to lead a professional staff are also expected.

The place of work will be the EMBO offices in Heidelberg, Germany. The appointment will be for five years with the possibility of a single renewal. Compensation will be internationally competitive and commensurate with the prestige of this position.

Applications should be sent to: Professors Gottfried Schatz and Hermann Bujard
EMBO
Meyerhofstr. 1
69117 Heidelberg
Germany

E-mail:
hermann.bujard@embo.org

Appication deadline: 15 April 2007

EMBO

---

www.mssm.edu

MOUNT SINAI SCHOOL OF MEDICINE

Faculty Positions in Molecular Cardiology

The Center for Molecular Cardiology at the Mount Sinai School of Medicine invites applications for independent, tenure-track faculty positions at the Assistant or Associate Professor level in molecular cardiology. Exceptionally well-qualified candidates at a more senior level may also be considered.

The successful candidates will have outstanding research qualifications. Areas of study interest include (but are not limited to): cardiogenesis, vasculogenesis, cardiovascular stem cell biology, genetic and systems level analyses of pathways involved in disease and development in animal models. Individuals should be highly interactive and receptive to multidisciplinary collaborations. Mount Sinai offers numerous shared research facilities including mouse transgenic and imaging cores and state-of-the-art animal facilities.

Applications should include a CV, a brief description of current research and future research plans, copies of no more than four primary publications, and names of and contact information for three references. Please send applications to: **Bruce D. Gelb, M.D., Director, Center for Molecular Cardiology, Box 1040, Mount Sinai School of Medicine, One Gustave L. Levy Place, New York, NY 10029. Call: (212) 241-3302. Email: bruce.gelb@mssm.edu.** Equal opportunity employer. We particularly welcome applications from women and underrepresented minorities in science.

SCRIPPS FLORIDA
THE SCRIPPS RESEARCH INSTITUTE

Department of Cancer Biology Faculty Positions

The Scripps Research Institute-Florida is seeking outstanding applicants for tenure-track faculty positions in the newly formed Department of Cancer Biology. The Department focuses on the molecular pathogenesis of cancer, using state-of-the-art, multi-disciplinary approaches and a variety of model systems for target identification, validation and pre-clinical studies.

The Department of Cancer Biology currently consists of four faculty, including **Dr. John L. Cleveland** (Myc, Apoptosis, Cancer Prevention and Therapeutics), **Dr. Nagi Ayad** (Ubiquitin Ligases in the Control of Cell Cycle, Differentiation and Cancer), **Dr. Michael Conkright** (Cyclic AMP Signaling and Transcriptional Regulatory Circuits), and **Dr. Kendall Nettles** (Nuclear Receptors, X-Ray Crystallography and Targeting Steroid Hormones in Breast Cancer).

The Department is seeking highly qualified and interactive investigators who will take advantage of the unique high-throughput Core Services of The Scripps Research Institute-Florida, including genomics, cell-based screening, proteomics, X-Ray crystallography, informatics and drug discovery.

Appointments are available at the Assistant, Associate and Full Professor levels. Scripps-Florida offers very attractive startup packages, unique core services, and the outstanding intellectual environment of The Scripps Research Institute for fostering top-tier basic and translational research. Interested candidates should submit their *Curriculum Vitae*, a synopsis of their past research accomplishments, and of their current and proposed research programs, along with complete contact information for at least four professional references, to: **Dr. John L. Cleveland, Chairman, Department of Cancer Biology, c/o Diane Wildman, The Scripps Research Institute-Florida, 5353 Parkside Drive, RE-1, Jupiter, FL 33458.**

SCIENTIFIC CURATOR

ZFIN, the zebrafish model organism database, seeks a scientific curator to join our dynamic, interactive team of biologists and computer scientists at the University of Oregon in Eugene, OR.

Scientific curation is emerging as an attractive, alternative career track for creative scientists. As a ZFIN curator you will:

- read the latest zebrafish literature, and add information about zebrafish genes, expression patterns and mutant phenotypes to the ZFIN database.
- work directly with research laboratories to facilitate the incorporation of their data into ZFIN.
- integrate the emerging whole-genome sequence with data available in ZFIN.
- collaborate with other bioinformatics professionals to create tools to aid cross-species comparisons.
- help design web interfaces to facilitate access to scientific data.

Required:

- Ph.D. or M.Sc. degree in the life sciences.
- Strong written and verbal communications skills.

Preferred:

- Experience in developmental genetics.
- Familiarity with biological databases or bioinformatics.

Please visit the ZFIN website (**http://zfin.org/zf_info/news/ZFIN_jobs.html**) for more information on this position.

Send curriculum vitae and references to: **Ellen McCumsey, Institute of Neuroscience, 1254 University of Oregon, Eugene, OR 97403-1254 USA; Fax: 541-346-4548; Email: ellenm@uoregon.edu**.

The University of Oregon is an Affirmative Action/Equal Opportunity/ADA Institution committed to cultural diversity. We invite applications from candidates who share our commitment to diversity. Applications received by March 9 receive first consideration.

University of California Davis, School of Medicine

and the

Shriners Hospitals for Children Northern California

Postdoctoral Fellowship Openings

The Institute for Pediatric Regenerative Medicine (IPRM), a collaborative initiative of The University of California Davis School of Medicine and Shriners Hospitals for Children Northern California, is recruiting for postdoctoral fellows in the laboratories of:

Paul Knoepfler, Ph.D. This opening is for a fellow to study genetic and epigenetic regulation of murine and human es stem cells. Postdoctoral fellows will have the opportunity to obtain experience and training in molecular genetics, transgenic technology, genomics, and ES stem cell biology. Candidates should have experienced and publications in developmental and stem cell biology, biochemistry, and/or molecular biology are desired.

Wenbin Deng, Ph.D. The fellow will study molecular mechanisms of nervous system development and disease. Emphasis is on signaling mechanisms of neuronal and glial cell death, excitotoxic, oxidative and inflammatory forms of injury to the developing brain, stem cell biology and regenerative medicine. Candidates will have the opportunity to obtain experience and training in animal models of human disease, neural culture techniques, and biochemical/molecular and morphological methods.

Candidates must have a Ph.D and/or M.D. Candidates should forward a letter indicating lab of interest to the appropriate PI describing their research, current interest, curriculum vitae, reprints of 3 publications, names and addresses of at least 3 reference to: Human Resources, c/o Paul Knoepfler, Ph.D. or Wenbin Deng, Ph.D. (depending on lab of interest), 2425 Stockton Blvd., Sacramento, CA 95817 or fax (916) 453-2388. The positions will remain open until filled.

University of California Davis & Shriners Hospitals for Children are EOE/Drug Free Workplace

EUROPE'S BRAIN GAIN

With significant increases in funding, and the creation of the European Research Council, Europe is quietly making its presence felt as a science and technology hub. We track the expansion of funding and career opportunities as the European Union continues to grow and strengthen as a global science leader. **Read the full story in the 2 March issue of *SCIENCE*.**

UPCOMING FEATURES:

March 2 — International Career Report: Science in Europe
April 6 — Careers in Cancer Research
April 20 — Postdoctoral Careers: Transferable Skills

www.sciencecareers.org/businessfeatures

ScienceCareers.org
We know science AAAS

UNIVERSITY OF HAWAI'I
DEAN, COLLEGE OF NATURAL SCIENCES

The University of Hawai'i at Mānoa (UHM), a leading institution of higher learning in the Pacific Basin and one of the nation's few land-, sea- and space-grant institutions, seeks an innovative, entrepreneurial and highly accomplished leader as Dean of the College of Natural Sciences.

The College of Natural Sciences is part of an international community of scholars in the physical and life sciences, mathematics and information and computer sciences, including library sciences. The Dean serves as the foremost academic and administrative leader for the College. As the University celebrates its centennial in 2007, the Dean will be called upon to develop an inspiring cohesive vision and strategic plan to guide the College toward new levels of excellence by building on the strong scientific accomplishments of existing programs and by pursuing an integrated, comprehensive academic program that balances scholarship, instruction and service. To implement this vision, the Dean must be a passionate, collaborative, engaging advocate for the College within the University, across the state, and beyond.

Nominations and applications are being accepted for the position. First screening of candidates will begin on Monday, **March 19, 2007**, and will continue until the position is filled. Candidates must submit a cover letter summarizing the candidate's interest and qualifications for the position, a current resume, and the names of five (5) professional references including postal and e-mail addresses and telephone numbers. For more information about the University of Hawai'i at Mānoa, please go to **www.uhm.hawaii.edu**. For a position description, application and nomination requirements, and other information, please visit University of Hawai'i web sites at **http://workatuh.hawaii.edu** and **www.hawaii.edu/executivesearch/naturalsciences**.

Inquiries, nominations, and applications should be directed to Edward W. Kelley and Partners at: **Edward W. Kelley and Partners, Attention: Sharon Tanabe, Principal, 1111 Corporate Center Drive, Suite 106, Monterey Park, CA 91754; Phone: 323-260-5045; Fax: 323-260-7889; E-Mail: sharon.tanabe@ewkp.com**. E-Mail correspondence is strongly encouraged.

The University of Hawai'i is an Equal Opportunity/Affirmative Action Institution and encourages applications from and nominations of women and minority candidates.

Yale School of Public Health
Yale University School of Medicine

Tenured Full Professor to Develop Program in Bioinformatics, Statistical Genomics or Genetic Epidemiology

Yale School of Public Health is currently seeking a tenured full professor to develop and lead programs in one of the related disciplines of bioinformatics, statistical genetics or genetic epidemiology. Expertise in any of these areas is of interest. The person holding this position will also assume a leadership role in the interface of their discipline with Yale's broader initiatives to expand genomic research in the Medical School and at the University. Further faculty recruitment in these genomic disciplines is planned.

The successful candidate will have an active research and training program; an extensive body of influential publications; a history of service to international/national-level committees, professional organizations, and scholarly journals; a reputation for mentoring successful academic careers; and an established international reputation in their chosen discipline.

Applications, nominations, and inquiries are all invited. For full consideration, applicants should submit a letter of interest, a complete curriculum vitae, and copies of recent publications, by **May 31, 2007**, in confidence to:

Michael Bracken, Search Committee Chair
Yale School of Public Health
Yale University School of Medicine
P.O. Box 208034
New Haven, CT 06520-8034

Yale University is an Affirmative Action/Equal Opportunity Employer. Men and women of diverse racial/ethnic backgrounds and cultures are encouraged to apply.

POSITIONS OPEN

INTRINSIC DISORDER RESEARCH
School of Informatics
Center for Computational Biology and Bioinformatics
Indiana University, Purdue University Indianapolis

The Center for Computational Biology and Bioinformatics and the School of Informatics at Indiana University, Perdue University, Indianapolis (IUPUI), are welcoming applications for a **TENURE-TRACK POSITION** at the junior level. The appointed faculty member will join our renowned intrinsic disorder research group, and will be expected to participate in ongoing research projects in collaboration with the other members of the group, as well as start a strong, externally funded research program. The appointed candidate will also be expected to teach in the School of Informatics' graduate program in bioinformatics. Candidates must have a Ph.D. in computer science with postdoctoral experience in bioinformatics, and a research program focused on the study of intrinsic disorder in proteins. Ample experience in the computational prediction and analysis of intrinsic disorder is essential. Candidates must also have experience in the computational analysis of biological pathways and be able to teach courses at the graduate level in structural bioinformatics, pattern recognition and machine learning, and theory of computation for bioinformatics students. Letter of application, curriculum vitae, statement of research, and the names and three letters of reference (under separate cover) must be postmarked by March 30, 2007, to: **A. Keith Dunker, Search Committee for Intrinsic Disorder Research, Medical Information Sciences Building, 410 W. 10th Street, Suite 5000, Indianapolis, IN 46202.** *The School of Informatics is eager to consider applications from women and people of color. Indiana University is an Affirmative Action/Equal Opportunity Employer.*

TRACE ELEMENT/TRACE METAL GEOCHEMIST (TENURE TRACK)

Stony Brook University's Marine Sciences Research Center (MSRC) announces the availability of a tenure-track faculty position (nine-month academic year salary) in trace element geochemistry of marine systems. The position will be filled at the rank of **ASSISTANT PROFESSOR,** and candidates must have a Ph.D. at the time of appointment. More information on MSRC is available at **website: http://www.msrc.sunysb.edu** and application details may be found at **website: http://www.msrc.sunysb.edu/news/empops.html.** Successful candidates will be expected to enhance and complement existing faculty and programs at MSRC, generate external funding to develop an active research program in marine science, and teach at the graduate and undergraduate levels. Applicants should submit curriculum vitae, statement of professional goals, and the names and contact information of at least three references to: **Chair, MSRC Trace Element Geochemist Search Committee, Marine Sciences Research Center, Stony Brook University, Stony Brook, NY 11794-5000.** Review of applications will begin March 12, 2007, and continue until the position is filled. *The MSRC has a diverse faculty and members of underrepresented groups are especially encouraged to apply.*

RESEARCH ASSISTANT PROFESSOR at the Center for Remote Sensing of Ice Sheets (CReSIS), University of Kansas. Full-time position. Required qualifications: Ph.D. or equivalent in electrical engineering, computer engineering, computer science, geophysics, physics, glaciology, or related field, evidence of independent research capabilities in remote sensing and field observations, two years of experience collecting and analyzing data from remote sensors, excellent written communication skills. Review of applications begins March 1, 2007. Salary commensurate with experience. Application instructions at **website: https://jobs.ku.edu** (position 00008546) or e-mail **Ms. Tommie Cassen** at **e-mail: tcassen@cresis.ku.edu.** *Equal Opportunity/Affirmative Action.*

POSITIONS OPEN

ADJUNCT ASSOCIATE PROFESSOR
University of California, San Francisco
Diabetes Center/Immune Tolerance Network

The Diabetes Center/Immune Tolerance Network (ITN) of the University of California at San Francisco (UCSF) is seeking to appoint a new faculty member whose focus will be on evaluating new technologies and develop core facilities for implementation of novel genetic and immunologic assays to support the clinical research of the ITN.

The ITN is a collaborative research project that seeks out, develops, and performs clinical trials and biological assays of immune tolerance. It is supported by a seven-year contract from the National Institute of Allergy and Infectious Diseases (NIAID), the National Institute of Diabetes and Digestive and Kidney Disorders (NIDDK), and the Juvenile Diabetes Research Foundation. ITN-supported researchers are developing new approaches to induce, maintain, and monitor tolerance with the goal of designing new immune therapies for solid organ and islet transplantation, autoimmune diseases and allergy and asthma.

The successful candidate will establish new approaches for understanding the basis for immunological disease and tolerance, including developing novel protocols, approaches, and assays for implementation at ITN core facilities. The appointee will design experiments and protocols, establish core facilities, and oversee core directors as they carry out experiments. The appointee will work in the Bethesda, Maryland, offices, and will be a member of the Diabetes Center and an appropriate academic department.

Candidates are expected to hold a Ph.D. in a scientific field relevant to the ITN with demonstrated achievement in their field. The deadline for application to be considered in a timely manner is April 1, 2007. Applicants should submit curriculum vitae, a one to two-page summary of research accomplishments, a one to two-page perspective on future research plans, and reprints of major publications, and arrange to have three to five letters of recommendation forwarded to:

Diabetes Center/Immune Tolerance Network
Faculty Search Committee
c/o Ms. Brigid E. Donnelly
3333 California Street
Suite 430, P.O. Box 1211
San Francisco, CA 94118

UCSF seeks candidates whose expertise, teaching, research, or community service has prepared them to contribute to our commitment to diversity and excellence. UCSF is an Affirmative Action/Equal Opportunity Employer. The University undertakes affirmative action to assure equal employment opportunity for underutilized minorities and women, for persons with disabilities, and for covered veterans. All qualified applicants are encouraged to apply, including minorities and women.

BIOLOGIST/BIOINFORMATICS

The Department of Biological Sciences at Marquette University has a tenure-track **ASSISTANT PROFESSOR** position available August 16, 2007. Applicants must have a Ph.D. with postdoctoral experience. The successful candidate is expected to develop an extramurally funded research program that will complement existing areas of research within the Department **(website: http://biology.marquette.edu).** Preference will be given to applicants who can also provide expertise in bioinformatics, genomics, or protein structure that enhances ongoing programs campuswide. Teaching responsibilities include an introductory biology course for undergraduate majors and a graduate course in the candidate's area of expertise each year. Review of applications until the position is filled. Candidates should apply online at **website: http://careers.marquette.edu/applicants/Central?quickFind=50566.** Application process requires curriculum vitae and statement of research and teaching interests. Three reference letters are to be sent to: **Dr. Robert Fitts, Chair, Department of Biological Sciences, Marquette University, WLS 112, P.O. Box 1881, Milwaukee, WI 53201-1881.**

Cooperative Ecosystem Studies Units Network

National Coordinator, Cooperative Ecosystem Studies Units. The Department of the Interior is looking for a demonstrated leader in directing a multi-disciplinary, multi-agency/institution partnership to provide research, technical assistance, and education to natural and cultural resource and environmental managers.

These units, named Cooperative Ecosystem Studies Units (CESUs), provide research, technical assistance, and education to Federal land management, environmental and research agencies, and their potential partners. Cooperative emphasizes that multiple Federal agencies and universities are among the partners in this program. Ecosystem studies involve the biological, physical, social, and cultural sciences needed to address resource issues and interdisciplinary problem solving at multiple scales and in an ecosystem context. Resources encompass natural and cultural resources.

Federal agencies contribute research scientists and/or other professionals located and working at CESUs under formal agreements between their respective bureaus and universities. Federal personnel are supervised and supported by their respective agencies, through existing administrative systems. Federal agencies provide other scientific staff, administrative support funds (for assistance beyond the basic support provided by the universities), and project funds for specific research projects and technical assistance. Federal agency participation in a CESU does not alter previous arrangements or cooperative agreements. CESUs create additional opportunities for interdisciplinary and multi-agency research, technical assistance, and education. More information on the program can be found at **www.cesu.org**.

Requirements include U.S. citizenship, an advanced degree in a natural, cultural, or social science, experience in management and/or scientific leadership, experience in multi-agency coordination, ability to achieve an integrated and cooperative inter-organizational and interdisciplinary program that contributes to the scientific and scholarly basis for federal agencies to achieve their resource stewardship and technical application missions, broad professional knowledge and familiarity with a wide range of professional and technical disciplines and ability to apply this knowledge to effectively develop, organize, and oversee CESU activities. Also, a knowledge and understanding of how the principles of conservation biology, ecosystem management, social science, and cultural resource scholarship and their interrelationships influence their application by federal, state, and private land and resource managing agencies, universities, and other partner entities that together form the CESU National Network is required.

The position is a GS 14 or 15 (salary range $87,533 -$133,850) depending on qualifications and organizationally located within the National Park Service in the Main Interior Building in Washington DC. The DOI is an Equal Opportunity Employer. To apply please visit **www.usajobs.opm.gov (Announcement NPS WASO-06-12)**. Applications will be accepted through **March 15, 2007**. For information about the application process contact **Kenyett Nicholson** at **202-354-1919**. For information about the position contact **Bert Frost, Deputy Associate Director, Natural Resource Stewardship and Science at 202-513-7210 or bert_frost@nps.gov**.

MEETINGS

PRIZES

KUWAIT PRIZE 2007
Invitation for Nominations

The **Kuwait Foundation for the Advancement of Sciences (KFAS)** institutionalized the **KUWAIT Prize** to recognize distinguished accomplishments in the arts, humanities and sciences. The Prizes are awarded annually in the following categories:

A. Basic Sciences
B. Applied Sciences
C. Economics and Social Sciences
D. Arts and Literature
E. Arabic and Islamic Scientific Heritage

The Prizes for **2007** will be awarded in the following fields:

1. **Basic Sciences:** Immunology
2. **Applied Sciences:** Pharmacology
3. **Economic and Social Sciences:** Energy and Development in the Arab World
4. **Arts and Literature:** Andalosian Literature
5. **Arabic and Islamic Scientific Heritage:** Veterinary and Zoology in Arab Heritage

Foreground and **Conditions** of the Prize:

1. Two prizes are awarded in each category:
   • A Prize to recognize the distinguished scientific research of a Kuwaiti citizen, and,
   • A Prize to recognize the distinguished scientific research of an Arab citizen.
2. The candidate should not have been awarded a Prize for the submitted work by any other institution.
3. Nominations for these Prizes are accepted from individuals, academic and scientific centers, learned societies, past recipients of the Prize, and peers of the nominees. No nominations are accepted from political entities.
4. The scientific research submitted must have been published during the last ten years.
5. Each Prize consists of a cash sum of K.D. 30,000/- (approx. U.S.$100,000/-), a Gold medal, a KFAS Shield and a Certificate of Recognition.
6. Nominators must clearly indicate the distinguished work that qualifies their candidate for consideration.
7. The results of KFAS decision regarding selection of winners are final.
8. The documents submitted for nominations will not be returned regardless of the outcome of the decision.
9. Each winner is expected to deliver a lecture concerning the contribution for which he was awarded the Prize.

Inquiries concerning the KUWAIT PRIZE and nominations including complete curriculum vitae and updated lists of publications by the candidate with **four copies** of each of the published papers should be received before **October 31, 2007** and addressed to:

The Director General
The Kuwait Foundation for the Advancement of Sciences
P.O. Box: 25263
Safat - 13113, Kuwait
Tel: (+965) 2429780
Fax: 2403891
E-Mail: prize@kfas.org.kw

GRANTS

PRIZES

The Daiwa Anglo-Japanese Foundation

Daiwa Adrian Prizes 2007

Daiwa Adrian Prizes are awarded by The Daiwa Anglo-Japanese Foundation on a triennial basis in recognition of significant collaboration between British and Japanese research teams in the field of pure science or the application of science.

The Prizes were established in 1992 and subsequently renamed to commemorate the late Lord Adrian, a founding Trustee of the Foundation, at whose initiative the Prizes were established. Since their launch, £280,000 in Prizes has been awarded to 47 different institutions, 25 from the UK and 22 from Japan.

All submissions will be judged on the basis of scientific quality and past performance but take into account future potential and the likely long-term contribution to UK-Japan scientific relations. Applications are handled by the Foundation with an assessment conducted by a panel of Fellows of The Royal Society.

Further information: www.dajf.org.uk/dap

EUROPEAN SCIENCE FOUNDATION

Opportunities for Europe-wide Collaborations

The European Science Foundation (ESF), with offices in Strasbourg and Brussels, is the European association of 75 major national research funding and performing organisations and academies in 30 countries devoted to excellence in scientific research. The ESF covers all research domains: physical and engineering sciences; life, earth and environmental sciences; medical sciences; humanities; and social sciences. The mission of the ESF is to provide a common European platform for its Member Organisations in order to advance research and explore its new directions at the European level.

In 2007 ESF announces the following Calls for Proposals

Proposals for ESF Exploratory Workshops (EWs)

Small, interactive group sessions, EWs aim to open up new directions in research and to explore emerging fields. Proposals should demonstrate the potential for initiating follow-up research activities and/or developing future collaborative actions. Interdisciplinary topics are greatly encouraged.

Awards will be to a maximum of €15,000

Submission: open from 1st March 2007 ■ Deadline: 27th April 2007

Workshops must take place during 2008

More information: **www.esf.org/workshops**

Proposals for ESF Research Networking Programmes (RNPs)

RNPs are the platform for nationally-funded research groups to address major scientific and research infrastructure issues. Proposals must deal with high-quality science and demonstrate the added value of being carried out at the European level with the goal to advance the frontiers of science.

Awards will be to a maximum of €120,000 annually, for a four or five-year period.

Submission: open from 2nd July 2007 ■ Deadline: 30th October 2007

More information: **www.esf.org/programmes**

Proposals for EUROCORES (European Collaborative Research)

The EUROCORES Scheme offers a flexible framework for researchers from Europe to address questions which are best addressed in larger scale collaborative research programmes.

Themes: Following the EUROCORES theme call around five new themes for collaborative research in and across all scientific fields will be selected through international peer review.

Submission: open from March 2007 ■ Deadline: 1st June 2007

Projects: Each year a call for Collaborative Research Projects (CRPs) is announced, based on EUROCORES themes selected the previous year.

Publication for the Calls for the approved EUROCORES Programme: March 2007 ■ Start of the research projects: May 2008

More information: **www.esf.org/eurocores**

Proposals for ESF Research Conferences 2009

The ESF Research Conferences Scheme allows scientists and young researchers to meet for discussions on the most recent developments in their fields of research. The Call for 2009 Research Conferences is addressed to leading European scientists for events to take place in: Biology + (Biology at the Interface with Other Science Disciplines), Environmental Sciences, Physics/Biophysics, Social Sciences and Humanities.

Submission: open from Spring 2007 ■ Deadline: 1st October 2007

More information: **www.esf.org/conferences** or for enquiries to **conferences-proposals@esf.org**

For further information on the calls and all ESF activities, please go to www.esf.org

---

CONFERENCE

ESF CONFERENCES

RESEARCH INTEGRITY

FOSTERING RESPONSIBLE RESEARCH

A Portuguese European Union Presidency and European Commission Event, Initiated and Organized by the European Science Foundation & the US Office of Research Integrity, in Partnership with the International Council for Science.

Lisbon, Portugal • 16-19 September 2007

Research regulations and commonly accepted research practices vary significantly from country to country and among professional organisations. There is no common definition world-wide for research misconduct, conflict of interest or plagiarism. Even where there is general agreement on key elements of research behaviour, the policies that implement this agreement can vary widely from country to country and organization to organization. The research community worldwide has to address these problems in order to retain public confidence and to establish a clear best practice frameworks at an international level. It must do so at a time when there are increased pressures on the research system.

The September 2007 Conference represents an initial effort to establish a framework for continued discussion of research integrity on a global level. It is the first global forum convened to provide researchers, research administrators, research sponsors, journal editors, representatives from professional societies, policymakers, and others an opportunity to discuss strategies for harmonizing research misconduct policies and fostering responsible conduct in research.

Attendance will be limited and by invitation to ensure geographical and experience balances. A maximum of 350 places will be available.

Confirmed Speakers will include:
Bertil Andersson, Chief Executive, European Science Foundation; Christine Boesz, Inspector General, US National Science Foundation; Jose-Mariano Gago, Minister of Science, Portugal; Manuel Heitor, Ministry of Science, Portugal; Motoyuki Ono, President, Japan Society for the Promotion of Science; Chris Pascal, Director, Office of Research Integrity; Janez Potočnick, European Commissioner for Research.

Pre-Registration Form & Conference Programme, available from

www.esf.org/conferences/researchintegrity

Closing Date for Applications 27 April 2007

www.esf.org

With Additional Support from:
- European Molecular Biology Organization (EMBO)
- Committee on Publication Ethics (COPE)
- Portuguese Ministry of Science, Technology and Higher Education (MCTES)
- Portuguese Science Foundation (FCT)
- Calouste Gulbenkian Foundation (FCG)
- UK Research Integrity Office (UKRIO).

POSITIONS OPEN

DARWIN POSTDOCTORAL FELLOW

The Earth Systems Initiative at MIT seeks Postdoctoral scientists to develop and explore cross-scale models of marine microbial communities, ocean biogeochemical cycles, and climate. Through the development and application of novel modeling approaches we seek to understand and simulate the ecological, biogeochemical, and physical regulators of marine microbial communities from the genomic and cellular scales, through metabolic networks, to emergent global biogeography.

Successful candidates will join a new, interdisciplinary effort which links several Departments at MIT (Earth, Atmospheric and Planetary Sciences; Civil and Environmental Engineering; and Computational and Systems Biology) under the auspices of the Earth Systems Initiative **(website: http://esi.mit.edu).** This interdisciplinary project provides an opportunity for motivated candidates to drive forward and explore cutting-edge and novel approaches to modeling marine microbes and their interactions with global biogeochemical cycles.

Candidates must have or must be close to completing a doctoral degree in a relevant scientific discipline. Predoctoral candidates must complete their doctoral degree prior to commencing employment. Candidates should have a background in one or more of the following fields: environmental genomics, ecology, systems biology or marine biogeochemistry with experience and interest in mathematical and/or numerical modeling.

Additional information may be obtained by contacting **Dr. Mick Follows (e-mail: mick@mit.edu; telephone: 617-253-5939), Prof. Penny Chisholm (e-mail: chisholm@mit.edu),** or **Prof. Bruce Tidor (e-mail: tidor@mit.edu).** Application material should include curriculum vitae and one-page statement of your research interests.

Interested candidates may apply online at **website: http://web.mit.edu/jobs.** Please reference job number mit-00003798.

MIT is an Equal Opportunity/Affirmative Action Employer. Applications from women, minorities, veterans, older workers, and individuals with disabilities are strongly encouraged.

POSTDOCTORAL FELLOW POSITION

The Department of Anatomy and Physiology invites applications for the position of Postdoctoral Fellow in the Tumor Physiology Laboratory engaged in studying lung carcinogenesis and the therapeutic applications of stem cells in lung cancer. A Ph.D. in cancer biology or biochemistry is required. Ideally, the successful candidate will have experience with basic biochemistry and molecular biology which include Western blotting, real time polymerase chain reaction, and Northern blotting. Isolation of epithelial cells and stromal fibroblasts as well as primary culture of these cells will be a part of the laboratory's daily work. Experience with immunohistochemistry and immunocytochemistry is desirable. Computer literacy is also essential. Applicants must submit electronically curriculum vitae, a short essay that describes their scientific experiences and/or future study, and the names of two to three references to: **Dr. Masaaki Tamura (e-mail: mtamura@vet.k-state.edu).** Screening of applications will begin February 26, 2007, and continue until position is filled. *Kansas State University is an Equal Opportunity, Affirmative Action Employer. Kansas State University actively seeks diversity among its employees.*

STAFF RESEARCH ASSOCIATE II ($3045 to $4900 per month). The University of California, Davis, is seeking a specialist to work in its Murine Cryopreservation and Recovery Laboratory in the Mutant Mouse Regional Resource Center. Must have experience in in vitro fertilization, cryopreservation, and resuscitation. For details and required application materials call **telephone: 530-752-1760, TDD 530-752-7140,** or apply at **website: http://www.hr.ucdavis.edu/Emp/Careers, VL 7401.** Final filing date: March 7, 2007. *Equal Opportunity Employer.*

POSITIONS OPEN

POSTDOCTORAL FELLOW POSITION

A Postdoctoral position is available to study the role of the RUNX transcription factor family in prostate and ovarian cancers. This position is available immediately. The selected individual will work within a Feist-Weiller Cancer Center-supported group of scientists studying the role of aberrant transcription and chromatin structure as it relates to cancer. Applicants must have a Ph.D. with experience in biochemistry and molecular and cellular biology. Candidates should have experience in mammalian tissue culture, general molecular biology techniques, immunohistochemistry, and in-situ analysis. All interested applicants should forward curriculum vitae/bibliography and list of three references to: **Shari Meyers, Ph.D., Department of Biochemistry and Molecular Biology, Louisiana State University Health Sciences Center, 1501 Kings Highway, Shreveport, LA 71130; e-mail: smeyer@lsuhsc.edu, fax: number: 318-675-5180.**

Further details can be found at **websites: http://www.fwcconline.com** and **www.shrevebiochem.com.**

Louisana State University Health Science Center is an Affirmative Action/Equal Opportunity Employer.

A POSTDOCTORAL POSITION is available in the Department of Molecular and Cellular Oncology to study the signal transduction pathways involved in tumorigenesis using the mouse model. We are particularly interested in the role of PTEN/Akt signaling and PML tumor suppressor in cancer development (*Nature* **431:** 205-211, 2004; *Nature* **436:** 725-730, 2005; *Mol. Cell* **24:** 331-339, 2006) and aim to identify the key regulators involved in this process. Applicants who have a strong background in molecular biology, cell biology, or mouse genetics are strongly preferred. Please send your curriculum vitae, past research background and accomplishments, and names of three references to: **Dr. Hui-Kuan Lin, Assistant Professor of Molecular and Cellular Oncology, e-mail: hklin@mdanderson.org** or **e-mail: huikuanlin@hotmail.com.**

The M.D. Anderson Cancer Center is an Equal Opportunity Employer and does not discriminate on the basis of race, color, national origin, gender, sexual orientation, age, religion, disability, veteran status, except where such distinction is required by law. All positions at the University of Texas M.D. Anderson Cancer Center are security-sensitive and subject to Texas education code 51-215, which authorizes the employer to obtain criminal history record information. Smokefree environment.

SHRINERS HOSPITAL/OREGON HEALTH and SCIENCE UNIVERSITY (OHSU). A Postdoctoral position is now available to study the developmental and biochemical functions of Hoxa13. Applicants with experience with in vitro cell expression assays, protein expression, purification, and crystallization will be given strong consideration. Curriculum vitae and the names of three references should be mailed to: **H. Scott Stadler, Ph.D., Shriners Hospital for Children, Mail Code SHC-Research, 3101 S.W. Sam Jackson Park Road, Portland, OR 97239,** or e-mailed to **e-mail: hss@shcc.org.** *Shriners Hospital and OHSU are Equal Opportunity Employers and drugfree and smoking-free workplaces.*

POSTDOCTORAL/RESEARCH SCIENTIST position for a highly-motivated individual available at the University of Michigan to study the mechanism of action of microsomal cytochrome P450 using techniques including stopped-flow-spectrophotometry, rapid chemical quench, and rapid freeze quench electron paramagnetic resonance under anaerobic conditions. Knowledge of enzyme kinetics and the structure and function of heme and flavo-proteins is desirable, as well as experience with mass spectrometry. Send resume and names of three references to **Dr. Waskell** at **e-mail: waskell@umich.edu.**

POSITIONS OPEN

MOLECULAR BIOLOGY LABORATORY TECHNICIAN and LABORATORY MANAGER

Position available in laboratory of **Dan Morse, Director,** Institute for Collaborative Biotechnologies, University of California, Santa Barbara. Experience and skills required in DNA and RNA manipulation and protein purification and characterization. Experience in laboratory management desired.

Sixty percent time: molecular biology of protein expression, purification, self-assembly, catalysis, optical properties and control; 30 percent time: laboratoroy management (equipment maintenance, regulatory compliance, hiring and supervising student assistant); five percent time: laboratory displays and presentations (preparation, transport, installation, and presentation of displays of research materials for visitors and conferences); five percent time: general assistance.

Salary commensurate with experience. Applications and inquiries to **Pam Wall (e-mail: wall@lifesci.ucsb.edu).** Position is opened until filled. *The University of California is an Equal Employment Opportunity/Affirmative Action Employer.*

VISITING ASSISTANT PROFESSOR
Invertebrate Biology

The Department of Biology, Hamilton College, invites applications for a two-year visiting assistant professorship, with the possibility of a second two-year appointment, effective July 1, 2007. Ph.D. and teaching experience expected. The successful applicant will supervise senior thesis research, and teach: (1) invertebrate biology and (2) an additional lecture/ laboratory course of the candidate's choosing, or an upper-level seminar and co-teach introductory biology, as complements the Department's offerings. Support is available for research and conference travel. Send curriculum vitae, a statement about teaching, and names of three references to: **Patrick D. Reynolds, Chair, Department of Biology, Hamilton College, 198 College Hill Road, Clinton, NY 13323-1292.** Review of application materials will begin March 2, 2007, and continue until the position is filled. *Women and members of minority groups are encouraged to apply. Hamilton College is an Affirmative Action, Equal Opportunity Employer and is committed to diversity in all areas of the campus community.*

MARKETPLACE